

Copper-Mediated Cross-Coupling Reactions Toward Tandem-Catalysis

Von der Fakultät für Mathematik, Informatik und Naturwissenschaften der RWTH Aachen
University zur Erlangung des akademischen Grades eines Doktors der Naturwissenschaften
genehmigte Dissertation

vorgelegt von

M. Sc.

Fabian Thomas

aus Düsseldorf

Berichter:

Universitätsprofessorin Dr. Sonja Herres-Pawlis

Universitätsprofessor Dr. Ulrich Schwaneberg

Tag der mündlichen Prüfung: 11.06.2021

Eidesstattliche Versicherung

Ich, Fabian Thomas, versichere hiermit an Eides Statt, dass ich die vorliegende Dissertation mit dem Titel:

Copper-Mediated Cross-Coupling Reactions Towards Tandem-Catalysis

selbstständig und ohne unzulässige fremde Hilfe erbracht habe. Ich habe keine anderen als die angegebenen Quellen und Hilfsmittel benutzt. Für den Fall, dass die Arbeit zusätzlich auf einem Datenträger eingereicht wird, erkläre ich, dass die schriftliche und die elektronische Form vollständig übereinstimmen. Die Arbeit hat in gleicher oder ähnlicher Form noch keiner Prüfungsbehörde vorgelegen.

Ort, Datum

Unterschrift

Belehrung:

§ 156 StGB: Falsche Versicherung an Eides Statt

Wer vor einer zur Abnahme einer Versicherung an Eides Statt zuständigen Behörde eine solche Versicherung falsch abgibt oder unter Berufung auf eine solche Versicherung falsch aussagt, wird mit Freiheitsstrafe bis zu drei Jahren oder Geldstrafe bestraft.

§ 161 StGB: Fahrlässiger Falscheid; fahrlässige falsche Versicherung an Eides Statt

(1) Wenn eine der in den §§ 154 bis 156 bezeichneten Handlungen aus Fahrlässigkeit begangen worden ist, so tritt Freiheitsstrafe bis zu einem Jahr oder Geldstrafe ein.

(2) Straflosigkeit tritt ein, wenn der Täter die falsche Angabe rechtzeitig berichtigt. Die Vorschriften des § 158 Abs. 2 und 3 gelten entsprechend

Die vorstehende Belehrung habe ich zur Kenntnis genommen:

Ort, Datum

Unterschrift

List of publications, presentations, posters and projects:

Publications as first or shared first author:

1. M. A. S. Mertens, F. Thomas, M. Nöth, J. Moegling, I. El-Awaad, D. F. Sauer, G. V. Dhoke, W. Xu, A. Pich, S. Herres-Pawlis, U. Schwaneberg, *Eur. J. Org. Chem.* **2019**, 2019, 6341.
2. F. Thomas, M. Oster, F. Schön, K. Göbgen, B. Amarouch, D. Steden, A. Hoffmann, S. Herres-Pawlis, *Dalton Trans.* **2021**, 50, 6444.
3. F. Thomas, D. Steden, A. Eith, A. Hoffmann, S. Herres-Pawlis, *Z. Naturforsch.* **2021**, 76b, 835.

Further publications:

1. J. Moegling, A. Hoffmann, F. Thomas, N. Orth, P. Liebhäuser, U. Herber, R. Rampmaier, I. Ivanović-Burmazović, S. Herres-Pawlis, *Angew. Chem.* **2018**, 57, 9154; *Angew. Chem. Int. Ed.* **2018**, 130, 9294.
2. D. Schäfer, F. Fink, D. Kleinschmidt, K. Keisers, F. Thomas, A. Hoffmann, A. Pich, S. Herres-Pawlis, *Chem. Commun.* **2020**, 56, 5601.

Presentations:

1. 3. Ligandendesignworkshop, 2019, *Maßgeschneiderte Bis(pyrazolyl)methan-Liganden zur Stabilisierung von Kupfer-Nitrenen*, Cologne (Germany).
2. 12th New Year's Symposium, 2020, *Copper nitrene complexes and their application in catalytic C–H amination reactions*, Aachen (Germany).
3. 16. Koordinationschemie-Treffen, 2020, *Kupfer-Bis(pyrazolyl)methan-Nitren-Komplexe in der C–H-Aminierung*, Freiburg (Germany).

Posters:

1. 15. Koordinationschemie-Treffen, 2019, *Kupfer(I)-Bis(pyrazolyl)methan-Komplexe in der katalytischen C–H-Aminierung*, Munich (Germany).
2. GDCh Wissenschaftsforum, 2019, *C–H-Aminierung mittels Kupfer(I)-Bis(pyrazolyl)methan-Komplexen*, Aachen (Germany).
3. Assessment of SFB 985, 2020, *Microgel-engineered chemoenzymatic cascades employing whole cells*, Aachen (Germany).

SFB-Projects:

SFB 985 (*Functional Microgels and Microgel Systems*), subproject A1 (funding period 2: *Microgel engineered enzymatic and chemical reactions – towards tandem catalysts*; funding period 3: *Microgel-engineered chemoenzymatic cascades employing whole cells*).

Abstract

Catalytic transformations are key to the development of atom efficient processes. An important functional group in biologically, synthetically and pharmacologically relevant molecules are amines. The central intermediates in atom efficient reactions to introduce an amine function are terminal nitrenes. Terminal nitrene complexes are an elusive species and rational ligand design helps to understand connection between the structure and the reactivity. Therefore, this PhD thesis includes the synthesis of a library of different bis(pyrazolyl)methane ligands. The aim was to investigate the influence of the ligand design on the formation and activity of the generated copper nitrene complexes. This was achieved by variation of the third *N* donor unit of the ligand, whose electronic as well as the steric properties were varied. By the application of the nitrene generating agent ^sPhINTs, six novel copper nitrene complexes were synthesized at low temperature in dichloromethane. These nitrene complexes were characterized by ultra-high resolution cryo ESI mass spectrometry, density functional theory, UV/Vis and NMR spectroscopy. It was shown that terminal nitrene complexes are generated as singlet species in high yields. In addition, the thermal stability and catalytic activity was investigated. By variation of the third *N* donor unit copper nitrene complexes with a high stability as well as a high catalytic activity were obtained. At room temperature the C–H amination of different benzylic, alkylic and aromatic substrates and the aziridination of different styrene derivatives is possible. Due to the relevance of enantiomeric pure products, also chiral precursor complexes were used in asymmetric catalytic reactions and enantiomeric enriched products could be obtained. To further increase the atom efficiency of the catalytic amination reaction under avoidance of ^sPhINTs, also aromatic azides were used as nitrene generating agents. A first success was achieved by the combination of benzoyl azide and electron rich bis(pyrazolyl)methane ligands. Beside copper(I) complexes also iron(II) complexes were investigated as precursor complexes to generate nitrene complexes. Another approach for the development of environmentally sustainable processes are tandem reactions. By the combination of two or more catalysts in one process, a purification of the intermediates is redundant. This leads to savings in energy and solvent consumption as well as in the investment costs. Therefore, in the framework of the SFB 985 in the Subproject A1 the aim was to develop a tandem reaction between a P450 BM3 variant and a copper bis(pyrazolyl)methane complex. Two possible tandem reactions were investigated. In the first tandem reaction a combination of an aromatic hydroxylation of dimethylbenzene to yield dimethylphenol followed by a copper catalyzed C–O cross-coupling to a diphenyl ether was planned. Both reactions could be performed separately, but a combination was not successful. The second approach is the combination of a copper catalyzed benzofuran synthesis from iodophenol and alkyne followed by a hydroxylation of the benzofuran by a P450 BM3 variant. The combination of both reactions could be realized in a stepwise reaction and the addition of EDTA.

Kurzzusammenfassung

Katalytische Reaktionen leisten einen wichtigen Beitrag zur Entwicklung von atomeffizienten Prozessen. Eine wichtige funktionelle Gruppe in biologisch, synthetisch und pharmakologisch relevanten Molekülen sind Amine. Atomeffiziente Methoden zur Einführung von Aminen haben häufig ein terminales Nitren als zentrales Intermediat. Terminale Nitren-Komplexe sind bisher wenig untersucht. Daher wurden in dieser Dissertation verschiedene Bis(pyrazolyl)methan-Liganden synthetisiert, um den Einfluss des Ligandendesigns auf Kupfer-Nitren-Komplexe zu erforschen. Dafür wurde die dritte *N*-Donoreinheit des Liganden variiert, sowohl bezüglich des elektronischen als auch des sterischen Einflusses. Mit Hilfe des Nitrenbildungsreagenz ^sPhINTs konnten sechs neue Kupfer-Nitren-Komplexe bei tiefen Temperaturen synthetisiert werden. Diese Nitren-Komplexe wurden mittels ultrahochauflösender Cryo-ESI Massenspektrometrie, Dichtefunktionaltheorie, UV/Vis-Spektroskopie und NMR-Spektroskopie charakterisiert. Dabei konnte gezeigt werden, dass es sich um terminale Singulett-Nitren-Komplexe handelt, welche mit einer hohen Ausbeute dargestellt werden können. Des Weiteren wurden die thermische Stabilität und die katalytische Aktivität der Nitren-Komplexe untersucht. Durch Variation der dritten *N*-Donoreinheit konnten sowohl sehr stabile als auch sehr aktive Nitren-Komplexe dargestellt werden. Bei Raumtemperatur ist eine C–H-Aminierung von benzyli-schen, alkylischen und aromatischen Substraten und die Aziridinierung von verschiedenen Styrol-Derivaten möglich. Aufgrund der Relevanz von enantiomerenreinen Produkten wurden chirale Precoursorkomplexe in asymmetrischen Katalysereaktionen eingesetzt. Um die Atomeffizienz der katalytischen Reaktionen weiter zu erhöhen, wurden neben ^sPhINTs auch organische Azide als Nitrenbildungsreagenz eingesetzt und erste Erfolge mit Benzoylazid und elektronenreichen Bis(pyrazolyl)methan-Ligand erzielt. Neben Kupfer-Komplexen wurden auch Eisen-Komplexe als mögliche Katalysatoren untersucht. Eine weitere Möglichkeit zur Erhöhung der Umweltverträglichkeit von chemischen Prozessen sind Tandemreaktionen. Dabei werden zwei oder mehr verschiedene Katalysatoren in einem Prozess vereint. Dadurch wird die Aufreinigung des Zwischenprodukts obsolet, was sowohl Energie, Lösungsmittel und Investitionskosten spart. Daher wurde im Rahmen des Sonderforschungsbereichs 985 im Teilprojekt A1 eine Tandemreaktion zwischen einer P450 BM3 Variante und einem Kupfer-Bis(pyrazolyl)methan-Komplex entwickelt. Dafür wurden zwei mögliche Tandemreaktionen untersucht. Die erste Tandemreaktion ist im ersten Schritt die aromatische Hydroxylierung von Dimethylbenzol. Das erhaltene Dimethylphenol wird dann mittels einer kupferkatalysierten C–O Kupplungsreaktion zu einem Diphenylether umgesetzt. In diesem Fall konnten beide Reaktionen getrennt erfolgreich durchgeführt werden, eine Kombination verlief nicht erfolgreich. Die zweite Tandemreaktion umfasst eine kupferkatalysierte Benzofuransynthese aus Iodphenol und einem Alkin und anschließend die enzymatische Hydroxylierung des Benzofurans. Eine funktionierende Tandemreaktion konnte durch die Zugabe von EDTA entwickelt werden.

Danksagung

Zuerst möchte ich mich bei Prof. Dr. Sonja Herres-Pawlis für die interessante und abwechslungsreiche Themenstellung der Dissertation bedanken. Darüber hinaus möchte ich mich für die anregenden Diskussionen und die Unterstützung während meiner Doktorarbeit bedanken, welche zum Gelingen dieser Arbeit beigetragen haben. Dank der gewährten Freiheiten hinsichtlich der Themenstellung konnte ich mein Forschungsinteresse frei entfalten und meine Fähigkeiten und Wissen vertiefen. Außerdem bin ich dankbar für die zahlreichen Eindrücke, welche ich bei Konferenzen sammeln konnte, die diese Arbeit stets mit neuen Ideen und Impulsen durch ungezwungenen Austausch von wissenschaftlichem Fachwissen bereichert haben.

Für die Übernahme des Zweitgutachtens und die Zusammenarbeit im Rahmen des Sonderforschungsbereichs 985 (Teilprojekt A1) möchte ich mich besonders bei Prof. Dr. Ulrich Schwaneberg bedanken.

Darüber hinaus möchte ich mich bei Dr. Alexander Hoffmann bedanken. Zum einen für die Durchführung aller in dieser Arbeit vorkommenden DFT-Rechnungen und zum anderen für die Unterstützung im Laboralltag und bei wissenschaftlichen Fragestellungen. Außerdem möchte ich mich für die Finalisierung der Kristallstrukturen und das Korrekturlesen dieser Arbeit bedanken.

Im Rahmen des Sonderforschungsbereichs 985 bedanke ich mich bei Dr. Stephanie Mertens, Maximilian Nöth und Dr. Islam El-Awaad (Arbeitskreis Prof. Dr. Ulrich Schwaneberg) für die sehr gute Zusammenarbeit im Projekt A1.

Den Angestellten der Institute für anorganische und organische Chemie der RWTH Aachen danke ich für das Durchführen der massenspektrometrischen und NMR-spektroskopischen Messungen. Einen besonderen Dank möchte ich Dr. Gerhard Fink und Brigitte Pütz für die Durchführung der Tieftemperatur-NMR- und Cryo-ESI-Messungen aussprechen. Für die röntgenkristallographischen Messungen möchte ich mich bei Prof. Dr. Ullrich Englert und seinem Arbeitskreis und Henrika Hüppe und Melanie Paul bedanken. Für die Unterstützung bei der Auswertung der EPR-Messungen möchte ich mich bei Regina Schmidt bedanken.

Bei Claudia Nelleßen möchte ich mich für stets freundliche Unterstützung in allen organisations- und bürotechnischen Belangen bedanken.

Bei meinen aktuellen und ehemaligen Kollegen (Alina, Angela, Christian, Dominic, Fabian, Florian, Henrika, Joshua, Julia, Julian, Konstantin, Kristina, Larissa, Lena, Martin, Matze, Melanie, Patricia, Pascal, Regina, Rosalie, Ruth und Thomas) bedanke ich mich für die stets sehr gute Arbeitsatmosphäre und die entstandenen Freundschaften. Besonders möchte ich mich bei meinem Vorgänger Julian Moegling für die hervorragende Einarbeitung und die vielen hilfreichen Ratschläge bedanken. Außerdem möchte ich mich bei Fabian Fink für die gute

Zusammenarbeit im Rahmen des SFB 985 bedanken. Des Weiteren möchte ich mich bei Joshua Heck und Konstantin Kröckert für die vielen anregenden Diskussionen bedanken.

Darüber hinaus bedanke ich mich bei allen meinen Bacheloranden (Benedikt, Dominik, Alexander), Forschungspraktikanten (Kai, Fabian E.), studentischen Hilfskräften (Benedikt, Dominik) und Auszubildenden (Helena) für ihre engagierte und motivierte Mitarbeit.

Weiterhin bedanke ich mich bei meinen Freunden für die stets vorhande moralische Unterstützung.

Abschließend möchte ich mich bei meinen Eltern und meiner Familie für die sehr große Unterstützung während meines gesamten Studiums und der Promotion bedanken.

We each need to find our own inspiration. Sometimes it's not easy.

- Kiki's Delivery Service, Hayao Miyazaki, (1989)

Inspiration unlocks the future.

- The Wind Rises, Hayao Miyazaki (2013)

Abbreviations

APT	Attached Proton Test
ATR	Attenuated Total Reflection
a.u.	atomic units
BDE	Bond Dissociation Energy
calc.	calculated
CamPz	(4 <i>S</i> ,7 <i>R</i>)-7,8,8-trimethyl-4,5,6,7-tetrahydro-2 <i>H</i> -4,7-methanoindazole
COSY	correlation spectroscopy
CSI	Cryo spray ionization
d	doublet (NMR)
DFT	Density Functional Theory
DKR	Dynamic Kinetic Resolution
EDA	Energy Decomposition Analysis
EDTA	Ethylenediaminetetraacetic acid
EPR	Electron Paramagnetic Resonance
equiv.	equivalent
ESI	Electrospray Ionization
GC	Gas Chromatography
HMBC	Heteronuclear Multiple Bond Correlation
HSQC	Heteronuclear Single Quantum Coherence
<i>J</i>	coupling constant (NMR)
m	multiplet (NMR), medium (IR)
MS	Mass Spectrometry
NacNac	1,3-Diketimines
NBO	Natural Bond Orbital
NMR	Nuclear Magnetic Resonance
NOESY	nuclear overhauser enhancement and exchange spectroscopy

^s Ph	<i>meta</i> -(<i>tert</i> -9butylsulfonyl)phenyl
PuIPz	(4R,7S)-7-(<i>tert</i> -butyl)-4-methyl-4,5,6,7-tetrahydro-2 <i>H</i> -indazol
R _f	retardation factor
r.t.	room temperature
s	singlet (NMR), strong (IR)
t	triplet (NMR)
THF	Tetrahydrofuran
Ts	<i>para</i> -toluene sulfonyl
UHR	Ultra High Resolution
UV/Vis	ultraviolet/visible
vs	very strong (IR)
vw	very weak (IR)
w	weak (IR)
XAS	X-ray absorption spectroscopy

List of synthesized ligands, complexes and nitrenes

Compounds marked with an ^x are resynthesized according to literature, compounds marked with a ^D were donated by coworkers and compounds marked with a * were analyzed with single crystal X-ray diffraction.

Ligands

L1^{DX} HC(PhPz) ₂ Py	L12 HC(CamPz) ₂ Py
L2* HC(Ph ₂ Pz) ₂ (4-ClPy)	L13^{DX} HC(Pz) ₂ Melm
L3* HC(Ph ₂ Pz) ₂ Melm	L14^{DX} HC(Me ₂ Pz) ₂ Melm
L4^{DX} HC(Ph ₂ Pz) ₂ Py	L15^x HC(Me ₃ Pz) ₂ Melm
L5^{DX} HC(PhPz) ₂ Qu	L16^{DX} H ₂ C(Pz) ₂
L6^{DX} HC(Et ₂ Pz) ₂ Py	L17^{DX} HC((CF ₃) ₂ Pz) ₂ Py
L7^{DX} HC(^t BuPz) ₂ Py	L18* {HC(^t BuPz) ₂ (4-PPh ₃ Py)}OTf
L8^{DX} HC(^t BuPz) ₂ Melm	L19 HC(^t BuPz) ₂ (4-DPy)
L9 HC(Pz) ₂ (6-CO ₂ MePy)	L20* HC(Ph ₂ Pz) ₂ DMAP
L10 HC(^t BuPz) ₂ (6-CO ₂ MePy)	L21^{DX} MeC(Py) ₂ Bpy
L11 HC(PulPz) ₂ Py	

Complexes

C1* [Cu{HC(PhPz) ₂ Py}(MeCN)]PF ₆	C11* [Cu{HC(PulPz) ₂ Py}(MeCN)]PF ₆
C2* [Cu{HC(Ph ₂ Pz) ₂ (4-ClPy)}(MeCN)]PF ₆	C12 [Cu{HC(CamPz) ₂ Py}(MeCN)]PF ₆
C3 [Cu{HC(Ph ₂ Pz) ₂ Melm}(MeCN)]PF ₆	C13* [Cu ₂ {HC(CamPz) ₂ Py} ₂](PF ₆) ₂
C4* [Cu ₂ {HC(Ph ₂ Pz) ₂ Melm} ₂](PF ₆) ₂	C14^x [CuCl{HC(^t BuPz) ₂ Melm}]
C5 [Cu{HC(Ph ₂ Pz) ₂ Melm}]SbF ₆	C15^x [CuCl ₂ {HC(Pz) ₂ Melm}]
C6^x [Cu{HC(Ph ₂ Pz) ₂ Py}(MeCN)]PF ₆	C16^x [Cu{HC((CF ₃) ₂ Pz) ₂ Py}(MeCN)]PF ₆
C7^x [Cu{HC(^t BuPz) ₂ Py}(MeCN)]PF ₆	C17^x [Cu{HC(^t BuPz) ₂ Py}]SbF ₆
C8^x [Cu{HC(^t BuPz) ₂ Melm}(MeCN)]PF ₆	C18^x [Cu{HC(^t BuPz) ₂ Melm}]SbF ₆
C9* [Cu{HC(Pz) ₂ (6-CO ₂ MePy)}(MeCN)]PF ₆	C19* [Cu{HC(Ph ₂ Pz) ₂ DMAP}(MeCN)]PF ₆
C10* [Cu{HC(^t BuPz) ₂ (6-CO ₂ MePy)}(MeCN)]PF ₆	C20^x [Fe{MeC(Py) ₂ Bpy}(MeCN) ₂]OTf ₂

Tosyl nitrenes

N1PF₆ [Cu{HC(PhPz) ₂ Py}(NTs)]PF ₆	N11PF₆ [Cu{HC(PulPz) ₂ Py}(NTs)]PF ₆
N2PF₆ [Cu{HC(Ph ₂ Pz) ₂ (4-ClPy)}(NTs)]PF ₆	N12PF₆ [Cu{HC(CamPz) ₂ Py}(NTs)]PF ₆
N3PF₆ [Cu{HC(Ph ₂ Pz) ₂ Melm}(NTs)]PF ₆	N19PF₆ [Cu{HC(Ph ₂ Pz) ₂ DMAP}(NTs)]PF ₆
N6PF₆ [Cu{HC(Ph ₂ Pz) ₂ Py}(NTs)]PF ₆	

Table of figures:

Figure 1. Comparison of the protocol of a multistep synthesis and a chemoenzymatic tandem reaction.	1
Figure 2. Visualization of the boat-like six-membered ring (left) and scorpionate coordination motif, exemplified with a copper(I) bis(pyrazolyl)methane complex (right).	3
Figure 3. Scorpionate ligand 6 and its regioisomer 6'	4
Figure 4. Commonly used iminoiodinane ^s PhINTs.	14
Figure 5. Different spin states and bonding situations in copper nitrenes from iminoiodinanes.	15
Figure 6. Dicopper nitrene complex.	16
Figure 7. Elusive copper guanidine nitrene.	17
Figure 8. Terminal copper nitrene complexes and the tautomeric form of 62	18
Figure 9. Structure of a dipyrin triplet copper nitrene complex 64	20
Figure 10. Polynorbene supported copper(I) tris(pyrazolyl)borate complex.	21
Figure 11. Copper stabilized phosphononitrenes.	23
Figure 12. Overview over the different colloid parts and microgel in the center. Adapted from the literature. ^[119]	29
Figure 13. Overview of all ligands used in this thesis sorted by their application. Blue: Copper nitrene chemistry, light blue: chiral copper nitrene chemistry, red: Sonogashira cross coupling reaction, black: oxidation of benzyl alcohols, orange: postmodification of bis(pyrazolyl)methane ligands, green: iron nitrene chemistry.	33
Figure 14. Molecular structure of L2 in the solid-state. Hydrogen atoms were omitted for clarity.	36
Figure 15. Molecular structure of L3 in the solid-state. Hydrogen atoms were omitted for clarity.	37
Figure 16. Molecular structure of {HC(^t BuPz) ₂ (4-PPh ₃ Py)} ⁺ in crystals of L18 in the solid-state. Hydrogen atoms were omitted for clarity.	39
Figure 17. Molecular structure of L20 in the solid-state. Hydrogen atoms were omitted for clarity.	40
Figure 18. Molecular structure of [Cu{HC(PhPz) ₂ Py}(MeCN)] ⁺ in crystals of C1 . Hydrogen atoms were omitted for clarity.	43
Figure 19. Molecular structure of [Cu{HC(Ph ₂ Pz) ₂ (4-ClPy)}(MeCN)] ⁺ in crystals of C2 . Hydrogen atoms were omitted for clarity.	44
Figure 20. Left: Molecular structure of [Cu ₂ {HC(Ph ₂ Pz) ₂ Melm} ₂] ²⁺ in crystals of C4 . Hydrogen atoms were omitted for clarity. Right: Side view on the molecular structure of C4 in the solid-state, substituents on the pyrazolyl are omitted for clarity.	46
Figure 21. Molecular structure of [Cu{HC(Pz) ₂ (6-CO ₂ MePy)}(MeCN)] ⁺ in crystals of C9 . Hydrogen atoms were omitted for clarity.	47
Figure 22. Molecular structure of [Cu{HC(^t BuPz) ₂ (6-CO ₂ MePy)}(MeCN)] ⁺ in crystals of C10 . Hydrogen atoms were omitted for clarity. In the asymmetric unit four molecules of C10 are present with a different torsion angle between the carbonyl group and the pyridinyl group.	49
Figure 23. Molecular structure of [Cu{HC(PuIPz) ₂ Py}(MeCN)] ⁺ in crystals of C11 . Hydrogen atoms were omitted for clarity.	50
Figure 24. Overlay of the ¹ H NMR spectra between 8.8 ppm and 6.8 ppm of L12 (red), C12 (green) and C13 (blue) in dichloromethane- <i>d</i> ₂ . The complex C12 was formed <i>in situ</i> from C13 by the addition of 10 equiv. of acetonitrile.	52
Figure 25. Left: Molecular structure of [Cu ₂ {HC(CamPz) ₂ Py} ₂] ²⁺ in crystals of C13 . Right: Different view on the molecular structure of C13 in the solid-state, substituents on the pyrazolyl are omitted for clarity. Hydrogen atoms were omitted for clarity.	52
Figure 26. Molecular structure of [Cu{HC(Ph ₂ Pz) ₂ DMAP}(MeCN)] ⁺ in crystals of C19 . Hydrogen atoms were omitted for clarity.	54

Figure 27. UV/Vis spectra of N1PF₆ , N2PF₆ , N3PF₆ , N6PF₆ , N11PF₆ , N12PF₆ and N19PF₆ .	58
Figure 28. Overview of different used nitrene generating agents.	59
Figure 29. Comparison of the calculated UV/Vis spectra and experimental UV/Vis spectra of the reaction between C18 and 110 in DCM.	60
Figure 30. UV/Vis spectra of the reaction of C18 and 113 in dichloromethane starting from -80 °C.	61
Figure 31. Comparison of the calculated UV/Vis spectra and the experimental spectra. Experimental spectrum is given in absorption.	62
Figure 32. UV/Vis spectra of the reaction between C19 and 113 in dichloromethane at different temperatures.	63
Figure 33. Reaction between C19 and 113 in dichloromethane at room temperature. Stored at -80 °C for A: 5 min, B: 10 d, C: 31 d.	63
Figure 34. Calculated DFT spectra and transitions.	64
Figure 35. X-band EPR spectra of a sample of the copper nitrene [Cu{HC(Ph ₂ Pz) ₂ DMAP}{NCOPh}] ⁺ and the decayed species [Cu{HC(Ph ₂ Pz) ₂ DMAP}{NHCOPh}] ⁺ in dichloromethane at 77 K.	65
Figure 36. UV/Vis spectra of the titration experiment of C1 against 58 in dichloromethane at -80 °C.	66
Figure 37. UV/Vis spectra of the decay of N1PF₆ in dichloromethane at -42 °C and a concentration of 3.4 mol L ⁻¹ . Inset: Absorption trace at 420 nm.	71
Figure 38. Comparison of the decay reaction in dichloromethane- <i>d</i> ₂ , dichloromethane and chloroform of N2PF₆ .	71
Figure 39. Comparison of the decay reaction of N2PF₆ in dichloromethane with different concentrations. The absorption for the reaction with a concentration of 6.8 mol L ⁻¹ was measured at 450 nm.	72
Figure 40. Connection between the change in the chemical shift of the apical hydrogen atom and the half-life time of the nitrene complexes.	73
Figure 41. Left: Molecular structure of [Cu{HC(PhPz) ₂ Py ₂ }] ²⁺ in crystals of [Cu{HC(PhPz) ₂ Py ₂ }] ₂ (PF ₆) ₂ . Right: different view of the molecular structure of [Cu{HC(PhPz) ₂ Py ₂ }] ²⁺ in the solid-state, substituents on the pyrazolyl are omitted for clarity. Hydrogen atoms were omitted for clarity.	74
Figure 42. Left: Example of both possible coordination motifs of the nitrene moiety (all other possibilities are given in Figure 109 in the Appendix). Shown is the κ^1 -N,O binding mode (left) and the κ^2 -N,O binding mode (right) of N1⁺ in the singlet state. Right: Schematic drawing of both coordination motifs.	75
Figure 43. Orbital representation of the covalent bond between a Cu d orbital and p orbital of the nitrene N atom (a) and the spin density of the nitrene N1⁺ (b), the nitrene N2⁺ (c) and the nitrene N3⁺ (d).	78
Figure 44. UV/Vis spectra of the reaction of C20 in THF and acetone at -80 °C.	88
Figure 45. Reaction between C20 , 58 and triphenylphosphane at -60 °C in dichloromethane.	89
Figure 46. Optimization of the Sonogashira cross-coupling reaction. *: phase transfer catalyst added. Reaction temperature: 80 °C, Reaction time: 12 h (DMF/water); 24 h (DMSO).	93
Figure 47. Novel bis(pyrazolyl)methane ligands.	98
Figure 48. Novel copper(I) acetonitrile bis(pyrazolyl)methane complexes.	99
Figure 49. Novel copper bis(pyrazolyl)methane complexes.	100
Figure 50. Novel copper nitrene complexes.	101
Figure 51. Molecular structures of L2 (top) and L3 (bottom). All hydrogen atoms are omitted for clarity. Displacement ellipsoids represent the 50% of probability level.	173
Figure 52. Molecular structures of L18 (top) and L20 (bottom). All hydrogen atoms are omitted for clarity. Displacement ellipsoids represent the 50% of probability level.	175

Figure 53. Molecular structures of C1 (top) and C2 · 1 DCM (bottom). All hydrogen atoms are omitted for clarity. Displacement ellipsoids represent the 50% of probability level.	177
Figure 54. Molecular structures of C4 · 4 THF (top) and C4 · 4 CHCl₃ (bottom). All hydrogen atoms are omitted for clarity. Displacement ellipsoids represent the 50% of probability level. Numberation is given in Figure 55 on the asymmetric unit for clarity.	179
Figure 55. Molecular structures of the asymmetric unit C4 · 4 THF (top) and C4 · 4 CHCl₃ (bottom). All hydrogen atoms are omitted for clarity. Displacement ellipsoids represent the 50% of probability level.....	180
Figure 56. Molecular structures of C9 (top) and C10 · DCM (bottom). All hydrogen atoms are omitted for clarity. Displacement ellipsoids represent the 50% of probability level.	182
Figure 57. Molecular structures of C11 (top) and C13 (bottom). All hydrogen atoms are omitted for clarity. Displacement ellipsoids represent the 50% of probability level.	184
Figure 58. Molecular structures of C19 · DCM (top) and [Cu{HC(Ph ₂ Pz) ₂ Melm} ₂](PF ₆) (bottom). All hydrogen atoms are omitted for clarity. Displacement ellipsoids represent the 50% of probability level. Numberation is given in Figure 60 on the asymmetric unit for clarity. ...	186
Figure 60. Molecular structure of the asymmetric unit of [Cu{HC(Ph ₂ Pz) ₂ Melm} ₂](PF ₆) ₂ . All hydrogen atoms are omitted for clarity. Displacement ellipsoids represent the 50% of probability level.....	187
Figure 61. Cryo-UHR-ESI mass spectrum (red) of [Cu{HC(Ph ₂ Pz) ₂ Py}{NTs}] ⁺ (N1 ⁺) at 183.15 K and simulation (black) of [Cu{HC(Ph ₂ Pz) ₂ Py}{NTs}-H] ⁺ (top), [Cu{HC(Ph ₂ Pz) ₂ Py}{NTs}] ⁺ (middle) and [Cu{HC(Ph ₂ Pz) ₂ Py}{NTs}+H] ⁺ (bottom).	189
Figure 62. Cryo-UHR-ESI mass spectrum (red) of [Cu{HC(Ph ₂ Pz) ₂ Melm}{NTs}] ⁺ (N3 ⁺) at 183.15 K and simulation (black) of [Cu{HC(Ph ₂ Pz) ₂ Melm}{NTs}-H] ⁺ (top), [Cu{HC(Ph ₂ Pz) ₂ Melm}{NTs}] ⁺ (middle) and [Cu{HC(Ph ₂ Pz) ₂ Melm}{NTs}+H] ⁺ (bottom).	190
Figure 63. Cryo-UHR-ESI mass spectrum (red) of [Cu{HC(Ph ₂ Pz) ₂ (4-ClPy)}{NTs}] ⁺ (N2 ⁺) at 183.15 K and simulation (black) of [Cu{HC(Ph ₂ Pz) ₂ (4-ClPy)}{NTs}+H] ⁺	191
Figure 64. Cryo-UHR-ESI mass spectrum (red) of [Cu{HC(Ph ₂ Pz) ₂ DMAP}{NCOPh}] ⁺ at 183.15 K and simulation (black) of [Cu{HC(Ph ₂ Pz) ₂ DMAP}{NCOPh}+H] ⁺	191
Figure 65. Titration experiment of C1 against ^s PhINTs in DCM at -80 °C. Inset: UV/Vis absorbance of N1PF₆ at 420 nm with equivalents of added ^s PhINTs.....	193
Figure 66. Titration experiment of C2 against ^s PhINTs in DCM at -80 °C. Inset: UV/Vis absorbance of N2PF₆ at 417 nm with equivalents of added ^s PhINTs.....	193
Figure 67. Titration experiment of C3 against ^s PhINTs in DCM at -80 °C. Inset: UV/Vis absorbance of N3PF₆ at 408 nm with equivalents of added ^s PhINTs.....	194
Figure 68. Titration experiment of C11 against ^s PhINTs in DCM at -80 °C. Inset: UV/Vis absorbance of N11PF₆ at 410 nm with equivalents of added ^s PhINTs.....	194
Figure 69. Titration experiment of C12 against ^s PhINTs in DCM at -63 °C. C12 was formed <i>in situ</i> by the addition of 10 equiv. of MeCN to C13 . Inset: UV/Vis absorbance of N12PF₆ at 412 nm with equivalents of added ^s PhINTs.	195
Figure 70. Titration experiment of C19 against ^s PhINTs in DCM at -80 °C. Inset: UV/Vis absorbance of N19PF₆ at 412 nm with equivalents of added ^s PhINTs.....	195
Figure 71. Thermal decay of N1PF₆ at -42 °C in DCM. Inset: absorption trace at 420 nm..	196
Figure 72. Thermal decay of N2PF₆ at -42 °C in DCM. Inset: absorption trace at 417 nm..	196
Figure 73. Absorption trace at 417 nm of the thermal decay of N2PF₆ at -42 °C in DCM- <i>d</i> ₂	197
Figure 74. Absorption trace at 417 nm of the thermal decay of N2PF₆ at -42 °C in DCM. Concentration: 1.7 mM.	197
Figure 75. Absorption trace at 450 nm of the thermal decay of N2PF₆ at -42 °C in DCM. Concentration: 6.8 mM.	198
Figure 76. Formation of N2PF₆ at -60 °C in chloroform. Inset: Absorption trace at 417 nm of the thermal decay of N2PF₆ at -42 °C.....	198
Figure 77. Thermal decay of N3PF₆ at -42 °C in DCM. Inset: absorption trace at 417 nm..	199

Figure 78. Reproduction of the thermal decay of N3PF₆ at -42 °C in DCM, absorption trace at 420 nm.	199
Figure 79. Thermal decay of N11PF₆ at -42 °C in DCM. Inset: absorption trace at 410 nm.	200
Figure 80. Thermal decay of N12PF₆ at -42 °C in DCM. Inset: absorption trace at 410 nm. C12 was formed <i>in situ</i> by the addition of 10 equiv. of MeCN.	200
Figure 81. Thermal decay of N19PF₆ at -42 °C in DCM. Inset: absorption trace at 412 nm.	201
Figure 82. Nitrene reduction in DCM at -80 °C with N1PF₆	201
Figure 83. Nitrene reduction in DCM at -80 °C with N2PF₆	202
Figure 84. Nitrene reduction in DCM at -80 °C with N3PF₆	202
Figure 85. Nitrene reduction in DCM at -80 °C with N11PF₆	203
Figure 86. Nitrene reduction in DCM at -63 °C with N12PF₆ . C12 was formed <i>in situ</i> by the addition of 10 equiv. of MeCN to C13	203
Figure 87. Nitrene reduction in DCM at -80 °C with N19PF₆	204
Figure 88. Nitrene formation test with <i>in situ</i> formed [Cu{HC(QuPz) ₂ Py}(MeCN)]PF ₆ ([CuL5(MeCN)]PF ₆) and ^s PhINTs in DCM at -80 °C.	204
Figure 89. Nitrene formation test with <i>in situ</i> formed [Cu{HC(Et ₂ Pz) ₂ Py}(MeCN)]PF ₆ ([CuL6(MeCN)]PF ₆) and ^s PhINTs in DCM at -80 °C.	205
Figure 90. Nitrene formation test with [Cu{HC(Ph ₂ Pz) ₂ (Py)}(MeCN)]PF ₆ (C4) and azobenzene in DCM at -80 °C.	205
Figure 91. Nitrene formation test with [Cu{HC(Ph ₂ Pz) ₂ (Py)}(MeCN)]PF ₆ (C4) and O-(4-nitrobenzoyl)hydroxylamine triflate in DCM at -80 °C.	206
Figure 92. Nitrene formation test with [Cu{HC(^t BuPz) ₂ (6-CO ₂ MePy)}(MeCN)]PF ₆ (C10) and ^s PhINTs in DCM at -80 °C.	206
Figure 93. Nitrene formation test with [Cu{HC(^t BuPz) ₂ Py}]SbF ₆ (C18) and bis(trifluoromethyl)phenyl azide in DCM at room temperature. Due to the formation of a precipitate a baseline shift occurs, which was corrected. Reaction time: 20 h.	207
Figure 94. Nitrene formation test with [Cu{HC(^t BuPz) ₂ Py}]SbF ₆ (C17) and bis(trifluoromethyl)phenyl azide in DCM starting from -42 °C ending at room temperature. Concentration: 3.4 mmol/L.	207
Figure 95. Nitrene formation test with [Cu{HC(^t BuPz) ₂ Melm}]SbF ₆ (C18) and adamantyl azide in DCM at room temperature. Reaction time: 72 h.	208
Figure 96. Nitrene formation test with [Cu{HC(^t BuPz) ₂ Melm}]SbF ₆ (C18) and mesityl azide in DCM at room temperature. Concentration: 5 mmol/L.	208
Figure 97. Nitrene formation test with [Cu{HC(^t BuPz) ₂ Py}]SbF ₆ (C18) and bis(trifluoromethyl)phenyl azide in DCM at room temperature. Reaction time: 20 h.	209
Figure 98. Nitrene formation test with [Fe{MeC(Py) ₂ Bpy}(MeCN) ₂]OTf ₂ (C20) and bis(trifluoromethyl)phenyl azide in DCM at room temperature. After the reaction with bis(trifluoromethyl)phenyl azide a precipitate form, which can be solved by addition of 2 mL of MeCN. Reaction time: 20 h.	209
Figure 99. Nitrene formation test with [Fe{MeC(Py) ₂ Bpy}(MeCN) ₂]OTf ₂ (C20) and ^s PhINTs in DCM.	210
Figure 100. Nitrene formation test with [Fe{MeC(Py) ₂ Bpy}(MeCN) ₂](OTf) ₂ (C20) and O-(4-Nitrobenzoyl)hydroxylamine triflate in DCM at room temperature. Due to the low solubility of O-(4-Nitrobenzoyl)hydroxylamine triflate in DCM, it was added in THF.	210
Figure 101. Nitrene formation test with [Fe{MeC(Py) ₂ Bpy}(MeCN) ₂](OTf) ₂ (C20) and O-(4-Nitrobenzoyl)hydroxylamine triflate in THF at -80 °C. Due to the low solubility of C20 in THF, C20 was added in DCM.	211
Figure 102. Nitrene formation test with [Fe{MeC(Py) ₂ Bpy}(MeCN) ₂]OTf ₂ (C20) and O-(4-Nitrobenzoyl)hydroxylamine triflate in acetone at -80 °C.	211

Figure 103. X-Band EPR spectrum of a sample of the reaction between C19 and 113 . (simulation parameters: $g_{\parallel} = 2.10$, $g_{\perp} = 2.33$, $A_{\parallel}(\text{Cu}) = 32$ MHz, $A_{\perp}(\text{Cu}) = 522$ MHz, $A_{\parallel}(\text{N}) = 41$ MHz, $A_{\perp}(\text{N}) = 41$ MHz, $A_{\parallel}(\text{H}) = 9$ MHz, $A_{\perp}(\text{H}) = 10$ MHz, Gaussian line shape linewidth: 9.3 mT).	212
Figure 104. X-Band EPR spectrum of a decayed sample of the reaction between C19 and 113 . (simulation parameters: $g_{\parallel} = 2.09$, $g_{\perp} = 2.31$, $A_{\parallel}(\text{Cu}) = 41$ MHz, $A_{\perp}(\text{Cu}) = 490$ MHz, $A_{\parallel}(\text{N}) = 44$ MHz, $A_{\perp}(\text{N}) = 49$ MHz, $A_{\parallel}(\text{H}) = 23$ MHz, $A_{\perp}(\text{H}) = 25$ MHz, Gaussian line shape linewidth: 6.0 mT).	212
Figure 105. X-Band EPR spectrum of a sample of N11PF₆ . (simulation parameters: $g_{\parallel} = 2.11$, $g_{\perp} = 2.32$, $A_{\parallel}(\text{Cu}) = 36$ MHz, $A_{\perp}(\text{Cu}) = 479$ MHz, $A_{\parallel}(\text{N}) = 31$ MHz, $A_{\perp}(\text{N}) = 97$ MHz, Gaussian line shape linewidth: 9.0 mT).	213
Figure 106. X-Band EPR spectrum of a decayed sample of N11PF₆ . (simulation parameters: $g_{\parallel} = 2.10$, $g_{\perp} = 2.34$, $A_{\parallel}(\text{Cu}) = 29$ MHz, $A_{\perp}(\text{Cu}) = 428$ MHz, $A_{\parallel}(\text{N}) = 31$ MHz, $A_{\perp}(\text{N}) = 54$ MHz, $A_{\parallel}(\text{H}) = 11$ MHz, $A_{\perp}(\text{H}) = 73$ MHz, Gaussian line shape linewidth: 7.0 mT).	213
Figure 107. X-Band EPR spectrum of a sample of N12PF₆ . (simulation parameters: $g_{\parallel} = 2.09$, $g_{\perp} = 2.32$, $A_{\parallel}(\text{Cu}) = 21$ MHz, $A_{\perp}(\text{Cu}) = 501$ MHz, $A_{\parallel}(\text{N}) = 4$ MHz, $A_{\perp}(\text{N}) = 52$ MHz, Gaussian line shape linewidth: 5.9 mT).	214
Figure 108. X-Band EPR spectrum of a decayed sample of N12PF₆ . (simulation parameters: $g_{\parallel} = 2.10$, $g_{\perp} = 2.32$, $A_{\parallel}(\text{Cu}) = 54$ MHz, $A_{\perp}(\text{Cu}) = 515$ MHz, $A_{\parallel}(\text{N}) = 31$ MHz, $A_{\perp}(\text{N}) = 39$ MHz, $A_{\parallel}(\text{H}) = 37$ MHz, $A_{\perp}(\text{H}) = 22$ MHz, Gaussian line shape linewidth: 5.5 mT).	214
Figure 109. Calculated UV/Vis spectra of $[\text{CuL19}(\text{NCOPh})]^+$ in dichloromethane.	215
Figure 110. κ^1 - and κ^2 -coordination motifs of the nitrene moieties in the copper nitrenes.	216

Table of schemes:

Scheme 1. Synthesis of tris(pyrazolyl)methane by Hückel and Bretschneider.	3
Scheme 2. Synthesis of tris(pyrazolyl)borate by Trofimenko.	3
Scheme 3. Optimized synthesis of poly(pyrazolyl)methanes.	4
Scheme 4. Synthesis of polar scorpionate ligands.	5
Scheme 5. Synthesis of bis(pyrazolyl)methane ligands by Thé and Peterson.	6
Scheme 6. Mechanism of the Peterson rearrangement.	6
Scheme 7. Syntheses of heteroscorpionate ligands from bis(pyrazolyl)methane.	7
Scheme 8. Enantioselective cyclopropanation of styrene.	8
Scheme 9. Copper(II) scorpionate catalyzed Sonogashira coupling.	9
Scheme 10. Tyrosinase-like oxidation with copper heteroscorpionate ligands.	10
Scheme 11. Copper-catalyzed selective oxidation of styrene to benzaldehyde.	11
Scheme 12. Copper(II) catalyzed Henry reaction.	12
Scheme 13. Mechanism of the benzofuran synthesis from a halidophenol and an alkyne.	12
Scheme 14. C–O coupling reaction between an arylhalide and an alcohol.	13
Scheme 15. Overview of nitrene basics.	14
Scheme 16. Mechanism of the insertion of a metal bound nitrene into a C–H bond.	16
Scheme 17. Mechanistic pathways of the copper(I) catalyzed aziridination.	18
Scheme 18. Reaction of alkynes with copper nitrenes.	22
Scheme 19. Catalytic C–H amination of heterocycles.	22
Scheme 20. Synthesis of sulfoximines from sulfoxides.	24
Scheme 21. Formation of an iron imido complex at low temperature.	25
Scheme 22. Formation of an iron(V) species and its catalytic activity.	25
Scheme 23. Reaction scheme of chemoenzymatic cascade reaction of a nitroaldol-DKR-esterification and scheme of a pore of the used MOF (Co^{2+} : pink, Pd NC and CalA).	27
Scheme 24. Stepwise tandem reaction, combining an aldol reaction and a subsequent enzymatic reduction using alcohol dehydrogenase (ADH).	27

Scheme 25. Compartmentalization of a Wacker oxidation and an enzymatic reduction.	28
Scheme 26. Ligand synthesized according to a modified Peterson rearrangement. The syntheses of the blue marked ligands were developed in this thesis. Ligands L1 ^[29] , L4 ^[137] , L5 ^[29] , L6 ^[137] , L7 ^[29] , L8 ^[40] , L13 ^[138] and L14 ^[139] were resynthesized according to literature. The synthesis of L15 ^[140] was modified from the literature.	35
Scheme 27. Overview of the synthesis of L18 and further post-modifications of L18	38
Scheme 28. Synthesis of L20 starting form L2	40
Scheme 29. Overview of the stable generated copper nitrene complexes.	57
Scheme 30. Formation of a terminal nitrene and a bridged nitrene complex.	66
Scheme 31. Proposed decay mechanism for bis(pyrazolyl)methane copper nitrene complexes.	67
Scheme 32. Nitrene yield determination by the reduction with ferrocene.	68
Scheme 33. Formation and decay of a copper nitrene complex.	70
Scheme 34. C–H amination of benzylic substrates.	80
Scheme 35. C–H amination of cyclohexane.	81
Scheme 36. C–H amination of aromatic substrates.	82
Scheme 37. Styrene aziridination with bis(pyrazolyl)methane copper complexes as catalyst.	83
Scheme 38. Aziridination of internal double bonds with bis(pyrazolyl)methane copper complexes as catalyst.	84
Scheme 39. Alkyne rearrangement into sulfonamides and isothiazoles.	85
Scheme 40. Planned iron nitrene generation.	87
Scheme 41. Planed cascade reaction. First step aromatic hydroxylation of dimethylbenzene followed by C–O cross-coupling in the second reaction.	90
Scheme 42. Planed cascade reaction. First step: Sonogashira coupling of iodophenol with an alkyne to a benzofuran; second step: hydroxylation of the benzofuran.	91
Scheme 43. Accomplished cascade reaction.	92
Scheme 44. Sonogashira cross-coupling reaction.	92
Scheme 45. Synthesis of copper loaded microgels.	95
Scheme 46. Oxidation of aliphatic alcohols.	96
Scheme 47. Henry reaction between nitrobenzyl aldehyde and nitromethane.	96

Table of tables:

Table 1. Selected bond lengths [Å] and angles [°] for L2	36
Table 2. Selected bond lengths [Å] and angles [°] for L3	37
Table 3. Selected bond lengths [Å] and angles [°] for L18	39
Table 4. Selected bond lengths [Å] and angles [°] for L20	41
Table 5. Selected bond lengths [Å] and angles [°] for C1	43
Table 6. Selected bond lengths [Å] and angles [°] for C2	45
Table 7. Selected bond lengths [Å] and angles [°] for C4	46
Table 8. Selected bond lengths, atom distance [Å] and angles [°] for C9	48
Table 9. Selected bond lengths, atom distance [Å] and angles [°] for C10	49
Table 10. Selected bond lengths [Å] and angles [°] for C11	51
Table 11. Selected bond lengths [Å] and angles [°] for C13	53
Table 12. Selected bond lengths [Å] and angles [°] for C19	54
Table 13. Comparison of selected bond lengths [Å] of C1 , C2 , C4 , C5 and C19	55
Table 14. Left: Calculated spin states and relative energies for the copper nitrene [Cu L19 (NCOPh)] ⁺ in the κ^1 - and κ^2 -mode. The energy is stated relative to the lowest spin state of the corresponding copper nitrene which is set to 0.0 kcal/mol ⁻¹ . Right: Key geometric parameters for the singlet and triplet state of copper nitrene [Cu L19 (NCOPh)] ⁺ in the κ^1 - and	

κ^2 -mode (Gaussian16; TPSSh/def2-TZVP and PCM solvent model for dichloromethane and the empirical dispersion correction with Becke-Johnson damping).	65
Table 15. Correlation of the half-life time and the difference of the chemical shift of the apical hydrogen ($\Delta\delta$ (H_{apical}) = $\delta_{\text{precursor}}(H_{\text{apical}})$ - $\delta_{\text{nitrene}}(H_{\text{apical}})$) for the nitrenes N1PF₆ – N3PF₆ , N6PF₆ and N19PF₆	73
Table 16. Selected bond lengths [Å] and angles [°] for [Cu{HC(PhPz) ₂ Py} ₂](PF ₆) ₂	74
Table 17. Key geometric parameters for the singlet and triplet state of copper nitrenes N1PF₆ – N3PF₆ in the κ^1 - and κ^2 -mode (Gaussian16; TPSSh/def2-TZVP and PCM solvent model for dichloromethane and the empirical dispersion correction with Becke-Johnson damping).	76
Table 18. Calculated spin states and relative energies for the copper nitrenes N1⁺ – N3⁺ in the κ^1 - and κ^2 -mode. The energy is stated relative to the lowest spin state of the corresponding copper nitrene which is set to 0.0 kcal/mol ⁻¹	76
Table 19. NBO charges (in e ⁻ units) and charge transfer energies (in kcal/mol) for selected atoms for the singlet state of copper nitrenes N1⁺ – N3⁺ and N6⁺ in the κ^2 -mode (NBO6.0. TPSSh/def2-TZVP and PCM solvent model for dichloromethane and the empirical dispersion correction with Becke-Johnson damping).	77
Table 20. Form and occupancy of the lone pairs of the nitrene N donor atom and of the bond of the copper ion and the N donor atom of the nitrene for the singlet state of copper nitrenes N1⁺ – N3⁺ and N6⁺ in the κ^2 -mode (NBO analysis with NBO6.0. TPSSh/def2-TZVP and PCM solvent model for dichloromethane and the empirical dispersion correction with Becke-Johnson damping).	78
Table 21. Fragmentation of N1⁺ for EDA and E _{orb}	79
Table 22. Yields* ([%]) of the catalytic C–H amination reactions of benzylic substrates.	80
Table 23. Yields* ([%]) of the catalytic C–H amination reactions of aliphatic and aromatic substrates.	82
Table 24. Yield* ([%]) of the aziridination of 4-substituted styrene derivatives. The enantiomeric excess for the reaction with C12 is given in the bracket.	83
Table 25. Yield* ([%]) of the aziridination of β -substituted styrene derivatives. The enantiomeric excess for the reaction with C12 and <i>trans</i> -substituted substrate is given in the bracket. For the <i>cis</i> -substituted substrate, the <i>cis/trans</i> -ratio is given in the brackets.	85
Table 26. Comparison of the yields* ([%]) for the alkyne rearrangement and the product distribution (A:B).	86
Table 27. Substrate scope of the Sonogashira cross-coupling reaction.	94
Table 28. Yields* of the performed Henry reaction.	97
Table 29. Commercial chemicals.	104
Table 30. Solvent residual signal and solvent signal of the used solvents. ^[148]	108
Table 31. Values of the effective magnetic moment μ_{eff} and the spin state for N1⁺ – N3⁺ , N6⁺ and N19⁺ . The respective calculated spin only value for μ_{eff} is 0 μ_{B} for a singlet, 1.73 μ_{B} for a doublet and 2.83 μ_{B} for a triplet spin state.	109
Table 32. Oxidation potentials and half-cell potentials of the measured complexes.	112
Table 33. Overview of nitrene formation tests.	139
Table 34. Measured nitrene yields.	141
Table 35. Measured half-life time at -42 °C.	141
Table 36. C–H amination of cyclohexane.	145
Table 37. C–H amination of toluene.	145
Table 38. C–H amination of toluene with benzoylazide.	146
Table 39. C–H amination ethylbenzene.	147
Table 40. C–H amination of ethylbenzene with benzoylazide.	148
Table 41. C–H amination of bibenzyl, neopentyl benzene and benzyl bromide with ^s PhINTs.	149
Table 42. C–H amination of benzene.	150

Table 43. C–H amination of naphthalene, anthracene, quinoline chlorobenzene and bromobenzene.	151
Table 44. Overview of styrene aziridination.	152
Table 45. Overview of aziridination using benzoylazide.	154
Table 46. Overview of alkyne rearrangement.	155
Table 47. Optimization of benzofuran synthesis.	156
Table 48. Oxidation of benzylic alcohols.	161
Table 49. Henry reaction.	162
Table 50. Oxidation of aliphatic alcohol.	163
Table 51. Crystallographic data of L2 and L3	174
Table 52. Crystallographic data of L18 and L20	176
Table 53. Crystallographic data of C1 and C2	178
Table 54. Crystallographic data of C4 · 4 CHCl₃ and C4 · 4 THF	181
Table 55. Crystallographic data of C9 and C10 · DCM . In C9 it was not possible to model the disordered solvent molecule CH₂Cl₂ in an adequate manner, and the data set was treated with the SQUEEZE routine as implemented in PLATON ^{[211],[212]}	183
Table 56. Crystallographic data of C11 and C13 . In C13 it was not possible to model the two disordered solvent molecule pentane in an adequate manner, and the data set was treated with the SQUEEZE routine as implemented in PLATON ^{[211],[212]}	185
Table 57. Crystallographic data of C19 · DCM and [Cu{HC(Ph₂Pz)₂Melm}₂](PF₆)₂ . In [Cu{HC(Ph₂Pz)₂Melm}₂](PF₆)₂ it was not possible to model the three disordered solvent molecule CD₂Cl₂ in an adequate manner, and the data set was treated with the SQUEEZE routine as implemented in PLATON ^{[211],[212]}	188
Table 58. Key geometric parameters of the complexes C1 – C4 and C6 (Gaussian16; TPSSh/def2-TZVP and PCM solvent model for dichloromethane and the empirical dispersion correction with Becke-Johnson damping).	215
Table 59. NBO charges (in e [−] units) and charge transfer energies (in kcal/mol) for selected atoms (<i>italic</i>) for C1 – C4 (NBO6.0. TPSSh/def2-TZVP and PCM solvent model for dichloromethane and the empirical dispersion correction with Becke-Johnson damping). ..	215

Table of contents

1. Localization of this thesis in the context of SFB 985	1
2. Introduction	2
2.1 Scorpionate ligands	2
2.1.1 Heteroscorpionate ligands	5
2.2 Copper poly(pyrazolyl)methane complexes as catalysts in organic transformations	7
2.2.1 Enantioselective cyclopropanation	8
2.2.2 Sonogashira coupling	9
2.2.3 Tyrosinase model systems.....	9
2.2.4 Oxidation of styrene	10
2.2.5 Stereoselective Henry reaction	11
2.3 Copper-mediated cross-coupling reactions	12
2.3.1 Benzofuran synthesis.....	12
2.3.2 C–O coupling reaction	13
2.4 Nitrenes	13
2.4.1 Copper nitrenes	15
2.4.2 Iron nitrenes.....	23
2.5 Chemoenzymatic tandem reactions	26
2.6 Microgels	28
3. Objectives and Contents.....	30
3.1. Objectives.....	30
3.2. Contents	31
4. Results and discussion	33
4.1 Ligand synthesis.....	33
4.1.1 Ligand synthesis by a Peterson rearrangement	34
4.1.2 Post-modification of bis(pyrazolyl)methane ligands.....	37
4.2 Synthesis and characterization of the complexes	42
4.2.1 Synthesis and characterization of copper(I) complexes of L1	42
4.2.2 Synthesis and characterization of copper(I) complexes of L2	44
4.2.3 Synthesis and characterization of copper(I) complexes of L3	45
4.2.4 Synthesis and characterization of copper(I) complexes of L9	47
4.2.5 Synthesis and characterization of copper(I) complexes of L10	48
4.2.6 Synthesis and characterization of copper(I) complexes of L11	50
4.2.7 Synthesis and characterization of copper(I) complexes of L12	51
4.2.8 Synthesis and characterization of copper(I) complexes of L20	53
4.2.9 Comparison of aromatic substituted copper(I) complexes	54
4.3 Copper nitrene chemistry.....	56
4.3.1 Variation of the ligand design.....	56

4.3.2 Variation of the nitrene generating agent	58
4.3.3 Characterization of stable tosyl copper nitrene complexes.....	66
4.3.4 DFT calculations	75
4.3.5 C–H amination	79
4.3.6 Aziridination	82
4.3.7 Alkyne rearrangement.....	85
4.4 Iron nitrene chemistry	87
4.5 Development of a chemoenzymatic cascade reaction	90
4.5.1 Combination of hydroxylation and C–O cross-coupling	90
4.5.2 Combination of Sonogashira cross-coupling and hydroxylation	91
4.6 Preliminary work on copper loaded microgels.....	95
4.6.1 Oxidation reaction.....	96
4.6.2 Henry reaction	96
5. Summary and Outlook.....	98
5.1 Summary.....	98
5.2 Outlook.....	102
6. Experimental part	104
6.1 General.....	104
6.2 Chemicals and solvents.....	104
6.3 Analytics.....	108
6.3.1 NMR spectroscopy.....	108
6.3.2 Evans NMR.....	108
6.3.3 UV/Vis spectroscopy.....	109
6.3.4 ESI mass spectrometry	110
6.3.5 Cryo ESI mass spectrometry	110
6.3.6 Single crystal x-ray diffractometry	110
6.3.7 IR spectroscopy	111
6.3.8 Column chromatography.....	111
6.3.9 Thin layer chromatography	111
6.3.10 Gas chromatography	111
6.3.11 Cyclic voltammetry.....	112
6.3.12 EPR spectroscopy	112
6.4.13 CHN Elemental analysis	113
6.4 Computational details	113
6.5 Synthesis of starting material.....	114
6.5.1 Synthesis approach of 1,3-bis(2,4,5-trichlorophenyl)propane-1,3-dione.....	114
6.6 Reagent synthesis	114
6.6.1 Synthesis approach of <i>N,N</i> -diisopropylprop-2-yn-1-amine	114

6.6.2 Synthesis approach of <i>N</i> -isopropylprop-2-yn-1-amine.....	115
6.6.3 Synthesis approach of <i>N,N</i> -diphenylprop-2-yn-1-amine	115
6.6.4 Synthesis approach of <i>N</i> -phenylprop-2-yn-1-amine	115
6.7 Ligand synthesis.....	116
6.7.1 Synthesis of HC(Ph ₂ Pz) ₂ (4-ClPy) (L2)	116
6.7.2 Synthesis of HC(Ph ₂ Pz) ₂ Melm (L3).....	117
6.7.3 Synthesis of HC(Pz) ₂ (6-CO ₂ MePy) (L9).....	118
6.7.4 Synthesis of HC(^t BuPz) ₂ (6-CO ₂ MePy) (L10)	119
6.7.5 Synthesis of HC(PulPz) ₂ Py (L11).....	120
6.7.6 Synthesis of HC(CamPz) ₂ Py (L12)	121
6.7.7 Resynthesis of HC(Me ₃ Pz) ₂ Melm (L15)	122
6.7.8 Synthesis of (HC(^t BuPz) ₂ (4-PPh ₃ Py))OTf (L18)	123
6.7.9 Synthesis of HC(^t BuPz) ₂ (4-DPy) (L19).....	124
6.7.10 Synthesis of HC(Ph ₂ Pz) ₂ DMAP (L20)	124
6.7.11 Synthesis approach of HC(^t BuPz) ₂ DMAP.....	125
6.7.12 Synthesis approach of MeC(CamPz) ₂ Py.....	126
6.8 Complex synthesis.....	127
6.8.1 Synthesis of [Cu{HC(PhPz) ₂ Py}(MeCN)]PF ₆ (C1)	127
6.8.2 Synthesis of [Cu{HC(Ph ₂ Pz) ₂ (4-ClPy)}(MeCN)]PF ₆ (C2)	128
6.8.3 Synthesis of [Cu{HC(Ph ₂ Pz) ₂ Melm}(MeCN)]PF ₆ (C3).....	129
6.8.4 Synthesis of [Cu ₂ {HC(Ph ₂ Pz) ₂ Melm}] ₂ (PF ₆) ₂ (C4).....	129
6.8.5 <i>In situ</i> synthesis of [Cu{HC(Ph ₂ Pz) ₂ Melm}]SbF ₆ (C5).....	130
6.8.6 Synthesis of [Cu{HC(Pz) ₂ (6-CO ₂ MePy)}(MeCN)]PF ₆ (C9).....	131
6.8.7 Synthesis of [Cu{HC(^t BuPz) ₂ (6-CO ₂ MePy)}(MeCN)]PF ₆ (C10)	132
6.8.8 Synthesis of [Cu{HC(PulPz) ₂ Py}(MeCN)]PF ₆ (C11).....	132
6.8.9 Synthesis of [Cu{HC(CamPz) ₂ Py}(MeCN)]PF ₆ (C12)	133
6.8.10 Synthesis of [Cu ₂ {HC(CamPz) ₂ Py}] ₂ (PF ₆) ₂ (C13).....	134
6.8.11 Synthesis of [Cu{HC(Ph ₂ Pz) ₂ DMAP}(MeCN)]PF ₆ (C19).....	136
6.8.12 Synthesis approach of [Cu{C(^t BuPz) ₂ Py}]	137
6.8.13 Synthesis approach of [Cu{HC(^t BuPz) ₂ Py}(C ₆ Me ₆)]PF ₆	138
6.9 Nitrene analytic.....	139
6.9.1 Nitrene formation test.....	139
6.9.2 Titration against ^s PhINTs	140
6.9.3 Nitrene yield determination	140
6.9.4 Thermal stability.....	141
6.9.5 Preparation of Cryo ESI MS sample	142
6.9.6 Preparation of low temperature Evans' NMR	143
6.9.7 Preparation of low temperature NMR.....	143

6.9.8 Preparation of EPR samples	143
6.10 Catalytic reactions	144
6.10.1 C–H amination	144
6.10.2 Aziridination	152
6.10.3 Alkyne rearrangement.....	155
6.10.4 Sonogashira coupling reaction	155
6.10.5 C–O coupling reaction	160
6.10.6 Preliminary work on copper loaded microgel.....	161
7. Literature	164
8. Appendix	173
8.1 Crystallographic data	173
8.2 Cryo-ESI-MS	189
8.3 Additional analytic of $[\text{Cu}\{\text{HC}(\text{Ph}_2\text{Pz})_2\text{Py}\}(\text{MeCN})]\text{PF}_6$	192
8.4 UV/Vis Spectra	193
8.4.1 Titration.....	193
8.4.2. Decay	196
8.4.3 Nitrene reduction with ferrocene	201
8.4.4 Nitrene formation test.....	204
8.5 EPR spectroscopy	212
8.6 Key parameters determined by DFT calculation	215

1. Localization of this thesis in the context of SFB 985

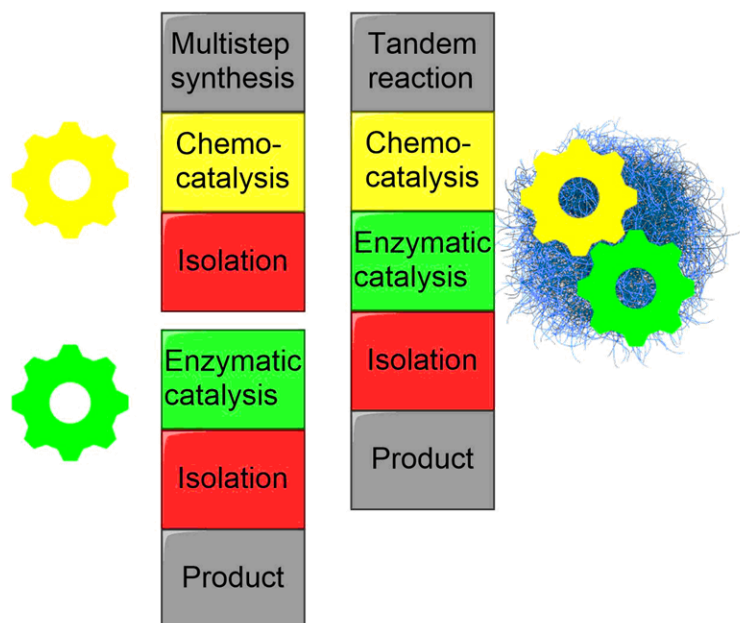


Figure 1. Comparison of the protocol of a multistep synthesis and a chemoenzymatic tandem reaction.

This thesis is located in the subproject A1 '*Microgel engineered enzymatic and chemical reactions – towards tandem catalysts*' of the SFB 985 '*Functional Microgels and Microgel Systems*'. Microgels are highly functional macromolecules and have many applications, including acting as mediator, protector and host of catalysts. The incorporation of enzymes and chemical catalysts, in this case bis(pyrazolyl)methane copper complexes, and their combina-

tion in chemoenzymatic tandem catalysis is the central research aim of the subproject A1. The microgel acts as a protector and will allow unprecedented environments for both catalysts. This leads to coexisting reaction conditions in a reaction mixture, which are otherwise orthogonal (Figure 1). The further development of microgel supported chemoenzymatic tandem reactions leads to more ecological and economical processes because the intermediate does not have to be isolated and the microgel supported catalyst should be easily recyclable.

The main part of this thesis is the development of copper bis(pyrazolyl)methane catalyzed C–N coupling reactions and the investigation of the copper nitrene intermediate. To achieve this, stable copper nitrene complexes are synthesized and analyzed by various methods, including UV/Vis spectroscopy, cryo-ESI-MS spectrometry and DFT calculations. The developed C–N coupling reactions can yield products with synthetically, biologically or pharmaceutically relevance. For these coupling reactions a broad range of possible nitrene generating agents were applied. Therefore, these reactions can be used as an interesting building block for further tandem reactions. Furthermore, microgel supported tandem reactions including C–N cross coupling reaction are a promising research field in the future. Further this thesis focuses on the development of a chemoenzymatic tandem reaction between a hydroxylation catalyzed by a P450 BM3 variant and a C–O or C–C coupling reaction catalyzed by a copper bis(pyrazolyl)methane complex. This tandem reaction should be enabled by incorporation of the enzyme or the copper complex into a microgel.

2. Introduction

In the broad field of complex compounds^[1] this thesis deals with copper complexes and their application as catalyst in different cross coupling reactions. Furthermore, the development of tandem reactions is part of this work. The reactions which are in the centre of this thesis are copper nitrene mediated C–N coupling reactions. These copper nitrene complexes can be stabilized with ligands from the bis(pyrazolyl)methane family which are part of the scorpionate family (chapter 2.1). In chapter 2.2 important catalytic applications of heteroscorpionate copper complexes are highlighted. Additionally, in chapter 2.3 some copper-catalyzed reactions with ligands which are not derived from the scorpionate family are discussed. The focus of these examples lies on catalytic reactions which are important for this thesis. Nitrene and metal nitrene complexes will be discussed in chapter 2.4, beside copper nitrene complexes also iron nitrene complexes are presented. In the last two parts of the introduction general information about tandem reactions (chapter 2.5) and microgels (chapter 2.6) are given.

2.1 Scorpionate ligands

Scorpionate ligands are defined as tridentate ligands, which have a facial coordination motif. In this coordination motif two pyrazolyl units form a boat-like six membered ring (RNNMNN, Figure 2, left). The name of the ligand family is inspired by its similarity to scorpions. Two pyrazolyl units bind to the central metal like the scorpion's claw, while the third donor binds from above like the tail of the scorpion (Figure 2, right). When the third donor is a pyrazolyl unit, the scorpionate is classified as a homoscorpionate, otherwise as heteroscorpionate.^{[2],[3]}

The definition originally applies to anionic poly(pyrazolyl)borate ligands by Trofimenko^{[4],[5]}, but it was extended to neutral poly(pyrazolyl)methane^[6] ligands. There is a huge variety of literature known pyrazoles^[7] and the bridging unit (R, Figure 2, left) of the scorpionate can be varied not only between CH or BH, but also arsenic^[8], silicon^[9] or phosphorus^[10] are possible. In addition, it is also possible to synthesize non-pyrazolyl based scorpionate ligands, which can be based on other various heterocycles, such as pyridine^[11]. Therefore, a huge number of structures of scorpionate ligands can be designed. Due to the large diversity of the scorpionate ligand family, in the following part, only poly(pyrazolyl)borates and poly(pyrazolyl)methanes are discussed.

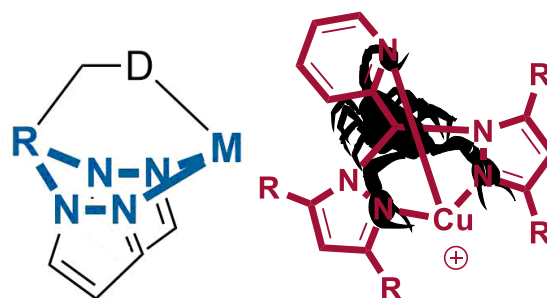
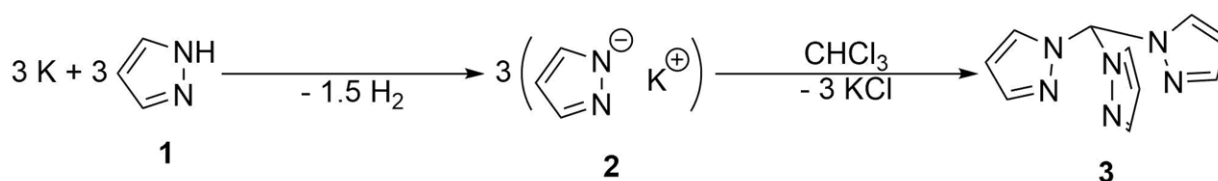


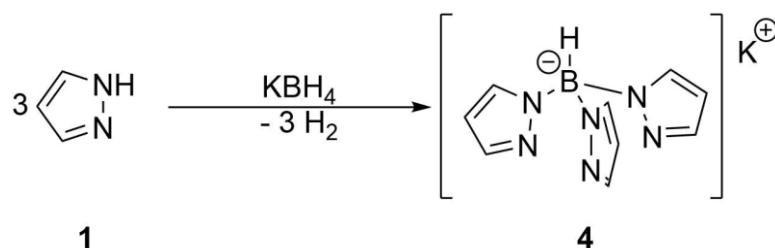
Figure 2. Visualization of the boat-like six-membered ring (left) and scorpionate coordination motif, exemplified with a copper(I) bis(pyrazolyl)methane complex (right).

In 1937, Hückel and Bretschneider synthesized tris(pyrazolyl)methane (**3**) from pyrazole (**1**), potassium and chloroform (Scheme 1). In the first step, pyrazole was deprotonated by potassium and the potassium pyrazolate (**2**) was isolated. In the second step, **2** was reacted with chloroform to yield **3**. The purification of **3** needed numerous steps of recrystallization and sublimation.^[12] Due to the challenging and time-consuming synthesis of poly(pyrazolyl)methane ligands, not many applications for these had been developed, until further synthesis routes were developed.



Scheme 1. Synthesis of tris(pyrazolyl)methane by Hückel and Bretschneider.

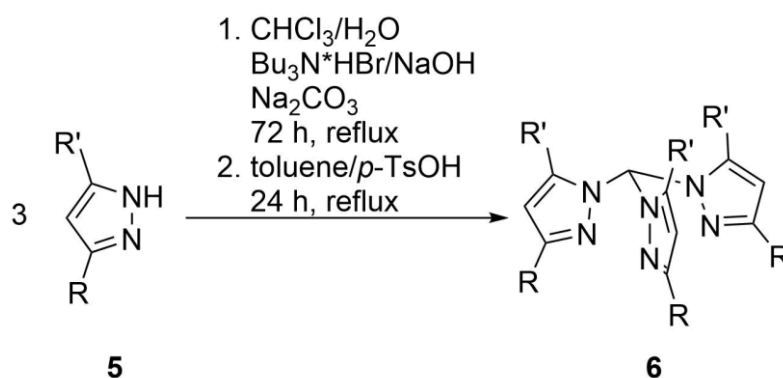
In 1966 Trofimenko synthesized tris(pyrazolyl)borate (**4**) from pyrazole (**1**) and potassium borohydride at high temperatures (Scheme 2). Because potassium borohydride also works as a base no additional base is needed. It also could be shown that most transition metal complexes with tris(pyrazolyl)borate ligands are stable against air and moisture, while the ligand itself is sensitive against moisture.^[13] In the following year, the synthesis was further investigated and it was reported that bis(pyrazolyl)borate can be synthesized at temperatures around 100 °C in DMF, while tris(pyrazolyl)borate are obtained in pyrazole melts at about 200 °C.^{[5],[14]}



Scheme 2. Synthesis of tris(pyrazolyl)borate by Trofimenko.

As this first generation of scorpionate ligands tends to the formation of bischelate complexes, Trofimenko introduced a second generation of scorpionate ligands with sterically demanding substituents in the 3-position of the pyrazolyl unit in 1987.^[15] With the second generation of scorpionate ligands the control of the coordination motif could be achieved.

In the 1990s, the synthesis of poly(pyrazolyl)methane was optimized. 3,5-substituted pyrazoles (**5**) and chloroform are converted into the desired ligand (**6**) in a mixture of chloroform and a basic aqueous solution aided by a phase transfer catalyst (Scheme 3).^{[2],[16]} This also led to the development of new applications.^[17]



Scheme 3. Optimized synthesis of poly(pyrazolyl)methanes.

One major side reaction occurring during this synthesis is the formation of different regioisomers. These regioisomers can be rearranged using *para*-toluene sulfonyl acid as a catalyst (Scheme 3, Figure 3).^{[2],[16]}

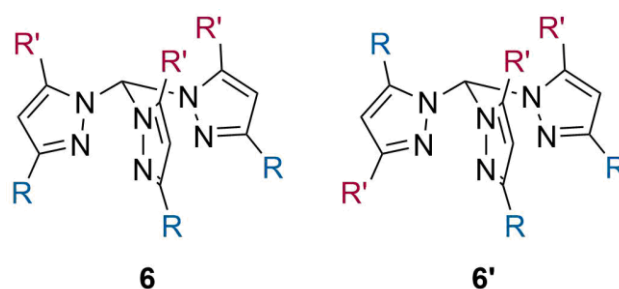
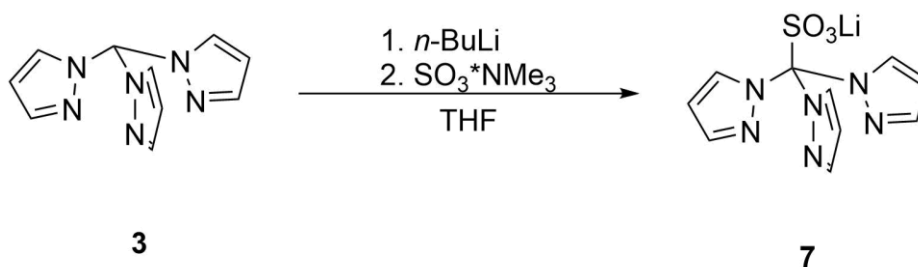


Figure 3. Scorpionate ligand **6** and its regioisomer **6'**.

For further optimization of the properties of the scorpionate ligands different non-coordinative groups were introduced on the apical atom of the ligand. These ligands are referred to as third generation of scorpionate ligands.^[18] For example, if polar groups like alcohols, ethers or methane sulfonic acid are introduced, the solubility in polar protic solvents increases.^[19] One possible introduction of polar groups is performed by deprotonation of **3** in the apical position with *n*-butyllithium followed by sulfonation with sulfur trioxide trimethyl amine complex to yield the modified ligand (**7**, Scheme 4).^[20]



Scheme 4. Synthesis of polar scorpionate ligands.

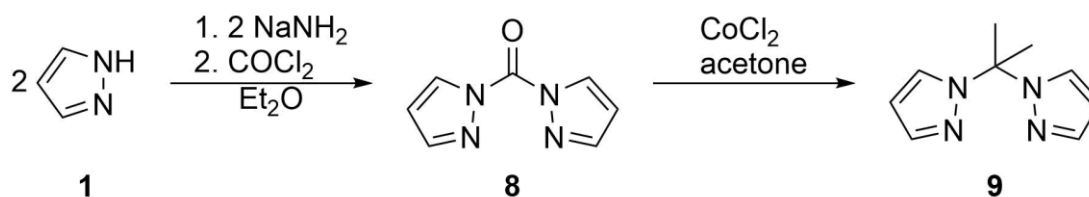
The bite angle of the donors can be adjusted by the introduction of sterically demanding groups like trimethylsilyl or large alkyl groups. One example is the utilization of a trimethylsilyl group, which can be achieved analogously to **7** by replacing the sulfur trioxide trimethyl amine complex by trimethylsilyl chloride.^[21] The same procedure can also be used to introduce a fourth donor group like a phosphane unit,^[22] for the synthesis of dinuclear complexes. As mentioned in chapter 1, the immobilization of complexes is an approach for more ecological and economical processes. In order to achieve an immobilization of scorpionate ligands one approach can be the backbone modification.

In addition, it is possible to form complexes with tris(pyrazolyl)methanide ligands. Therefore, at first a complex with a tris(pyrazolyl)methane ligand is formed. Subsequently the complex is deprotonated in the apical position.^{[23],[24]}

2.1.1 Heteroscorpionate ligands

The substitution of one pyrazolyl unit by another group containing Lewis basic sites leads to the class of heteroscorpionate ligands. The synthesis of poly(pyrazolyl)borate based heteroscorpionate ligands is possible by a stepwise addition of different groups to the central boron atom or by the isomerization of a homoscorpionate ligand.^[25] However as the synthesis of heteroscorpionate borate ligands is complex only few examples were reported.^[4]

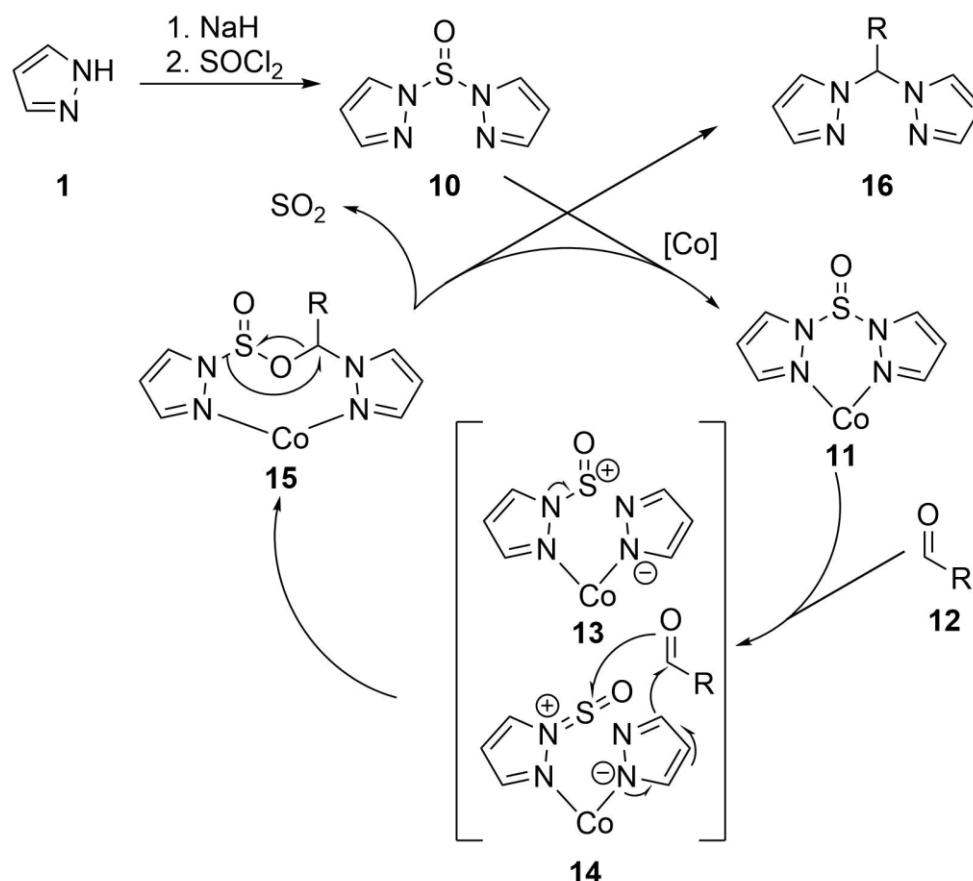
In contrast, the chemistry of poly(pyrazolyl)methane heteroscorpionate ligands has developed a rich chemistry with numerous examples and applications.^[26] In the 1970s, Thé and Peterson developed a method to synthesize modified bis(pyrazolyl)methane ligands. Therefore, pyrazole (**1**) is deprotonated by sodium amide. The pyrazolate reacts with phosgene to form bis(pyrazolyl)methanone (**8**). The last step is a cobalt(II) chloride catalyzed rearrangement with ketones to form the desired ligand (**9**, Scheme 5). It is noted that the reaction also can be performed when phosgene is substituted with thionyl chloride. While the intermediate is isolated in higher yields for the use of phosgene, the rearrangement is faster for the use of thionyl chloride.^[27]



Scheme 5. Synthesis of bis(pyrazolyl)methane ligands by Thé and Peterson.

This synthesis route can be used not only with ketones but also with aldehydes like salicylaldehyde to yield heteroscorpionate ligands.^[28]

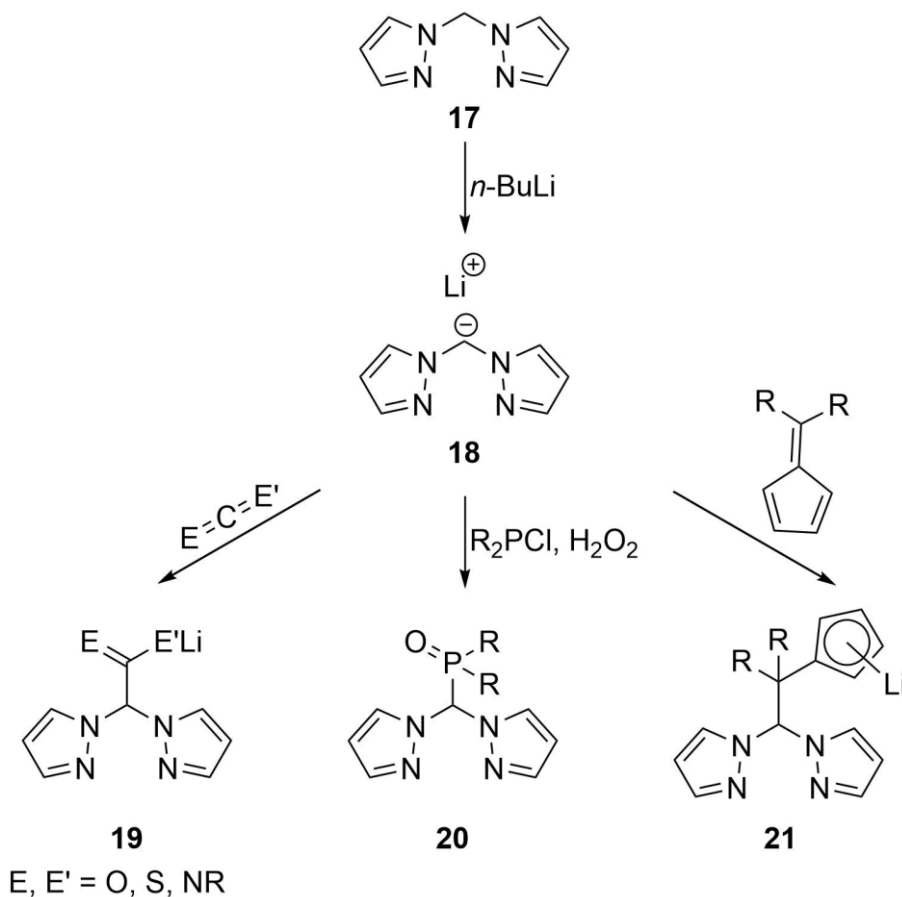
This protocol was further optimized, and an one-pot synthesis approach was presented in 2010.^[29] A variety of different aldehydes and pyrazole derivatives can be used to yield heteroscorpionate ligands (Scheme 6). In the first step pyrazole (**1**) is deprotonated with sodium hydride and further converted with thionyl chloride to yield bis(pyrazolyl)sulfoxide (**10**). Cobalt(II) and **10** form a coordination compound (**11**). By a Peterson rearrangement (**13-15**) and insertion of the aldehyde (**12**) the desired ligand (**16**) is obtained (Scheme 6).



Scheme 6. Mechanism of the Peterson rearrangement.

Another approach to synthesize heteroscorpionate ligands is starting from bis(pyrazolyl)methane (**17**). The synthesis of **17** is similar to the previously discussed synthesis of tris(pyrazolyl)methane (Scheme 3), using dichloromethane instead of chloroform.^{[30],[31]} The synthesis

of the heteroscorpionate ligands start with the lithiation of **17** in the apical position. The lithium salt of bis(pyrazolyl)methane (**18**) reacts with carbodiimide,^[32] isocyanate,^{[33],[34]} isothiocyanate,^{[33],[34]} chlorophosphane^[35] or substituted fulvene^[36] to yield different heteroscorpionates (**19-21**, Scheme 7). These syntheses are carried out as a one-pot syntheses. If **18** reacts with a fulvene or a heterocumulene, the lithium complex is obtained directly, while the neutral ligand is obtained after hydrolysis.



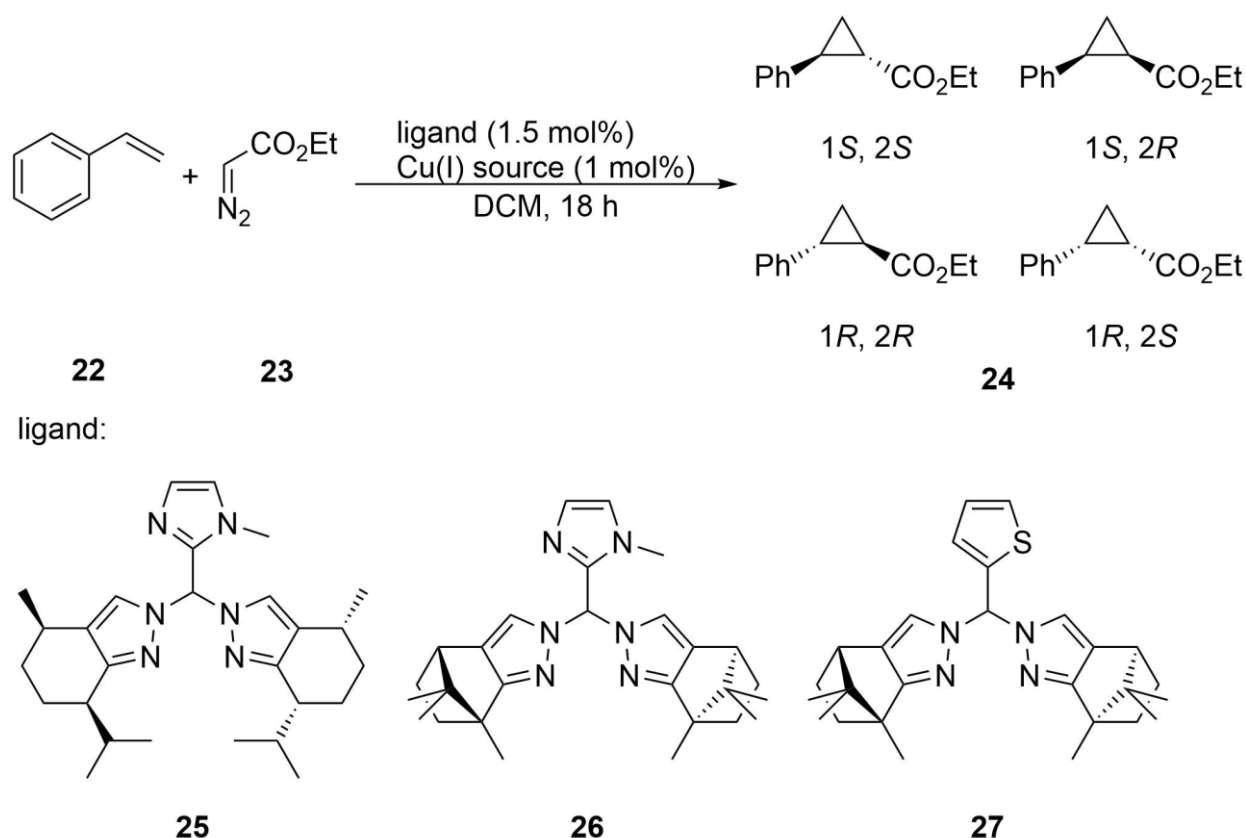
Scheme 7. Syntheses of heteroscorpionate ligands from bis(pyrazolyl)methane.

2.2 Copper poly(pyrazolyl)methane complexes as catalysts in organic transformations

Copper compounds have been used in a large array of applications including catalysis^[37] or photocatalysis.^[38] One class of copper compounds, that has a variety of applications, are the copper poly(pyrazolyl)methane complexes. Prominent examples are medical applications,^[39] bioinspired oxidation^[40] or homogenous catalysis.^[41] In the following chapter some examples will be highlighted. Examples including C–N coupling reactions and copper nitrene complexes will be discussed in chapter 2.4.

2.2.1 Enantioselective cyclopropanation

The working group of Burzlaff synthesized a series of enantiopure heteroscorpionate ligands. These ligands have chiral pyrazole units, which originate from (+)-camphor or (-)-menthone. Both substrates are part of the chiral pool. As the third donor unit different O, S and N donor units were used.^{[42],[43]} Copper(I) acetonitrile complexes with a chiral heteroscorpionate ligand and weak coordinating anions can be used in the enantioselective cyclopropanation of styrene (**22**) with ethyldiazoacetate (**23**) to yield four different cyclopropane enantiomers (**24**, Scheme 8). In this reaction three different heteroscorpionate ligands were used (**25-27**), the third donor unit was varied between imidazolyl and thiofuran. As pyrazole unit the above mentioned derivatives of (+)-camphor and (-)-menthone are used.^[43]

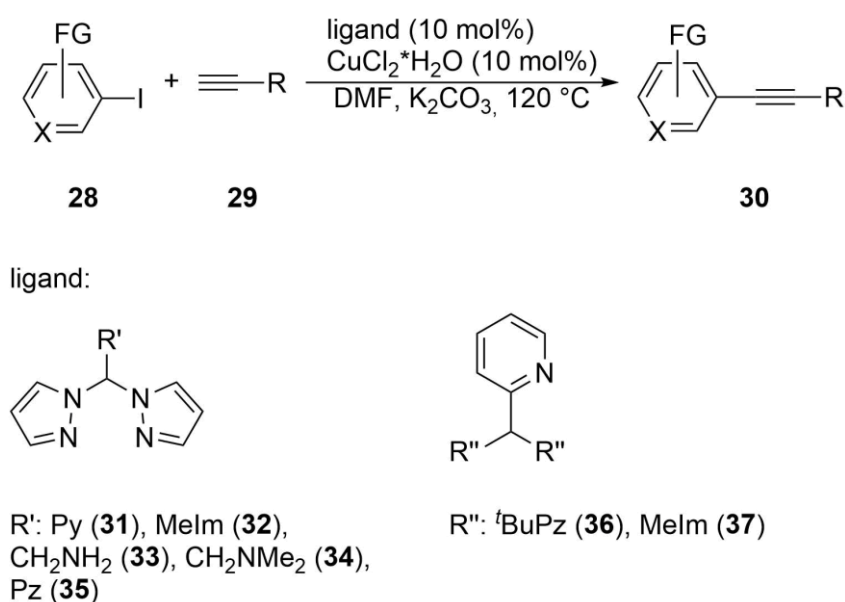


Scheme 8. Enantioselective cyclopropanation of styrene.

It could be shown that the yield of the desired cyclopropane (**24**) can be increased up to 90%, while the *cis/trans*-ratio only could be increased to 39/61. Also, the enantiomeric excess is limited to 69 for the *trans*-product and only 13 for the *cis*-product.^[43]

2.2.2 Sonogashira coupling

In 1975, the Sonogashira coupling was presented as a reaction between an alkyne and an aryl or vinyl halide catalyzed by palladium and copper.^[44] The Sonogashira coupling has some major drawbacks, which include the high cost and toxicity of palladium salts and the need for inert conditions. One possible way to overcome the drawbacks is using copper(II) heteroscorpionate complexes. These copper(II) complexes enable a palladium-free aerobic Sonogashira coupling.^[45] The developed reaction protocol can tolerate a variety of different aryl iodides (**28**) and various terminal alkynes (**29**) to yield numerous internal alkynes (**30**). In addition, the influence of the ligand design was investigated. A series of heteroscorpionate ligands were tested (Scheme 9).



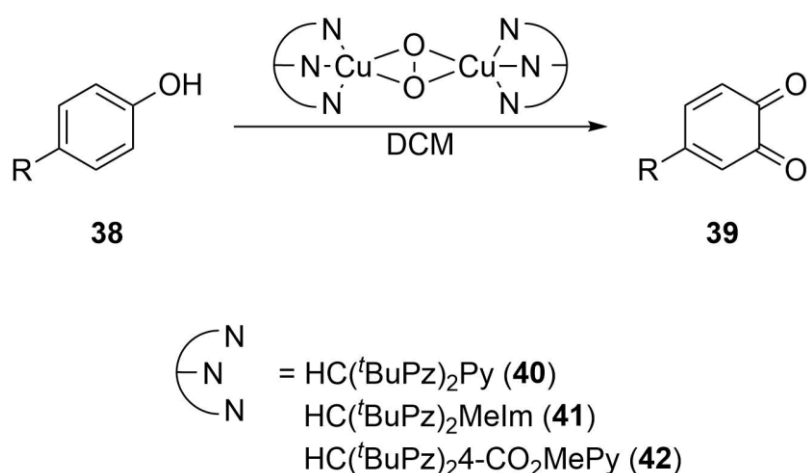
Scheme 9. Copper(II) scorpionate catalyzed Sonogashira coupling.

The ligand design of the used scorpionate ligands was varied between different third *N* donor units (**31-35**). In addition, the other two *N* donor units were varied (**36, 37**). The optimal ligand design for this type of Sonogashira coupling was found in ligand **32**.^[45]

2.2.3 Tyrosinase model systems

Dioxygen is a widely used oxidizing agent in biological and biomimetic oxidation reactions and industrial applications.^[46] In the biosynthesis of melanin the enzyme tyrosinase utilizes dioxygen for the oxidation of tyrosine to 3,4-dihydroxyphenylalanine.^[47] To obtain a deeper insight into the oxidation step, model systems are studied. One model system are copper(I) heteroscorpionate complexes in the oxidation of phenol (**38**) to catechol (**39**, Scheme 10).

Therefore, three different bis(pyrazolyl)methane ligands were used with different third *N* donor units. The used *N* donors were pyridine^[48] (**40**), methylimidazole^[40] (**41**) and 4-methyl picolinate^[49] (**42**). For the formation of a bis(μ -peroxide) copper complex a precursor complex is formed *in situ*. It is crucial for the formation of the peroxide complex that the precursor possesses a vacant coordination site. This can be achieved by an anion exchange. Therefore, silver hexafluoroantimonate is added to a copper(I) chloride complex. The bis(μ -peroxide) copper complex with **42** as ligand is highly stable with a half-life time of 50 min at 20 °C and is highly reactive and can reach TONs up to 19 in 7.5 min.^[49]

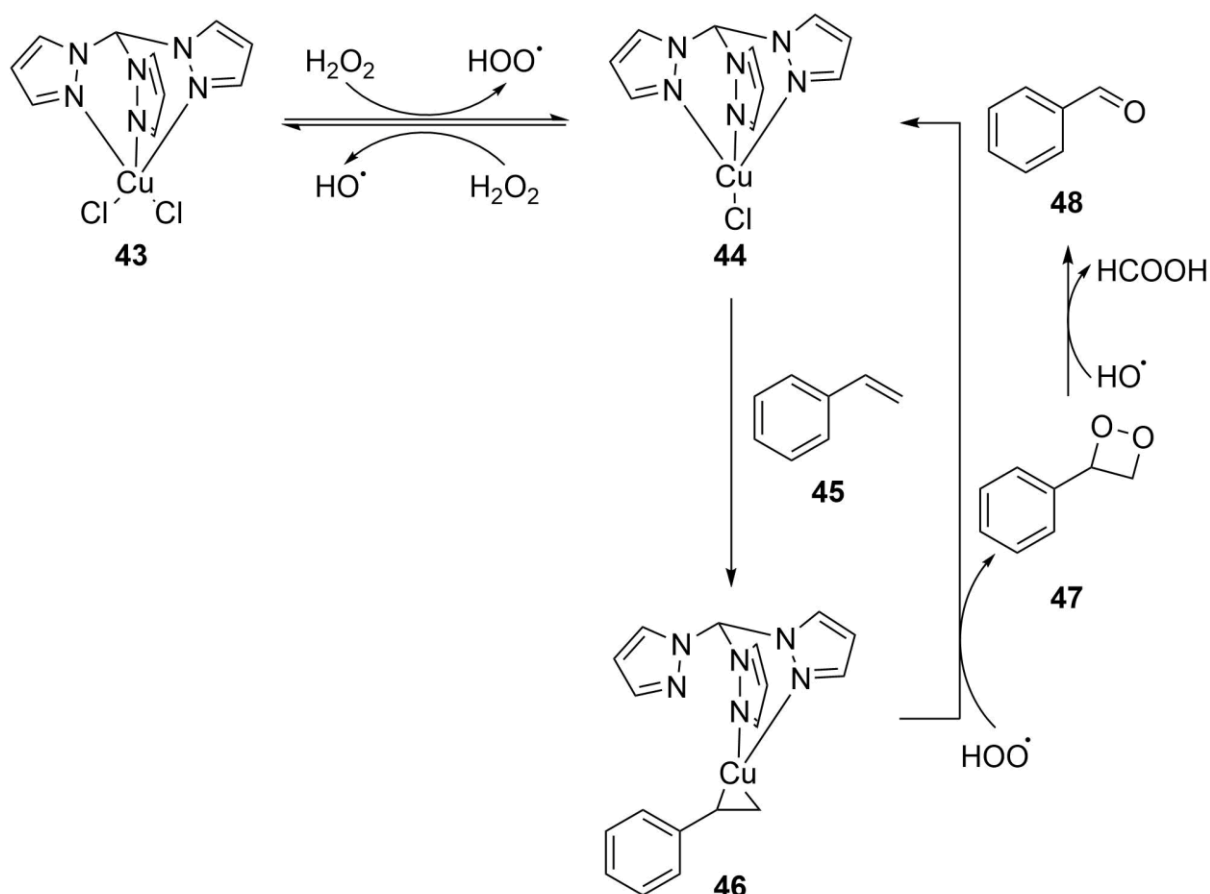


Scheme 10. Tyrosinase-like oxidation with copper heteroscorpionate ligands.

2.2.4 Oxidation of styrene

Besides the tyrosinase-like oxidation, as described before, copper heteroscorpionate complexes are also suitable for the oxidation of styrene (**45**) to benzaldehyde (**48**, Scheme 11).^[50]

The used catalyst (**43**) has shown an extremely high activity for the oxidation of **45** to **48**, a yield of 70% is reached after 5 minutes. Furthermore, it could be shown that **43** can be easily recovered. However, the recovered catalyst loses the catalytic activity, which will be addressed in further studies.^[50]

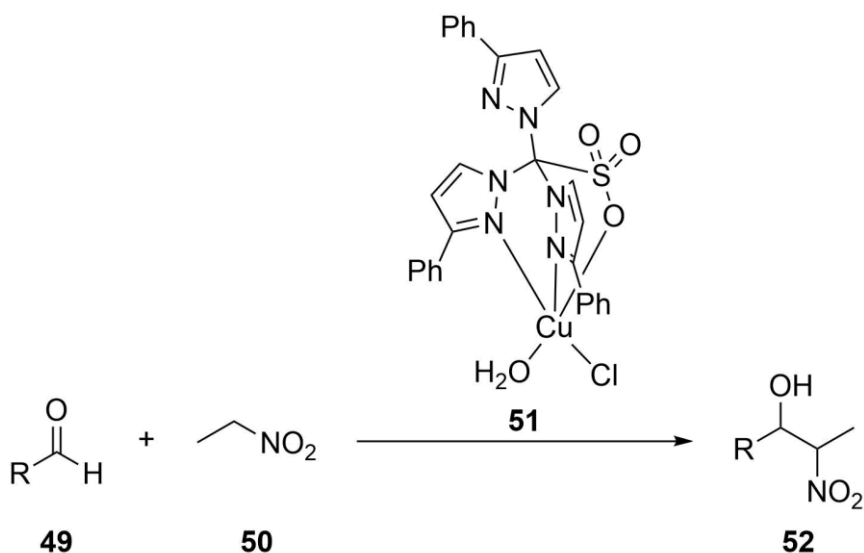


Scheme 11. Copper-catalyzed selective oxidation of styrene to benzaldehyde.

2.2.5 Stereoselective Henry reaction

The Henry reaction is an aldol reaction between an aldehyde (**49**) and a nitroalkane (**50**) to yield a nitro alcohol (**52**, Scheme 12). One possible catalyst for the Henry reaction is the copper(II) heteroscorpionate complex (**51**).^[51]

Complex **51** has shown to be highly active as a catalyst with yields up to 99%. Another advantage is the stereoselectivity. The reaction product shows an enrichment with the *anti* diastereoisomer and *anti/syn* ratios up to 2.3 are reached.^[51]



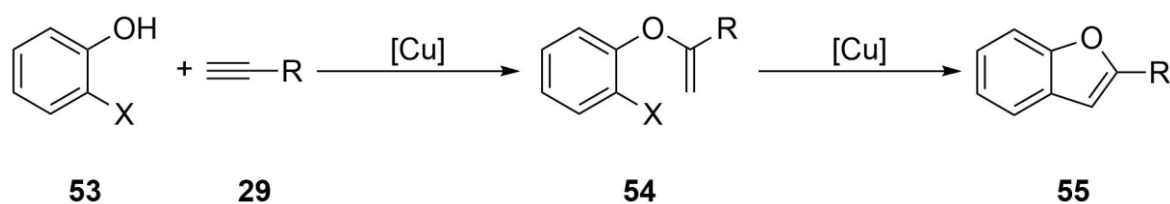
Scheme 12. Copper(II) catalyzed Henry reaction.

2.3 Copper-mediated cross-coupling reactions

As mentioned before, copper compounds have many applications, including their suitability as catalyst in various reactions. In the following chapter some copper catalyzed reactions with importance for this thesis will be discussed.

2.3.1 Benzofuran synthesis

In chapter 2.2.2 the Sonogashira coupling reaction was described. A similar reaction between a halidophenol (**53**) and an alkyne (**29**) can be catalyzed by copper(II) pincer complexes to yield a benzofuran derivative (**55**). It could be shown that the reaction does not follow a Sonogashira pathway. The intermediate of this reaction (**54**) is not the product of a C–C coupling but of a C–O bond formation (Scheme 13).^[52] Additionally, it was shown that a variety of different benzofurans could be synthesized using this route. Although the reaction does not follow a Sonogashira mechanism it is often referred to as a Sonogashira reaction.^[53]

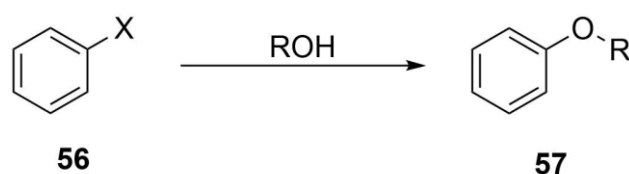


Scheme 13. Mechanism of the benzofuran synthesis from a halidophenol and an alkyne.

Furthermore, it is not only possible to synthesize **55** from **53**, but also to synthesize indoles from halide anilines. It could be shown that introducing one protective group to the amine leads to increased yields from 30% to 92%.^[54]

2.3.2 C–O coupling reaction

The formation of C–O bonds under classic Ullmann conditions^[55] using an arylhalide (**56**) and phenol has been known for a long time (Scheme 14). However due to the harsh reaction condition not many C–O couplings have been developed so far. The coupling reactions were usually performed in high-boiling polar solvents such as nitrobenzene or DMF, at temperatures as high as 210 °C.^[56]



Scheme 14. C–O coupling reaction between an arylhalide and an alcohol.

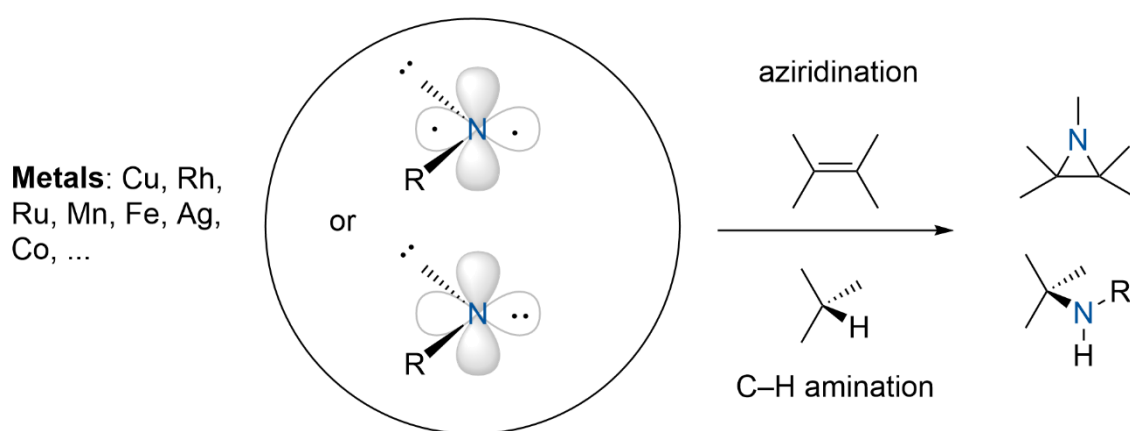
In 2006, a new reaction protocol was developed to perform C–O coupling reactions at room temperature. The two major drawbacks of this protocol are that it is limited to activated aryl halides and a high catalyst loading of 30 mol% is used.^[57] By using 2,2,6,6-tetramethyl-3,5-heptadione^[58] or pyrrolidine-2-phosphonic acid phenyl monoester^[59] as ligand the substrate scope can be increased, but higher temperatures are needed.

2.4 Nitrenes

Nitrogen-containing motifs are found in synthetically,^[60] biologically^[61] and pharmaceutically^[62] relevant molecules, this requires novel synthetic ways for the formation of C–N bonds. One way to achieve this motif is the direct functionalization of C–H bonds. C–H bond functionalization is one of the most efficient strategies to derivatize inert sites of organic molecules, but often requires directing groups.^[63] On the one hand C–H functionalization allows the step-economical access to valuable building blocks for the synthesis of complex molecules. On the other hand a late-stage approach can be used to generate a compound library.^[64] One way to achieve this are copper-mediated reactions. There is a variety of copper-based catalytic C–H amination reactions^{[65],[66],[67]–[69]} and N-group transfer^{[65],[70],[71],[72]} reactions. Experimental^{[73],[74]}

and theoretical investigations^{[65],[69],[72],[75]–[79]} indicate that the key intermediate of these reactions are nitrenes.

A nitrene is a monovalent nitrogen species with a valence-electron sextet and therefore an open valence electronic structure, which can be in a singlet or triplet state. The nitrene is often described as the nitrogen analogous of the carbene. Due to its valence-electron sextet, the nitrene is a highly reactive species and it represents the central intermediate of aziridinations and the direct C–H amination. Nitrenes can be stabilized by different transition metal complexes with *N* donor ligands.^{[80],[81]} A large variety of different copper complexes (Chapter 2.4.1), iron complexes (Chapter 2.4.2) and cobalt complexes^{[82],[83]} has been reported which are used to stabilize a nitrene moiety (Scheme 15).^[81]



Scheme 15. Overview of nitrene basics.

In the literature few efficient nitrene generating agents, like halogenated amines or amines incorporating an oxidant like di(acetyl)iodobenzene are applied. The most common used nitrene generating agents are iminoiodinanes (for example ^sPhINTs (**58**), Figure 4) and organic azides. Both families have advantages and disadvantages. While iminoiodinanes are poorly soluble and the synthetic effort is high, they are very reactive. Organic azides are well soluble and the synthetic effort is lower, but they are less reactive and require higher temperatures or radiation for reactions.^[84]

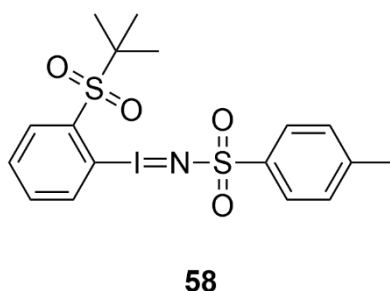


Figure 4. Commonly used iminoiodinane ^sPhINTs.

2.4.1 Copper nitrenes

Due to their low cost and low toxicity, copper compounds were studied extensively as nitrene precursors and a variety of different *N* donor ligands was applied. One essential factor for the reactivity is the presence of terminal copper nitrenes, which is considered to mediate the reactivity.^{[65],[69],[72]–[79]}

In general, a terminal copper nitrene complex generated from **58** can have two different bonding situations. On the one hand, it is possible that the nitrene moiety only coordinates by the nitrogen atom (κ^1 -isomer, Figure 5 top left) and, on the other hand, the nitrene moiety can coordinate by the nitrogen atom and an oxygen atom (κ^2 -isomer, Figure 5 top right).^[72] Additionally, the copper nitrene complex can have five different spin states (Figure 5 bottom). The five different spin states can be approached from the homolytic bond scission of a copper nitrene into a copper(I) and a nitrene fragment. All five spin states are discussed in the literature.^{[72],[85],[86]}

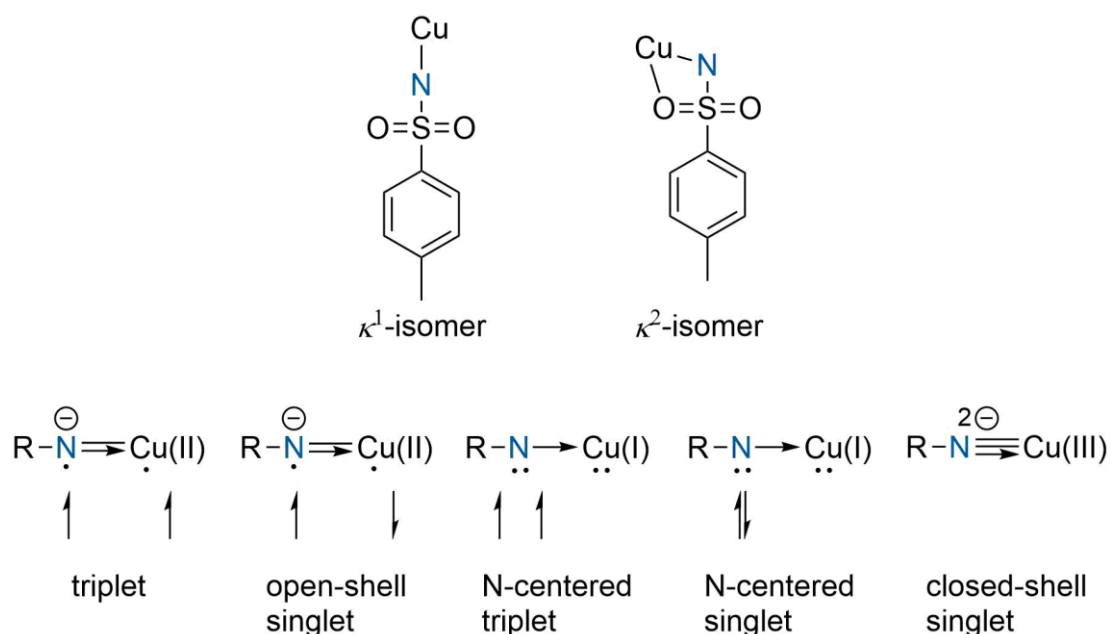
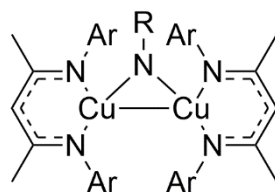


Figure 5. Different spin states and bonding situations in copper nitrenes from iminoiodinanes.

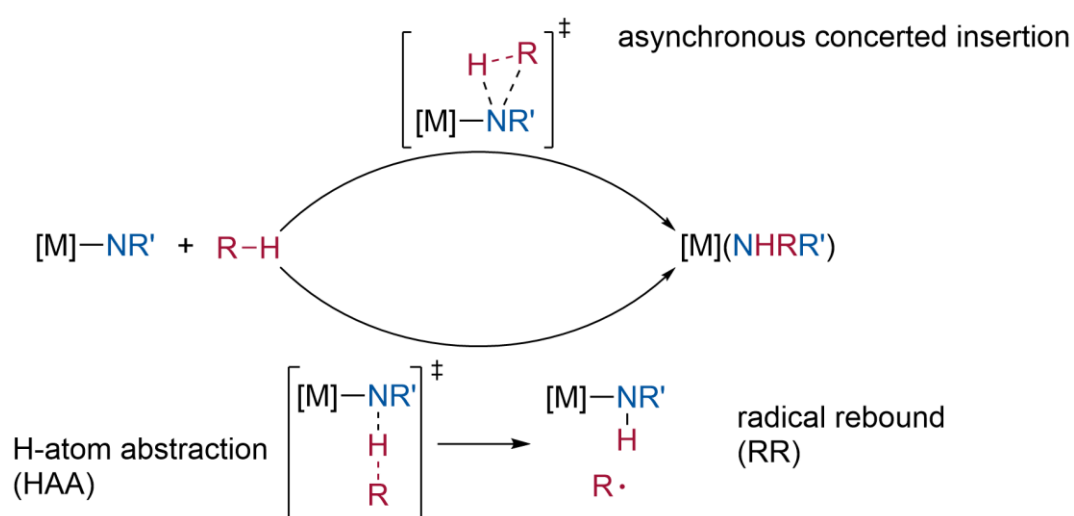
In the past, a limited number of stable copper nitrenes were presented in the literature. One of the first examples was synthesized by Warren *et al.* in 2006.^[87] They reported discrete dicopper nitrene complexes (**59**, Figure 6). The dicopper nitrene complexes were synthesized from a copper(I) NacNac complex and an aromatic azide. The dicopper nitrene was characterised *via* ¹H NMR spectroscopy and X-ray crystallography.



59

Figure 6. Dicopper nitrene complex.

In addition, it could be indicated that the dicopper nitrene complex slowly dissociates into a terminal nitrene and a nitrene transfer to trimethyl phosphane and *tert*-butyl isocyanide was achieved. In the following years this system was further optimized. On the one hand, different nitrene sources like benzoyl azide were utilized, which also prevent the formation of a dicopper nitrene complex,^[88] or amines with organic peroxides^[89]. On the other hand, the reactivity was investigated. At higher temperatures, the C–H amination of benzylic and aliphatic substrates was successful.^[90] Using NacNac ligands with sterically demanding aromatic substituents the selectivity of the amination reaction can be driven to primary and secondary C–H sites^[88], while the amination with less sterically demanding, aromatic substituent leads to an amination in the position with the lowest bond dissociation energy. Furthermore, the mechanism of the C–H amination *via* a dicopper nitrene complex was investigated. In a first step, the dicopper nitrene complex needs to disintegrate into a terminal nitrene complex and a copper complex.^[73] The mechanism for the insertion of a metal bound nitrene into a C–H bond was described for rhodium nitrenes.^[91] The insertion of the metal bound nitrene can be either an one-step asynchronous concerted insertion or a two-step reaction. The first step is a H-atom abstraction from the substrate by the nitrene followed by a radical rebound (Scheme 16).



Scheme 16. Mechanism of the insertion of a metal bound nitrene into a C–H bond.

For the dicopper nitrene it could be shown that, in a first step, a terminal nitrene must be formed by dissociation of the dicopper nitrene and the mechanism of the formal nitrene insertion

follows the two-step mechanism. The dissociation of the dicopper nitrene can be observed, when the kinetics of the amination of ethylbenzene are analyzed. Furthermore, the presence of a radical intermediate in the two-step mechanism can be proven by a radical clock experiment.^[73]

The working group of Stavropoulos studied the mechanism of the copper nitrene catalyzed aziridination of styrene extensively using a copper(I) guanidine precursor complex to yield the copper nitrene complex (**60**, Figure 7) when reacted with PhINTs. One disadvantage of the nitrene complex **60** is the presence of various methyl groups in close contact to the nitrene center. This decreases the stability of the copper nitrene, as the nitrene can insert into a C–H bond of a methyl group. Therefore, it was not possible to observe the nitrene, but only the decay products.^[65]

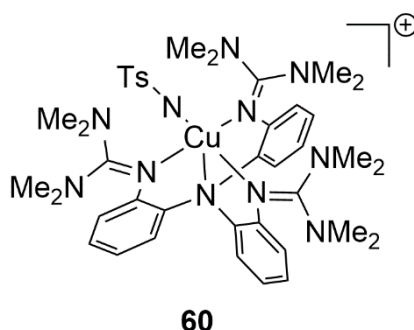
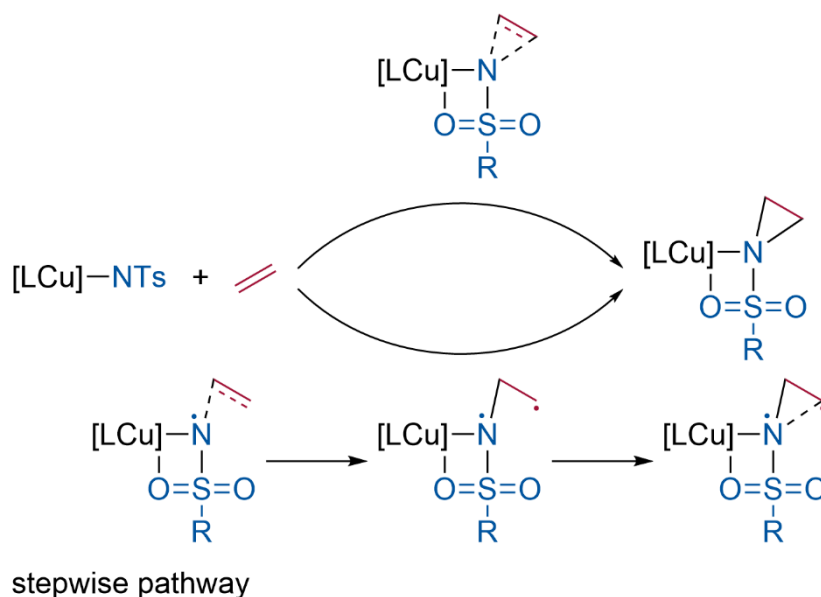


Figure 7. Elusive copper guanidine nitrene.

Nevertheless, it was possible to develop a reaction protocol for the efficient C–H amination of aliphatic and benzylic substrates and for the aziridination of a variety of different styrene derivatives and alkenes.^[65] For the C–H amination it could be shown, in accordance with the previously discussed results of Warren *et al.*, that a radical reaction occurs. In addition, the mechanism of the aziridination was investigated. Two mechanistic pathways for the aziridination of olefins are possible, which were described for copper bispidine complexes (Scheme 17).^{[71],[72]} Similar to the C–H amination a concerted pathway and a radical stepwise pathway are possible. DFT calculations and experimental observations of a radical intermediate show that the radical stepwise pathway is favored over the concerted one.^{[71],[72]}

concerted pathway



Scheme 17. Mechanistic pathways of the copper(I) catalyzed aziridination.

If the aziridination is performed with α - or β -deuterated styrene it can be observed that a kinetic isotope effect is measurable only for the β -deuterated styrene. This indicates that the β -styrene position is associated with the electrophilic nitrenoid moiety in the transition state. Also the aziridination with *para*-substituted *trans*-deuterated styrene derivatives showed that no 1,2 H/D exchange is observable and that the nature of the *para*-substituent does not affect the barriers for a rotation of the C_α – C_β bond.^[65]

To investigate the nitrene intermediate further stable terminal nitrene species are needed. The working group of Ray reported two strategies to stabilize nitrenes. The first strategy was presented in cooperation with the working groups of Company and Ribas and is illustrated by the synthesis of a nitrene incorporated into a macrocycle (**61**, Figure 8).^[92] The second strategy is to add a Lewis acid, like scandium triflate, for the stabilization of the terminal copper nitrene complex (**62**+**63**, Figure 8).^{[93]–[95]}

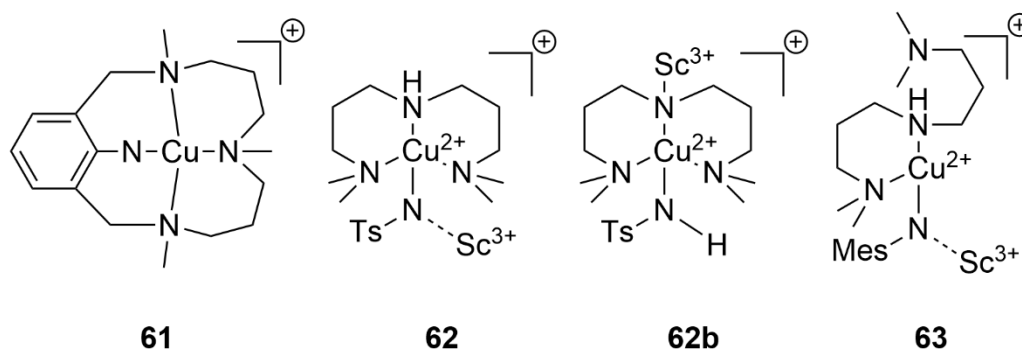


Figure 8. Terminal copper nitrene complexes and the tautomeric form of **62**.

To yield the copper nitrene **61** first an aromatic azide was synthesized, which is located inside a macrocycle. This azide reacts with copper(I) tetrakisacetonitrile triflate to yield compound **61**. The formation of this stable green compound ($t_{1/2}$ (25 °C) \approx 45 h) can be observed in the UV/Vis spectra in acetonitrile at room temperature. The UV/Vis spectra show three distinct absorption bands at 360 nm, 710 nm and 980 nm. **61** was further analyzed using cold spray ionization mass spectrometry, which showed the expected signal at m/z 351.1597, and EPR spectroscopy, which showed that the majority of the species are EPR silent. This indicates a singlet state of the formed nitrene. Additionally, the singlet state could be further proven by Evans NMR spectroscopy. The reaction was proven by the absence of an azide vibration at about 2200 cm^{-1} in the IR spectra, too. The copper nitrogen bond lengths in **61** were determinate to be 2.04 Å for all four nitrogen atoms. As the nitrene originates from the ligand, no catalytic reactions are possible. Nevertheless, it could be shown that **61** can undergo stoichiometric nitrogen-transfer reactions to phosphanes and abstract hydrogen atoms from weak C–H bonds.^[92] In order to obtain a catalytic system the complex $[\text{Cu}\{3,3'\text{-iminobis}(N,N\text{-dimethyl propylamine})\}]\text{BF}_4$ can be converted to **62** or **63** using either $^9\text{PhINTs}$ or mesityl azide. For both **62** and **63** similar properties to **61** were found. In contrast to **61** both species are only stable at -90 °C, but for **62** an equilibrium between the nitrene species and the tautomeric species **62b** (Figure 8) was observed.^{[93]–[95]}

The development of reaction protocols for the amination of toluene and cyclohexane as well as the aziridination of cyclohexene was possible.^[93] In addition, it could be shown that **63** is superior to **62** in nitrene-transfer reactions, while the opposite is true for hydrogen atom abstraction reactions.^[94] Furthermore, a method for the determination of the nitrene yield was introduced. If ferrocene is added to a solution of the nitrene a two-electron reduction process can be observed in the UV/Vis spectra and the yield can be extracted from the absorption of the ferrocenium band.^{[93]–[95]}

The working group of Betley presented a stable terminal triplet copper nitrene (**64**, Figure 9), which was stabilized by a dipyrin ligand with sterically encumbered substituents. The nitrene **64** could be obtained by the reaction of an aromatic azide with a copper(I) precursor complex. For the synthesis of a stable nitrene compound a ligand with a modified s-indacene substituent (1,1,7,7-tetraethyl-1,2,3,5,6,7-hexahydro-3,3,5,5-tetramethyl-s-indacene) on the pyrrole and a 3,5-bis(trifluoromethyl)phenyl backbone was used with different azides with ether or aliphatic substituents. For catalytic reactions the ligand design was modified to a mesityl backbone and a (2,4,6-trisphenyl)phenyl substituted pyrrole with fluorinated azides.^[86]

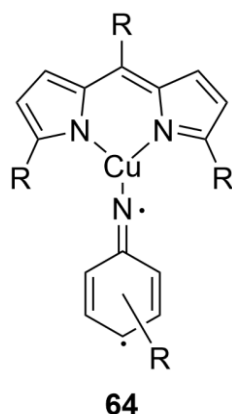


Figure 9. Structure of a dipyrin triplet copper nitrene complex **64**.

Compound **64** was investigated with a variety of methods including NMR spectroscopy, XAS, single crystal X-ray diffraction and theoretic investigations with a truncated model. With these methods the copper(I) character and the triplet spin state could be proven. The reactivity of the system was demonstrated by the stoichiometric C–H amination of toluene, cyclohexene and cyclohexane and the stoichiometric aziridination of styrene. It also could be shown that a catalytic process for the amination of cyclohexene is possible, but the yield is lower compared to the stoichiometric amination.^[86]

A more application driven research was performed by the working group of Perez. They investigated a series of different reactions, where copper nitrenes are a central intermediate. The copper complexes used are scorpionate complexes, mainly tris(pyrazolyl)borate ligands and tris(pyrazolyl)methane ligands were applied. One early example is the C–H amination of benzene, toluene and cyclohexane.^{[67],[68]} The C–H amination of simple substrates and aziridination were further investigated and a recyclable polynorbornene based reaction system was developed (**65**, Figure 10).^[96]

The successful incorporation of copper into the polymer was shown by inductively coupled plasma mass spectrometry (ICP-MS) and by FTIR spectroscopy. For the FTIR spectroscopy the compound **65** was reacted with carbon monoxide to form the corresponding copper carbonyl complex. The characteristic carbonyl band was observed in the FTIR spectra. It could be shown that the C–H amination of cyclohexane and the aziridination of styrene can be performed with **65** as catalyst and the iminoiodinane PhINTs with high yields. Additionally it was reported that the catalyst can be recycled up to three times.^[96]

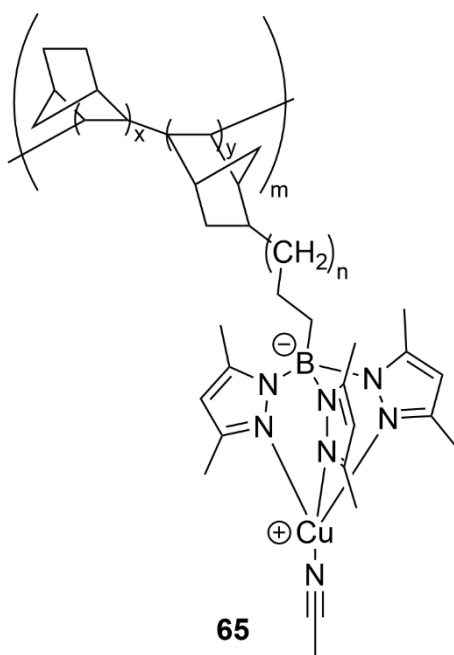
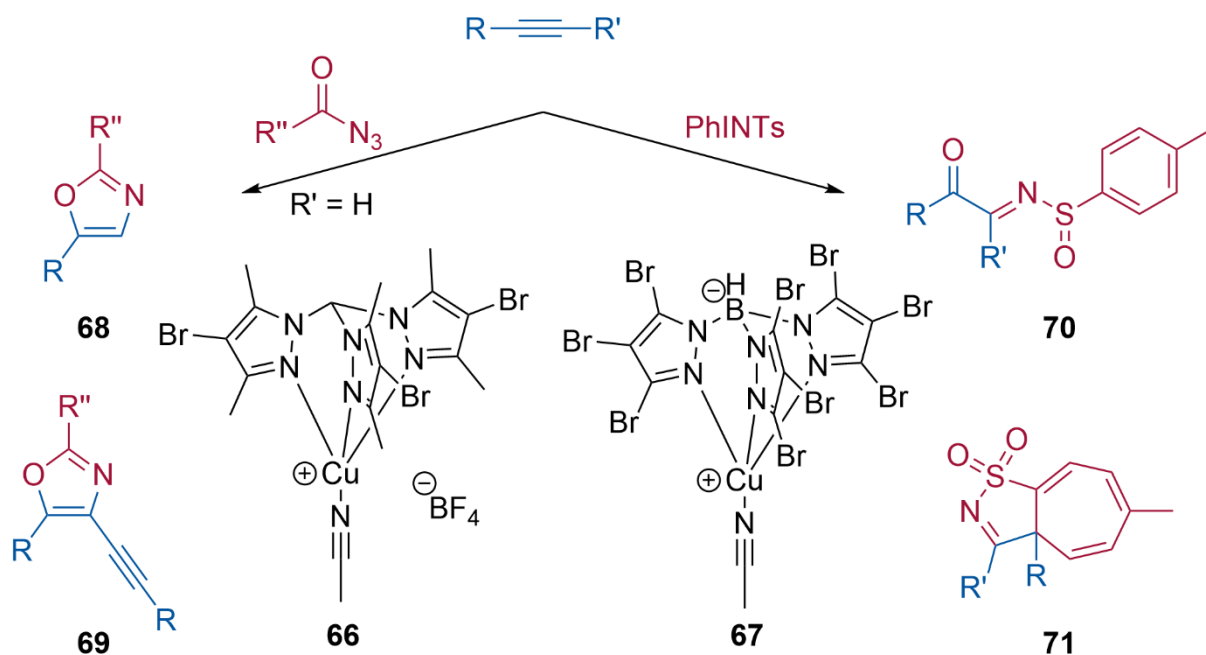


Figure 10. Polynorbornene supported copper(I) tris(pyrazolyl)borate complex.

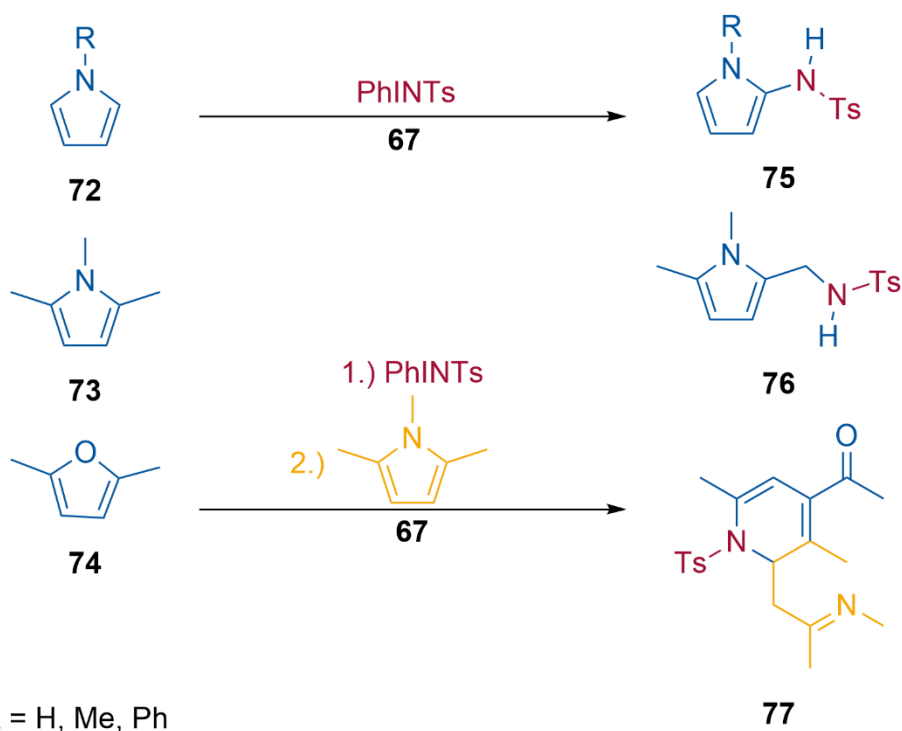
Besides the C–H amination reaction and the aziridination, the reactions of copper nitrene complexes with alkynes were investigated. Terminal alkynes could be converted to oxazoles (**68+69**), if reacted with benzoic azides in the presence of a copper tris(pyrazolyl)methane catalyst (**66**, Scheme 18, left). It could be shown that different tris(pyrazolyl)methylamine complexes are active as catalysts and that the reaction protocol tolerates different functional groups on the alkynes as well as on the azides. Furthermore, the mechanism of the reaction was investigated with DFT calculations.^[97]

Terminal and internal alkynes were transformed into sulfonamides (**70**) and isothiazoles (**71**), in a reaction with PhINTs catalyzed by a copper tris(pyrazolyl)borate complex (**67**, Scheme 18, right). For the conversion of terminal alkynes only the product **70** can be observed, while for internal alkynes a mixture of both products was observed. The product mixture is rich in **70**. In addition, the ratio of both products can be shifted to be richer in **70**, if alkynes with more sterically demanding substituents are used. The mechanism was investigated by DFT calculations as well.^[98]



Scheme 18. Reaction of alkynes with copper nitrenes.

With the use of the established catalyst **67** it was also possible to aminate the different pyrrole derivatives (**72+73**) and to perform a tandem reaction of a furan derivative (**74**) and **73** (Scheme 19).^[99]



Scheme 19. Catalytic C–H amination of heterocycles.

The reaction is selective to the α -position of the pyrrole and it tolerates NH groups. When the α -position of the pyrrole is blocked by a methyl group, this methyl group is aminated selectively.^[99]

The working group of Bertrand investigated phosphinonitrenes, which can either be isolated as a metal free nitrene^[100], as a bridged or terminal coinage metal nitrene^[101] (Figure 11, **78**). As coinage metal copper and silver can be used.

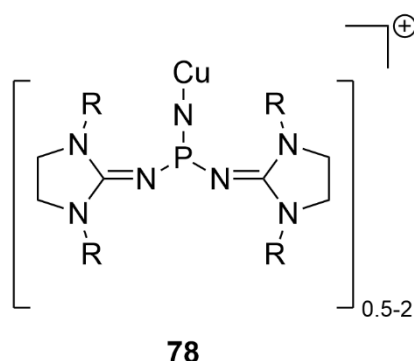


Figure 11. Copper stabilized phosphinonitrenes.

The copper nitrene species can be synthesized from the metal free phosphinonitrene and copper triflate and can coordinate to the copper in three different forms. A μ -nitrene-bridged species, a terminal nitrene species or a twofold coordinated species can be obtained. However only the μ -nitrene-bridged species and the twofold coordinated species can be isolated, due to further isomerization of the terminal nitrene species. The stable copper phosphinonitrenes can be analyzed *via* single crystal X-ray diffraction and NMR spectroscopy.^[101] The metal free phosphinonitrene can be used as a nitrogen atom-transfer agent.^[100]

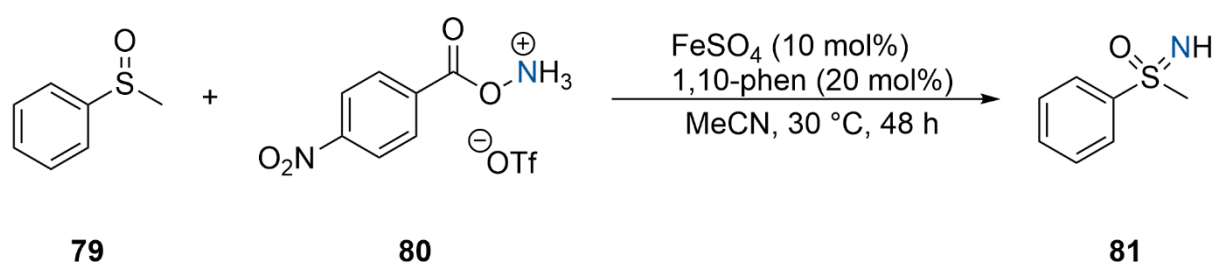
Another way for the stabilization of nitrenes is the use of bis(pyrazolyl)methane copper(I) acetonitrile complexes. It was shown that the reaction between ^sPhINTs (**58**) and a copper(I) bis(pyrazolyl)methane complex in dichloromethane leads to a singlet nitrene complex with a κ^2 -coordination motif of the tosyl nitrene (Figure 4). This reaction can be observed with UV/Vis spectroscopy by the formation of two characteristic absorption bands: a strong one at about 400 nm and a weaker one at 650 nm. Further, the nitrene complexes can be observed using cryo ESI mass spectrometry. These nitrene complexes are stable at -80 °C and can be used as efficient catalysts for the C–H amination of toluene and cyclohexane and the aziridination of styrene derivatives.^{[102],[103]}

2.4.2 Iron nitrenes

Iron is one of the most common metals on the earth^[104] and is highly biocompatible.^[105] Therefore, iron complexes are very interesting as catalysts in green reactions.

Iron nitrenes can be generated in several ways, but the most commonly used is by the reaction of a low-valent iron complex and an oxidizing nitrene transfer reagent. In earlier studies

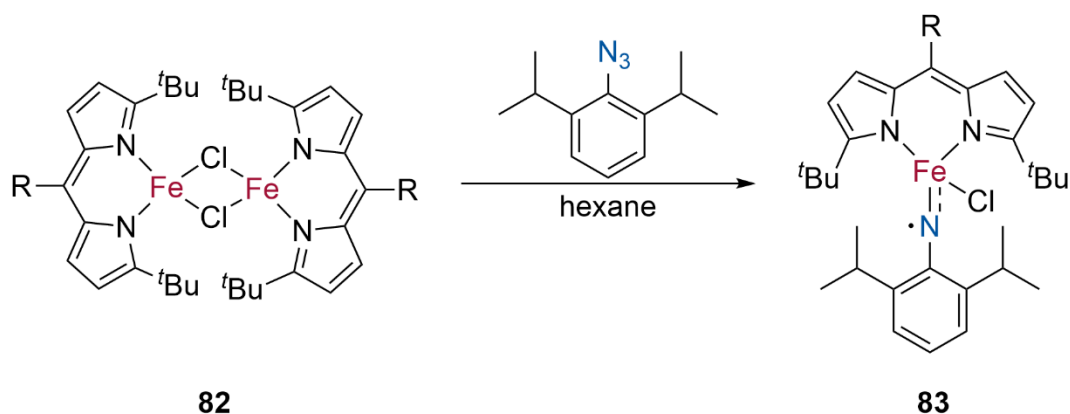
bromamine-T and iminodianes were used often, however they suffer from a low atom efficiency, overoxidation and selectivity issues. Mostly organic azides were used as nitrene transfer reagents in recently reported catalytic processes.^{[83],[106]} Another possibility to generate an iron nitrene is the usage of carbamates (**80**) as a nitrene generating agents. The working group of Bolm developed a catalytic process for the iron catalyzed synthesis of sulfoximines (**81**) from sulfoxides (**79**, Scheme 20). It could be shown that the most active catalyst is iron(II) sulfate with two equivalents of 1,10-phenanthroline and that a variety of different functional groups are tolerated. As the study is focused on the synthetic application, the iron nitrene intermediate was not proven yet. However the formation of an iron nitrene intermediate is plausible from the reaction observed.^[107]



Scheme 20. Synthesis of sulfoximines from sulfoxides.

Another way to achieve an iron catalyzed nitrene transfer process is the use of *Pseudomonas savastoni* ethylene-forming enzyme, a non-heme iron enzyme. It is possible to catalyze the olefin aziridination and the nitrene C–H insertion. Additionally, the reactivity can be improved by directed evolution.^[108] Furthermore, it is possible to perform a visible light driven nitrene transfer reaction with an iron porphyrin and organic azides. This method enables the amination and aziridination of a huge variety of different substrates.^[109]

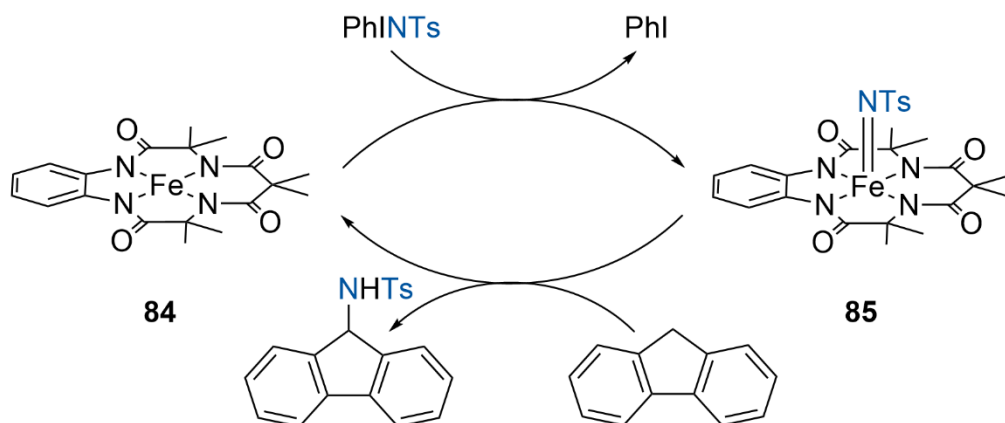
In general, the isolation of a stable iron nitrene is challenging. In most iron based nitrene transfer processes the only isolated intermediates are iron imido complexes. Beside their work on copper nitrene, the Betley group also investigated iron nitrene chemistry. For the synthesis of iron complexes also dipyrin ligands were used.^{[110],[111]} One possibility is to start from a μ -bridged iron(II) complex (**82**) in a hexane solution at $-40\text{ }^\circ\text{C}$. By the addition of 2,6-diisopropylphenylazide the formation of the iron imido complex can be observed (**83**, Scheme 21). The iron imido complex **83** could be characterized with Mössbauer spectroscopy, single crystal X-ray diffraction and SQUID magnetometry.^[110]



Scheme 21. Formation of an iron imido complex at low temperature.

When, instead of 2,6-diisopropylphenylazide, 3,5-bis(trifluoromethyl)phenylazide is used, a bridged iron imido complex is obtained. This iron imido complex can be used for nitrene transfer reactions. It is possible to achieve the aziridination of styrene or the amination of toluene.^[110]

Another way to use iron complexes in nitrene transfer reactions is the iron(III) non-heme complex (**84**) presented by the Nam working group. When this complex reacts with PhINTs an iron(V) imido complex (**85**) is obtained. This iron(V) complex can be used for amination reactions (Scheme 22). The iron(V) imido species was analyzed *via* CSI-MS, UV/Vis spectroscopy, Mössbauer and XAS.^[112]



Scheme 22. Formation of an iron(V) species and its catalytic activity.

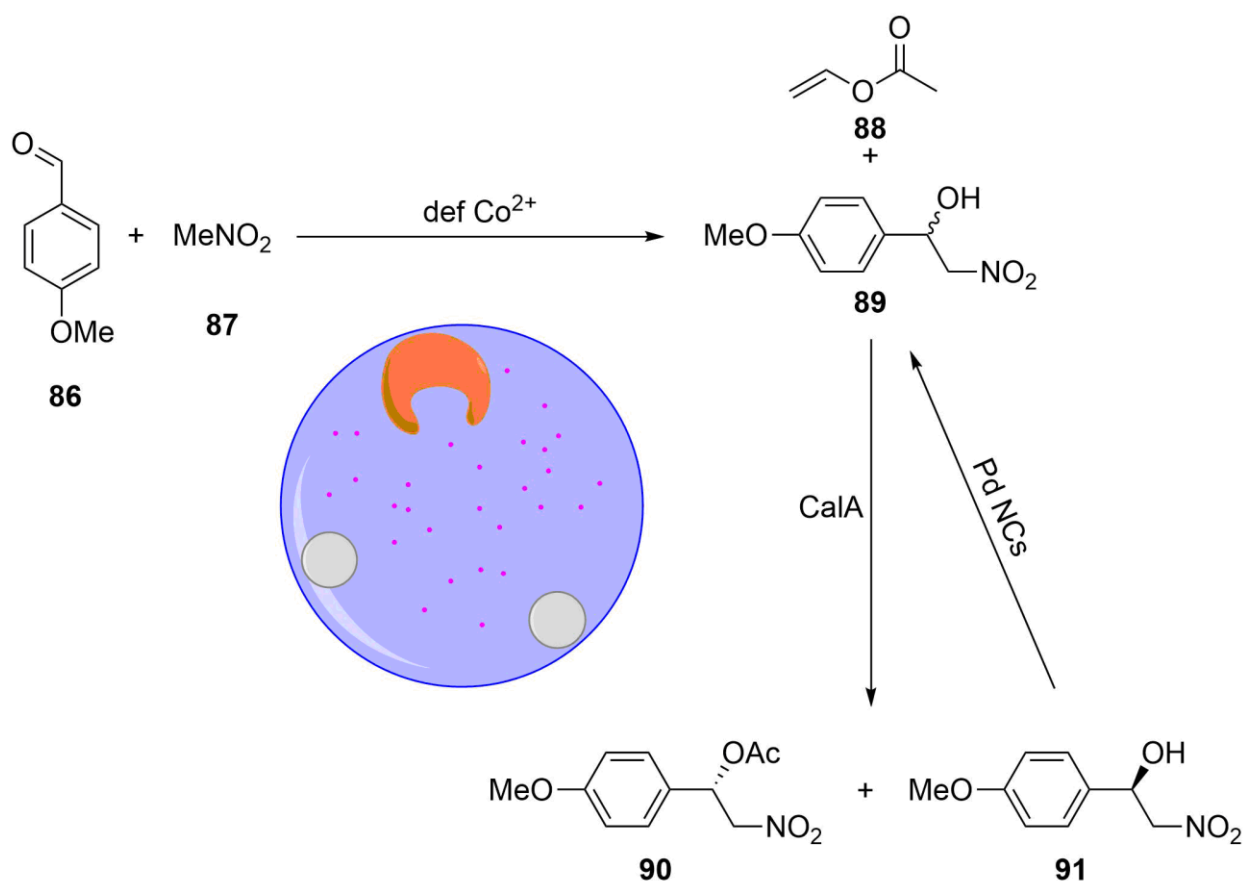
In addition, it could be shown that, if the ligand of **85** is oxidized, the reactivity can be increased. As one-electron oxidants $[\text{Fe}(\text{bpy})_3]^{3+}$, $[\text{Ru}(\text{bpy})_3]^{3+}$ and $[(4\text{-BrC}_6\text{H}_4)_3\text{N}]\text{SbCl}_6$ were used. The metastable product of the one-electron oxidation can be characterized with various methods including EPR, CSI-MS, XAS and NMR spectroscopy. When the reactivity of **85** and the oxidized iron(V) imido complex is compared it can be observed that the amination reaction is enhanced by a factor of 2.5 while the nitrene transfer reaction is enhanced by a factor of 17000.^[113]

2.5 Chemoenzymatic tandem reactions

Even though a great effort is needed for the combination of chemo- and biocatalysis, the advantages of a combination of both leads to the development of new tandem reactions. The main challenge to overcome for a successful tandem reaction is the requirement that the reaction conditions of both catalytic steps have to be compatible.^{[114],[115]} One problem is that there is no general concept to set-up combined reactions. The advantages of combined chemoenzymatic tandem reactions are especially that the intermediates are not isolated, less waste is produced, higher yields and high selectivities are obtained. Hence, for industrial application the investment costs are lower.^[114] Therefore, the use of microgels as a protector of one or both catalysts is a very interesting approach, which may lead to a general concept (see Chapter 1).

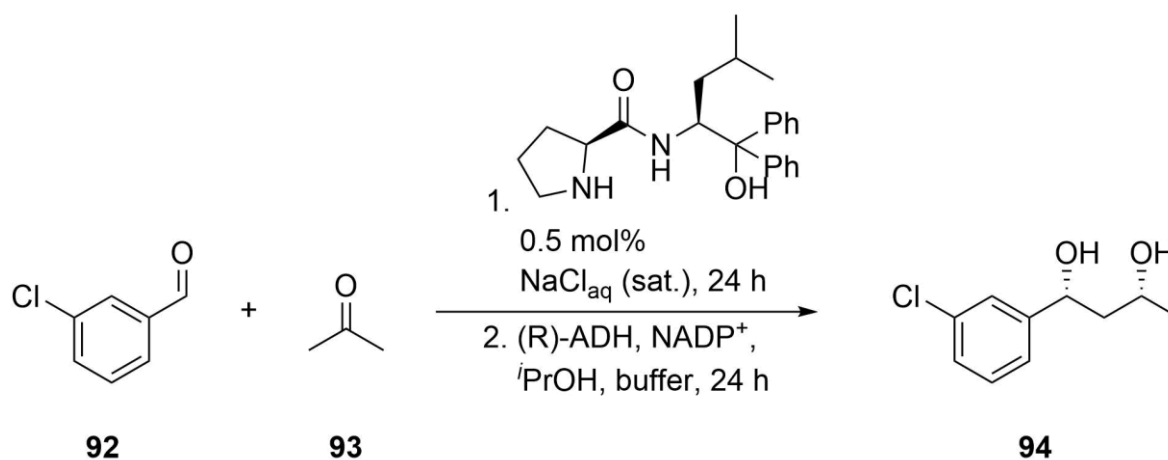
A few concepts are already used for some chemoenzymatic tandem reactions. On the one hand, it is possible to separate the reaction temporally and use a stepwise reaction or the two reactions can be separated locally by a membrane or in a two-phase system. On the other hand, the catalyst can be immobilized on a surface, in nanoparticles or in supramolecular structures. For immobilized catalysts also flow chemistry can be used. In the following part selected examples for the successful application of these different concepts are given.^[114]

One way to immobilize and protect different catalysts is the use of metal-organic frameworks (MOF). Lee *et al.*^[116] presented a MOF, which was functionalized with a cobalt(II) methylimidazole complex, Palladium nanocrystals (NC) and candida antarctica lipase A (CalA). This MOF can be used for a nitroaldol-DKR(dynamic kinetic resolution)-esterification, where the cobalt(II) ion activates the aldehyde (**86**) for a nitroaldol reaction, while the CalA selectively converts the *R*-enantiomer of the racemic nitroaldol product (**89**) in an esterification with vinyl acetate (**88**). An enrichment of the *S* enantiomer (**91**) is prevented by racemization of **91** catalyzed by the Pd NC (Scheme 23). Another advantage of the MOF is that it can be easily separated from the reaction mixture and can be recycled, even though there is a loss in activity.^[116]



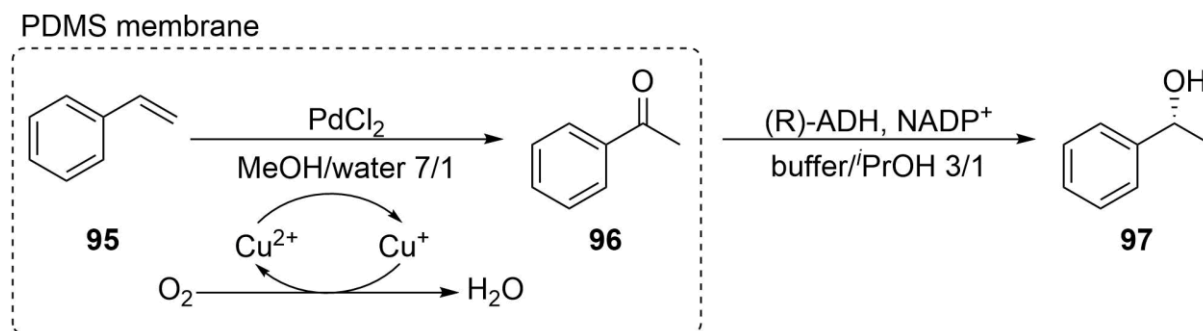
Scheme 23. Reaction scheme of chemoenzymatic cascade reaction of a nitroaldol-DKR-esterification and scheme of a pore of the used MOF (Co²⁺: pink, Pd NC and CalA).

An additional way to combine an enzymatic and a chemical catalyst is by separation in a temporal or spatial manner. For example, in a stepwise reaction a stereoselective aldol reaction of 3-chloro benzyl aldehyde (**92**) with acetone (**93**) is followed by a stereoselective enzymatic reduction to yield (1*R*,3*R*)-1-(3-chlorophenyl)butane-1,3-diol (**94**, Scheme 24).^[117]



Scheme 24. Stepwise tandem reaction, combining an aldol reaction and a subsequent enzymatic reduction using alcohol dehydrogenase (ADH).

A Wacker oxidation using $\text{CuCl}/\text{PdCl}_2$ as catalyst can be successfully combined with an enzymatic reduction of the ketone *via* compartmentalization of the two reactions. A polydimethylsiloxane (PDMS) membrane enables diffusion of the organic substrate and intermediate but withholds the copper ions (Scheme 25). Firstly, styrene (**95**) is oxidized to acetophenone (**96**). **96** can diffuse through the PDMS membrane and the ketone is reduced by ADH to finally yield phenylethanol (**97**).^[118]



Scheme 25. Compartmentalization of a Wacker oxidation and an enzymatic reduction.

2.6 Microgels

Microgels are macromolecular networks in the colloidal size range and are swollen by the solvent. Colloids are divided in three major groups: micellar aggregates, flexible macromolecules and rigid particles. However, microgels cannot be categorized in one of these three parts, as they show properties of all three categories (Figure 12).^[119]

The microgel architecture can be modified by the used monomers, the crosslinker concentration and the polymerization technique. Therefore, a huge variety of different architecture can be synthesized: for example core shell microgels,^[120] Janus-like microgels,^[121] rod-like microgels,^[122] hollow microgels^[123] or ultra-low crosslink microgels.^[124] The variety of different architectures leads to microgels with tunable properties. For example, temperature responsible microgels,^[125] pH responsible microgels^[126] or light responsible microgels have been reported.^[127] Building on the different architectures and properties many applications of microgels are possible.^[128] Microgels can be used as carrier for guest molecules,^[129] for a more efficient delivery of nutrients to plants,^[130] for the immobilization of catalysts^[131] and enzymes^[132] or to stabilize liquid-liquid interfaces^[133].

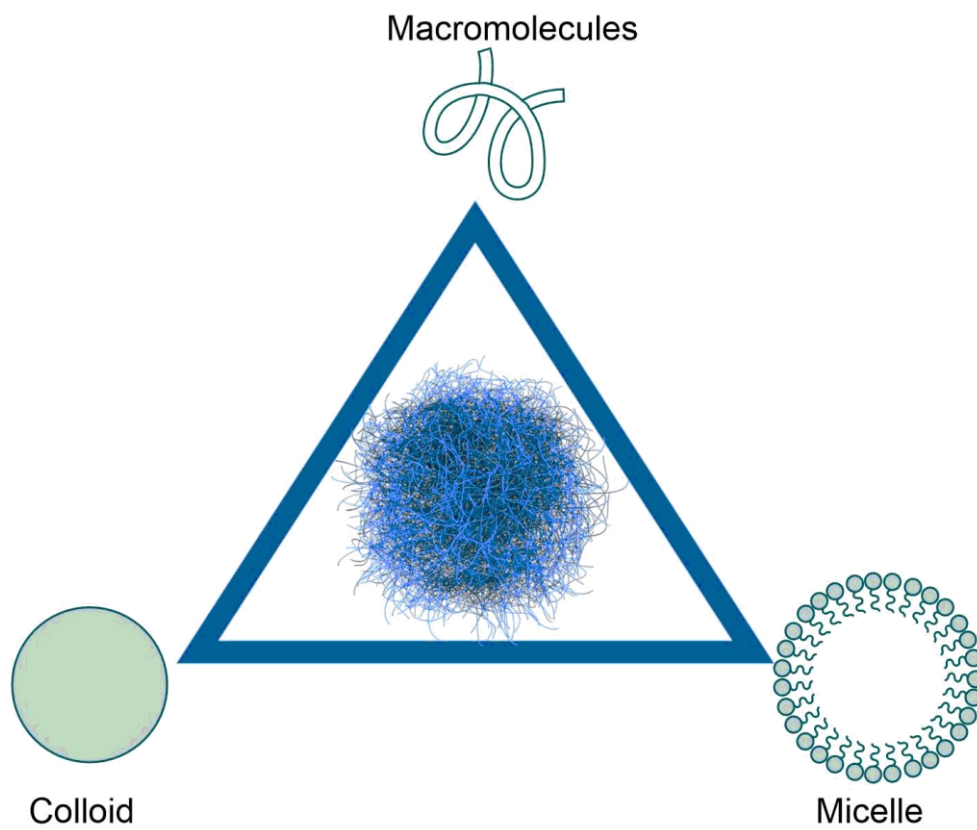


Figure 12. Overview over the different colloid parts and microgel in the center. Adapted from the literature.^[119]

3. Objectives and Contents

3.1. Objectives

This PhD thesis is motivated by the exploration of the reactivity of bis(pyrazolyl)methane complexes in a variety of cross-coupling reactions. In the introduction the predominance of poly(pyrazolyl)methane and poly(pyrazolyl)borate as ligand in catalytic reactions was described (chapter 2.1). In contrast the investigation of the potential of heteroscorpionate is still in its infancy. One reason for the predominance of poly(pyrazolyl) homoscorpionate ligands is the limited synthetic accessibility of carbon-based heteroscorpionate ligands. However, the development of new synthetic approaches for the synthesis of carbon-based heteroscorpionate ligands leads to more catalytic applications for them (see chapter 2.2). The reactivity of bis(pyrazolyl)methane complexes, which are the focus of this thesis, is on the one hand the amination of unactivated C–H bonds *via* a nitrene intermediate and, on the other hand, the synthesis of benzofurans *via* a modified Sonogashira coupling reaction.

The first reactivity investigated is the transfer of a nitrene moiety by a copper complex to different substrates. Beside the reactivity also the key intermediate of these reactions, a copper nitrene complex, should be investigated. As explained in chapter 2.4 copper nitrene complexes are elusive species and only few examples were described before. In this thesis it is aimed to synthesize a series of modified bis(pyrazolyl)methane ligands to yield copper nitrene complexes. It is envisioned to develop a general concept from this series for the ligand design to achieve either a very stable or a very reactive copper nitrene complex or to join both properties. Therefore, a series of ligands with different third *N* donor groups is synthesized. While the general coordination geometry is only changed in details the electronic structure is influenced significantly by the variation of the third *N* donor group. In the next step, the catalytic scope of bis(pyrazolyl)methane copper nitrene complexes is increased. The aziridination of internal double bond and the amination of aromatic substrates is evaluated. Not just the reactivity is investigated but also the enantioselectivity of the mediated reactions. To achieve this, chiral pyrazolyl units were used. Parallel to the optimization of the ligand design, also the use of nitrene generating agent with a high atom efficiency is investigated. In the last step, the metal in the complex was changed from copper to iron and the potential formation of iron nitrene complexes was investigated.

In the context of the SFB 985 in the subproject A1 the development of tandem reactions was targeted. The tandem reaction should combine the hydroxylation chemistry of the enzyme P450 and the cross-coupling chemistry of copper bis(pyrazolyl)methane complexes. The enzymatic part of the tandem reaction was investigated in collaboration with the Schwaneberg

working group (RWTH Aachen University, Institute of Biotechnology). Two approaches for the tandem reaction were investigated. The first is the combination of the aromatic hydroxylation of *para*-xylene by a P450 BM3 variant. The obtained phenol derivative can then be further converted by a copper catalyzed *O*-arylation. The second approach is to combine the copper catalyzed synthesis of benzofuran derivatives from iodophenol and alkynes *via* an enzymatic hydroxylation. Modified benzofuran derivatives are a motif which shows interesting pharmaceutical behavior.^[134] Further optimization of the tandem reaction should be obtained by immobilization of the enzyme and the copper catalyst in a microgel. On the one hand, this should protect both catalysts and, on the other hand, it should enable facile recycling of the catalyst.

3.2. Contents

The results of this PhD thesis are discussed in chapter 4. The basis is a library of bis(pyrazolyl)methane ligands, which has been prepared in order to achieve higher activity and stability of the copper nitrene complexes and enantio-selective reactivity. In chapter 4.1 the synthesis of literature-known and novel ligands with a focus on the synthesis of novel ligands will be presented. The ligands are divided into two groups based on their synthetic strategy. The first group is synthesized by the Peterson rearrangement (see chapter 2.1.1), this group includes the majority of the ligands. The second group is synthesized *via* postmodifying ligands of the first group. This was achieved by the introduction of a leaving group either into the aldehyde before the Peterson rearrangement or into the ligand itself. The leaving group was subsequently substituted by the desired functional group.

In the next step, the ligands were used for the synthesis and crystallization of copper(I) complexes with a weak coordinating coligand. The aim was to obtain structural information about the copper complexes from single crystal X-ray analysis and further information from different spectroscopic methods. This is discussed in chapter 4.2. The desired complex coordination motif is a monofacial coordination motif and the parameters towards their formation are discussed.

Afterwards, copper nitrene complexes were generated from different copper(I) acetonitrile complexes with various nitrene generating agents. The successfully generated stable copper nitrene complexes are characterized by a variety of experimental (including cyro-ESI-MS, UV/Vis- and NMR spectroscopy) and theoretical methods, and catalytic C–H aminations and aziridinations were performed, which are described in chapter 4.3. Besides the often used iminoiodane ^sPhINTs different organic azides were used as nitrene generating agent. The influence of the ligand design on the copper nitrene complex and on the generating reaction

will be discussed. The generated nitrenes were stabilized by low temperature in dichloromethane. Additionally, the substrate scope of the catalytic C–H amination and the aziridination reaction were increased. Furthermore, a successful C–H amination and aziridination protocol with benzoyl azide as nitrene generating agent and $[\text{Cu}\{\text{HC}(\text{Ph}_2\text{Pz})_2\text{DMAP}\}(\text{MeCN})]\text{PF}_6$ was developed.

The next aim was to generate iron nitrenes from $[\text{Fe}\{\text{Me}(\text{Py})_2\text{Bpy}\}(\text{MeCN})_2](\text{OTf})_2$ and different nitrene generating agents. This is discussed in chapter 4.4. The reaction was performed in different solvents at different temperatures.

In the framework of the SFB 985 in the subproject A1 the aim was to perform a successful tandem reaction between a copper bis(pyrazolyl)methane catalyzed cross-coupling reaction and a hydroxylation by a P450 BM3 variant. Therefore, two different tandem reactions were designed, a C–C coupling followed by the hydroxylation and a hydroxylation followed by a C–O cross-coupling. The successful optimization of the reaction conditions of the first tandem reaction is presented in chapter 4.5.

The last step was to increase the reaction scope of copper loaded microgels. Therefore, these microgels were tested as catalyst for the Henry reaction. This is described in chapter 4.6.

4. Results and discussion

4.1 Ligand synthesis

In this thesis different ligands of the bis(pyrazolyl)methane family were synthesized. These ligands will be discussed by their synthesis approach and not by their application. For every application the ligand design was adapted on different aspects (Figure 13).

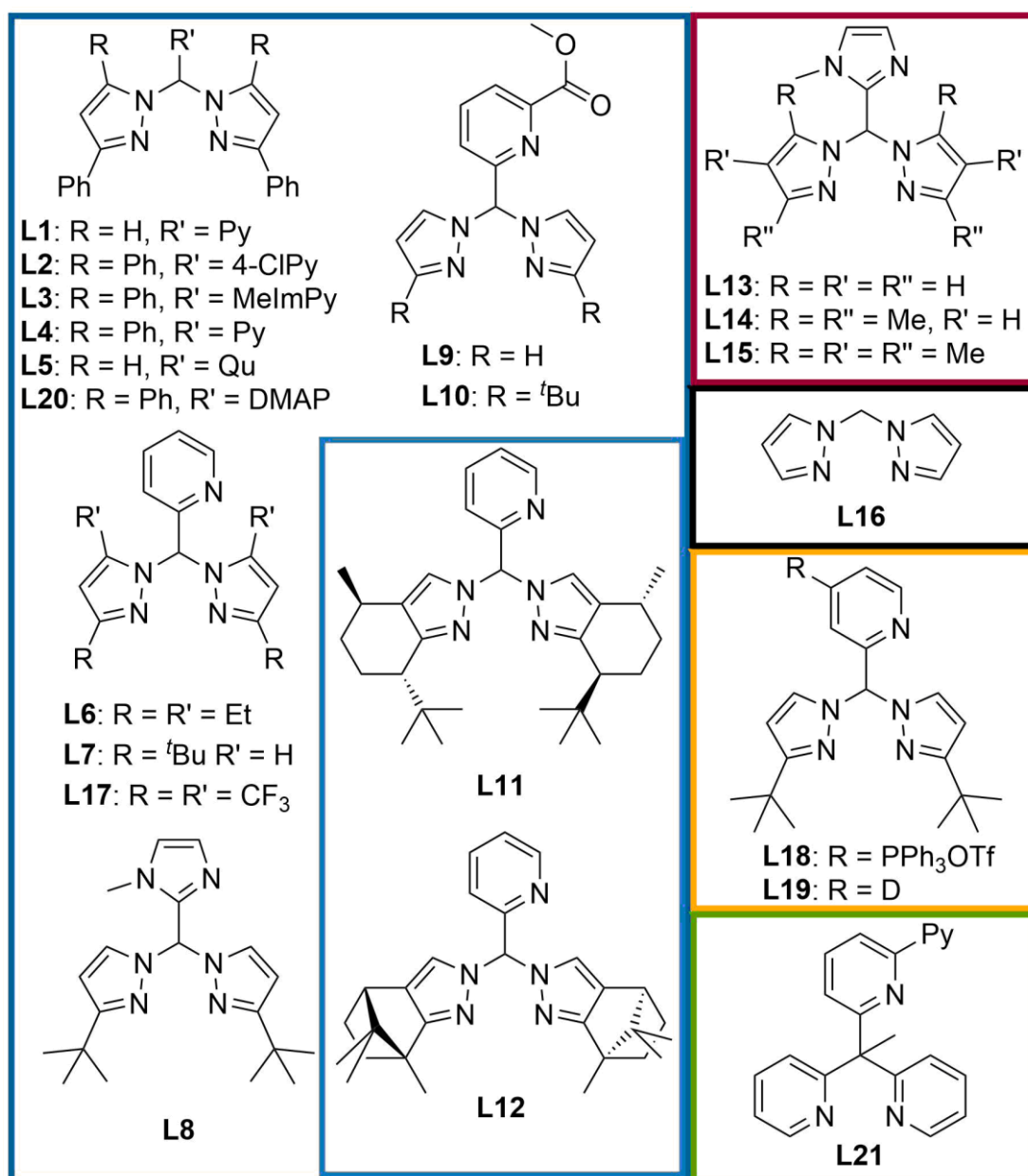
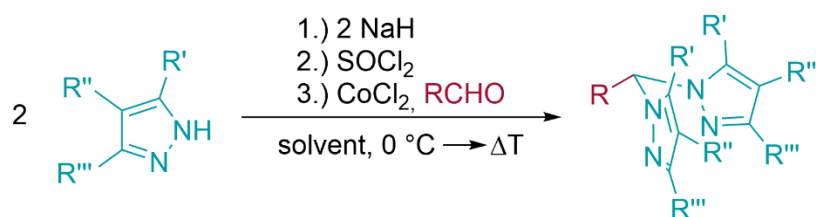


Figure 13. Overview of all ligands used in this thesis sorted by their application. Blue: Copper nitrene chemistry, light blue: chiral copper nitrene chemistry, red: Sonogashira cross coupling reaction, black: oxidation of benzyl alcohols, orange: postmodification of bis(pyrazolyl)methane ligands, green: iron nitrene chemistry.

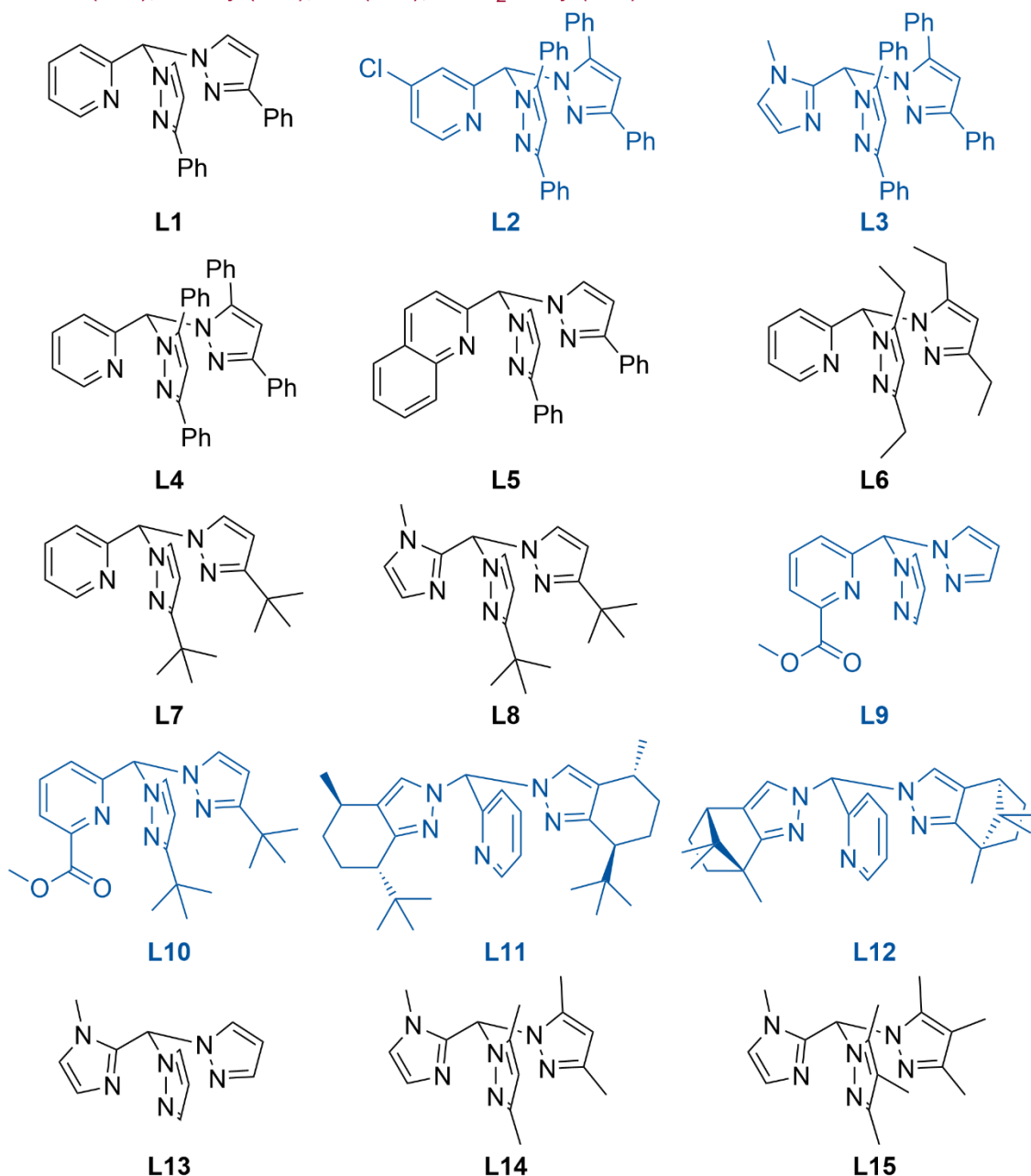
For the copper nitrene chemistry, ligands with different third *N* donor units and aromatic substituted pyrazole units were synthesized (**L1-L5**, **L20**). As third *N* donor unit pyridine, methyl imidazolyl, 4-chloropyridine and dimethylamine pyridine were used. In addition, the phenyl substituent of the pyrazole unit should be modified by chlorido substituents, but the desired diketone could not be reproduced from the literature.^{[135],[136]} Also, different aliphatic pyrazole units were tested (**L6-L8**, **L11**, **L12**, **L17**). For the enantio-enriched C–H amination and aziridination reactions, two chiral ligands were synthesized (**L11**, **L12**). The ligands **L11** and **L12** have pyrazolyl units which are based on molecules from the chiral pool. To increase steric demand on the third *N* donor unit an ester group in the 6 position of pyridine was introduced (**L9**, **L10**). For Sonogashira cross-coupling reactions ligands with an increasing number of methyl groups on the pyrazole were synthesized (**L13-L15**). For the oxidation of benzyl alcohol in addition a bidentate ligand (**L16**) was resynthesized. Also, a new way of post modifying bis(pyrazolyl)methane ligands was developed to synthesize new ligands (**L18**, **L19**). For the iron nitrene chemistry, a tetradentate ligand was resynthesized (**L21**). In the following chapters only, aspects of the synthesis of ligands will be discussed, which were not reported in the literature before.

4.1.1 Ligand synthesis by a Peterson rearrangement

The first synthesis approach for bis(pyrazolyl)methane ligands is the Peterson rearrangement, which leads to various ligands (Scheme 26). The Peterson rearrangement is a well-established one-pot reaction to yield different bis(pyrazolyl)methane ligands in good yields starting from various pyrazoles and aldehydes (see Chapter 2.1.1, Scheme 6).^{[29],[137]} In the first reaction step a pyrazole derivative (**1**, **97-104**) is deprotonated by sodium hydride in THF. The deprotonated step can be completed often at 0 °C, while for the pyrazole **98** heating of the reaction mixture is mandatory to achieve a complete deprotonation to ensure a high yield of the desired ligand (**L2-L4**). After the deprotonation two pyrazolates are bridged with thionyl chloride. The bis(pyrazolyl)sulfonyl reacts with a suitable aldehyde in a cobalt(II) chloride catalyzed rearrangement (**105-109**).



R' = R'' = H, R''' = Ph (**97**); R' = Ph, R'' = H, R''' = Ph (**98**); R' = Et, R'' = H, R''' = Et (**99**); R' = R'' = H, R''' = *t*Bu (**100**); R' = R'' = R''' = H (**1**); R' = H, R'' = R''' = Pul (**101**); R' = H, R'' = R''' = Cam (**102**); R' = Me, R'' = H, R''' = Me (**103**); R' = R'' = R''' = Me (**104**); **R = Py (105), Melm (106), 4-ClPy (107), Qu (108), 6-CO₂MePy (109)**



Scheme 26. Ligand synthesized according to a modified Peterson rearrangement. The syntheses of the blue marked ligands were developed in this thesis. Ligands **L1**^[29], **L4**^[137], **L5**^[29], **L6**^[137], **L7**^[29], **L8**^[40], **L13**^[138] and **L14**^[139] were resynthesized according to literature. The synthesis of **L15**^[140] was modified from the literature.

By this synthetic protocol the ligands **L1-L15** were synthesized in overall good yields (above 59%, Scheme 26). Only for the ligands **L3**, **L12** and **L15** lower yields were obtained. The yield of ligand **L3** can be increased when the solvent of the reaction is switched from THF to toluene (from 5% up to 49%). For **L12** the main reason for the low yield of 26% is the problematic isolation of the ligand. During the work-up of **L12** a series of chromatographic columns were performed, but only parts of the product could be isolated, even though different stationary phases and a variety of eluents mixtures were applied. In contrast the literature known reaction protocol for the synthesis of the ligand **L15** was successfully modified.^[140] In the literature the Peterson rearrangement is catalyzed by pyridine and the yield is 22%, while the performed synthesis with cobalt(II) chloride as catalyst leads to a yield of 33%.

For the ligand **L2** crystals suitable for single crystal X-ray diffraction were obtained from a concentrated solution in dichloromethane and vapor diffusion of pentane. The molecular structure is shown in Figure 14 and selected bond lengths and angles are presented in Table 1. The crystallographic details are provided in Table 51 in the Appendix. The ligand crystallizes triclinic in the space group $P\bar{1}$ with $Z = 2$. The bond angles around C(ap) deviate slightly from ideal tetrahedral angles.

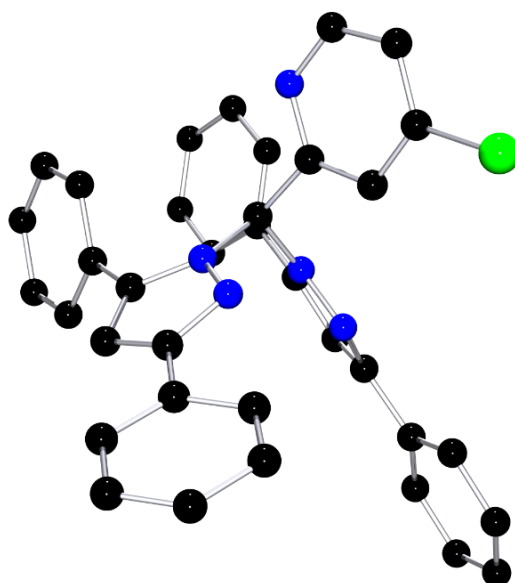


Figure 14. Molecular structure of **L2** in the solid-state. Hydrogen atoms were omitted for clarity.

Table 1. Selected bond lengths [Å] and angles [°] for **L2**.

Bond lengths		Bond angles	
C(ap) – C(Py)	1.521(4)	N(Pz) – C(ap) – N(Pz')	110.3(2)
C(ap) – N(Pz)	1.458(4)	N(Pz) – C(ap) – C(Py)	111.3(2)
C(ap) – N(Pz')	1.461(1)	N(Pz') – C(ap) – C(Py)	113.7(2)

Suitable crystals for single X-ray diffraction of **L3** were obtained analogously to **L2**. In Figure 15 the molecular structure is shown and selected bond angles and lengths are highlighted in Table 2. The crystallographic details are provided in Table 51 in the Appendix. Ligand **L2** crystallizes monoclinic in the space group $P2_1/n$ with $Z = 4$. In accordance with **L2** the bond angles around the apical carbon atom in **L3** deviate slightly from ideal tetrahedral angles.

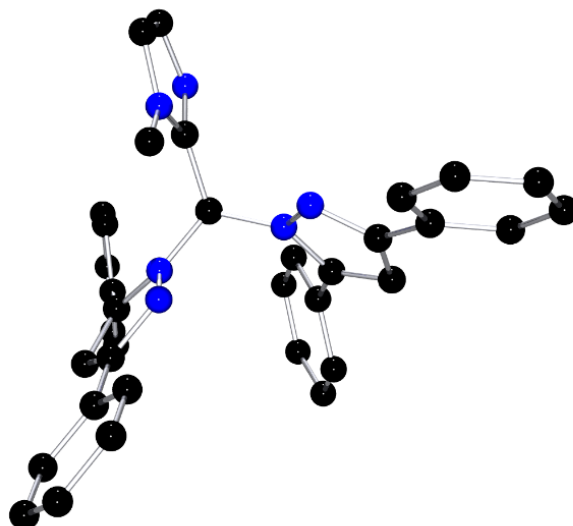


Figure 15. Molecular structure of **L3** in the solid-state. Hydrogen atoms were omitted for clarity.

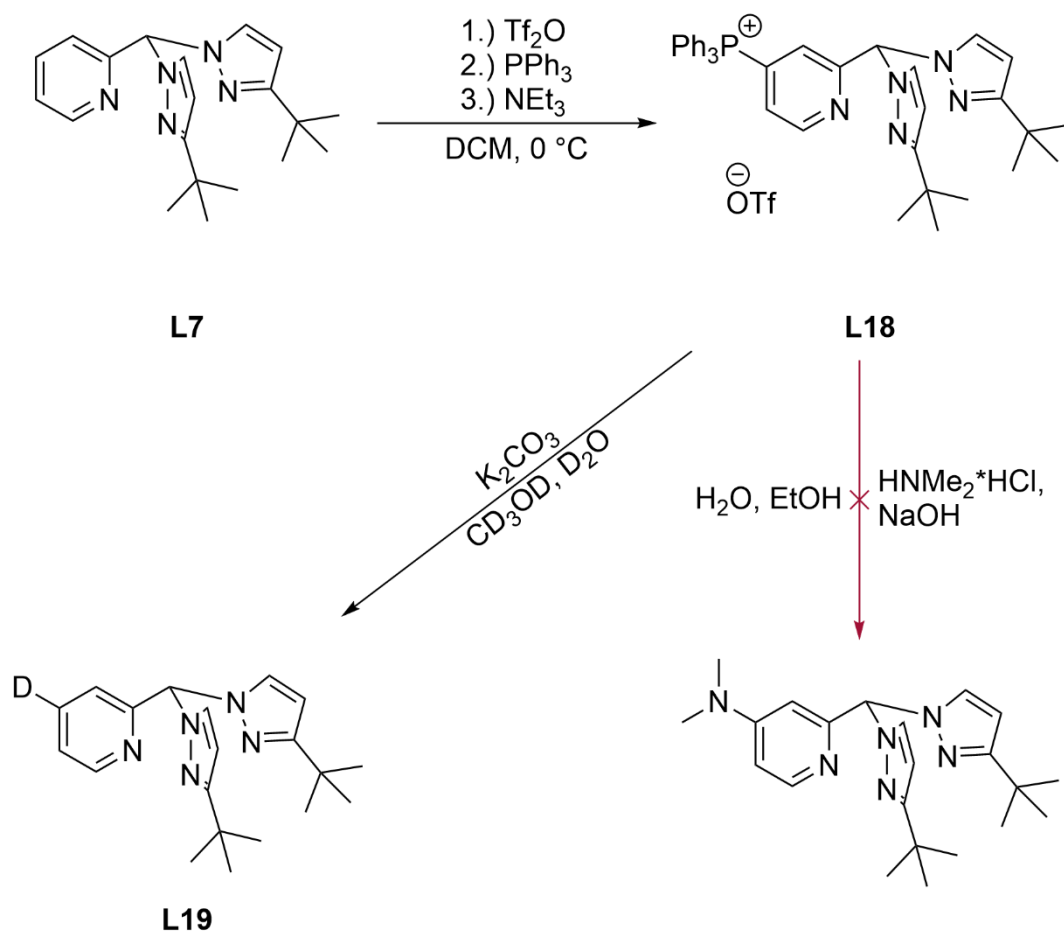
Table 2. Selected bond lengths [Å] and angles [°] for **L3**.

Bond lengths		Bond angles	
C(ap) – C(Melm)	1.509(3)	N(Pz) – C(ap) – N(Pz')	110.7(2)
C(ap) – N(Pz)	1.456(3)	N(Pz) – C(ap) – C(Melm)	112.6(2)
C(ap) – N(Pz')	1.464(3)	N(Pz') – C(ap) – C(Melm)	116.3(2)

4.1.2 Post-modification of bis(pyrazolyl)methane ligands

The second approach for the synthesis of new bis(pyrazolyl)methane ligands in this thesis is the post-modification of a bis(pyrazolyl)methane ligand which was investigated, because there are some pyridinyl carboxaldehydes which are not suitable for the Peterson rearrangement.^{[103],[141]} In this thesis three different ways for the post-modification were investigated. The first route starts from a bis(pyrazolyl)methane ligand, in this case **L7**, to synthesize a phosphonium salt (**L18**, Scheme 27). In the first step trifluoromethanesulfonic anhydride is added to **L7** to form a 1-((trifluoromethyl)sulfonyl)pyridin-1-ium cation. In this cation the *para*-position is activated so the added triphenylphosphane can attack this position. By the addition of a suitable base, in this case triethylamine, the desired ligand is obtained. It was shown by the working group of McNally that the synthesis of the phosphonium salt starting from different pyridine

derivatives forms selectively the *para*-substituted phosphonium salt. These salts can be used in a variety of C–X cross-coupling reactions.^{[142]–[146]}



Scheme 27. Overview of the synthesis of **L18** and further post-modifications of **L18**.

The obtained ligand **L18** was isolated and fully characterized and in the next step the triphenyl phosphonium unit should be further substituted. On the one hand, the pyridine should be modified with a deuterium atom, as a prove of principle for the possible substitution of the phosphonium group. And on the other hand, a dimethylamine group should be introduced to the ligand (Scheme 27). While the substitution of the phosphonium group with a deuterium atom could be achieved by a reaction with potassium carbonate in methanol-*d*₄ and deuterium oxide at room temperature to yield **L19**, the substitution with dimethylamine under high pressure at high temperature in a mixture of water and ethanol was not successful and only **L7** was observed in the NMR spectra. Another possible reaction could be the palladium-catalyzed Buchwald-Hartwig cross-coupling, which might be used in further investigations. In addition, it could be shown by Regina Schmidt that the ligand **L18** can coordinate to copper(I) chloride and that the substitution of the phosphonium group with an alcohol does not yield the desired ether.¹

¹ Unpublished results from the bachelor thesis of Johannes Beißmann, RWTH Aachen University, 2020 supervised by Regina Schmidt in the working group of Prof. Sonja Herres-Pawlis.

Crystals suitable for single crystal X-ray diffraction were achieved for the ligand **L18** at -32 °C in a mixture of diethyl ether and dichloromethane. The molecular structure of the cation of **L18** is shown in Figure 16 and selected bond lengths and angles are pointed out in Table 3. The crystallographic details are provided in Table 52 in the Appendix. The space group of **L18** is $P\bar{1}$ and it crystallizes triclinic with $Z = 2$. The bond angles around the phosphorous atom as well as the bond angles around C(ap) differ only slightly from the angles of an ideal tetrahedron. The bonds lengths between the phosphorus atom to the four surrounding carbon atoms do not vary significantly.

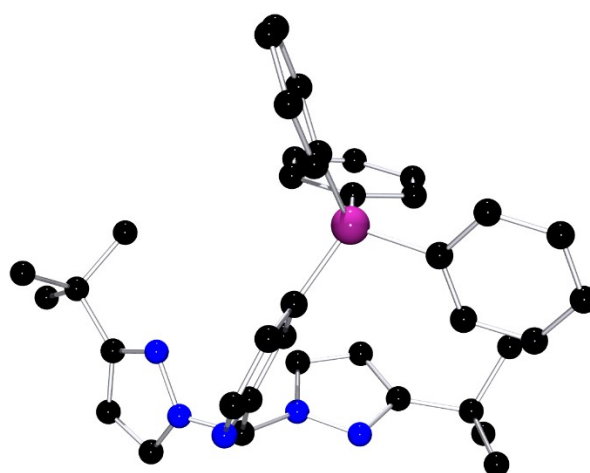


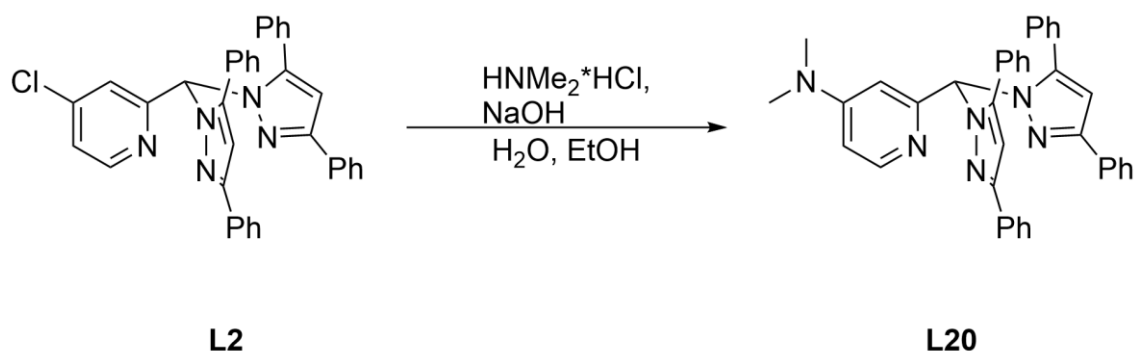
Figure 16. Molecular structure of $\{HC('BuPz)_2(4-PPh_3Py)\}^+$ in crystals of **L18** in the solid-state. Hydrogen atoms were omitted for clarity.

Table 3. Selected bond lengths [Å] and angles [°] for **L18**.

Bond lengths		Bond angles	
C(ap) – C(Py)	1.526(3)	N(Pz) – C(ap) – N(Pz')	109.6(2)
C(ap) – N(Pz)	1.440(3)	N(Pz) – C(ap) – C(Py)	112.1(2)
C(ap) – N(Pz')	1.465(3)	N(Pz') – C(ap) – C(Py)	109.3(2)
P – C(Py)	1.810(2)	C(Py) – P – C(Ph)	113.1(1)
P – C(Ph)	1.798(2)	C(Py) – P – C(Ph')	107.1(1)
P – C(Ph')	1.796(2)	C(Py) – P – C(Ph'')	105.8(1)
P – C(Ph'')	1.794(2)	C(Ph) – P – C(Ph')	110.7(1)
		C(Ph) – P – C(Ph'')	111.3(1)
		C(Ph') – P – C(Ph'')	108.7(1)

The second synthetic route for the post-modification of bis(pyrazolyl)methane ligands is to synthesize a chlorido substituted ligand, in this case **L2**. In the next step the chlorine atom can be substituted by a suitable nucleophile. As a first reaction the substitution with dimethylamine

under high pressure in a mixture of ethanol and water was chosen (Scheme 28). The substitution reaction was successful and ligand **L20** was isolated in good yields.



Scheme 28. Synthesis of **L20** starting from **L2**.

Crystals of **L20** suitable for single crystal X-ray diffraction were obtained, analogous to **L2** and **L3**, from a concentrated solution in dichloromethane by vapor diffusion of pentane. The molecular structure of **L20** is presented in Figure 17 and selected bond lengths and angles are highlighted in Table 4. The crystallographic details are provided in Table 52 in the Appendix. **L20** crystallizes monoclinic in the space group $P2_1/n$ with $Z = 4$. In addition, it is observable that the dimethylamine pyridine group is almost planar. The environment found around C(ap) is almost perfect tetrahedral. When the bond lengths and bond angles of **L2** and **L20** are compared it can be observed that the substitution of the chloride with a dimethylamine group does not influence the solid-state structure significantly.

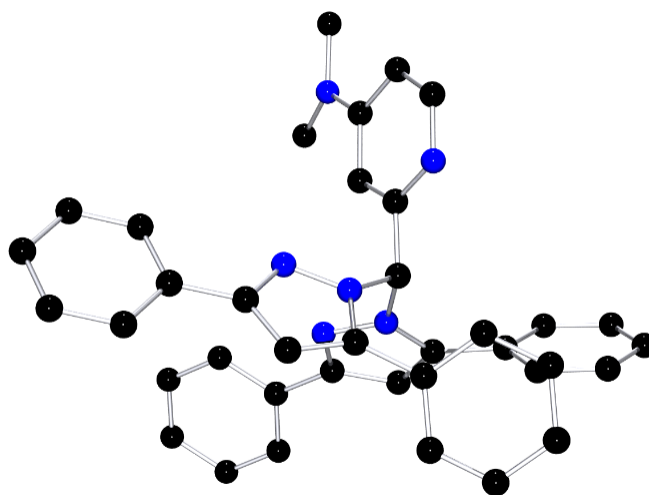


Figure 17. Molecular structure of **L20** in the solid-state. Hydrogen atoms were omitted for clarity.

Table 4. Selected bond lengths [Å] and angles [°] for **L20**.

Bond lengths		Bond angles	
C(ap) – C(Py)	1.516(2)	N(Pz) – C(ap) – N(Pz')	110.0(1)
C(ap) – N(Pz)	1.456(2)	N(Pz) – C(ap) – C(Py)	110.8(1)
C(ap) – N(Pz')	1.467(2)	N(Pz') – C(ap) – C(Py)	114.5(1)

The last post-modification was the methylation of **L12** in the apical position of the ligand. Therefore, **L12** was deprotonated by different bases in apical position and subsequently methylated with methyl iodide. However, the desired product was not obtained.

4.2 Synthesis and characterization of the complexes

A variety of different copper and iron complexes have been synthesized from the previously described ligand library. The complexes were used for different C–X cross-coupling reactions. While for some application (C–O, C–C cross-coupling) the complexes were synthesized *in situ*, for other applications (C–N cross-coupling, nitrene chemistry) a well-defined complex is crucial. For a tailor-made catalyst not only the ligand design of the used bis(pyrazolyl)methane ligand is important, but also the coligand and the copper source. The mainly used copper source was tetrakis(acetonitrile)copper(I) hexafluoridophosphate, but also copper halides and bis(hexamethylbenzene)copper(I) hexafluoridophosphate were used. However, the desired coordination motif $[\text{CuL}(\text{coligand})]\text{PF}_6$ was only achieved by using tetrakis(acetonitrile)copper(I) hexafluoridophosphate. When bis(hexamethylbenzene)copper(I) hexafluoridophosphate was used only complexes with $[\text{Cu}_2\text{L}_2](\text{PF}_6)_2$ or $[\text{CuL}_2]\text{PF}_6$ coordination motif were observed. For the application in C–N cross-coupling reactions also the synthesis of neutral complexes of **L7** and **L8** was targeted. The synthesis approach is based on the synthesis of neutral iron(II) tris(pyrazolyl)methanide complexes.^[23] Therefore, it was tried to deprotonate the apical position with *n*-butyllithium, potassium *tert*-butoxide or sodium bis(trimethylsilyl)amide as free ligand or when coordinated on a copper atom. In all cases either a coordination of the bis(trimethylsilyl)amide or a disproportionation can be observed.

Most copper(I) acetonitrile complexes ($[\text{CuL}(\text{MeCN})]\text{PF}_6$) were successfully synthesized by the slow addition of a solution of the ligand to a solution of tetrakis(acetonitrile)copper(I) hexafluoridophosphate in dichloromethane. The complexes were isolated by the addition of pentane. Both solutions can have high a concentration. In some cases, the formation of a complex with a $[\text{Cu}_2\text{L}_2](\text{PF}_6)_2$ or $[\text{CuL}_2]\text{PF}_6$ coordination motif can be observed. To prevent the formation of this coordination motif the concentration can be decreased, and the solvent can be switched to THF or acetone. All copper(I) acetonitrile complexes synthesized are highly air-stable in the solid-state, while a solution of the copper(I) complex will be oxidized within a few hours.

In the following chapters aspects of the synthesis of the used complexes will be discussed, which were not reported in the literature before. The complexes will be discussed in the order of the ligand used in the complex.

4.2.1 Synthesis and characterization of copper(I) complexes of **L1**

The complex **C1** ($[\text{Cu}\{\text{HC}(\text{PhPz})_2\text{Py}\}(\text{MeCN})]\text{PF}_6$) can be synthesized from ligand **L1** and $[\text{Cu}(\text{MeCN})_4]\text{PF}_6$ in THF. In principle the synthesis is also possible in DCM, but the THF facilitates the crystallization of **C1**, which leads to a more efficient isolation procedure. For the

copper(I) complex **C1** crystals suitable for single crystal X-ray diffraction were received from a concentrated solution in THF by layering with diethyl ether. The cation structure is shown in Figure 18 and chosen bond lengths and angles are highlighted in Table 5. The crystallographic details are provided in Table 53 in the Appendix. The complex crystallizes monoclinic with $Z = 4$ in the space group $P2_1/n$. The coordination geometry of a copper complex with four coordination sites can be described with the help of the τ_4 parameter.^[147] For a tetrahedral coordination geometry a value of 1 is obtained, while a square planar coordination geometry leads to value of 0. The τ_4 parameter is calculated from the two largest angles (α and β) at the copper ion and is defined as $\tau_4 = (360^\circ - (\alpha + \beta))/141^\circ$.

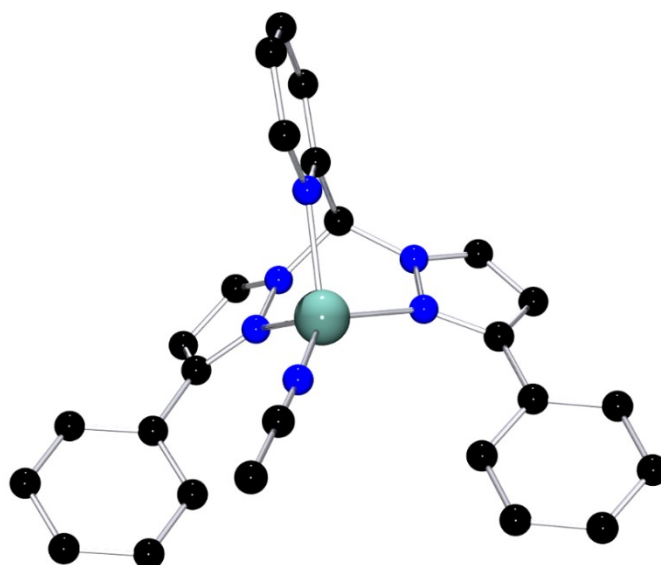


Figure 18. Molecular structure of $[\text{Cu}\{\text{HC}(\text{PhPz})_2\text{Py}\}(\text{MeCN})]^+$ in crystals of **C1**. Hydrogen atoms were omitted for clarity.

Table 5. Selected bond lengths [\AA] and angles [$^\circ$] for **C1**.

Bond lengths		Bond angles	
C(ap) – C(Py)	1.515(4)	N(Pz) – C(ap) – N(Pz')	109.7(3)
C(ap) – N(Pz)	1.458(4)	N(Pz) – C(ap) – C(Py)	118.3(3)
C(ap) – N(Pz')	1.456(4)	N(Pz') – C(ap) – C(Py)	112.4(3)
Cu – N(MeCN)	1.872(3)	N(MeCN) – Cu – N(Pz)	122.2(1)
Cu – N(Pz)	2.066(3)	N(MeCN) – Cu – N(Pz')	132.3(1)
Cu – N(Pz')	2.067(3)	N(MeCN) – Cu – N(Py)	123.3(1)
Cu – N(Py)	2.090(3)	N(Py) – Cu – N(Pz)	89.0(1)
		N(Py) – Cu – N(Pz')	89.6(1)
		τ_4^a	0.74

^a $\tau_4 = \frac{360^\circ - (\alpha + \beta)}{141^\circ}$ [147]

The complex **C1** adopts a distorted tetrahedral geometry with a τ_4 parameter of 0.74, it also can be observed that the bond lengths of the three *N* donors of the ligand do not vary significantly. Additionally, the structure of **C1** was calculated using a dichloromethane solvent model and only insignificant deviations to the solid-state structure are observed (Table 58).

4.2.2 Synthesis and characterization of copper(I) complexes of **L2**

The complex **C2** ($[\text{Cu}\{\text{HC}(\text{Ph}_2\text{Pz})_2(4\text{-ClPy})\}(\text{MeCN})]\text{PF}_6$) was synthesized analogously to **C1** in dichloromethane and can be isolated by the addition of pentane. To achieve crystals suitable for X-ray diffraction a concentrated solution of **C2** in dichloromethane was layered with pentane. Selected bond lengths and angles are shown in Table 6 and in Figure 19 the cation structure is displayed. The crystallographic details are provided in Table 53 in the Appendix. The complex crystallizes triclinic in the space group $P\bar{1}$ with $Z = 2$. The solid-state structure of **C2** features two almost identical copper(I) complexes per asymmetric unit as well as three dichloromethane molecules. Only the bond lengths and bond angles of one copper(I) complex are given in Table 6. The coordination geometry of **C2** is distorted tetrahedral with a τ_4 parameter of 0.67. The Cu–N bonds length of the three *N* donors do not vary significantly. Furthermore, the structure of **C2** in solution was calculated using a dichloromethane solvent model and only insignificant deviations to the solid-state structure are observed (Table 58).

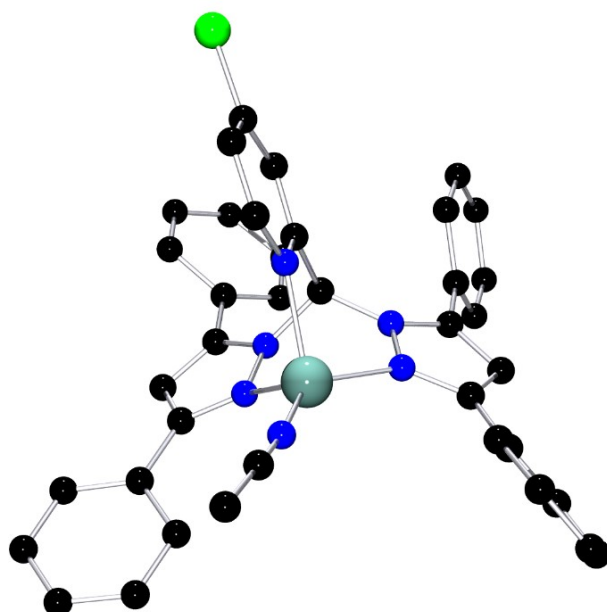


Figure 19. Molecular structure of $[\text{Cu}\{\text{HC}(\text{Ph}_2\text{Pz})_2(4\text{-ClPy})\}(\text{MeCN})]^+$ in crystals of **C2**. Hydrogen atoms were omitted for clarity.

Table 6. Selected bond lengths [Å] and angles [°] for **C2**.

Bond lengths		Bond angles	
C(ap) – C(Py)	1.514(10)	N(Pz) – C(ap) – N(Pz')	110.2(5)
C(ap) – N(Pz)	1.473(9)	N(Pz) – C(ap) – C(Py)	112.8(6)
C(ap) – N(Pz')	1.456(9)	N(Pz') – C(ap) – C(Py)	112.9(6)
Cu – N(MeCN)	1.888(6)	N(MeCN) – Cu – N(Pz)	142.1(3)
Cu – N(Pz)	2.047(6)	N(MeCN) – Cu – N(Pz')	123.4(3)
Cu – N(Pz')	2.124(6)	N(MeCN) – Cu – N(Py)	109.6(3)
Cu – N(Py)	2.116(6)	N(Py) – Cu – N(Pz)	90.7(2)
		N(Py) – Cu – N(Pz')	89.1(2)
		τ_4^a	0.67

$$^a \tau_4 = \frac{360^\circ - (\alpha + \beta)}{141^\circ} \quad [147]$$

4.2.3 Synthesis and characterization of copper(I) complexes of **L3**

Complex **C3** ($[\text{Cu}\{\text{HC}(\text{Ph}_2\text{Pz})_2(\text{Melm})\}(\text{MeCN})]\text{PF}_6$) was synthesized in dichloromethane and can be isolated by vapor diffusion of pentane. The product of the synthesis was not suitable for single crystal X-ray diffraction. Therefore, the complex was recrystallized from dichloromethane and pentane or chloroform and hexane or THF and diethyl ether. Further crystallization attempts used acetonitrile and diethyl ether, but stayed unsuccessful. While the first method leads to a microcrystalline product the latter two methods yielded crystal suitable for single crystal X-ray diffraction. Both methods do not yield crystals of **C3** but of the dinuclear complex **C4** ($[\text{Cu}_2\{\text{HC}(\text{Ph}_2\text{Pz})_2(\text{Melm})\}_2](\text{PF}_6)_2$). As the structure of the cation of **C4** are in both cases almost identical in the following only the data of the THF structure are given. The molecular structure of the cation is shown in Figure 20 and selected bonds length and bond angles are presented in Table 7. The crystallographic details for both structures are provided in Table 54 in the Appendix. In both cases four solvent molecules are included in the solid-state structure of **C4**. While **C4** crystallizes monoclinic in the space group $P2_1/c$ with $Z = 2$ from chloroform, it crystallizes triclinic in the space group $P\bar{1}$ with $Z = 1$ from THF. The complex adopts a distorted tetrahedral geometry with a τ_4 parameter of 0.69 and the copper–copper bond length is 2.568(1) Å.

In addition, it was investigated if **C3** also reacts to **C4** when in solution or only when recrystallized and if **C4** reacts to a monometallic complex when in solution. A reaction from **C3** in solution to **C4** could not be observed. On the one hand, the electrochemical properties of a solution of **C3** and **C4** are significantly different (Table 32) and, on the other hand, also the ^1H NMR spectra of **C3** and **C4** in dichloromethane- d_2 show that both species are different, for example

the apical hydrogen atom in **C3** has a chemical shift of 7.57 ppm, while in **C4** a chemical shift of 7.39 ppm is observed. Also, the coordination of the acetonitrile can be observed: while acetonitrile has a chemical shift of 2.10 ppm^[148] in **C3** a chemical shift of 2.15 ppm is observed. To investigate if there is a reaction of **C4** to a monometallic complex the complex [Cu{HC(Ph₂Pz)₂(Melm)}]SbF₆ (**C5**) was synthesized *in situ*. The synthesis of copper(I) bis(pyrazolyl)methane complexes with an empty coordination site is well-established and used for the synthesis of copper peroxide complexes.^[49] For the synthesis of **C5** copper(I) chloride and **L3** were combined in dichloromethane-*d*₂ and stirred overnight. Then silver hexafluoroantimonate was added for an anion exchange and a precipitate formed. The supernatant can be analyzed using ¹H NMR spectroscopy.

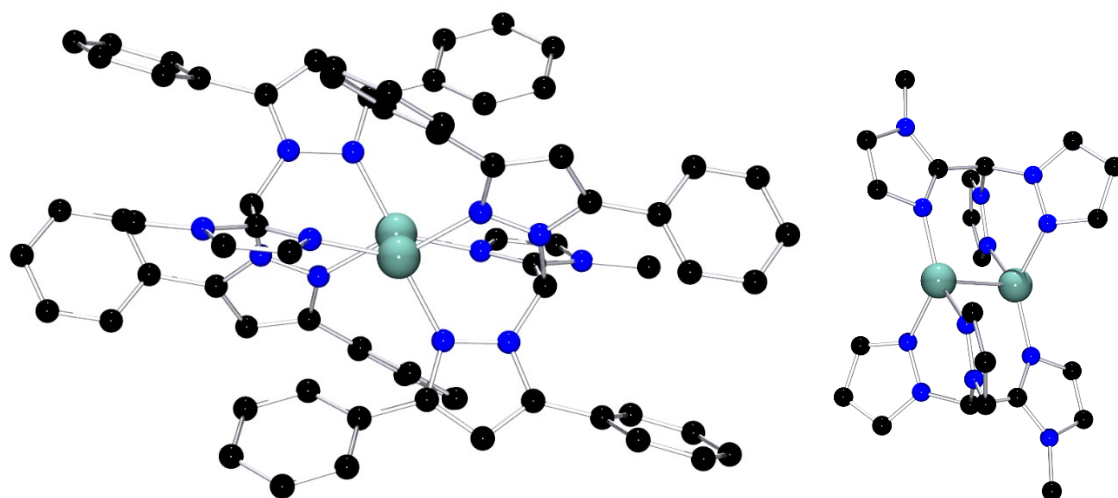


Figure 20. Left: Molecular structure of [Cu₂{HC(Ph₂Pz)₂Melm}₂]²⁺ in crystals of **C4**. Hydrogen atoms were omitted for clarity. Right: Side view on the molecular structure of **C4** in the solid-state, substituents on the pyrazolyl are omitted for clarity.

Table 7. Selected bond lengths [Å] and angles [°] for **C4**.

Bond lengths		Bond angles	
C(ap) – C(Melm)	1.499(4)	N(Pz) – C(ap) – N(Pz')	111.6(2)
C(ap) – N(Pz)	1.452(3)	N(Pz) – C(ap) – C(Melm)	114.1(2)
C(ap) – N(Pz')	1.463(3)	N(Pz') – C(ap) – C(Melm)	114.8(2)
Cu – Cu'	2.568(1)	Cu' – Cu – N(Pz)	99.7(1)
Cu – N(Pz)	2.014(2)	Cu' – Cu – N(Pz')	89.4(1)
Cu – N(Pz')	1.979(2)	Cu' – Cu – N(Melm)	99.2(1)
Cu – N(Melm)	1.913(2)	N(Melm) – Cu – N(Pz)	132.0(1)
		N(Melm) – Cu – N(Pz')	130.4(1)
		τ_4^a	0.69

$$^a \tau_4 = \frac{360^\circ - (\alpha + \beta)}{141^\circ} \quad [147]$$

It was observed that there is a significant difference in the chemical shift of the imidazole hydrogen atoms of **C4** and **C5**. Therefore, a reaction of **C4** to a monometallic complex in solution can be excluded. This also shows that **C3** and **C4** are stable in solution and the reaction only occurs when **C3** is recrystallized.

Additionally, the structure of **C3** and **C4** were calculated using a dichloromethane solvent model. For **C4** only insignificant deviations to the solid-state structure is observed (Table 58). For **C3** no molecular structure in the solid-state could be achieved. Therefore, no comparison is possible.

4.2.4 Synthesis and characterization of copper(I) complexes of **L9**

The complex **C9** ($[\text{Cu}\{\text{HC}(\text{Pz})_2(6\text{-CO}_2\text{MePy})\}(\text{MeCN})]\text{PF}_6$) was synthesized in acetone and can be isolated by the addition of pentane. Acetone was chosen as solvent, because the solubility of **C9** in dichloromethane is very low. Crystals of **C9** which are suitable for single crystal X-ray diffraction were obtained from a concentrated solution in dichloromethane by layering with pentane. The cation structure is shown in Figure 21 and selected bond lengths and angles are presented in Table 8. The crystallographic details are provided in Table 55 in the Appendix. **C9** crystallizes monoclinic with $Z = 4$ in the space group $P2_1/c$. The coordination geometry is a distorted tetrahedral geometry with a τ_4 parameter of 0.71 and the torsion angle between the carbonyl group and the pyridine is $4.8(1)^\circ$. The distance between the copper ion and the carbonyl oxygen atom is $2.820(2) \text{ \AA}$. Therefore, the oxygen atom does not coordinate the copper ion.

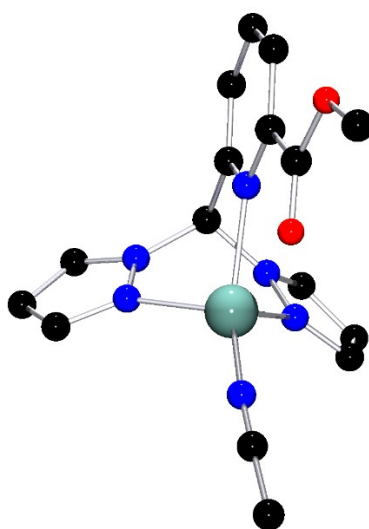


Figure 21. Molecular structure of $[\text{Cu}\{\text{HC}(\text{Pz})_2(6\text{-CO}_2\text{MePy})\}(\text{MeCN})]^+$ in crystals of **C9**. Hydrogen atoms were omitted for clarity.

Table 8. Selected bond lengths, atom distance [Å] and angles [°] for **C9**.

Bond lengths		Bond angles	
C(ap) – C(Py)	1.512(5)	N(Pz) – C(ap) – N(Pz')	110.3(3)
C(ap) – N(Pz)	1.450(5)	N(Pz) – C(ap) – C(Py)	112.2(3)
C(ap) – N(Pz')	1.455(5)	N(Pz') – C(ap) – C(Py)	111.8(3)
Cu – N(MeCN)	1.900(4)	N(MeCN) – Cu – N(Pz)	119.3(1)
Cu – N(Pz)	2.096(3)	N(MeCN) – Cu – N(Pz')	119.4(1)
Cu – N(Pz')	2.102(3)	N(MeCN) – Cu – N(Py)	140.8(1)
Cu – N(Py)	2.168(3)	N(Py) – Cu – N(Pz)	87.1(1)
Atom distance		N(Py) – Cu – N(Pz')	84.8(1)
Cu ... O(Carb)	2.820(2)	N(Py) – C – C – O(Carb)	4.8(1)
		τ_4^a	0.71

$$^a \tau_4 = \frac{360^\circ - (\alpha + \beta)}{141^\circ} \quad [147]$$

4.2.5 Synthesis and characterization of copper(I) complexes of **L10**

Complex **C10** ($[\text{Cu}\{\text{HC}(\text{tBuPz})_2(6\text{-CO}_2\text{MePy})\}(\text{MeCN})]\text{PF}_6$) was synthesized in dichloromethane and can be isolated by the addition of pentane. By layering a concentrated solution of **C10** in dichloromethane with pentane crystals suitable for X-ray diffraction were obtained. The cation structure is shown in Figure 22 and selected bond lengths and angles are presented in Table 9. The crystallographic details are provided in Table 55 in the Appendix. The complex crystallizes monoclinic in the space group Pn with Z = 8. It adopts a distorted tetrahedral geometry with a τ_4 parameter of 0.76. In the asymmetric unit four distinct complexes are present. The coordination sphere for all four complexes is almost identical, while the torsion angle of the carbonyl group varies between the complexes. Only the bond lengths and bond angles of one copper(I) complex are given in Table 9 and only the cation structure of one copper(I) complex is shown in Figure 22. The four torsion angles found in the solid-state structure of **C10** are $16.7(1)^\circ$, $-41.5(1)^\circ$, $-15.1(1)^\circ$ and $43.7(1)^\circ$. The four distances between the copper(I) ion and the oxygen atom are 3.072(1) Å, 3.113(1) Å, 3.030(1) Å and 3.231(1) Å leading to an average copper(I) oxygen distance of 3.112(1) Å.

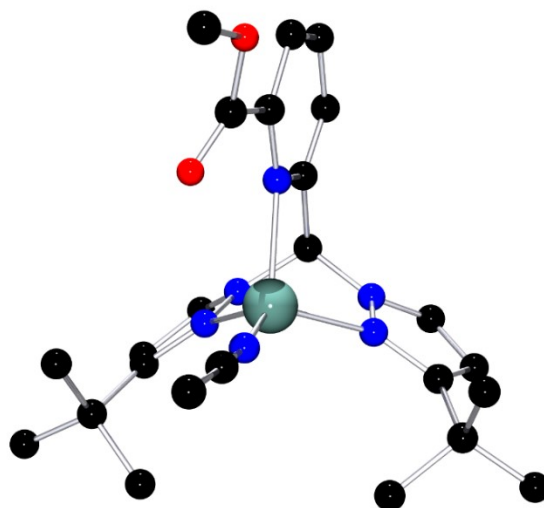


Figure 22. Molecular structure of $[\text{Cu}\{\text{HC}(\text{tBuPz})_2(6\text{-CO}_2\text{MePy})\}(\text{MeCN})]^+$ in crystals of **C10**. Hydrogen atoms were omitted for clarity. In the asymmetric unit four molecules of **C10** are present with a different torsion angle between the carbonyl group and the pyridinyl group.

Table 9. Selected bond lengths, atom distance [Å] and angles [°] for **C10**.

Bond lengths		Bond angles	
C(ap) – C(Py)	1.511(10)	N(Pz) – C(ap) – N(Pz')	109.9(1)
C(ap) – N(Pz)	1.458(9)	N(Pz) – C(ap) – C(Py)	114.1(1)
C(ap) – N(Pz')	1.465(9)	N(Pz') – C(ap) – C(Py)	111.3(1)
Cu – N(MeCN)	1.905(7)	N(MeCN) – Cu – N(Pz)	125.8(1)
Cu – N(Pz)	2.055(6)	N(MeCN) – Cu – N(Pz')	125.1(1)
Cu – N(Pz')	2.103(6)	N(MeCN) – Cu – N(Py)	126.4(1)
Cu – N(Py)	2.194(6)	N(Py) – Cu – N(Pz)	86.8(1)
Atom distance		N(Py) – Cu – N(Pz')	91.2(1)
Cu ... O(Carb)	3.072(1)	N(Py) – C – C – O(Carb)	-16.7(1)
		τ_4^a	0.76

$$^a \tau_4 = \frac{360^\circ - (\alpha + \beta)}{141^\circ} \quad [147]$$

A comparison between the two complexes with a methylester group **C9** and **C10** shows that the copper oxygen distance in **C10** is approximately 0.3 Å longer than in **C9** while the copper nitrogen bond lengths are not significantly different. Also, it can be observed that the coordination geometry in **C10** is slightly less distorted than in **C9**. In addition, it is noticeable that for **C10** the position of the ester group can have four different torsion angles to the pyridine group in the solid-state structure while for **C9** the torsion between the ester and the pyridine group is fixed in the solid-state. The difference between both complexes lies in the steric influence of the *tert*-butyl group. In comparison to the cation structure of the complex $[\text{Cu}\{\text{HC}(\text{tBuPz})_2\text{Py}\}\text{MeCN}]\text{ClO}_4^{[102]}$ it can be observed that the copper pyridine bond length is elongated in **C10**. This indicates that through the introduction of the ester group the donor

strength is lowered. The higher donor strength of pyridine in comparison to methyl picolinate was shown in the literature before.^[49] When compared to the complex $[\text{Cu}\{\text{HC}(\text{iBuPz})_2(4\text{-CO}_2\text{MePy})\}\text{Br}]$ ^[49] it can be observed that the difference in the copper nitrogen bonds length are in the same range as expected for the difference between a halide and an acetonitrile coligand.^{[40],[102]} This indicates that the influence of the ester group on the coordination properties of the copper complex is similar for a substitution in the 4- and the 6-position.

4.2.6 Synthesis and characterization of copper(I) complexes of **L11**

Complex **C11** ($[\text{Cu}\{\text{HC}(\text{PuIPz})_2\text{Py}\}(\text{MeCN})]\text{PF}_6$) was synthesized in acetone from **L11** and $[\text{Cu}(\text{MeCN})_4]\text{PF}_6$ and was isolated by reducing the volume to half and the addition of hexane. A synthesis approach in dichloromethane indicated a formation of a dinuclear complex, while the isolated complex **C11** did not show any tendency to form a dinuclear complex when solved. For complex **C11** crystals suitable for single X-ray diffraction were achieved by layering the reaction solution with pentane instead of the addition of hexane. In Figure 23 the obtained cation structure is shown and selected bond lengths and angles are presented in Table 10. The crystallographic details are provided in Table 56 in the Appendix. The complex crystallizes monoclinic in the space group $P2(1)$ with $Z = 2$ and it adopts a distorted tetrahedral geometry with a τ_4 parameter of 0.70.

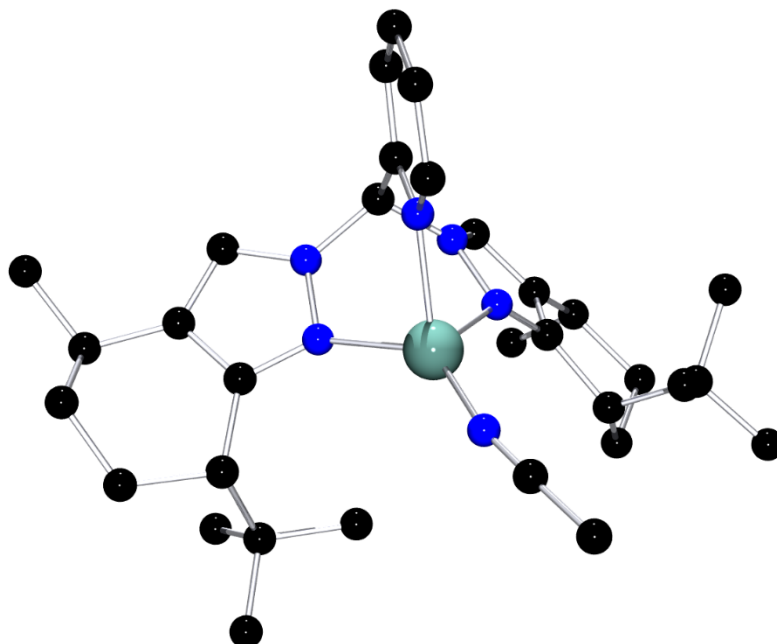


Figure 23. Molecular structure of $[\text{Cu}\{\text{HC}(\text{PuIPz})_2\text{Py}\}(\text{MeCN})]^+$ in crystals of **C11**. Hydrogen atoms were omitted for clarity.

Table 10. Selected bond lengths [Å] and angles [°] for **C11**.

Bond lengths		Bond angles	
C(ap) – C(Py)	1.511(7)	N(Pz) – C(ap) – N(Pz')	110.9(4)
C(ap) – N(Pz)	1.447(7)	N(Pz) – C(ap) – C(Py)	113.6(5)
C(ap) – N(Pz')	1.464(7)	N(Pz') – C(ap) – C(Py)	109.4(5)
Cu – N(MeCN)	1.872(5)	N(MeCN) – Cu – N(Pz)	125.2(2)
Cu – N(Pz)	2.100(5)	N(MeCN) – Cu – N(Pz')	136.6(2)
Cu – N(Pz')	2.046(4)	N(MeCN) – Cu – N(Py)	115.4(2)
Cu – N(Py)	2.120(5)	N(Py) – Cu – N(Pz)	89.1(2)
		N(Py) – Cu – N(Pz')	89.3(2)
		τ_4^a	0.70

$$^a \tau_4 = \frac{360^\circ - (\alpha + \beta)}{141^\circ} \text{ [147]}$$

4.2.7 Synthesis and characterization of copper(I) complexes of **L12**

Complex **C12** ($[\text{Cu}\{\text{HC}(\text{CamPz})_2\text{Py}\}(\text{MeCN})]\text{PF}_6$) was synthesized in THF from **L12** and $[\text{Cu}(\text{MeCN})_4]\text{PF}_6$ and was isolated as a pale-yellow solid by the addition of diethyl ether. For the isolation of **C12** it is mandatory to have a low concentration of the ligand and the copper salt and that the addition of the ligand is very slow to avoid the formation of the dinuclear complex **C13** ($[\text{Cu}_2\{\text{HC}(\text{CamPz})_2\text{Py}\}_2](\text{PF}_6)_2$). The formation of **C13** is indicated by a change in the color from pale yellow to intense yellow. Furthermore, it can be observed that **C12** is not stable in solution of dichloromethane, acetone or THF and **C13** forms *in situ*. Due to the low stability in solution the synthesis of **C12** is limited to a scale of 0.05 mmol. In acetonitrile **C12** and **C13** are also instable and the decomposition into **L12** and $[\text{Cu}(\text{MeCN})_4]\text{PF}_6$ can be observed. However, it is possible to stabilize a solution of **C12** by the addition of 10 equivalents of acetonitrile. Additionally, it is also possible to form **C12** *in situ* from **C13** by the addition of 10 equivalents of acetonitrile. This was proven by NMR spectroscopy (Figure 24) and CV measurements (Table 32). When the NMR spectra of **L12**, *in situ* formed **C12** and **C13** are compared in the range from 8.8 ppm to 6.8 ppm, it can be observed that the three species show major differences in the NMR spectra.

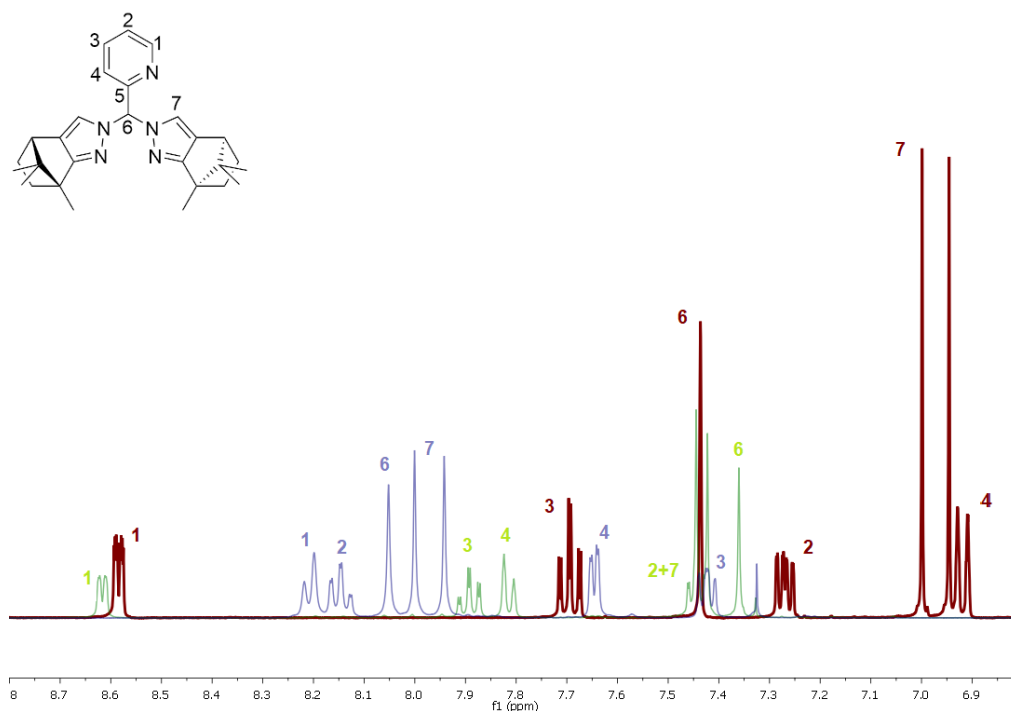


Figure 24. Overlay of the ^1H NMR spectra between 8.8 ppm and 6.8 ppm of **L12** (red), **C12** (green) and **C13** (blue) in dichloromethane- d_2 . The complex **C12** was formed *in situ* from **C13** by the addition of 10 equiv. of acetonitrile.

Crystals suitable for single crystal X-ray diffraction were obtained from a concentrated solution of **C13** in dichloromethane by layering with pentane. The cation structure is shown in Figure 25 and selected bond lengths and angles are presented in Table 11. The crystallographic details are provided in Table 56.

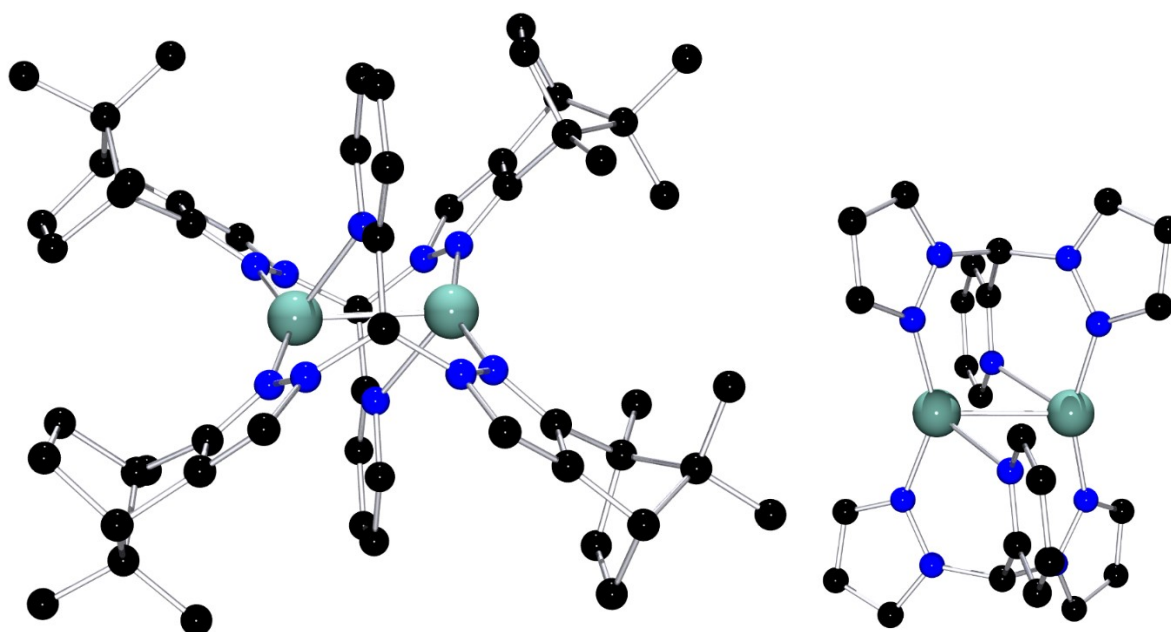


Figure 25. Left: Molecular structure of $[\text{Cu}_2\{\text{HC}(\text{CampPz})_2\text{Py}\}_2]^{2+}$ in crystals of **C13**. Right: Different view on the molecular structure of **C13** in the solid-state, substituents on the pyrazolyl are omitted for clarity. Hydrogen atoms were omitted for clarity.

Table 11. Selected bond lengths [Å] and angles [°] for **C13**.

Bond lengths		Bond angles	
C(ap) – C(Py)	1.527(4)	N(Pz) – C(ap) – N(Pz')	113.3(2)
C(ap) – N(Pz)	1.462(4)	N(Pz) – C(ap) – C(Py)	113.0(2)
C(ap) – N(Pz')	1.449(4)	N(Pz') – C(ap) – C(Py)	114.1(2)
Cu – Cu'	2.586(1)	Cu' – Cu – N(Pz)	104.6(1)
Cu – N(Pz)	1.935(2)	Cu' – Cu – N(Pz')	99.8(1)
Cu – N(Pz')	1.930(2)	Cu' – Cu – N(Py)	51.9(1)
Cu – N(Py)	2.194(3)	Cu' – Cu – N(Py')	57.1(1)
Cu – N(Py')	2.336(3)	N(Pz) – Cu – N(Pz')	155.2(1)
		N(Py) – Cu – N(Py')	109.0(1)
		Cu – N(Py) – Cu'	68.1(1)
		Cu – N(Py') – Cu'	68.4(1)
		τ_4^a	0.68

$$^a \tau_4 = \frac{360^\circ - (\alpha + \beta)}{141^\circ} \quad [147]$$

The complex **C13** crystallizes monoclinic in the space group $P2_1$ with $Z = 2$ and it adopts a distorted tetrahedral geometry with a τ_4 parameter of 0.68 in the solid-state.

When the two dinuclear complexes **C4** and **C13** are compared it can be observed that the copper copper bond lengths and the distortion of the tetrahedral coordination geometry do not vary significantly between the two complexes. In addition, the coordination geometry of both complexes is not the same. In **C4** both pyrazolyl units are coordinated to one copper ion and the methyl imidazolyl unit is coordinated to the other copper ion (Figure 20, right), in contrast in **C13** each copper ion is coordinated by a pyridine and a pyrazolyl unit of one ligand and another pyrazolyl unit of the second ligand (Figure 25, right).

4.2.8 Synthesis and characterization of copper(I) complexes of **L20**

Complex **C19** ($[\text{Cu}\{\text{HC}(\text{Ph}_2\text{Pz})_2\text{DMAP}\}(\text{MeCN})]\text{PF}_6$) was synthesized in dichloromethane and can be isolated by the addition of pentane. By layering a concentrated solution of **C19** in dichloromethane with pentane crystals suitable for single crystal X-ray diffraction were obtained. The resulting cation structure is shown in Figure 26 and selected bond lengths and angles are highlighted in Table 12. The crystallographic details are provided in Table 57 in the Appendix. The complex crystallizes orthorhombic with $Z = 8$ in the space group $Pbca$ with and one dichloromethane molecule in the asymmetric unit. The coordination geometry **C19** adopts is a distorted tetrahedral geometry with a τ_4 parameter of 0.82.

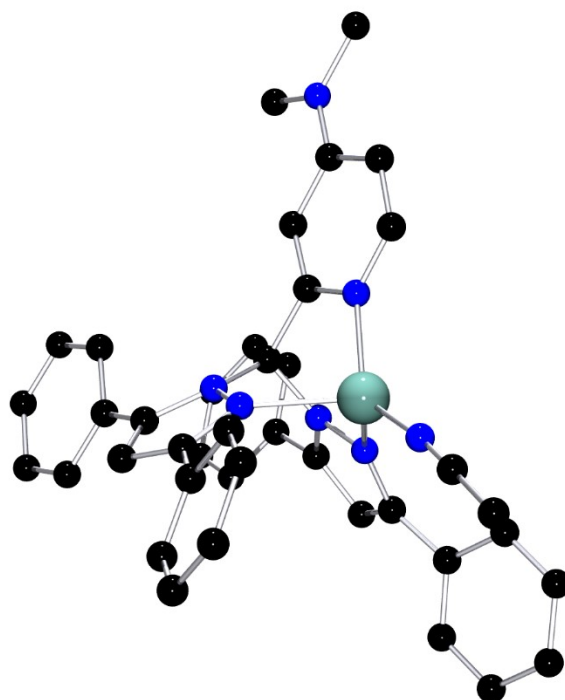


Figure 26. Molecular structure of $[\text{Cu}\{\text{HC}(\text{Ph}_2\text{Pz})_2\text{DMAP}\}(\text{MeCN})]^+$ in crystals of **C19**. Hydrogen atoms were omitted for clarity.

Table 12. Selected bond lengths [Å] and angles [°] for **C19**.

Bond lengths		Bond angles	
C(ap) – C(Py)	1.523(3)	N(Pz) – C(ap) – N(Pz')	109.5(2)
C(ap) – N(Pz)	1.460(2)	N(Pz) – C(ap) – C(Py)	112.4(2)
C(ap) – N(Pz')	1.458(2)	N(Pz') – C(ap) – C(Py)	112.8(2)
Cu – N(MeCN)	1.874(2)	N(MeCN) – Cu – N(Pz)	121.3(1)
Cu – N(Pz)	2.184(1)	N(MeCN) – Cu – N(Pz')	123.1(1)
Cu – N(Pz')	2.094(1)	N(MeCN) – Cu – N(Py)	133.4(1)
Cu – N(Py)	2.032(1)	N(Py) – Cu – N(Pz)	88.5(1)
		N(Py) – Cu – N(Pz')	91.0(1)
		τ_4^a	0.82

$$^a \tau_4 = \frac{360^\circ - (\alpha + \beta)}{141^\circ} \quad [147]$$

4.2.9 Comparison of aromatic substituted copper(I) complexes

Starting from the known complex $[\text{Cu}\{\text{HC}(\text{Ph}_2\text{Pz})_2\text{Py}\}(\text{MeCN})]\text{PF}_6$ (**C5**)^{[102],[141]} different copper(I) bis(pyrazolyl)methane complexes with an aromatic substituted pyrazolyl unit were synthesized (**C1**, **C2**, **C3**, **C4** and **C19**). Of these five complexes the solid-state structures of four could be analyzed with single crystal X-ray diffraction (**C1**, **C2**, **C4** and **C19**). While the complex **C3** was successfully isolated, recrystallization yields complex **C4** with a different coordination

motif ($[\text{Cu}_2\text{L}_2](\text{PF}_6)_2$) than the other complexes ($[\text{CuL}(\text{MeCN})]\text{PF}_6$). For the synthesis of the new ligands, the ligand design was varied on different aspects. The complexes **C2**, **C3** and **C19** have a different third *N* donor, while the complex **C1** has a different substituent in the 5-position of the pyrazolyl unit.

Selected bond lengths and the τ_4 parameter of these complexes are presented in Table 13. The copper pyrazolyl and copper acetonitrile bond lengths do not vary significantly between the five copper complexes. In contrast the bond lengths between the third *N* donor unit and the copper center vary: in **C4** the shortest Cu–N(third *N* donor) bond length is observable, while in **C2** the largest bond length is observable. Due to the different coordination motif, an interpretation is difficult but it is reported that methyl imidazolyl is a stronger donor than pyridine.^{[40],[149]} This is also indicated by the shorter bond length in **C4** compared to **C5**. It also can be observed that the variation in the 5-position of the pyrazolyl unit has no significant effect on the copper pyridine bond length. By the introduction of a chlorido substituent in the 4-position of the pyridine the Cu–N bond length can be increased and by the introduction of a dimethyl amino group the bond length can be decreased.

When the τ_4 parameter is compared it can be noticed that all complexes are distorted tetrahedrally coordinated. For the pyridine-based complexes an electron-rich pyridine unit leads to a less distorted coordination moiety.

Table 13. Comparison of selected bond lengths [Å] of **C1**, **C2**, **C4**, **C5** and **C19**.

	C1	C2	C4	C5 ^{[102],[141]}	C19
Cu – N(MeCN)	1.872(3)	1.888(6)	-	1.879(7)	1.874(2)
Cu – Cu	-	-	2.568(1)	-	-
Cu – N(Pz)	2.066(3)	2.047(6)	2.014(2)	2.080(6)	2.184(1)
Cu – N(Pz')	2.067(3)	2.124(6)	1.979(2)	2.103(6)	2.094(1)
Cu – N(Py/Melm)	2.090(3)	2.116(6)	1.913(2)	2.080(6)	2.032(1)
τ_4 ^a	0.74	0.67	0.69	0.73	0.82

^a $\tau_4 = \frac{360^\circ - (\alpha + \beta)}{141^\circ}$ [147]

4.3 Copper nitrene chemistry

Parts of this chapter are already published:

F. Thomas, D. Steden, A. Eith, A. Hoffmann, S. Herres-Pawlis, *Z. Naturforsch.* **2021**, *76b*, 835.

F. Thomas, M. Oster, F. Schön, K. Göbgen, B. Amarouch, D. Steden, A. Hoffmann, S. Herres-Pawlis, *Dalton Trans.* **2021**, *50*, 6444.

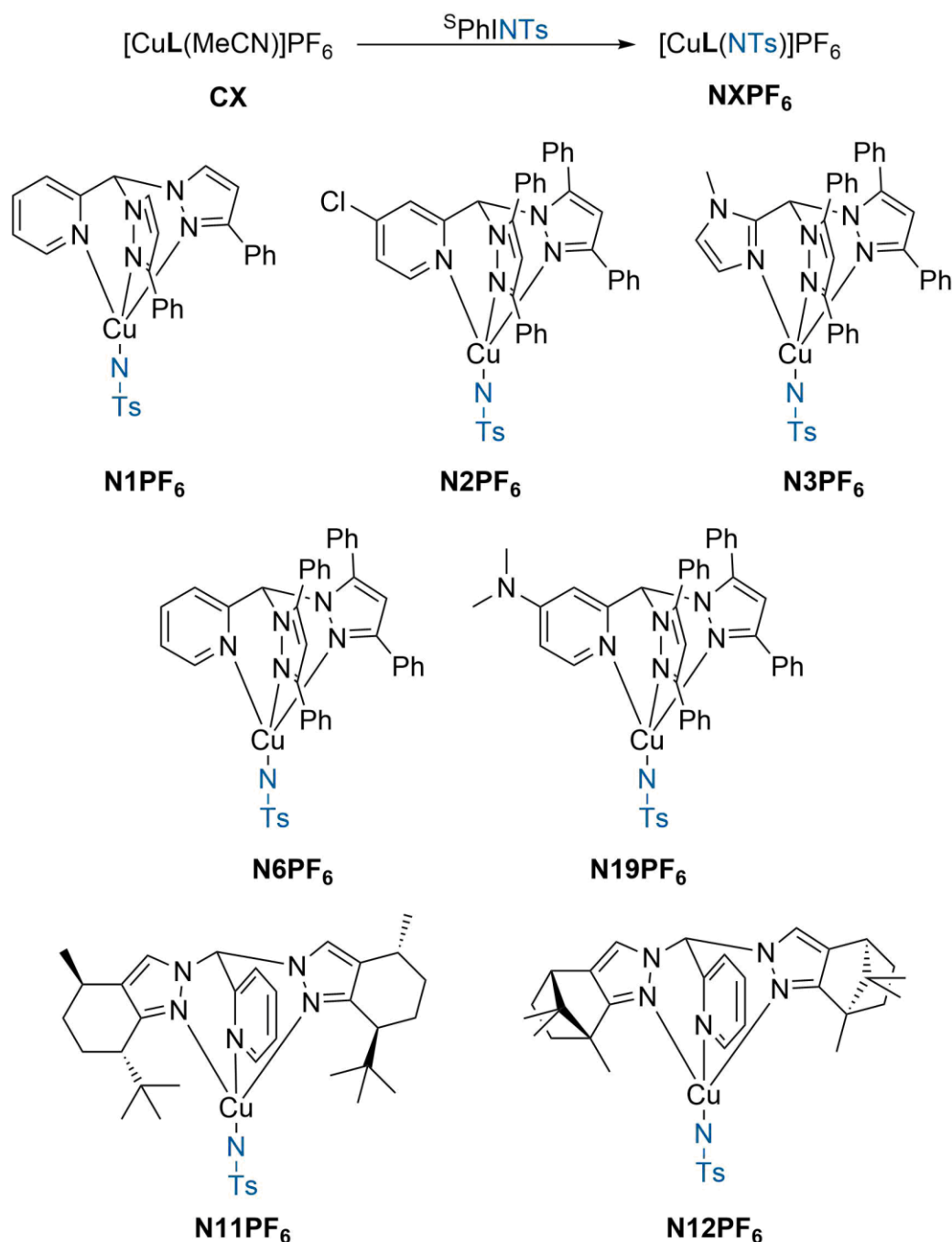
J. Moegling, A. Hoffmann, F. Thomas, N. Orth, P. Liebhäuser, U. Herber, R. Rampmaier, I. Ivanović-Burmazović, S. Herres-Pawlis, *Angew. Chem.* **2018**, *57*, 9154, *Angew. Chem. Int. Ed.* **2018**, *130*, 9294.

In this thesis a variety of different copper nitrenes were generated. Therefore, in a first step different ligands were screened (**L1-L12**, **L20**) using ^sPhINTs (**58**) as nitrene generating agent. In a second step different nitrene generating agents were screened (3,5-bis(trifluoromethyl)phenyl azide (**110**), mesityl azide (**111**), adamantyl azide (**112**) and benzoyl azide (**113**), azobenzene (**114**) O-(4-nitrobenzoyl) hydroxylamine triflate (**115**)) with different copper complexes. The screening was performed using dichloromethane as solvent at low temperature and the reaction was monitored by UV/Vis spectroscopy. When no reaction was observed the temperature was increased. When a stable copper nitrene complexes was identified further characterization steps were accomplished and catalytic reactions were performed. The number of the stable tosyl nitrene complexes in the following chapter refers directly to the precursor complex. For example, the tosyl nitrene complex generated from **C19** is the tosyl nitrene complex **N19PF₆**.

4.3.1 Variation of the ligand design

The first step was the investigation to which extent a change in the ligand design or in the coordination moiety influences the formation of stable nitrene complex. Therefore, a variety of different copper(I) complexes were used (Table 33). It can be observed that the dinuclear complexes (**C4**, **C13**) do not form a stable copper nitrene complex. In addition, not only the coordination motif influences the generating but also the ligand design is crucial. For example, the presence of aliphatic C–H bonds close to the nitrene nitrogen atom leads to highly instable nitrene complexes. While it is possible to generate a nitrene complex from the *in situ* formed complex [Cu{HC(Et₂Pz)₂Py}(MeCN)]PF₆ the nitrene complex is highly instable even at -80 °C. Furthermore, a sterically demanding third *N* donor interferes with the formation of a copper

nitrene complex. The reaction of **C10** and the *in situ* formed complex $[\text{Cu}\{\text{HC}(\text{PhPz})_2\text{Qu}\}(\text{MeCN})]\text{PF}_6$ both show the formation of a shoulder in the UV/Vis spectra in the range of 300-500 nm. While both complexes can be used as catalyst for C–H amination reactions the formation of a stable nitrene cannot be observed. Nevertheless, the complexes **C1**, **C2**, **C3**, **C6**, **C11**, **C12** and **C19** form the stable copper nitrene complexes **N1PF₆**, **N2PF₆**, **N3PF₆**, **N6PF₆**, **N11PF₆**, **N12PF₆** and **N19PF₆** (Scheme 29).



Scheme 29. Overview of the stable generated copper nitrene complexes.

The UV/Vis spectra of **N1PF₆**, **N2PF₆**, **N3PF₆**, **N6PF₆**, **N11PF₆**, **N12PF₆** and **N19PF₆** are given in Figure 27, while the UV/Vis spectra of the reaction of **58** with **C10**,

$[\text{Cu}\{\text{HC}(\text{Et}_2\text{Pz})_2\text{Py}\}(\text{MeCN})]\text{PF}_6$ and $[\text{Cu}\{\text{HC}(\text{PhPz})_2\text{Qu}\}(\text{MeCN})]\text{PF}_6$ are given in the Appendix (Figure 87, Figure 88, Figure 91).

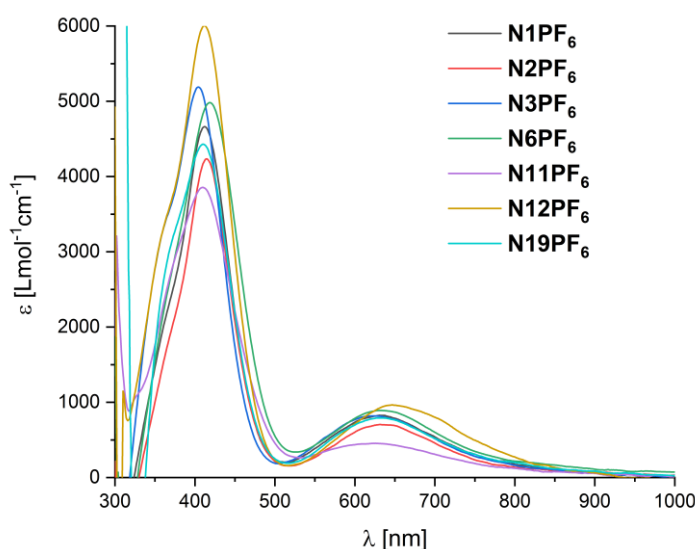


Figure 27. UV/Vis spectra of **N1PF₆**, **N2PF₆**, **N3PF₆**, **N6PF₆**, **N11PF₆**, **N12PF₆** and **N19PF₆**.

All stable tosyl nitrene complexes have a deep green color and most nitrenes can be generated by the addition of $^{\text{S}}\text{PhINTs}$ at $-80\text{ }^{\circ}\text{C}$. Only for the formation of **N12PF₆** the temperature needs to be increased to $-63\text{ }^{\circ}\text{C}$. When the UV/Vis spectra of the different stable copper nitrene complexes are compared it can be noticed that all nitrene complexes have two characteristic bands, one strong band at 400–450 nm ($\epsilon = 4000\text{--}6000\text{ Lmol}^{-1}\text{cm}^{-1}$) and a weaker one between 600 and 700 nm ($\epsilon = 500\text{--}1000\text{ Lmol}^{-1}\text{cm}^{-1}$). The concentration used to calculate the extinction coefficient was corrected by the nitrene yield (see Chapter 4.3.3, Table 34).

4.3.2 Variation of the nitrene generating agent

Beside the usage of $^{\text{S}}\text{PhINTs}$ (**58**) it was investigated if bis(pyrazolyl)methane copper nitrene complexes can be formed with other nitrene generating agents. The use of **58** has some major drawbacks, for instance the solubility is low in most solvents and the stability in solution is also very low. Also, the multi-step synthesis of **58** is time consuming and includes the use of toxic and explosive reactants. In addition, the formation of $^{\text{S}}\text{PhI}$ as couple products leads to a low atom-efficiency of catalytic reactions. Possible alternatives are organic azides (**110–113**), azo compounds (**114**) or carbamates (**115**), which are either commercially available or can be synthesized in a one-step synthesis. These nitrene generating agents were converted with different copper(I) complexes at low temperatures in dichloromethane (Figure 28), in the following

part only reactions are highlighted where a reaction was observed. An overview over all performed reaction is given in Table 33.

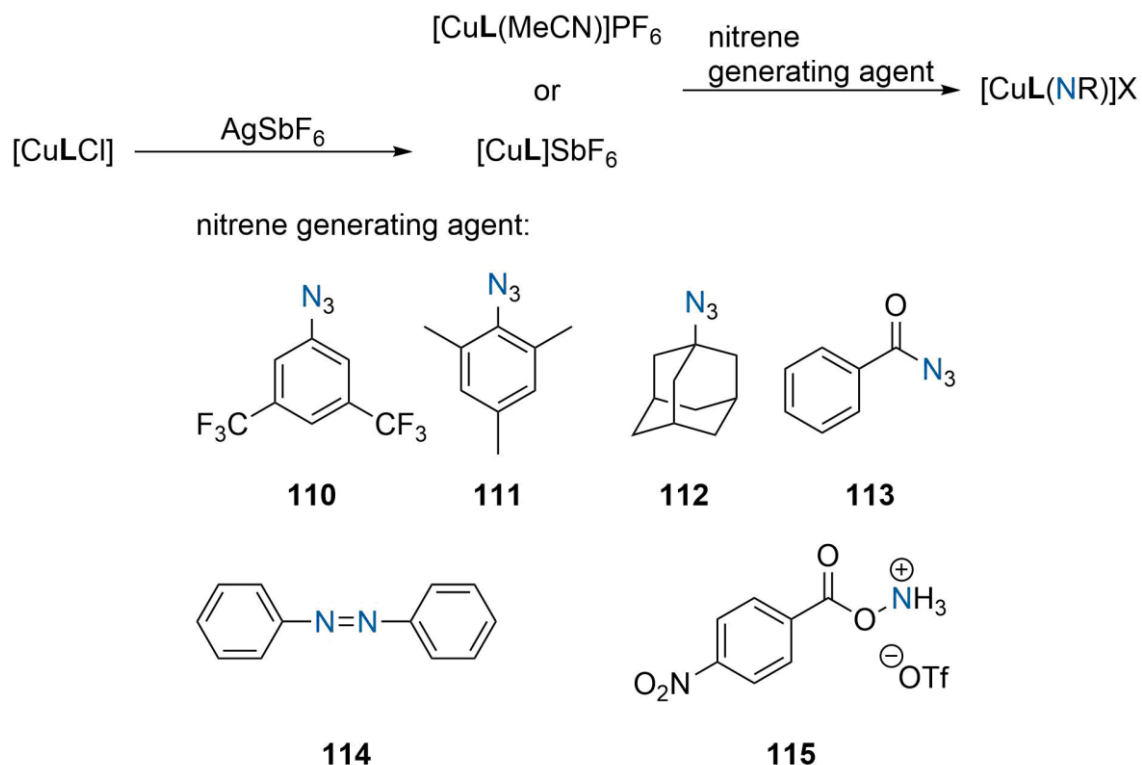


Figure 28. Overview of different used nitrene generating agents.

For the reaction between organic azides (3,5-bis(trifluoromethyl)phenyl azide (**110**), mesityl azide (**111**), adamantyl azide (**112**)), it was observed that only complexes with an empty coordination site can react with these azides and complexes with methyl imidazolyl as third *N* donor unit show a higher reactivity against organic azides. Bis(pyrazolyl)methane copper(I) complexes with an empty coordination site can be synthesized *in situ* from the copper(I) chloride complex by addition of silver(I) hexafluoroantimonate. On the one hand, this indicates that for the utilization of organic azides electron richer copper(I) complexes are beneficial. On the other hand, this shows that a reaction of an organic azide is hindered by a coligand, which coordinates too strong. Therefore, also complexes with hexamethylbenzene as coligand were tried to be synthesized. The aim was to yield a copper complex with a weak coordinating coligand, which can be stored and has a defined structure. As mentioned in Chapter 4.2 the synthesis was not successful. The reaction between a copper(I) complex and an organic azide is slow and only occurs at room temperature. During the reaction a weak band at 400 nm in the UV/Vis spectrum is formed. Additionally, it could be shown that the reaction with the aromatic azides is faster than with the aliphatic adamantyl azide (**112**). Due to the slow reaction between the organic azides and the copper(I) complex a reactive intermediate like a nitrene complex cannot be directly observed in the UV/Vis spectra. Therefore, the organic azides were applied to catalytic C–H amination reactions, but no conversion of the substrate was observed.

For a better understanding, if the reaction observed is the formation of a copper nitrene complex the UV/Vis spectra of the possible copper nitrene complex $[\text{Cu}\{\text{HC}(\text{tBuPz})_2(\text{Melm})\}(\text{NPh}(\text{CF}_3)_2)]$ was calculated by DFT using TPSSh/def2TZVP GD3BJ. The UV/Vis spectra were calculated for a singlet and a triplet nitrene (Figure 29). When the calculated and the experimental spectra are compared it appears that the extinction coefficient of the experimental spectra is significantly lower than the calculated spectra. It can be observed that the shoulder of the experimental data at 350 nm is in the same range with the band of the calculated triplet nitrene complex. This may imply the formation of a triplet nitrene, but this species is too instable to perform a selective reaction or to be observed, but neither a nitrene complex nor a decayed nitrene complex could be observed using (cryo) ESI mass spectrometry. The formation of a triplet nitrene is also implied from the calculated energy of the nitrene complex, as the singlet energy is 16.15 kcal/mol higher than the triplet energy.

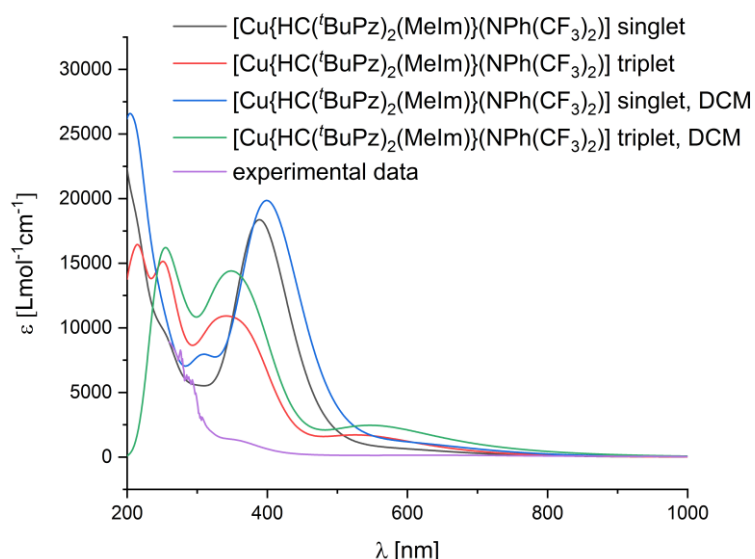


Figure 29. Comparison of the calculated UV/Vis spectra and experimental UV/Vis spectra of the reaction between **C18** and **110** in DCM.

When the complex **C6** is reacted with azo benzene (**114**) or the carbamate **115** a reaction can be monitored using UV/Vis spectroscopy (Figure 89, Figure 90), but no reactivity was detected. The reaction between **C6** and **110** is most presumably the coordination of **114** or a *cis/trans*-isomerization of **114**.

The last used nitrene generating agent was benzoyl azide (**113**) which was used owing to the carbonyl functional group. Therefore, it is possible that the nitrene can coordinate in a κ^2 coordination motif. This should lead to more stable nitrene complex. Due to the previous experiments with organic azides it was at first investigated if **113** reacts with the *in situ* formed complex $[\text{Cu}\{\text{HC}(\text{tBuPz})_2(\text{Melm})\}]\text{SbF}_6$ (**C18**) in dichloromethane starting at low temperature (Figure 30). In the UV/Vis spectra a slow reaction can be detected for temperatures above -60 °C.

While at -50 °C a band at about 600 nm forms a shift to 710 nm appears when the temperature is further increased. When the reaction is performed at room temperature, an intensively blue intermediate forms, which decays too fast for further analysis. However, the decomposition products of the reaction at low temperature and at room temperature show the same UV/Vis spectra.

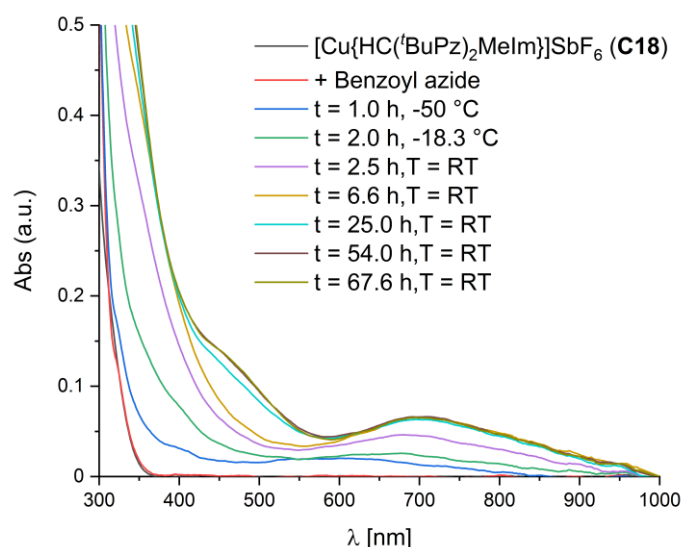


Figure 30. UV/Vis spectra of the reaction of **C18** and **113** in dichloromethane starting from -80 °C.

To gain a better insight if the observed species is a copper nitrene complex the UV/Vis spectrum of $[\text{Cu}\{\text{HC}(\text{tBuPz})_2\text{Melm}\}(\text{NCOPh})]^+$ was calculated using TPSSh/def2TZVP GD3BJ. for a triplet and a singlet nitrene complex with a κ^2 coordination moiety (Figure 31). The position of the UV/Vis features of the calculated triplet spectra and the experimental data are similar, while the extinction coefficient of the of the calculated spectra is higher by a magnitude, which gives a hint to the formation of a nitrene complex that cannot be observed due to its high reactivity. In addition, it was investigated if it is possible to achieve a catalytic C–H amination reaction. Therefore, the amination of ethyl benzene with **C18** and **C8** ($[\text{Cu}\{\text{HC}(\text{tBuPz})_2(\text{Melm})\}(\text{MeCN})]\text{PF}_6$) was investigated. With both complexes a conversion of ethyl benzene was observed. While for **C18** a yield of 4% could be reached, for **C8** a yield of 12% was achieved. This shows that using benzoyl azide the copper(I) acetonitrile complexes can be used. Therefore, it was also investigated if the use of ligands with a pyridine as a third *N* donor unit is feasible with benzoyl azide, but for the C–H amination reaction of ethyl benzene the complex **C7** ($[\text{Cu}\{\text{HC}(\text{tBuPz})_2(\text{Py})\}(\text{MeCN})]\text{PF}_6$) shows no conversion of ethylbenzene.

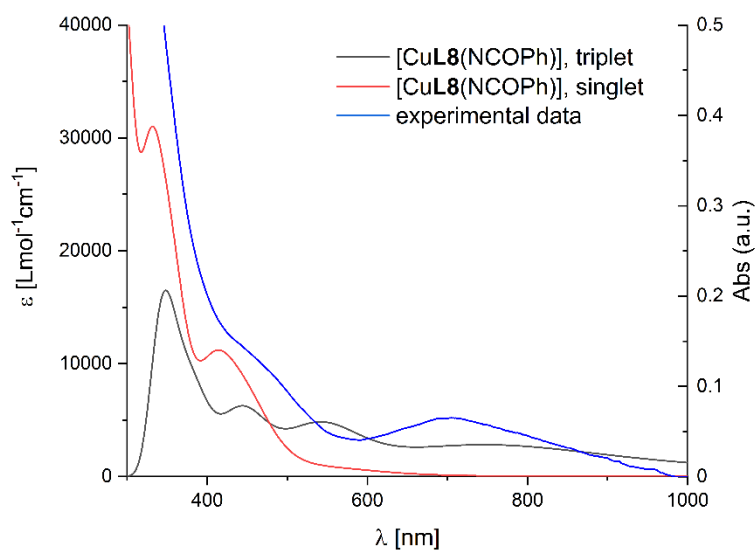


Figure 31. Comparison of the calculated UV/Vis spectra and the experimental spectra. Experimental spectrum is given in absorption.

To increase the stability of a possible copper nitrene intermediate the complex **C19** ($[\text{Cu}\{\text{HC}(\text{Ph}_2\text{Pz})_2\text{DMAP}\}(\text{MeCN})]\text{PF}_6$) was used in the reaction with **113**. The stability should be increased in comparison to complex **C8**, because the aliphatic *tert*-butyl groups in the ligand are substituted with aromatic phenyl groups where C–H bonds are more stable. The reaction between **C19** and **113** was performed in dichloromethane at different temperatures (room temperature, 0 °C, -42 °C and -80 °C, Figure 32). Comparing the reaction of **C8** and **C19** with **113** at room temperature shows that the stability of the possible copper nitrene complex was successfully increased. And the formed species of the reaction between **C19** and **113** is observable for a few seconds at room temperature. When the UV/Vis spectra of the reactions at different temperatures are compared, it can be noticed that for the reaction between **C19** and **113** at room temperature the highest intensity is reached. Once the temperature is decreased also the intensity decreases. The reason is that the reaction between **C19** and **113** is decelerated more than the decay reaction by a decreased temperature. However, it is possible to stabilize the intermediate formed at room temperature and cooling down to -80 °C. The characteristic blue color of the solution can be observed even after one month, even though the intensity decreases slowly (Figure 33). Another hints that the formed species is a nitrene complex can be obtained from the ESI mass spectra of the decayed species, while not the expected decay product $[\text{Cu}\{\text{HC}(\text{Ph}_2\text{Pz})_2\text{DMAP}\}(\text{NHCOPh})]^+$ could be detected in the mass spectra but the copper(II) complex $[\text{Cu}\{\text{HC}(\text{Ph}_2\text{Pz})_2\text{DMAP}\}_2]^{2+}$. Similar complexes are found in the mass spectra of the tosyl nitrene complexes (see Chapter 4.3.3). In addition, benzoyl amine was observable in the ESI mass spectra. Furthermore, the reaction between **C19** and **113** was also investigated by cryo ESI mass spectrometry. The mass for the expected nitrene

$[\text{Cu}\{\text{HC}(\text{Ph}_2\text{Pz})_2\text{DMAP}\}(\text{NCOPh})]^+$ as well as the decay product with an additional hydrogen atom are found (Figure 63).

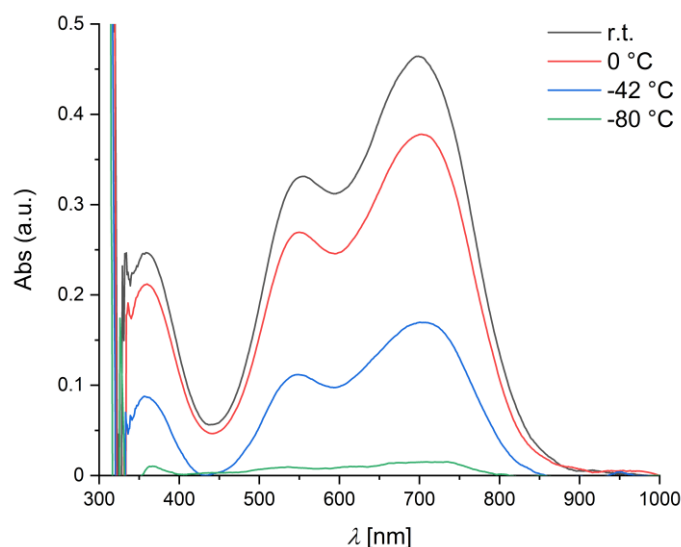


Figure 32. UV/Vis spectra of the reaction between **C19** and **113** in dichloromethane at different temperatures.

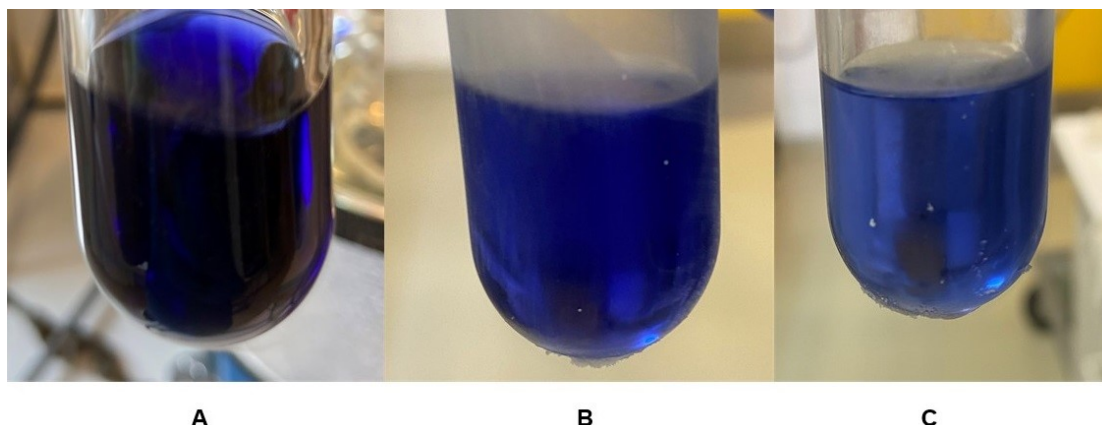


Figure 33. Reaction between **C19** and **113** in dichloromethane at room temperature. Stored at $-80\text{ }^{\circ}\text{C}$ for A: 5 min, B: 10 d, C: 31 d.

Another evidence is that the complex **C19** can successfully aminate ethylbenzene in the presence of benzoyl azide and aziridine styrene.

One further evidence can be obtained by DFT calculation of the UV/Vis spectra of the expected nitrene complex. The calculation was performed using TPSSh/def2TZVP GD3BJ. The UV/Vis spectra were calculated for both spin-states and both possible coordination motifs (Figure 34, Figure 108). Additionally, the energy was calculated showing that the singlet κ^2 state has the lowest energy (Table 14), for the singlet κ^2 state also the key geometric parameters are given in Table 14. When the structure is compared to the tosyl nitrene complex (Table 17) it is

noticeable that the Cu–N(nitrene) and the Cu–O bond length vary only insignificant between the tosyl and the benzoyl nitrene.

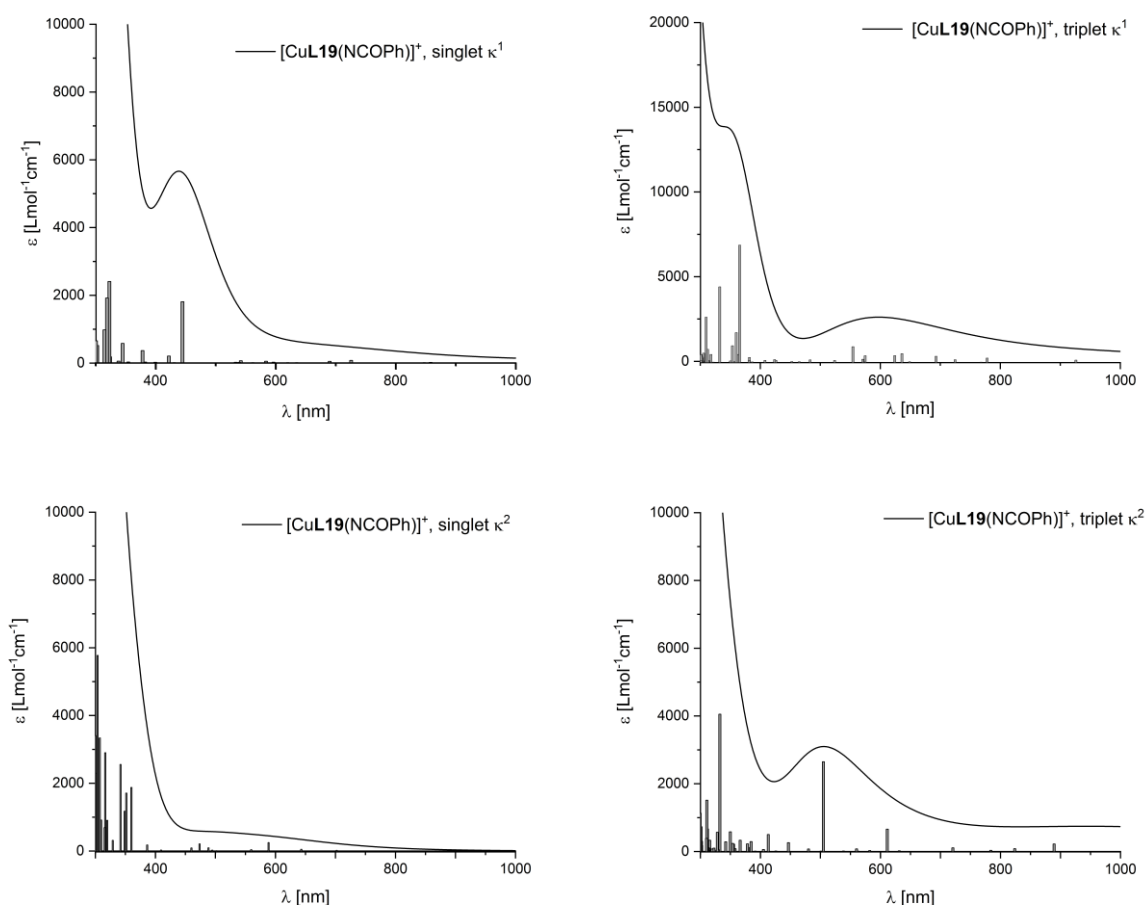


Figure 34. Calculated DFT spectra and transitions.

The calculated UV/Vis spectra feature one intensive band at 200 nm ($\epsilon \approx 100000 \text{ Lmol}^{-1}\text{cm}^{-1}$) and weaker bands between 300 and 800 nm ($\epsilon \approx 1000\text{--}6000 \text{ Lmol}^{-1}\text{cm}^{-1}$). In the experimental spectrum three bands at 360, 560 and 700 nm are present. For the band at 360 nm in all four spectra similar transitions can be observed, but for the singlet κ^2 state the transitions fit best to the experiment. For the other two bands at 560 and 700 nm the accordance between the theoretical and experimental data is not as good as for the band at 360 nm. Transitions suitable for the observed band at 560 nm are found in the calculated spectra of the singlet κ^2 state and the triplet κ^1 state. For the band at 700 nm transitions in accordance with the experiment are found in the calculated spectra of the triplet κ^1 state. This might be an evidence that there are both spin states present at higher temperatures, which is also supported by the calculated energies which are close-lying for both spin states.

Table 14. Left: Calculated spin states and relative energies for the copper nitrene $[\text{CuL19}(\text{NCOPh})]^+$ in the κ^1 - and κ^2 -mode. The energy is stated relative to the lowest spin state of the corresponding copper nitrene which is set to 0.0 kcal/mol⁻¹. Right: Key geometric parameters for the singlet and triplet state of copper nitrene $[\text{CuL19}(\text{NCOPh})]^+$ in the κ^1 - and κ^2 -mode (Gaussian16; TPSSh/def2-TZVP and PCM solvent model for dichloromethane and the empirical dispersion correction with Becke-Johnson damping).

Relative energy [kcal mol ⁻¹]		Bond length [Å]	
singlet κ^1	11.6	Cu – N(Pz/Pz')	1.995/2.361
triplet κ^1	7.3	Cu – N(Py)	1.934
singlet κ^2	0.0	Cu – N(nitrene)	1.876
triplet κ^2	10.9	Cu – O	1.880

Additionally, the formed nitrene species (black) and the decayed species (red) were analyzed with EPR spectroscopy (Figure 35). For both species an EPR signal can be recorded. In the EPR spectra of the formed species a weak signal is observed which intensifies when the nitrene sample decays and an axial copper(II) spectrum is observed. The signal observed in the nitrene sample originates most likely from decayed species which is formed during the nitrene generation at room temperature. Therefore, it can be assumed that the formed nitrene is a singlet nitrene. The changes in the spectra of the nitrene sample and the decayed sample may be due to the formation of different decay species which are observed in the mass spectra.

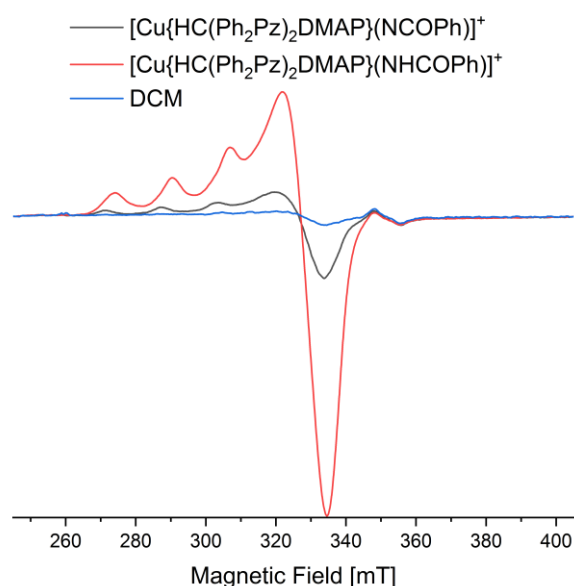
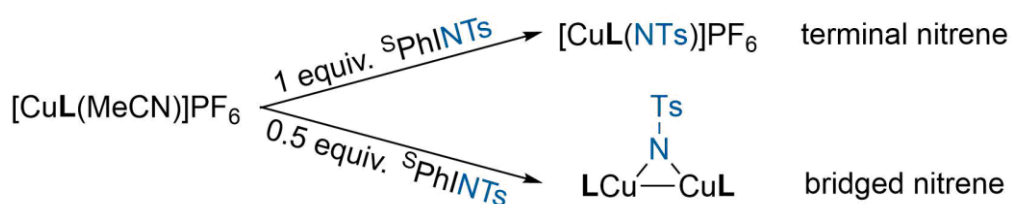


Figure 35. X-band EPR spectra of a sample of the copper nitrene $[\text{Cu}\{\text{HC}(\text{Ph}_2\text{Pz})_2\text{DMAP}\}(\text{NCOPh})]^+$ and the decayed species $[\text{Cu}\{\text{HC}(\text{Ph}_2\text{Pz})_2\text{DMAP}\}(\text{NHCOPh})]^+$ in dichloromethane at 77 K.

Therefore, it can be concluded from the UV/Vis spectra, the EPR spectra, the cryo-ESI mass spectra and the reactivity of the formed species from the reaction of **C19** and **113** that this species is a terminal singlet copper nitrene.

4.3.3 Characterization of stable tosyl copper nitrene complexes

The first aspect to be analyzed for the stable tosyl copper nitrene complexes is whether a terminal nitrene or a bridged nitrene is formed. To determine this question a titration was performed. Therefore, one equivalent of the copper(I) precursor complex was dissolved in dichloromethane and cooled to -80 °C and a solution of **58** in dichloromethane was added stepwise. The nitrene formation was monitored by UV/Vis spectroscopy and between each addition the maximum of the absorption was awaited. For the formation of a terminal nitrene complex the absorption maximum is expected at 1.0 equivalents while for the formation of a bridged nitrene complex the absorption maximum is expected at 0.5 equivalents (Scheme 30).



Scheme 30. Formation of a terminal nitrene and a bridged nitrene complex.

The UV/Vis spectra reveal a linear trend between the absorption and the added amount of **58** and the maximum of absorption is reached after the addition of 1.0 equivalents (Figure 36, exemplary the titration experiment of **C1** is shown, the other UV/Vis spectra are given in the Appendix.).

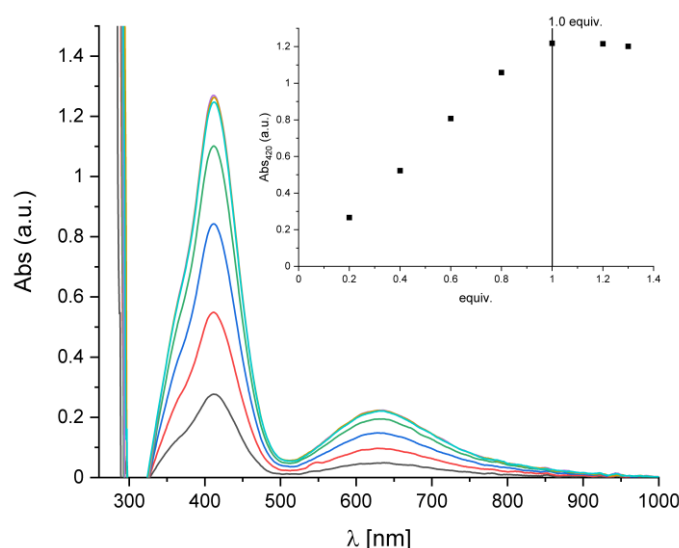
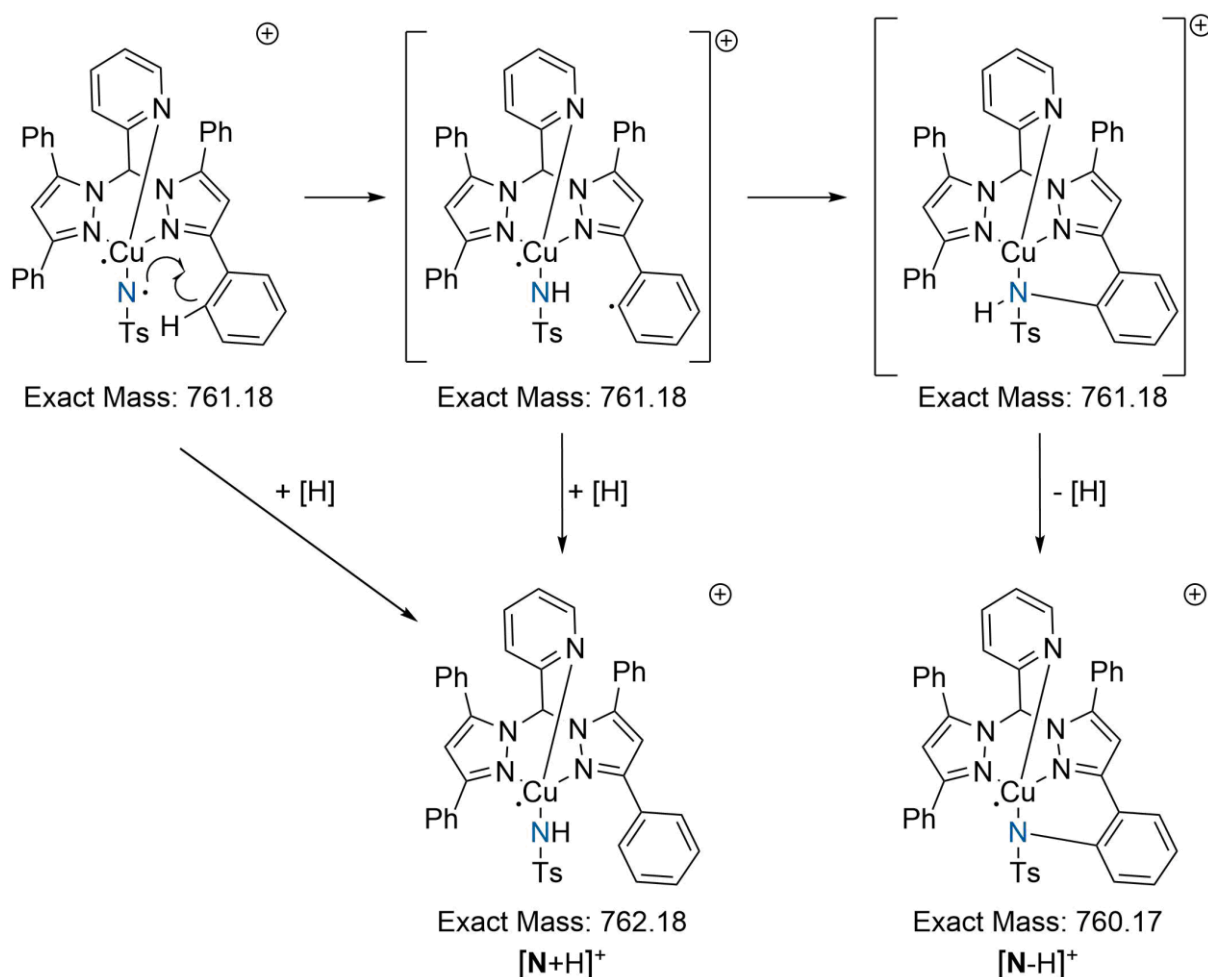


Figure 36. UV/Vis spectra of the titration experiment of **C1** against **58** in dichloromethane at -80 °C.

The titration experiment was performed also with **C2**, **C3**, **C6**, **C11**, **C12** and **C19**; in all cases analogue results were obtained. The titration procedure for the reaction with **C12** had to be

modified: because the formation reaction at $-80\text{ }^{\circ}\text{C}$ was too slow, the reaction was performed at $-63\text{ }^{\circ}\text{C}$. Due to the still slow nitrene formation and therefore decay of the solution of **58** the maximum was reached at 0.8 equivalents. Therefore, it can be concluded that all the formed stable tosyl nitrene complexes are terminal nitrene complexes. This was further proven by cryo ESI mass spectrometry for the nitrene complexes **N1PF₆**, **N2PF₆** and **N3PF₆**. In the mass spectra of **N1PF₆** and **N3PF₆** an overlay of three species can be observed. Beside the nitrene cation, two decay products are detected. The first decay product is formed by an addition of a hydrogen atom to the nitrene cation ($[\text{N}^+ + \text{H}]$). And the second decay product is the product of an abstraction of a hydrogen atom from the nitrene cation ($[\text{N}^+ - \text{H}]$, Figure 60, Figure 61). In the mass spectra of **N2PF₆** only one species can be observed ($[\text{N2}^+ + \text{H}]$). Due to the higher reactivity of **N2PF₆** not the nitrene cation is found but only the decay product of the addition of a hydrogen atom (Figure 62).

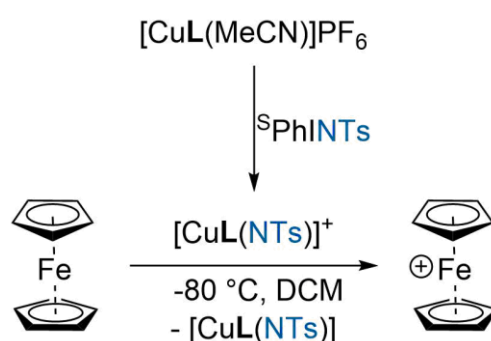


Scheme 31. Proposed decay mechanism for bis(pyrazolyl)methane copper nitrene complexes.

For the other nitrene only the decay products were analyzed with ESI mass spectrometry. Thereby, for **N6PF₆** that both decay products ($[\text{N6}^+ - \text{H}]$ and $[\text{N6}^+ + \text{H}]$) are found,^[141] while for **N19PF₆** only the decay product $[\text{N19}^+ - \text{H}]$ was detected, showing that the choice of the third *N* donor influences the decay mechanism. While with pyridine as third *N* donor both decay

products are found, for an electron-rich system (like DMAP) only the hydrogen abstraction decay product is obtained and for an electron-poorer system (like 4-chloropyridine) only the hydrogen addition decay product is obtained. Both possible mechanism pathways are shown in Scheme 31 on the example of **N6⁺**. The mechanism of the decay of bis(pyrazolyl)methane copper complexes was stated before.^{[102],[141]} While it is possible that the nitrene decay occurs from a reaction with the solvent or ^sPhINTs from the solution directly to [**N⁺**+H], it is also possible that the nitrene abstracts a hydrogen from the ligand and is protonated or abstracts a hydrogen atom afterwards. For the nitrene **N11PF₆** no decay products were observed, whereas for the nitrene **N12PF₆** also both decay products are detected in the ESI mass spectrum.

In the next step, the completeness of the nitrene formation reaction was studied. One possible way to determine the nitrene yield is by the reduction of the nitrene with ferrocene (Scheme 32). The reduction is accomplished by forming the nitrene in dichloromethane at -80 °C and adding an excess of ferrocene. The reduction can be monitored by UV/Vis spectroscopy, the formed ferrocenium has a characteristic UV/Vis band at 624 nm. The UV/Vis spectra of all performed reductions are given in the Appendix.



Scheme 32. Nitrene yield determination by the reduction with ferrocene.

The nitrene concentration is then calculated using the Lambert-Beer law, leading to the following equation for the nitrene yield determination from the reduction of the copper nitrene complex with ferrocene.

$$Y(\text{nitrene}) = \frac{V \cdot E_{624 \text{ nm}}}{n(\text{sPhINTs}) \cdot d \cdot \epsilon_{624 \text{ nm}}(\text{ferrocenium})} \cdot 100\%$$

V: Volume of the reaction solution

E: Extinction

d: Optical path length

ε: Extinction coefficient

The extinction coefficient of ferrocenium at a wavelength of 624 nm was determined in the literature^[102] to 507 Lmol⁻¹cm⁻¹. For the copper nitrene complexes **N1PF₆**, **N2PF₆**, **N3PF₆** and

N6PF₆^{[102],[141]} high nitrene yields, above 82%, were obtained, while for the nitrene **N11PF₆**, **N12PF₆** and **N19PF₆** lower yields, 50-58%, were confirmed (Table 34). Reasons for the lower yields can be the low stability of the copper nitrene complex (**N11PF₆**), the slow reaction between **58** and the copper(I) complex (**N12PF₆**) and the slow nitrene reduction reaction with ferrocene (**N19PF₆**). Therefore, more side reactions can occur resulting in a lower nitrene yield, whereby the side reactions are the decay of the nitrene complex before a reduction of the nitrene occur or the decay of **58** in solution before a reaction with the copper complex takes place. As for the nitrene **N19PF₆** the reason for the low nitrene yield is presumably the slow reaction between ferrocene and **N19PF₆**, also a second approach was used to determine the yield. Therefore, a nitrene transfer reaction with triphenylphosphane was performed. The nitrene transfer reaction of bis(pyrazolyl)methane copper nitrene is known in the literature^[102] and it was shown that the nitrene yield is underestimated in contrast to the reaction with ferrocene when a fast reaction with ferrocene occurs. **N19PF₆** was formed at low temperature in dichloromethane and an excess of triphenylphosphane was added, the yield was determined by ³¹P {¹H} NMR spectroscopy (16%), showing that the reactivity of **N19PF₆** is also low against triphenylphosphane. A third method for the estimation of the nitrene yield for **N19PF₆** uses the Evans NMR method. A comparison of the theoretical and the experimental value of μ_{eff} indicates a nitrene yield of 93%. This further shows that the nitrene yield for **N19PF₆** is underestimated by the other two methods.

Another important characteristic of copper nitrene complexes is the spin state. Nitrenes can be present as singlet or triplet nitrenes (Figure 5). The spin state can be investigated with different methods. On the one hand, it can be determined with the Evans NMR method at low temperature and, on the other hand, it can be studied with EPR spectroscopy at low temperature. For the nitrene complexes **N1PF₆**, **N2PF₆**, **N3PF₆**, **N6PF₆** and **N19PF₆** the spin state was determined with the Evans NMR method, while for the nitrene complexes **N11PF₆** and **N12PF₆** the spin state was determined using EPR spectroscopy. By using the Evans NMR method, it was shown for the five nitrene complexes that all five are singlet nitrene complexes and that the decay product has a doublet spin state. Due to the low solubility of the decay product in dichloromethane a precipitate is observed and therefore a lower effective magnetic field is present. For the other two nitrene EPR spectroscopy was used, because of the low stability of **N11PF₆** and the mandatory addition of acetonitrile to **C13** to yield **C12** *in situ*. In the EPR spectra of both nitrenes a signal is observed. However, the signal recorded in the nitrene sample and the decayed sample are very similar and shows a typical axial copper(II) signal (Figure 104-Figure 107). Due to the low stability of **N11PF₆** and the slow formation of **N12PF₆** at -63 °C, it is possible that even in the nitrene sample decay product is present, which leads to the observed signal. The small change in the original and the decayed sample are presumably due to the formation of the different decay products, which can be obtained from the nitrene

complex. This indicates that both nitrenes are also a singlet nitrene. This is expectable as the bis(pyrazolyl)methane tosyl copper nitrene complexes reported before are singlet nitrenes and also the similar nitrene $[\text{Cu}\{\text{HC}(\text{tBuPz})_2\text{Py}\}(\text{NTs})]\text{PF}_6$ is a singlet nitrene.^[102]

Also, the thermal stability of the copper nitrene complexes was investigated. Therefore, the nitrene was generated at $-80\text{ }^\circ\text{C}$ and then warmed to $-42\text{ }^\circ\text{C}$. The decay was monitored by UV/Vis spectroscopy (Scheme 33). The primary decay reaction can be an intermolecular reaction between the nitrene complex and the solvent or the ^5PhI or another nitrene complex. The second option for the decay reaction is an intramolecular decay reaction.



Scheme 33. Formation and decay of a copper nitrene complex.

During the decay reaction it can be observed for all copper nitrene complexes that both characteristic nitrene bands in the UV/Vis spectra are transformed to bands with a similar absorption maximum with a lower intensity. The UV/Vis spectra of the decay of **N1PF₆** is shown in Figure 37 exemplary, while the others UV/Vis spectra are given in the Appendix. The time-resolved measurements (Figure 37 inset) show that the decay is neither a reaction of first nor second order but of non-integer order. This further reveals that different reactions are responsible for the decay of the copper nitrene complexes. In addition, the influence of different factors on the stability of the nitrene complexes were examined. On the one hand, the presence of aliphatic C–H bonds in close distance to the nitrene nitrogen leads to a low stability. When the distance between aliphatic C–H bonds and the nitrene nitrogen is larger, a higher stability is observed. Therefore, for **N11PF₆** a half-life time of two minutes is obtained and for **N12PF₆** a half-life time of 21 minutes. On the other hand, it can be observed that aromatic C–H bonds in close distance to the nitrene nitrogen increase the stability compared to aliphatic C–H bonds, for **N6PF₆** a half-life time of 14 minutes is obtained. This was expected due to higher bond energy in aromatic C–H bonds. For the choice of the third donor the trend for the stability is: 4-chloropyridine (5 min) \leq dimethylamine pyridine (6 min) $<$ pyridine (14 min) $<$ methyl imidazolyl (42 min). Beside a trend for the third *N* donor unit also a clear trend is observed for substitution in the 5-position of the pyrazolyl. For the nitrene **N1PF₆**, without a substitution in the 5-position a significantly higher half-life time of 50 minutes is obtained in contrast to the 14 minutes of **N6PF₆**.

For better understanding of the decay, the influence of the solvent was investigated. Therefore, the fragile nitrene **N2PF₆** was chosen for further investigation. In a first step the solvent was switched to dichloromethane-*d*₂. If the decay reaction is mainly a reaction between dichloromethane and the nitrene a higher half-life time is expected.

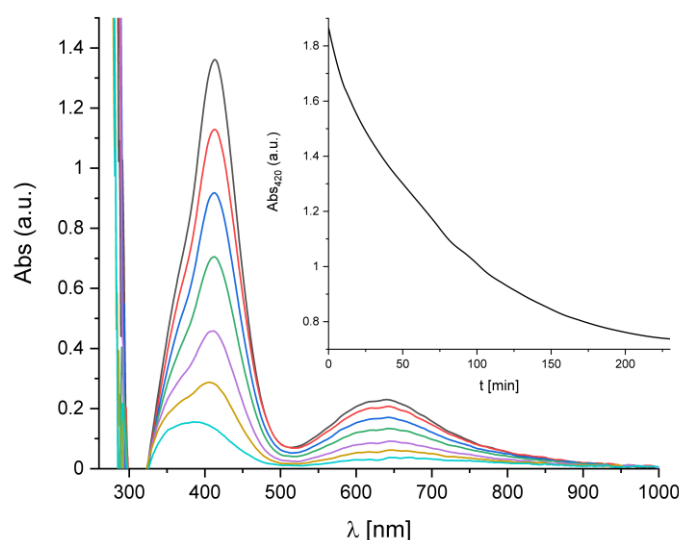


Figure 37. UV/Vis spectra of the decay of **N1PF₆** in dichloromethane at -42 °C and a concentration of 3.4 molL⁻¹. Inset: Absorption trace at 420 nm.

However, only an insignificant increase of the half-life time from five minutes to six minutes can be observed for the decay in dichloromethane-*d*₂. Therefore, the main decay reaction is not the reaction between dichloromethane and the nitrene compound. In a second experiment the decay was performed in chloroform as solvent. Beside the lower solubility of **58** compared to dichloromethane an incomplete nitrene formation and also a lower stability can be observed (Figure 38). This emphasizes the influence of the solvent choice especially when a solvent with lower C–H bond energy^[32] is chosen.

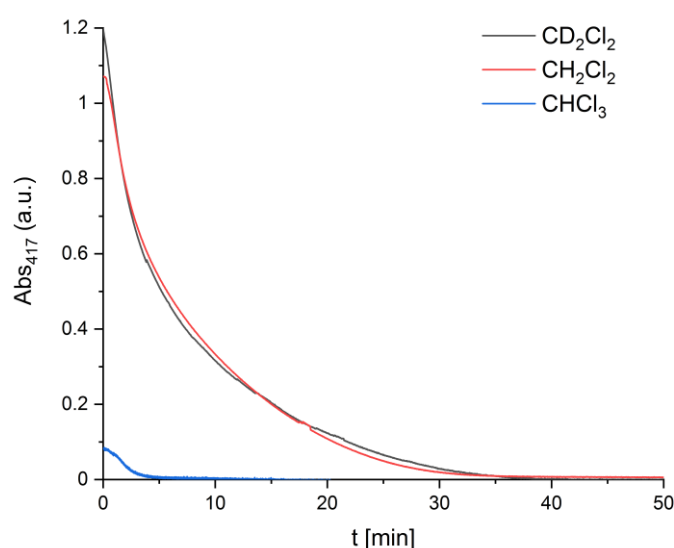


Figure 38. Comparison of the decay reaction in dichloromethane-*d*₂, dichloromethane and chloroform of **N2PF₆**.

Beside the solvent also the influence of the nitrene concentration on the stability was investigated. Therefore, the decay of **N2PF₆** was monitored by UV/Vis spectroscopy at three different concentration in dichloromethane (1.7 mmolL⁻¹, 3.4 mmolL⁻¹ and 6.8 mmolL⁻¹) at a temperature of -42 °C (Figure 39). Due to limitation of the detector for the highest concentration a different wavelength was chosen. Nevertheless, the decay of the same band was observed. When the decay at the three different concentration are compared it is noticeable that for a higher concentration a higher stability is obtained. For a concentration of 6.8 mmolL⁻¹ a half-life time of 25 minutes is obtained and for a concentration of 1.7 mmolL⁻¹ a half-life time of two minutes. Also, for all three concentration the decay is neither first nor second order, but a mixed order. This further shows that the decay is due to at least two decay reactions, one reaction with the solvent and one of an inter- or intramolecular reaction of the nitrene complex.

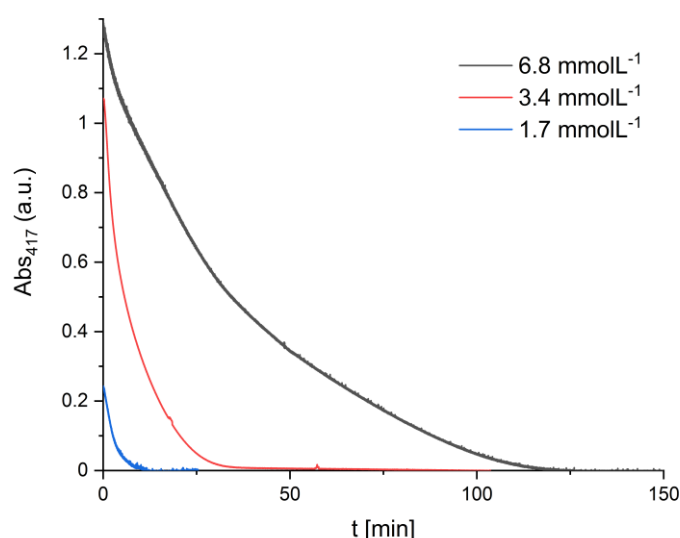


Figure 39. Comparison of the decay reaction of **N2PF₆** in dichloromethane with different concentrations. The absorption for the reaction with a concentration of 6.8 molL⁻¹ was measured at 450 nm.

To further characterize the copper nitrene complexes, the nitrenes **N1PF₆**, **N2PF₆**, **N3PF₆**, **N6PF₆** and **N19PF₆** were analyzed by ¹H NMR spectroscopy in dichloromethane-*d*₂ at -80 °C. Due to the low solubility of ^sPhINTs the concentration is limited to 10 mmolL⁻¹. This limited the possible NMR experiments to ¹H NMR, COSY and HSQC. Owing to the limited experiments and the overlap between most signals not all signals could be assigned. Due to the characteristic shift of the apical carbon atom it was possible to assign the apical hydrogen atom with the HSQC experiment. When the difference in the chemical shift of the apical hydrogen in the nitrene complex and the copper precursor complex ($\Delta\delta(\text{H}_{\text{apical}}) = \delta_{\text{precursor}}(\text{H}_{\text{apical}}) - \delta_{\text{nitrene}}(\text{H}_{\text{apical}})$) is compared with the thermal stability of the nitrene complex, the stabilization of the nitrene complex is correlated linearly with the chemical shift of the H_{apical} atom in the nitrene complex (Figure 40, Table 15), with the exception of **N19PF₆**.

Table 15. Correlation of the half-life time and the difference of the chemical shift of the apical hydrogen ($\Delta\delta(H_{\text{apical}}) = \delta_{\text{precursor}}(H_{\text{apical}}) - \delta_{\text{nitrene}}(H_{\text{apical}})$) for the nitrenes **N1PF₆**-**N3PF₆**, **N6PF₆** and **N19PF₆**.

	$t_{1/2}$ [min]	$\Delta\delta(H_{\text{apical}})$ [ppm]
N1PF₆	50	0.17
N2PF₆	5	0.00
N3PF₆	42	0.12
N6PF₆	14	0.03
N19PF₆	6	-0.36

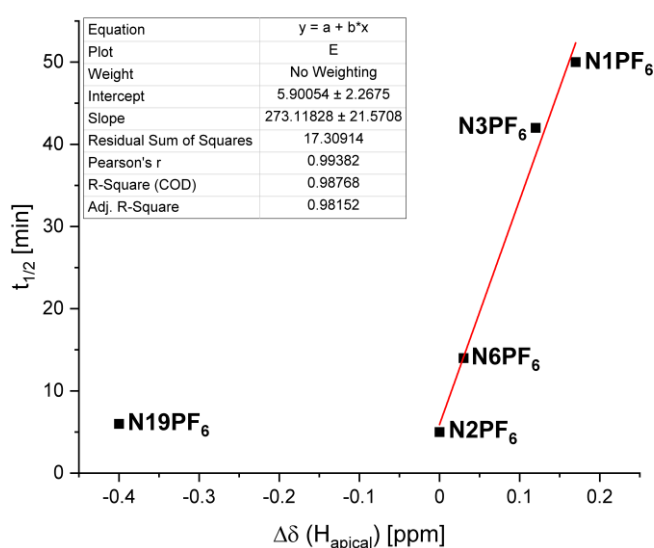


Figure 40. Connection between the change in the chemical shift of the apical hydrogen atom and the half-life time of the nitrene complexes.

Furthermore, it is noticeable that **N19PF₆** is the only nitrene complex with a higher chemical shift in the nitrene than in the precursor complex and the only nitrene complex with leads to a decay product with is enriched in the $[N-H]^+$ decay product. If this is a coincidence or if there is a trend needs to be further investigated in the future.

When the 10 mM solution of **N3PF₆** in dichloromethane- d_2 is slowly warmed to room temperature crystal suitable for single crystal X-ray diffraction were obtained. The crystallized decay product is not the expected complex $[Cu\{HC(Ph_2Pz)_2Melm\}(NHTs)]PF_6$ but the copper(II) complex $[Cu\{HC(Ph_2Pz)_2Melm\}_2](PF_6)_2$. The decay product of the nitrene **N3PF₆** crystallizes monoclinic in the space group $C2/c$ with $Z = 4$. The cation structure is shown in Figure 41 and selected bond lengths and angles are presented in Table 16. The crystallographic details are provided in Table 57 in the Appendix. The second ligand in the complex is symmetry adapted. Therefore, the angles $N(Pz) - Cu N^*(Pz)$, $N(Pz') - Cu N^*(Pz')$ and $N(Melm) - Cu N^*(Melm)$

are fixed. The coordination motif is a Jahn-Teller distorted octahedron. The octahedron is compressed along the N(Melm)–Cu–N(Melm) axis.

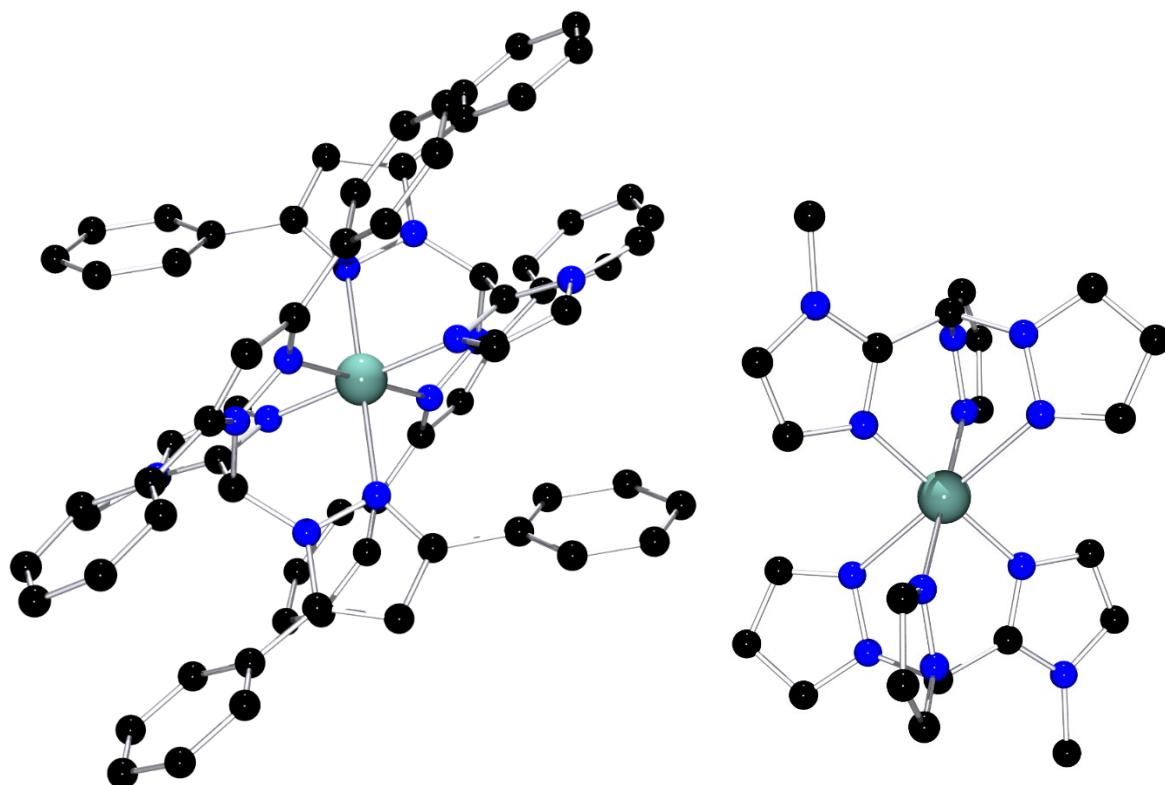


Figure 41. Left: Molecular structure of $[\text{Cu}\{\text{HC}(\text{PhPz})_2\text{Py}\}_2]^{2+}$ in crystals of $[\text{Cu}\{\text{HC}(\text{PhPz})_2\text{Py}\}_2](\text{PF}_6)_2$. Right: Different view of the molecular structure of $[\text{Cu}\{\text{HC}(\text{PhPz})_2\text{Py}\}_2]^{2+}$ in the solid-state, substituents on the pyrazolyl are omitted for clarity. Hydrogen atoms were omitted for clarity.

Table 16. Selected bond lengths [Å] and angles [°] for $[\text{Cu}\{\text{HC}(\text{PhPz})_2\text{Py}\}_2](\text{PF}_6)_2$.

Bond lengths		Bond angles	
C(ap) – C(Melm)	1.499(8)	N(Pz) – C(ap) – N(Pz')	110.6(4)
C(ap) – N(Pz)	1.451(7)	N(Pz) – C(ap) – C(Melm)	111.3(4)
C(ap) – N(Pz')	1.460(6)	N(Pz') – C(ap) – C(Melm)	110.2(4)
Cu – N(Pz)	2.257(4)	N(Pz) – Cu – N*(Pz)	180.0
Cu – N(Pz')	2.311(5)	N(Pz') – Cu – N*(Pz')	180.0
Cu – N(Melm)	1.947(4)	N(Melm) – Cu – N*(Melm)	180.0
		N(Pz) – Cu – N(Pz')	78.2(2)
		N(Melm) – Cu – N(Pz)	87.2(2)
		N(Melm) – Cu – N(Pz')	88.7(2)
		N(Melm) – Cu – N*(Pz')	88.7(2)
		N(Melm) – Cu – N*(Pz')	91.3(2)
		τ_4^a	0.00

$$^a \tau_4 = \frac{360^\circ - (\alpha + \beta)}{141^\circ} \quad [147]$$

4.3.4 DFT calculations

Additional information about the electronic structure of the copper nitrene complexes **N1**⁺, **N2**⁺ and **N3**⁺ were obtained by DFT calculations; performed by Dr. A. Hoffmann. For the calculation the hybrid functional TPSSh with the Ahlrichs type basis set def2-TZVP, a PCM solvent model for dichloromethane and an empirical dispersion correction with Becke-Johnson damping were used. This combination was applied because it could be shown before that good results with larger molecules can be obtained.^[150] The synthesized copper nitrene complexes with ^sPhINTs (**58**) have two possible binding modes of the nitrene moiety, the κ^1 -N,O binding mode and the κ^2 -N,O binding mode (Figure 42).

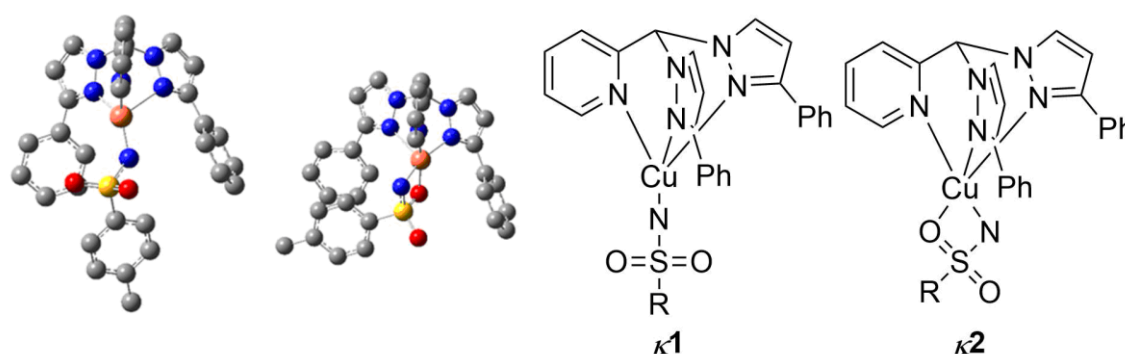


Figure 42. Left: Example of both possible coordination motifs of the nitrene moiety (all other possibilities are given in Figure 109 in the Appendix). Shown is the κ^1 -N,O binding mode (left) and the κ^2 -N,O binding mode (right) of **N1**⁺ in the singlet state. Right: Schematic drawing of both coordination motifs.

For the copper nitrene complexes **N1PF₆**, **N2PF₆** and **N3PF₆** the structure in solution of the singlet and triplet spin state of the two possible coordination motifs have been calculated (Table 17). All energies are close with the exception of the energy of the singlet state of the κ^1 -N,O binding mode (Table 18). The singlet κ^2 -N,O binding mode is the most stable for **N1**⁺ and **N2**⁺ and the spin state is in accordance with the experimentally determined spin state, while for **N3**⁺ the singlet κ^2 -N,O binding mode is within the accuracy of the calculations the lowest configuration. In the literature^[150] it is known for Cu₂O₂ cores, that the donor flexibility and possible conformers complicate the calculation, this might as well be true for copper nitrene complexes. A more accurate method for the determination of the energy is the domain-based local pair natural orbital coupled cluster single-double-triple (DLPNO-CCSD(T)) calculation.^{[151]–[153]} Due to the size of the copper nitrene complexes the bases are limited to 2z bases. The calculation is also theoretically possible with a truncated system, but the use of a truncated system is not appropriate for the description of reactive copper compounds.^[154] The DLPNO-CCSD(T) calculations also show that the singlet spin state is favoured and that the κ^2 -N,O binding mode is favoured as well (Table 18).

Table 17. Key geometric parameters for the singlet and triplet state of copper nitrenes **N1PF₆** – **N3PF₆** in the κ^1 - and κ^2 -mode (Gaussian16; TPSSh/def2-TZVP and PCM solvent model for dichloromethane and the empirical dispersion correction with Becke-Johnson damping).

	Cu – N(Pz)	Cu – N(Pz')	Cu – N(Py/Im)	Cu – N(nitrene)	Cu – O(nitrene)
<i>Bond lengths of N1PF₆ [Å]</i>					
singlet κ^1	1.945	2.292	1.983	1.752	-
triplet κ^1	1.983	2.087	2.059	1.805	-
singlet κ^2	1.979	2.487	1.951	1.868	1.902
triplet κ^2	2.089	2.150	2.036	1.947	2.076
<i>Bond lengths of N2PF₆ [Å]</i>					
singlet κ^1	1.942	2.335	1.981	1.759	-
triplet κ^1	1.987	2.073	2.059	1.803	-
singlet κ^2	1.981	2.488	1.946	1.870	1.897
triplet κ^2	2.082	2.175	2.053	1.944	2.122
<i>Bond lengths of N3PF₆ [Å]</i>					
singlet κ^1	1.974	2.307	1.964	1.764	-
triplet κ^1	1.986	2.126	2.023	1.811	-
singlet κ^2	1.980	2.516	1.950	1.870	1.890
triplet κ^2	2.047	2.381	1.980	1.955	2.103

Table 18. Calculated spin states and relative energies for the copper nitrenes **N1⁺** – **N3⁺** in the κ^1 - and κ^2 -mode. The energy is stated relative to the lowest spin state of the corresponding copper nitrene which is set to 0.0 kcalmol⁻¹.

Spin state	Relative energy [kcalmol ⁻¹]					
	N1⁺	N2⁺	N3⁺	N1⁺	N2⁺	N3⁺
	DFT			DLPNO-CCSD(T)		
singlet κ^1	12.9	11.9	13.8	17.5	17.4	15.0
triplet κ^1	0.3	0.6	0.0	8.5	9.0	3.6
singlet κ^2	0.0	0.0	3.8	0.0	0.0	0.0
triplet κ^2	3.3	3.9	1.3	2.1	3.1	*

* This calculation stopped due to memory problems.

Further information can be obtained from the NBO charges and charge transfer energies of the copper nitrene complexes **N1⁺** – **N3⁺** and **N6⁺** (Table 19). A more negative NBO charge reveals that the donor is more basic. Therefore, the basicity trend of the different *N* donors present in the copper nitrene complexes is methyl imidazole > pyridine = 4-chloropyridine > pyrazole. It can also be observed that the substitution on the pyridine and the pyrazole does not influence the basicity of the *N* donor. The charge transfer energies show the relative donor

character. For these bis(pyrazolyl)methane copper nitrene complexes the charge transfer energies demonstrate that pyrazolyl is the weaker donor compared to pyridine and methyl imidazolyl. This leads to a donor competition between the different donors in these copper nitrene complexes. And even a small change in the ligand design effects the donor character. This effect is known for bis(pyrazolyl)methane ligands and has a strong influence on catalytic reactions.^[49]

Table 19. NBO charges (in e^- units) and charge transfer energies (in kcalmol^{-1}) for selected atoms for the singlet state of copper nitrenes **N1⁺** – **N3⁺** and **N6⁺** in the κ^2 -mode (NBO6.0. TPSSh/def2-TZVP and PCM solvent model for dichloromethane and the empirical dispersion correction with Becke-Johnson damping).

	N1⁺	N2⁺	N3⁺	N6⁺
<i>NBO charges</i>				
Cu	1.3	1.3	1.3	1.3
N(Pz/Pz')	-0.34/-0.37	-0.33/-0.37	-0.33/-0.34	-0.37/-0.33
N(Py/Im)	-0.472	-0.47	-0.53	-0.46
N(nitrene)	-1.04	-1.04	-1.00	-1.04
O(nitrene)	-0.88	-0.88	-0.87	-0.88
<i>Charge transfer energies</i>				
N(Pz/Pz') → Cu	13.1/33.3	13.0/33.3	9.3/37.5	12.9/31.8
N(Py/Im) → Cu	36.6	36.4	33.0	36.5
N(nitrene) → Cu	19.9	19.6	20.5	19.4

The bonding situation in the copper nitrene complexes can be explained by NBO analysis combined with Wiberg bond indices (WBI). Two interactions between the nitrene nitrogen atom and the copper ion are shown by NBO analysis. One covalent bond between the nitrene nitrogen atom and the copper ion (Figure 43a) and one donor acceptor interaction from the LP(1) of the nitrene to the copper is present. The covalent bond is polar and located with 60% on a copper d orbital and with 40% on a p orbital of the nitrene nitrogen atom (Table 20). The covalency of this bond is shown by a WBI of 0.76 for all four copper nitrene complexes. The donor acceptor interaction is present with a charge transfer of 19-20 kcalmol^{-1} . The NBO charge of the copper ion is 1.3 e^- units representing a copper(II) ion. In addition, the spin density is focused on the copper ion and the nitrene nitrogen atom (Figure 43b-d).

Table 20. Form and occupancy of the lone pairs of the nitrene N donor atom and of the bond of the copper ion and the N donor atom of the nitrene for the singlet state of copper nitrenes **N1⁺** – **N3⁺** and **N6⁺** in the κ^2 -mode (NBO analysis with NBO6.0. TPSSh/def2-TZVP and PCM solvent model for dichloromethane and the empirical dispersion correction with Becke-Johnson damping).

Nitrene		Occupancy [electrons]		Hybridization [%]	Polarization	Localization [%]
N1⁺	LP1 (nitrene)	1.94		s(77.7) p ^{0.29} (22.2)		
	LP2 (nitrene)	1.77		p ^{99.9} (99.2)		
	Cu – N(nitrene)	1.95	Cu	d ^{65.6} (98.5)	0.78	60.4
			N	p ^{67.1} (97.9)	0.63	39.6
N2⁺	LP1 (nitrene)	1.94		s(77.5) p ^{0.29} (22.4)		
	LP2 (nitrene)	1.77		p ^{99.9} (99.2)		
	Cu – N(nitrene)	1.95	Cu	d ^{65.2} (98.5)	0.78	60.4
			N	p ^{66.3} (97.8)	0.63	39.6
N3⁺	LP1 (nitrene)	1.94		s(78.4) p ^{0.27} (21.5)		
	LP2 (nitrene)	1.77		p ¹ (99.4)		
	Cu – N(nitrene)	1.95	Cu	d ^{64.2} (98.4)	0.78	60.4
			N	p ^{75.7} (97.9)	0.63	39.6
N6⁺	LP1 (nitrene)	1.94		s(77.5) p ^{0.29} (22.4)		
	LP2 (nitrene)	1.77		p ^{99.9} (99.2)		
	Cu – N(nitrene)	1.95	Cu	d ^{63.9} (98.4)	0.78	60.3
			N	p ^{65.4} (97.8)	0.63	39.7

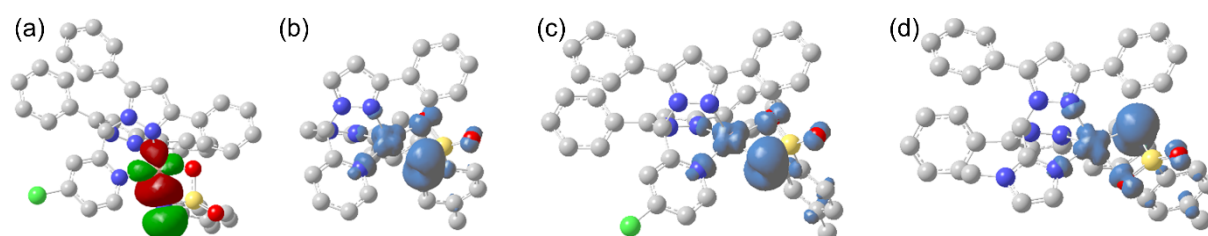


Figure 43. Orbital representation of the covalent bond between a Cu d orbital and p orbital of the nitrene N atom (a) and the spin density of the nitrene **N1⁺** (b), the nitrene **N2⁺** (c) and the nitrene **N3⁺** (d).

Further information on the character of the nitrene can be obtained by energy decomposition analysis (EDA), this was performed exemplarily for **N1⁺**.^[155] The singlet κ^2 and triplet κ^1 isomer are both possible and close in energy, so we decompose both isomers in three fragments: the nitrene moiety, the copper ion and the ligand. Due to the different spin states we have to

distinguish between two possible isomers for the triplet state (nitrene and iminyl) and three for the singlet state (nitrene, iminyl and imido). AOMix wavefunction method determines the orbital interaction energy (E_{orb}) of each possible isomer. The smallest absolute value for E_{orb} is found for the Cu(I) nitrene interpretation (Table 21). Further evidence can be provided by the effective oxidation state of the copper ion determined by Salvador's method:^[156] for the singlet κ^2 conformer of **N1**⁺ an oxidation state of +I is obtained. Therefore, the copper nitrene complexes can be characterized as a singlet nitrene.

Table 21. Fragmentation of **N1**⁺ for EDA and E_{orb} .

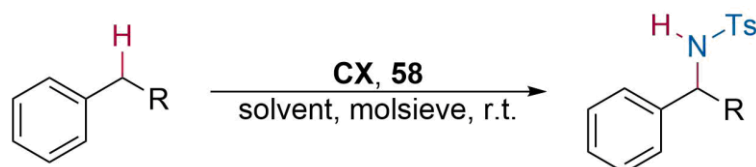
	singlet κ^2 nitrene: Cu(I)– ¹ NR	singlet κ^2 iminyl: Cu(II)– ² NR [•]	singlet κ^2 imido Cu(III)–NR ²⁻	triplet κ^1 nitrene: Cu(I)– ³ NR	triplet κ^1 iminyl Cu(II)– ² NR [•]
<i>ligand</i>					
charge	0	0	0	0	0
multiplicity	1	1	1	1	1
<i>copper ion</i>					
charge	1	2	3	1	2
multiplicity	1	2	1	3	2
<i>nitrene</i>					
charge	0	-1	-2	0	-1
multiplicity	1	2	1	1	2
E_{orb} [kcalmol ⁻¹]	-209	-782	-741	-158	-264

4.3.5 C–H amination

The complexes **C1**, **C2**, **C3**, **C6**, **C11**, **C12** and **C19** were investigated regarding their capability as catalyst for C–H amination reactions of different substrates classes. While the complexes **C1**, **C2**, **C3**, **C6**, and **C19** were investigated for their reactivity, for the two chiral complexes **C11** and **C12** the focus was on asymmetric reaction. Moreover, with **C19** the catalytic reaction with benzoyl azide (**113**) as nitrene generating agent was tested. While different nitrene generating agents were used in catalytic reactions, only those will be discussed in the following part where a successful conversion of the substrate was detected. For the reaction with **58** also the iminoiodinane PhINTs (**116**) can be used as nitrene generating agent, but this leads to a lower yield. All reaction details are given in the experimental part. The reaction protocols for the amination of toluene and cyclohexane with **58** were optimized before^[102] and transferred to the new complexes.

The first substrate class used in the catalytic C–H amination with **58** and **113** are benzylic substrates (Scheme 34). For comparison of the reactivity toluene and ethyl benzene were investigated, while for asymmetric reactions beside ethyl benzene also neopentyl benzene, bibenzyl and benzyl bromide were applied. For these substrates the reaction conditions were

optimized using **C7** ($[\text{Cu}\{\text{HC}(\text{tBuPz})_2\text{Py}\}(\text{MeCN})]\text{PF}_6$). Complex **C7** was chosen for the optimization, because the ligand has an aliphatic substituent like the ligands in **C11** and **C12**, the ligand^[29] and the complex^[102] synthesis are established and can be scaled up. The syntheses of complexes **C11** and **C12** are not easily scaled up. For all used substrates it was observed that the amination takes selectively place in the benzylic position.



Scheme 34. C–H amination of benzylic substrates.

When the reactivity of the different complexes is compared it can be observed that the substitution in the 5-position of the pyrazole only has a minor influence and the yield for **C1** for toluene is a bit lower than for **C6**, but for ethylbenzene the opposite is true. However, for the different third *N* donor a major effect can be found. Methyl imidazolyl leads to lower yields compared to the pyridinyl based *N* donor (Table 22).

Table 22. Yields* ([%]) of the catalytic C–H amination reactions of benzylic substrates.

R =	H	Me	^t Bu	Br	Bz
C1	69	49			
C2	21	57			
C3	22	10			
C6	76	32			
C7		40	traces	traces	23
C11	56	43 (50:50)			
C12^a	8	7 (52:48)	traces	traces	3
C19	76	56			

*Yields were determined using ¹H NMR spectroscopy and nitromethane as internal standard.

^a Formed *in situ* by the addition of 10 equiv. of acetonitrile.

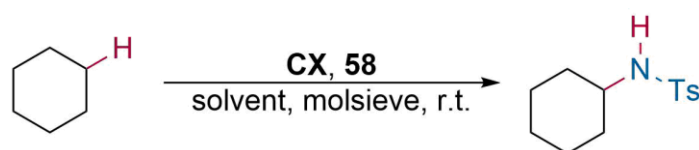
In addition, the established reaction protocol was further optimized. Therefore, the amination of toluene with **C6** was performed solvent-free (41%), with less solvent and only 1 equivalent of substrate (57%), with only 10 equivalents of substrate (43%), with 10 equivalents of substrate and only 30 minutes of reaction time (32%). The yield decreases from 76% to 57%, when no excess instead of 188 equivalents of substrate is used. Even though the use of less substrate is beneficial for applications with valuable substrates.

For the asymmetric C–H amination reaction **C11** displays a good activity and the yields for both benzylic substrates are comparable to the other used complexes. However, no enantio-

enriched product was obtained. In contrast when **C12** is used for the amination reaction of ethylbenzene a slightly lower yield of 25% is obtained, but also a slightly enantio-enriched product is obtained with an enantiomeric excess of 10. One reason for the lower yield is that **C12** does not dissolve in phenylchloride, which is the optimal solvent for this reaction. Therefore, the reaction was performed in dichloromethane. Due to the problematic synthesis of isolated **C12** for further investigations **C12** was synthesized *in situ* from **C13** by the addition of acetonitrile. This leads to both a lower yield and a lower enantiomeric excess. However, the enantiomeric excess can be increased from 4 to 10 when the reaction temperature is decreased to 0 °C.

For the C–H amination reaction with **C19** and **113** different solvents, different concentrations of the solution of **113** and different addition speeds were used. The optimal reaction conditions apply dichloromethane as solvent, a concentration of 0.1 mM of the stock solution of **113** and the addition of **113** in one load. This leads to a yield of 16% for the amination of ethylbenzene and 4% of toluene. While this reaction protocol still leads to lower yields in comparison to the amination with **58**, it is the first protocol for a bis(pyrazolyl)methane copper(I) complex which utilizes aromatic azides for the amination of C–H bonds. Beside **C19** also **C7** ($[\text{Cu}\{\text{HC}(\text{tBuPz})_2\text{Py}\}(\text{MeCN})]\text{PF}_6$, 0%), **C8** ($[\text{Cu}\{\text{HC}(\text{tBuPz})_2\text{MeIm}\}(\text{MeCN})]\text{PF}_6$, 12%), and **C18** ($[\text{Cu}\{\text{HC}(\text{tBuPz})_2\text{MeIm}\}]\text{SbF}_6$, 4%) were used as catalyst for the C–H amination of ethylbenzene with **113**. On the one hand, it can be shown that for a successful reaction with **113** pyridine is not a suitable third *N* donor group and, on the other hand, a well-defined complex is better suited than an *in situ* formed complex.

The second substrate class used in catalytic C–H aminations with **58** are aliphatic substrates (Scheme 35). The only used substrate from this substrate class was cyclohexane.

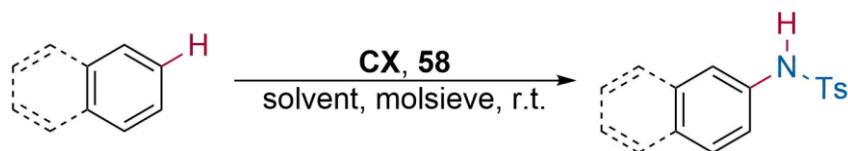


Scheme 35. C–H amination of cyclohexane.

For the C–H amination of cyclohexane, the aromatic substituted complex **C1** has the highest yields and the other complexes show similar yields (Table 23). For the two chiral complexes **C11** and **C12** the same trend as for the benzylic substrates is found. **C11** gives a high yield comparable to the other used catalyst. In contrast **C12** does not dissolve in the optimized reaction condition and therefore, the reaction was performed in dichloromethane which decreases the yield of substrate.

The third substrate class used in catalytic C–H aminations with **58** are aromatic substrates (Scheme 36). The reaction conditions of the amination of aromatic substrates were optimized

using the complex **C6** and it could be shown that the optimal reaction condition is in acetonitrile with 5 equivalents of substrate. Also, different aromatic substrates were used, and benzene and naphthalene were both successfully aminated. Naphthalene was aminated selectively in the 2-position.



Scheme 36. C–H amination of aromatic substrates.

Comparing the yield for benzene the pyridine-based complexes **C1** and **C6** display higher yields compared to **C2** and **C3**. Contrary to this for naphthalene the complexes **C2**, **C3** and **C6** display yields of around 25%, only **C1** has a lower yield of 7% (Table 23).

Table 23. Yields* ([%]) of the catalytic C–H amination reactions of aliphatic and aromatic substrates.

	cyclohexane	benzene	naphthalene
C1	30	35	7
C2	18	24	25
C3	18	22	23
C6	19	45	27
C7		29	
C11	38		
C12^a	7		
C16		28	

*Yields were determined using ^1H NMR spectroscopy and nitromethane as internal standard.

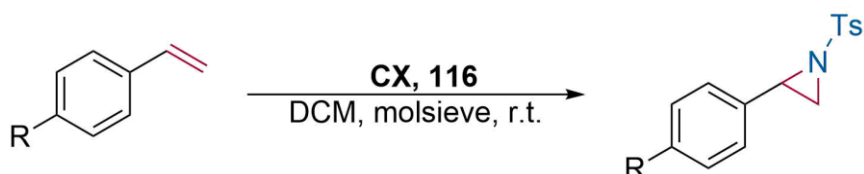
^a Formed *in situ* by the addition of 10 equiv. of acetonitrile.

Overall, it can be concluded that for the C–H amination pyridine as third *N* donor unit in bis(pyrazolyl)methane complexes leads to the highest yields. Also, the substitution in the 5-position has a minor effect, as **C6** is slightly more reactive than **C1**. And in addition, it was observed that the C–H amination proceeds selectively in the position with the lowest bond dissociation energy. The only side reaction is the copper(I) catalyzed cleavage of $^s\text{PhINTs}$ into H_2NTs and ^sPhI , which is well known in literature for other copper catalyzed reactions with $^s\text{PhINTs}$.^[157]

4.3.6 Aziridination

The complexes **C1**, **C2**, **C3**, **C6**, **C11**, **C12** and **C19** were investigated regarding their capability as catalyst for the aziridination of different substituted styrene derivatives. While the complexes

C1, **C2**, **C3**, **C6**, and **C19** were investigated for their reactivity, for the two chiral complexes **C11** and **C12** the focus was on asymmetric reaction. For **C19** the focus was on catalytic reaction with benzoyl azide (**113**) as nitrene generating agent. In contrast to the C–H aminations for the aziridination reaction PhINTs (**116**) was used as nitrene generating agent instead of ^sPhINTs (**58**). **116** has the disadvantage of an even lower solubility in solvents beside dichloromethane compared to **58**, but the synthesis of **116** is less time consuming and has a higher atom efficiency.



Scheme 37. Styrene aziridination with bis(pyrazolyl)methane copper complexes as catalyst.

The first investigated styrene derivatives as substrate were 4-substituted styrenes (Scheme 37). The aziridination was performed by a reaction protocol which was optimized before.^[102] The protocol was tried to be optimized further, by using an excess of substrate and reducing the reaction time. The variation did not lead to an increased yield or the same yield in a shorter reaction time. For the aziridination of 4-substituted styrene derivatives it can be observed that in accordance with the C–H amination bis(pyrazolyl)methane copper complexes with pyridine as third *N* donor lead to the highest yields (Table 24).

Table 24. Yield* ([%]) of the aziridination of 4-substituted styrene derivatives. The enantiomeric excess for the reaction with **C12** is given in the bracket.

R =	H	CF ₃	NO ₂	OMe
C1	69	29	41	14
C2	50	32	13	4
C3	39	56	40	7
C6	64	64	25	24
C11	16	46	42	
C12^a	55(4)	52(10)	58(8)	32
C19	58			

*Yields were determined using ¹H NMR spectroscopy and nitromethane as internal standard.

^a Formed *in situ* by the addition of 10 equiv. of acetonitrile.

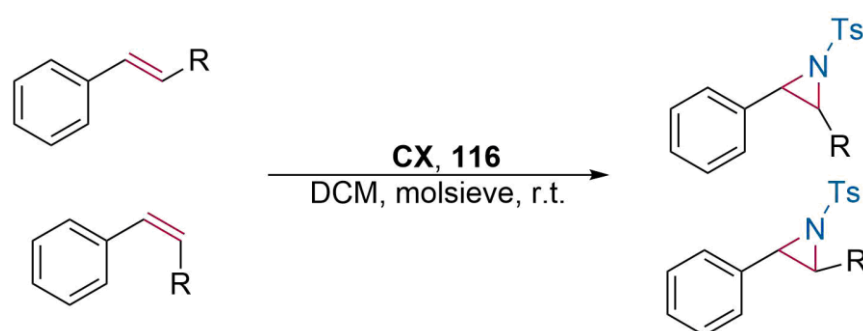
To gain insight into the mechanism of the aziridination also styrene-β-*d*₂ was used as substrate with **C1** as catalyst. A reaction with a mixture of styrene and styrene-β-*d*₂ was conducted. The standard protocol was slightly adjusted and of each styrene derivative one equivalent was added to the reaction mixture. When the ratio of both styrene derivatives in the substrate (*d*₀/*d*₂, 52.1/47.9) and the product (*d*₀/*d*₂, 50.5/49.5) is compared a slight enrichment of the styrene-β-

d_2 is observed. This is an indicator for an N–C association between the electrophilic nitrene moiety and the β -styrene position in the electrophilic transition state.^[65]

For the asymmetric aziridination it can be observed that **C11** and the *in situ* formed **C12** both have a good activity and the yields are comparable to the other used complexes. However, no enantio-enriched product was obtained for **C11**. When **C12** is used for the aziridination a slightly enantio-enriched product is obtained with an enantiomeric excess of 4 to 10. However, the enantiomeric excess for the aziridination of styrene can be increased from 4 to 12, by decreasing the reaction temperature to 0 °C.

For the aziridination of styrene with **C19** beside **116** also **113** could be utilized but this also leads to a lower yield of 5%, while the aziridination with **116** leads to a yield of 58%.

The second investigated styrene derivatives as substrate were β -substituted styrenes (Scheme 38). Therefore, *cis*- and *trans*- β -methyl styrene and *cis*- and *trans*-stilbene were used as substrate.



Scheme 38. Aziridination of internal double bonds with bis(pyrazolyl)methane copper complexes as catalyst.

For the aziridination of internal double bonds it is known in the literature that a *trans*-substrate will be converted to the *trans*-product, while for a *cis*-substrate a product mixture will be obtained. The main product depends on the used catalyst. The loss in stereoinformation is due to the reaction mechanism, which is reported to be a radical two step mechanism (Scheme 17).^{[65],[71],[72]} When bis(pyrazolyl)methane copper complexes are used the same general trend can be observed. Most notable is that for the three complexes **C1**, **C2** and **C6** a high amount of stereoinformation is preserved when *cis*- β -methyl styrene is converted (Table 25). One reason for the high amount of preserved stereoinformation can be that bis(pyrazolyl)methane nitrene complexes enable not only the radical two step mechanism, but also a concerted mechanism. DFT calculation² of the reaction mechanism of the aziridination of styrene with **C1** as

² DFT calculation were performed by Dr. Florian Schön, more informations are given in the publication.^[158]

catalyst have demonstrated that both mechanisms are possible and the concerted mechanism is favored by around 10 kcalmol⁻¹.

For the amination of internal double bonds with the chiral complexes it can be observed that for **C11** no increase of the enantiomeric excess is observed, while with **C12** and the use of β -methyl styrene the enantiomeric excess can be increased from 4 to 8 and by the use of stilbene it can be further increased to 30. Besides, the yield for stilbene is lower compared to styrene and β -methyl styrene.

Table 25. Yield* ([%]) of the aziridination of β -substituted styrene derivatives. The enantiomeric excess for the reaction with **C12** and *trans*-substituted substrate is given in the bracket. For the *cis*-substituted substrate, the *cis/trans*-ratio is given in the brackets.

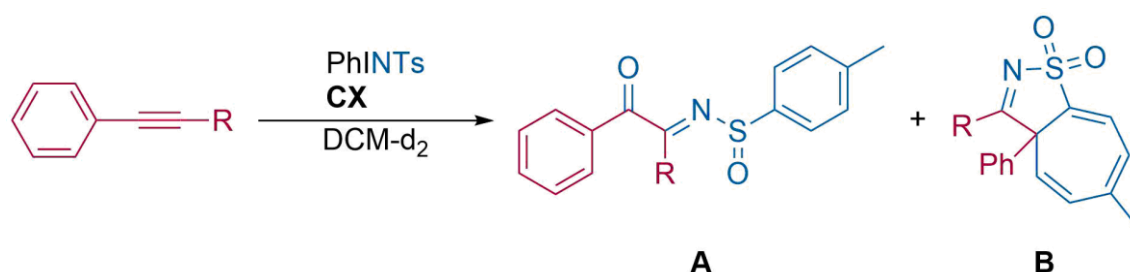
R =	<i>cis</i> -Me	<i>trans</i> -Me	<i>cis</i> -Ph	<i>trans</i> -Ph
C1	57 (86/14)	45		
C2	39 (90/10)	41		
C3	32 (63/37)	47		
C6	42 (88/12)	48		
C7			38 (81/19)	41
C11	39 (33/67)	38		
C12^a	49 (57/43)	55 (8)	24 (49/51)	13 (30)

*Yields were determined using ¹H NMR spectroscopy and nitromethane as internal standard.

^a Formed *in situ* by the addition of 10 equiv. of acetonitrile.

4.3.7 Alkyne rearrangement

In chapter 2.4.1 the tris(pyrazolyl)borate copper nitrene catalyzed rearrangement of alkynes into sulfonamides and isothiazoles was introduced.^[98] In this thesis the reaction protocol was transferred to bis(pyrazolyl)methane copper nitrene complexes (Scheme 39).



Scheme 39. Alkyne rearrangement into sulfonamides and isothiazoles.

As substrate phenylacetylene, prop-1-yn-1ylbenzene and diphenylacetylene was chosen. As catalyst the two complexes **C6** and **C16** were chosen to investigate if the size of the substituents of the pyrazolyl unit has an influence on the products (Table 26). It can be observed that

for the terminal alkyne only the sulfonamide product (**A**) is obtained, while for the internal alkyne a mixture of both products is obtained. For **C6** an enrichment in **A** is observed while for **C16** an enrichment in **B** is found and a higher yield. When these results are compared to the literature^[98] for terminal alkynes a similar yield is obtained with **C6** and a lower yield for **C16**. For internal alkynes the yield obtained in the literature is higher, but in the literature (54:46) and for **C6** (60:40) a slight enrichment in the sulfonamide product (**A**) is obtained. In contrast for **C16** an enrichment in **B** (36:64) is observed.

Table 26. Comparison of the yields* ([%]) for the alkyne rearrangement and the product distribution (A:B).

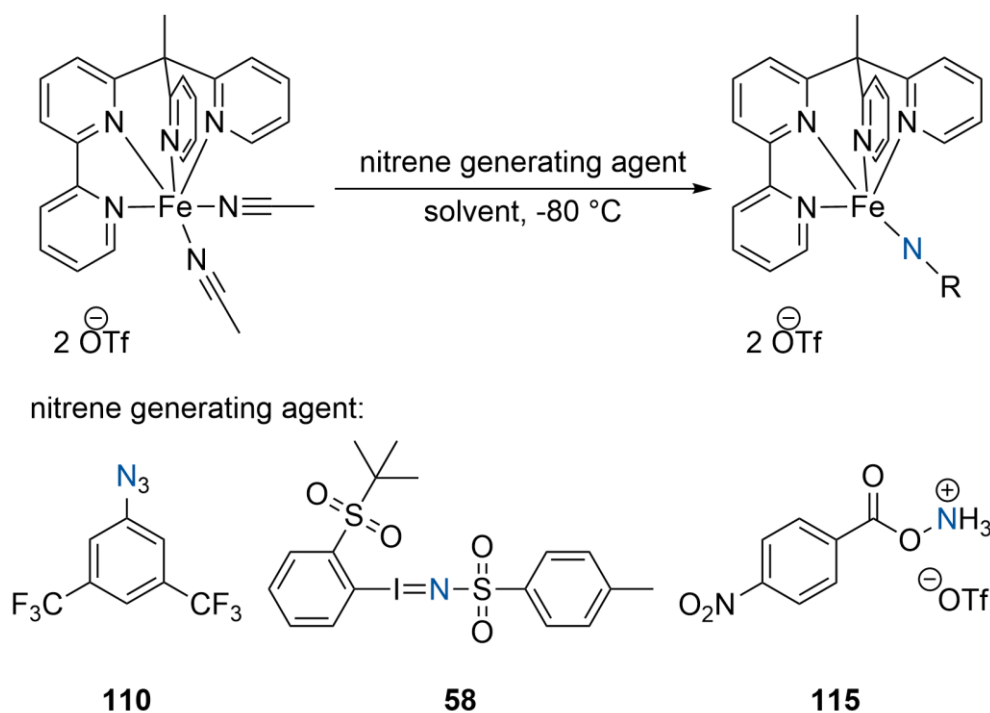
R =	H	Me	Ph
C6	91 (100:0)	22 (60:40)	10 ^a
C16	30 (100:0)	21 (36:64)	0
Tp ^{Br3} Cu(NCMe) ^[98]	89 (100:0)	70 (54:46)	16 ^a

*Yields were determined using ¹H NMR spectroscopy. ^a Due to the low yield the product distribution could not be determined.

4.4 Iron nitrene chemistry

For the synthesis of iron nitrene complexes and their application in different nitrene transfer reactions the complex **C20** ($[\text{Fe}\{\text{MeC}(\text{Py})_2(\text{Bpy})\}(\text{MeCN})_2](\text{OTf})_2$) was used. This complex was chosen because this complex is a suitable precursor complex for the formation and stabilization of highly reactive iron(IV) oxo complexes^[159] and has a good solubility in different solvents. Additionally, the complex $[\text{Fe}\{\text{HC}(\text{Me}_2\text{Pz})_2(\text{Melm})\}(\text{MeCN})_3](\text{BF}_4)_2$ was used in catalytic reactions with ^sPhINTs (**58**) and toluene, but no conversion was observable.³ This complex was chosen because iron acetonitrile triflate complexes tend to form equilibria for the coordination of the coligand and a ligand exchange between triflate and acetonitrile takes place in solution.^[160] This equilibrium could influence the formation of iron nitrene complexes. Therefore, a triflate free complex was used as well.

To form an iron nitrene starting from **C20** three different nitrene generating agents were evaluated. The utilized nitrene generating agents were 3,5-bis(trifluoromethyl)phenyl azide (**110**), ^sPhINTs (**58**) and O-(4-nitrobenzoyl) hydroxylamine triflate (**115**, Scheme 40). The reaction between **C20** and the nitrene generating agent was monitored with UV/Vis spectroscopy in different solvents and at different temperatures. When a reaction between **C20** and the nitrene generating agent could be observed it was investigated if a reaction of the formed species with different substrates takes place.



Scheme 40. Planned iron nitrene generation.

³ The catalytic reactions were performed by Julian Moegling.

The first examined nitrene generating agent was *O*-(4-nitrobenzoyl) hydroxylamine triflate (**115**) and the reaction was performed in acetone, THF, dichloromethane and acetonitrile. In acetone, THF and dichloromethane a reaction was observed. The reactions in acetone and THF were performed at -80 °C. After the addition of *O*-(4-nitrobenzoyl) hydroxylamine triflate to **C20** the band of **C20** at 400 nm and 498 nm disappeared, while new bands at 422 nm in acetone and at 394 nm and 492 nm in THF appear (Figure 44). The addition of methylphenyl sulfoxide does not lead to changes in the UV/Vis spectra. Therefore, no reaction between the formed species and methylphenyl sulfoxide is observable. Also *via* NMR spectroscopy no products could be detected. In dichloromethane the reaction was performed at room temperature, due to the bad solubility of *O*-(4-nitrobenzoyl) hydroxylamine triflate. During the reaction a precipitates forms, which can be dissolved in acetonitrile. Also, the formation of a band at 358 nm was observed, but no reaction with methylphenyl sulfoxide.

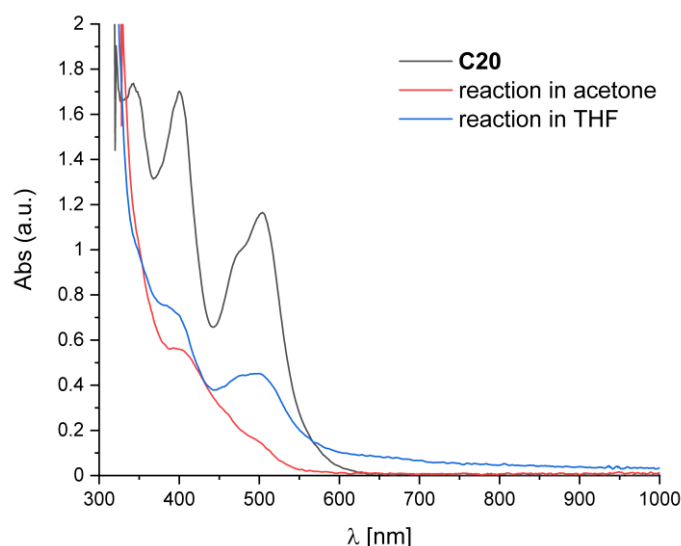


Figure 44. UV/Vis spectra of the reaction of **C20** in THF and acetone at -80 °C.

The next tested nitrene generating agent was 3,5-bis(trifluoromethyl)phenyl azide (**110**). The reaction was carried out at room temperature in dichloromethane. In the UV/Vis spectra, **C20** can be observed with two bands at 395 nm and 484 nm, after the addition of **110** a shift of the band from 484 nm to 470 nm was monitored as well as a formation of a shoulder at 363 nm. Also, a precipitate is formed, which can be redissolved by the addition of acetonitrile. After the formation of the new species different substrates were added (styrene, cyclohexadiene and triphenylphosphane), although only for the addition of triphenylphosphane a reaction can be monitored. The reaction of organic azides and triphenylphosphane is well known in the literature.^[161] Therefore, the reaction between the species and triphenylphosphane does not indicate that the species formed is an iron nitrene intermediate. Another possible explanation would be that the organic azide coordinates to the iron complex and forms the new species.

The last investigated nitrene generating agent is $^{\text{S}}\text{PhINTs}$ (**58**). The reaction was carried out in dichloromethane at $-42\text{ }^{\circ}\text{C}$, $-60\text{ }^{\circ}\text{C}$ and $-80\text{ }^{\circ}\text{C}$. After the addition of **58** to the solution of **C20** the formation of a broad new band at 525 nm can be observed. While at $-80\text{ }^{\circ}\text{C}$ the formation of the new species is very slow, at $-42\text{ }^{\circ}\text{C}$ the new species is only present for 15 minutes. However, at $-60\text{ }^{\circ}\text{C}$ the formation reaction takes about 1 hour, and the new species is present for a few hours. Therefore, after the addition of **58** to a solution of **C20** the formation of a new reactive species can be observed. In order to obtain hints for the formation of an iron nitrene, different substrates were added to the formed species (cyclohexadiene, triphenylmethane, xanthene, 4-nitro styrene and triphenylphosphane). A reaction between the new formed species and triphenylphosphane was observed. The band at 525 nm decayed, while a new band at 460 nm was formed. The new formed band decays when the mixture is warmed to room temperature (Figure 45). Therefore, first hints for the formation of an iron nitrene from **C20** were obtained. However, further proof needs to be obtained by future research.

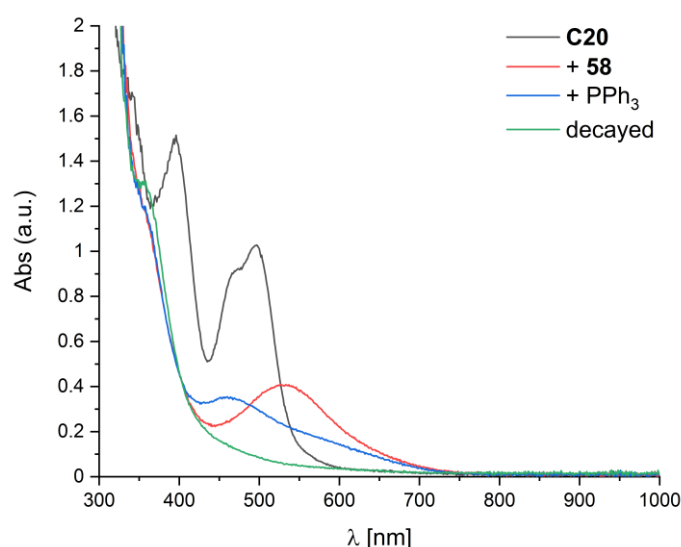


Figure 45. Reaction between **C20**, **58** and triphenylphosphane at $-60\text{ }^{\circ}\text{C}$ in dichloromethane.

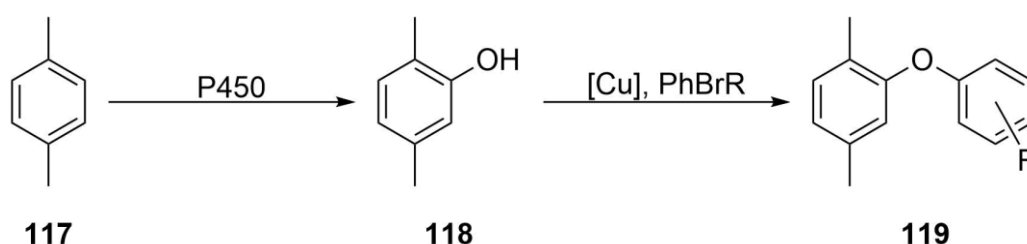
4.5 Development of a chemoenzymatic cascade reaction

The work presented in this chapter was accomplished in close collaboration with Stephanie Mertens and Maximilian Nöth from the Schwaneberg group and Julian Moegling. Stephanie Mertens performed the enzymatic reactions and Maximilian Nöth performed the microgel supported enzymatic reactions. Parts of this chapter are already published:

M. A. S. Mertens, F. Thomas, M. Nöth, J. Moegling, I. El-Awaad, D. F. Sauer, G. V. Dhoke, W. Xu, A. Pich, S. Herres-Pawlis, U. Schwaneberg, *Eur. J. Org. Chem.* **2019**, 2019, 6341.

4.5.1 Combination of hydroxylation and C–O cross-coupling

The first planned cascade reaction is a combination of an aromatic enzymatic hydroxylation of dimethylbenzene (**117**) to yield dimethylphenol (**118**) followed by a copper catalyzed C–O cross-coupling reaction to obtain a diphenyl ether derivative (**119**, Scheme 41). The reaction is planned in a stepwise way, since the C–O cross-coupling reaction needs higher temperature, which will lead to a denaturation of the applied enzyme.



Scheme 41. Planned cascade reaction. First step aromatic hydroxylation of dimethylbenzene followed by C–O cross-coupling in the second reaction.

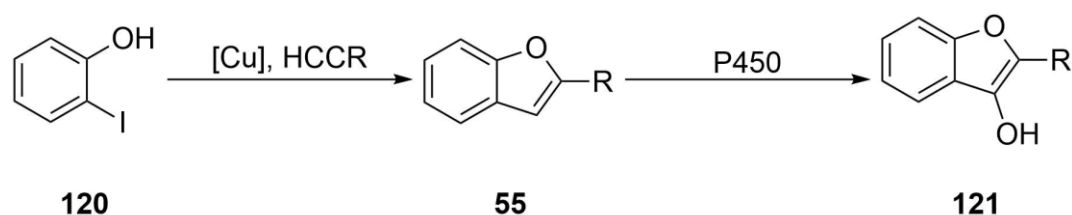
Therefore, the C–O cross-coupling reaction of commercial dimethylphenol with different bromoarenes was investigated. As catalyst *in situ* formed $[\text{Cu}\{\text{HC}(\text{Me}_2\text{Pz})_2\text{Melm}\}]$ (obtained from copper(I) iodide and $\text{HC}(\text{Me}_2\text{Pz})_2\text{Melm}$ (**L14**)) was used. As solvent DMF is used with potassium phosphate as base. The reaction is performed at 100 °C. From commercial **118** the desired diphenyl ether can be isolated in good yields up to 88%.

Due to the high temperatures required for the C–O cross-coupling, the cascade reaction is performed in two steps. First, dimethylbenzene is hydroxylated by a P450 BM3 variant in a low concentrated aqueous solution. The C–O cross-coupling reaction does not work in aqueous solution and needs a higher concentration. **118** was extracted with diethyl ether and applied to perform the C–O cross-coupling reaction. For the reaction using the enzymatic produced dimethylphenol only trace amounts of product were observed.

The incompatibility of the both desired reactions was too high to lead to a working cascade reaction. Therefore, another cascade reaction was planned.

4.5.2 Combination of Sonogashira cross-coupling and hydroxylation

The second planned cascade reaction is a combination of a palladium-free copper catalyzed Sonogashira cross-coupling reaction followed by an enzymatic hydroxylation (Scheme 42). Therefore, iodophenol (**120**) is converted into a benzofuran (**55**) which is converted to a hydroxylated benzofuran (**121**). Benzofuran derivatives are pharmacologically active, for example they feature antimicrobial activity.^[134] For the Sonogashira cross-coupling reaction temperatures above 80 °C are needed, which is not tolerated by P450 BM3 variant. Therefore, the cascade reaction is designed as a stepwise reaction. In the first step the Sonogashira reaction is completed, the reaction mixture is then added to an aqueous solution for the enzymatic hydroxylation.

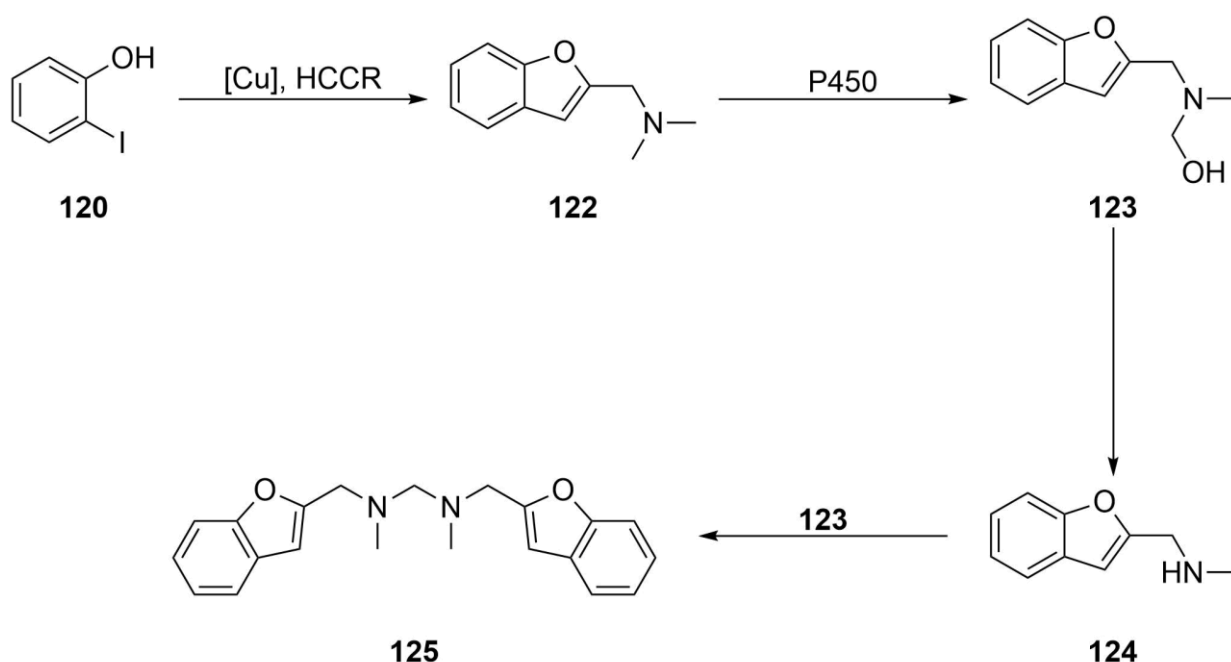


Scheme 42. Planned cascade reaction. First step: Sonogashira coupling of iodophenol with an alkyne to a benzofuran; second step: hydroxylation of the benzofuran.

The literature^[45] known protocol for copper bis(pyrazolyl)methane catalyzed Sonogashira cross-coupling reaction was extended to synthesize benzofurans. The applied catalyst was $[\text{CuCl}_2\{\text{HC}(\text{Pz})_2(\text{Melm})\}]$ (**C15**); besides the high activity in the Sonogashira cross-coupling reaction the complex synthesis is easy to scale up. The solvent of the reaction was switched from DMF/water to DMSO. Even though the reaction is enhanced in DMF/water in comparison to DMSO, DMSO was used for the cascade reaction. The reason is that the compatibility of the enzyme is better with DMSO than with DMF.^[162] When the reaction is performed at 120 °C in DMSO full conversion of iodophenol is observed after 24 h, while in DMF/water the reaction is completed after 12 h. A series of different alkynes can be used in this reaction protocol. Limitation is that only alkynes without primary alcohols, primary and secondary amines or esters can be employed.

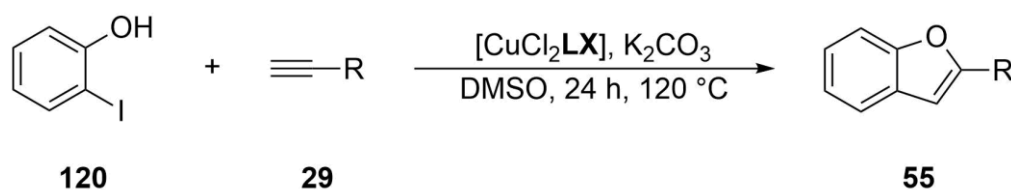
Different purified benzofurans were then tested in the enzymatic hydroxylation. It could be shown that benzofurans containing a tertiary amine are converted by the used P450 BM3 variant. Nevertheless, it could be observed that not the planned cascade reaction was achieved

(Scheme 42). The side chain of the benzofuran derivative was hydroxylated (**123**) and after the elimination of formaldehyde (**124**) an autocatalytic dimerization is observed (**125**, Scheme 43). While the product of enzymatic hydroxylation could only be identified for the dimethylamine functionalized benzofuran (**122**), also the diethyl and *n*-dipropyl amine functionalized benzofuran can be converted. When the crude reaction mixture was used instead of the purified benzofuran the yield was significantly lower, the reason for the lower yield is presumable that the used P450 BM3 variant is deactivated by the copper catalyst. The goal to utilize the raw reaction mixture could be achieved by adding EDTA. To protect the enzyme and enable recycling, the enzyme was immobilized in a microgel. As only an electrostatic and not a covalent immobilization could be achieved, the pH had to be adjusted which lead to a lower conversion.^[163]



Scheme 43. Accomplished cascade reaction.

Beside, the development of a cascade reaction combining the Sonogashira cross-coupling with an enzymatic hydroxylation the Sonogashira cross-coupling reaction was investigated further (Scheme 44). Besides the influence of the solvent, the ligand design, and different alkynes (**29**) were investigated.



Scheme 44. Sonogashira cross-coupling reaction.

To avoid full conversion of **120** the optimization reactions were performed at 80 °C and *N,N*-dimethylprop-2-yn-1-amine was used as alkyne. The problem with reactions with a full conversion is, that a comparison between reactions with a full conversion does not show the influence a change in the ligand design or the solvent choice makes. At first the solvent choice was optimized. Therefore, the reaction was performed in DMSO and DMF/water and DMF/water with tetrabutylammonium bromide as phase transfer catalyst with **C15** as catalyst. The reaction in DMSO led to conversion of 70% after 24 h. When the reaction is performed in DMF/water, a conversion of 70% is reached after 12 h. When a phase transfer catalyst like tetrabutylammonium bromide is added, the conversion can be increased to 83% (Figure 12).

In the next step the ligand was varied. Three ligands were used: HC(Pz)₂(Melm) (**L13**), HC(Me₂Pz)₂(Melm) (**L14**) and HC(Me₃Pz)₂(Melm) (**L15**). Only the pyrazolyl unit was changed in this thesis as the third *N* donor unit was varied in previous studies^[45] using iodobenzene. There the optimum for the third *N* donor unit was found for methyl imidazolyl. It was determined that by adding methyl groups to the pyrazolyl unit the activity of the catalyst can be increased from 70% over 80% to 83% (Figure 46). In all cases no side reaction was observed in the GC spectra or the NMR spectra of the crude reaction mixture.

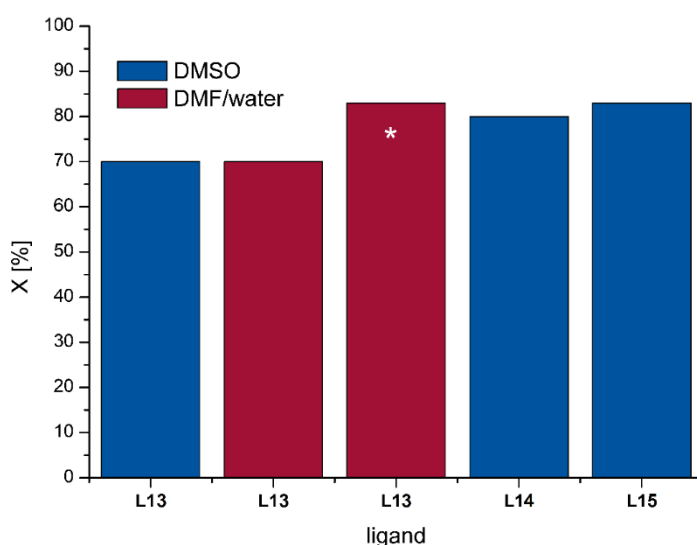


Figure 46. Optimization of the Sonogashira cross-coupling reaction. *: phase transfer catalyst added. Reaction temperature: 80 °C, Reaction time: 12 h (DMF/water); 24 h (DMSO).

In the last step the substrate scope was investigated (Table 27). A variety of different alkynes were applied for the Sonogashira cross-coupling reaction. The presented protocol tolerates tertiary amines and alcohols as well as ethers and aromatics and good isolated yields up to 94% are obtained. However, primary alcohol and primary/secondary amines and ester are not tolerated. It was also tempted to synthesize indoles with the presented protocol, but only traces

of the indoles were observed when iodoaniline was used as substrate. The substrate scope should be further increased by synthesizing different alkynes with secondary and tertiary amines from propargyl bromide and different amines with a base, but the synthesis could not be reproduced from the literature. The employed amines were aniline^[164], diphenylamine^[165], *iso*-propyl amine^[166] and di*iso*-propyl amine^{[167],[168]}.

Table 27. Substrate scope of the Sonogashira cross-coupling reaction.

R	Y(isolated) [%]	Enzymatic hydroxylation
CO ₂ Me	traces	
CO ₂ Et	traces	
CH ₂ NMe ₂	77	+
CH ₂ NEt ₂	94	+
CH ₂ NPr ₂	88	+
CH ₂ NHMe	traces	
CH ₂ NH ₂	traces	
CH ₂ NBoc ₂	traces	
CH ₂ OH	traces	
CH ₂ OMe	30 ^b	-
CMe ₂ OH	62 ^b	-
Ph ^a	85	-
CH ₂ OBn ^a	67	-

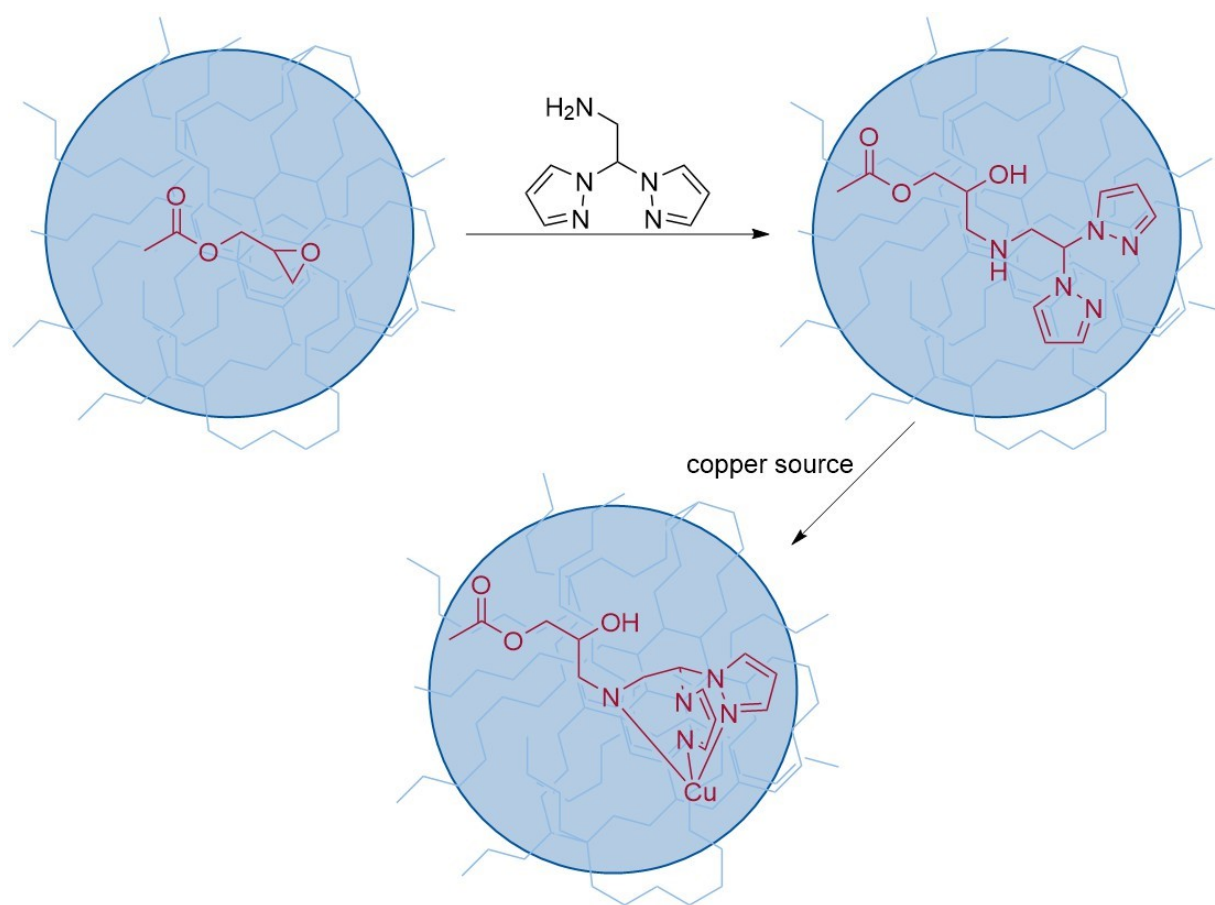
^a Reaction performed by Julian Moegling. ^b Yield determined by GC spectroscopy.

4.6 Preliminary work on copper loaded microgels

The work presented in this chapter was done in close collaboration with Fabian Fink. Parts of this chapter are published.

D. Schäfer, F. Fink, D. Kleinschmidt, K. Keisers, F. Thomas, A. Hoffmann, A. Pich, S. Herres-Pawlis, *Chem. Commun.* **2020**, 56, 5601.

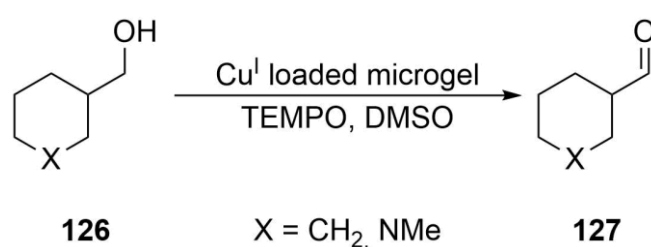
The pVCL-GMA-microgels used in this thesis were synthesized and analyzed by Denise Kleinschmidt from the Pich working group. The microgels were synthesized by precipitation polymerization and have a hydrodynamic radius of about 340 nm. In the next step the pVCL-GMA-microgels were functionalized with 2,2-di(1*H*-pyrazol-1-yl)ethan-1-amine and purified *via* dialysis by Fabian Fink. After the functionalization, the microgels shrink to a hydrodynamic radius of about 300 nm. The functionalized microgels can be loaded with different copper sources to yield a copper loaded microgel (Scheme 45).



Scheme 45. Synthesis of copper loaded microgels.

4.6.1 Oxidation reaction

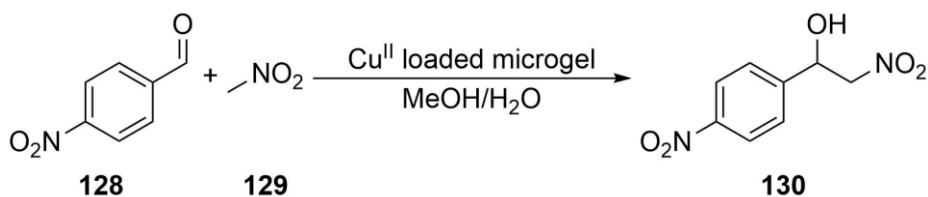
Within the subproject A1 of the SFB 985 copper loaded microgels were investigated. To show its potential for organic reactions a test reaction was needed. Therefore, the oxidation of benzyl alcohol to benzyl aldehyde was investigated. It could be shown that bis(pyrazolyl)methane copper complexes are possible catalysts for this oxidation reaction using TEMPO as cocatalyst. The reaction protocol was transferred and optimized for copper bis(pyrazolyl)methane loaded microgels by Fabian Fink. To further increase the substrate scope for the oxidation reaction a cyclic aliphatic alcohol (**126**) were tested (Scheme 46). The reaction mixture was analyzed with ^1H NMR spectroscopy, which only showed trace amounts of the desired product.



Scheme 46. Oxidation of aliphatic alcohols.

4.6.2 Henry reaction

In the next step the reaction scope of the copper bis(pyrazolyl)methane loaded microgel should be increased. For this purpose, the Henry reaction between nitrobenzyl aldehyde (**128**) and nitromethane (**129**) was investigated (Scheme 47). The Henry reaction also opens the opportunity for tandem reactions, which should be part of future studies. One example is the combination with the oxidation of benzyl alcohol discussed above. Furthermore, this reaction would enable the application of copper loaded microgels as catalyst at water oil interfaces. One possible set up would be a liquid-liquid extractor system. In this system a reaction with simultaneous extraction would be possible, due to the change in polarity between the substrate and the product. A similar system is in development in the subproject C5 of the SFB 985.



Scheme 47. Henry reaction between nitrobenzyl aldehyde and nitromethane.

For the Henry reaction the microgel was loaded *in situ* and dialyzed.⁴ For the reaction performed with *in situ* loaded microgel different copper(II) salts were used and for copper(II) bromide the highest yield with 16% was achieved (Table 28). In contrast the dialyzed copper(II) chloride loaded microgel was used to optimize the reaction solvent. When the reaction is performed in pure water the microgel collapses and no reaction is observed. This can be avoided by the addition of a methanol or acetonitrile. Another option is the use of DMSO as a solvent. The highest yield was obtained for a 2:1 mixture of water and methanol with 54% (Table 28).

One major problem concerning microgels is that the microgel structure highly depends on the reaction conditions. Little variation can have a huge influence on the structure and the properties of the microgel. Therefore, the reproducibility of the performed Henry reaction depends on the microgel batch. The challenge of a higher reproducibility of the microgel synthesis is currently under investigation in the subproject C6 of the SFB 985. Overcoming this challenge also will enable further optimization of the copper loaded microgel catalyzed Henry reaction.

Table 28. Yields* of the performed Henry reaction.

Copper source	<i>In situ</i> or dialyzed	Solvent	Y [%]
[Cu(MeCN) ₄](OTf) ₂	<i>In situ</i>	H ₂ O/MeOH (1/1)	15
CuBr ₂	<i>In situ</i>	H ₂ O/MeOH (1/1)	16
CuCl ₂	<i>In situ</i>	H ₂ O/MeOH (1/1)	4
CuCl ₂	dialyzed	DMSO	47
CuCl ₂	dialyzed	H ₂ O/MeOH (2/1)	54
CuCl ₂	dialyzed	H ₂ O/MeOH (1/1)	40
CuCl ₂	dialyzed	H ₂ O/MeCN (1/1)	10

* Yields determined by ¹H NMR spectroscopy.

⁴ All reactions with dialyzed copper loaded microgels were performed by Julian Moegling.

5. Summary and Outlook

5.1 Summary

In this thesis, copper bis(pyrazolyl)methane complexes were investigated as catalysts for different cross-coupling reactions. For this purpose, a series of literature-known and newly designed ligands (Figure 47) were synthesized. This ligand library was applied to C–C and C–O cross-coupling reactions and to copper nitrene mediated reactions. The ligand design was tailored for different aims, one aim was to investigate the correlation between the ligand design and the reactivity. Therefore, different synthetic strategies were applied to synthesize ligands with a third *N* donor unit with different donor abilities and various steric demand. In addition, also chiral ligands were developed and synthesized.

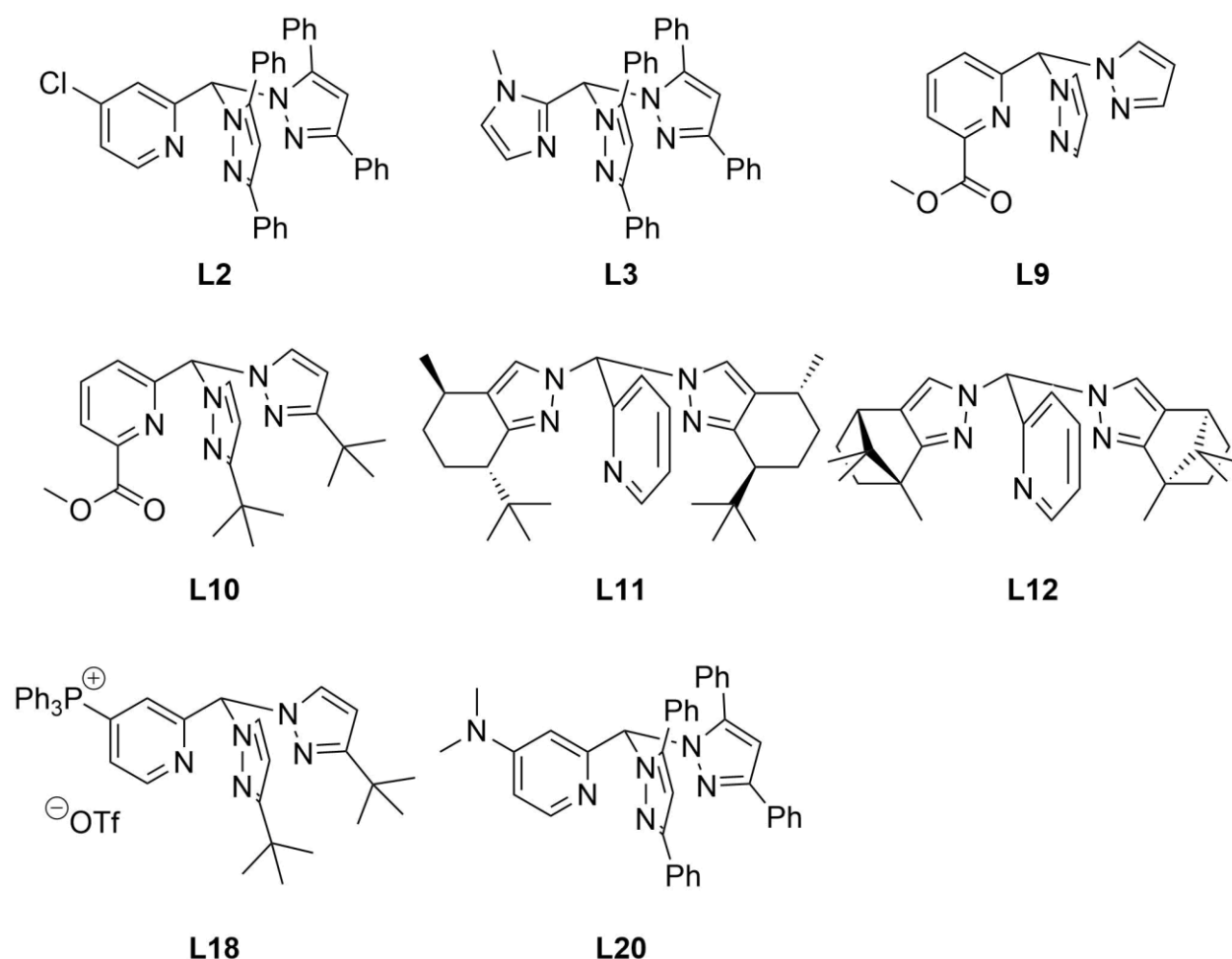


Figure 47. Novel bis(pyrazolyl)methane ligands.

The majority of the ligands were synthesized by the well-established Peterson rearrangement and in general good yields were obtained by modifying the reaction protocol. For example, for the synthesis of **L3** the solvent was switched from THF to toluene to increase the yield. Further

ligands were obtained by postmodifying bis(pyrazolyl)methane ligands. The ligand **L20** was synthesized from **L2** and dimethylamine under high pressure, while the ligand **L18** was obtained based on $\text{HC}(\text{tBuPz})_2\text{Py}$ (**L7**). The aim was to achieve a synthesis strategy to postmodify the pyridine functionality in the 4-position in different bis(pyrazolyl)methane ligands and introduce new functional groups. This strategy was based on literature known modification of pyridines by the formation of a phosphonium salt intermediate.^{[142]–[146]}

Starting with the various developed ligands the aim was to synthesize and characterize a library of copper(I) complexes. Novel isolated complexes were synthesized from the ligand and $[\text{Cu}(\text{MeCN})_4]\text{PF}_6$ (Figure 48, Figure 49), while *in situ* complexes were also synthesized from copper(I) and copper(II) chloride.

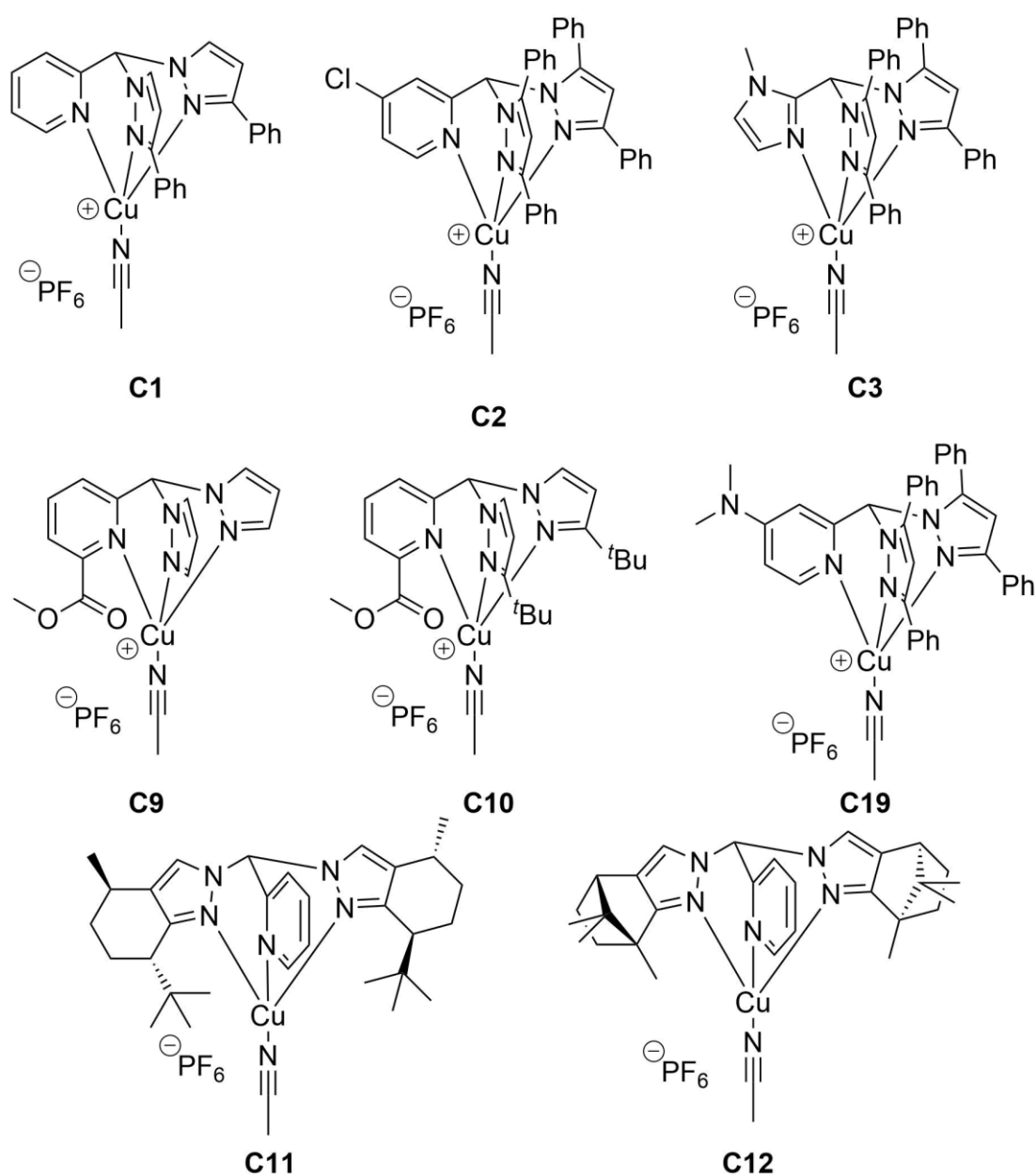


Figure 48. Novel copper(I) acetonitrile bis(pyrazolyl)methane complexes.

For the application as catalyst a monofacial complex is desired. Except for **L12** the formation of a monofacial complex, which is stable in solution, is obtained for all applied ligands. However, **C12** can be stabilized in solution by addition of acetonitrile. For the complex **C3** no suitable crystal for single crystal X-ray diffraction could be obtained, due to a rearrangement to the binuclear complex **C4** when recrystallized.

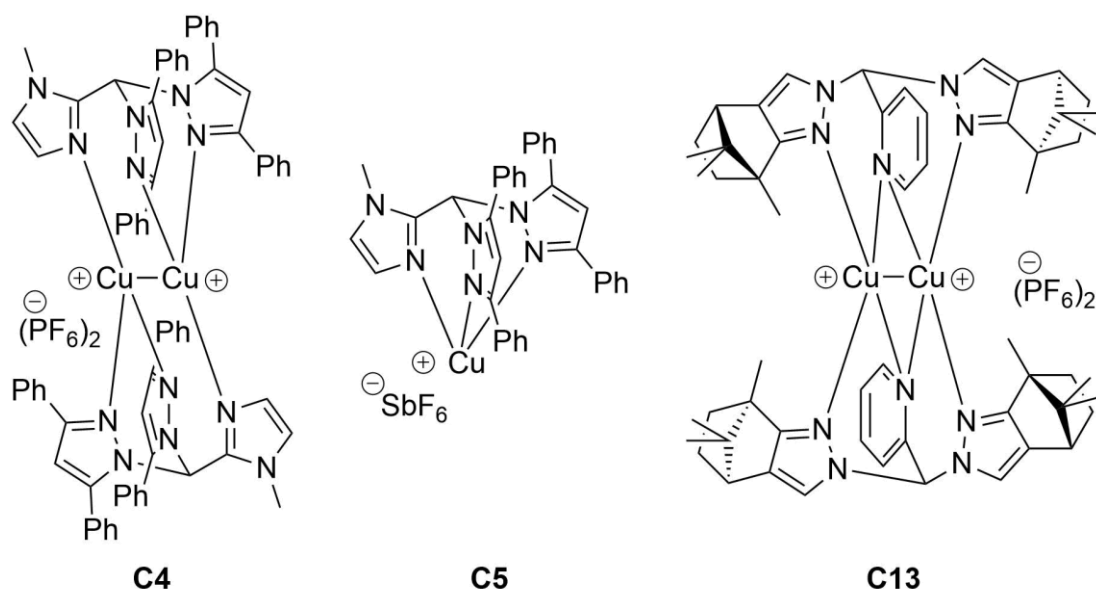


Figure 49. Novel copper bis(pyrazolyl)methane complexes.

The bond length of the third *N* donor unit shows that 4-chloropyridine and 6-CO₂Me pyridine are weaker donors compared to pyridine while methylimidazole and DMAP are stronger donors. Furthermore, it can be observed that the aromatic substituted pyrazolyl units tend to have a slightly shorter bond length than the aliphatic substituted pyrazolyl units.

In this thesis copper nitrenes and their reaction properties were investigated. Therefore, different aspects were focused and six novel copper nitrene complexes were synthesized (Figure 50). On the one hand, the influence of the third *N* donor unit in the bis(pyrazolyl)methane ligand towards the reactivity of the copper nitrene was investigated and, on the other hand, the scope of different substrates and reactions should be increased. By variation of the third *N* donor unit it could be shown that the spin-state and the constitution of the copper nitrene is not changed but the reactivity and stability is influenced. While for catalytic reaction with ⁹PhINTs pyridine as third *N* donor unit was the best choice, for reactions with benzoyl azide DMAP showed the highest yields. Overall high yields were obtained in the performed catalytic aziridination and C–H amination reactions, especially with benzene (45%) and toluene (76%) as substrate. The highest stability of the copper nitrene complexes was obtained using methyl imidazole as third donor. The stability can also be increased with an unsubstituted pyrazole residue in the 5-position of the pyrazole. The substrate scope was increased by aromatic substrates and β -substituted styrene derivatives. A first hint for the stability can be extracted from ¹H NMR

measurement of the precursor complex; a high shift of the apical proton is connected to a high stability. The reaction scope was increased by the nitrene mediated rearrangement of alkynes and enantio-selective aziridination and C–H amination. For the C–H amination of aromatic substrates yields up to 45% were achieved. For the aziridination of β -substituted styrene derivatives a high preservation of the stereo information was achieved for the *cis*-derivative. The rearrangement of alkynes could be achieved, but for internal alkynes the yield was low. Also, an enantioenriched aziridination and C–H amination was achieved, but the enantiomeric excess was limited to 30%. Furthermore, the application of nitrene generating agents apart from iminoiodinanes and the use of iron complexes was investigated. A reaction between organic azides and copper(I) bis(pyrazolyl)methane complexes with a free coordination sphere was achieved. And a first protocol for the C–H amination of ethylbenzene with a copper(I) bis(pyrazolyl)methane complex and benzoyl azide was developed.

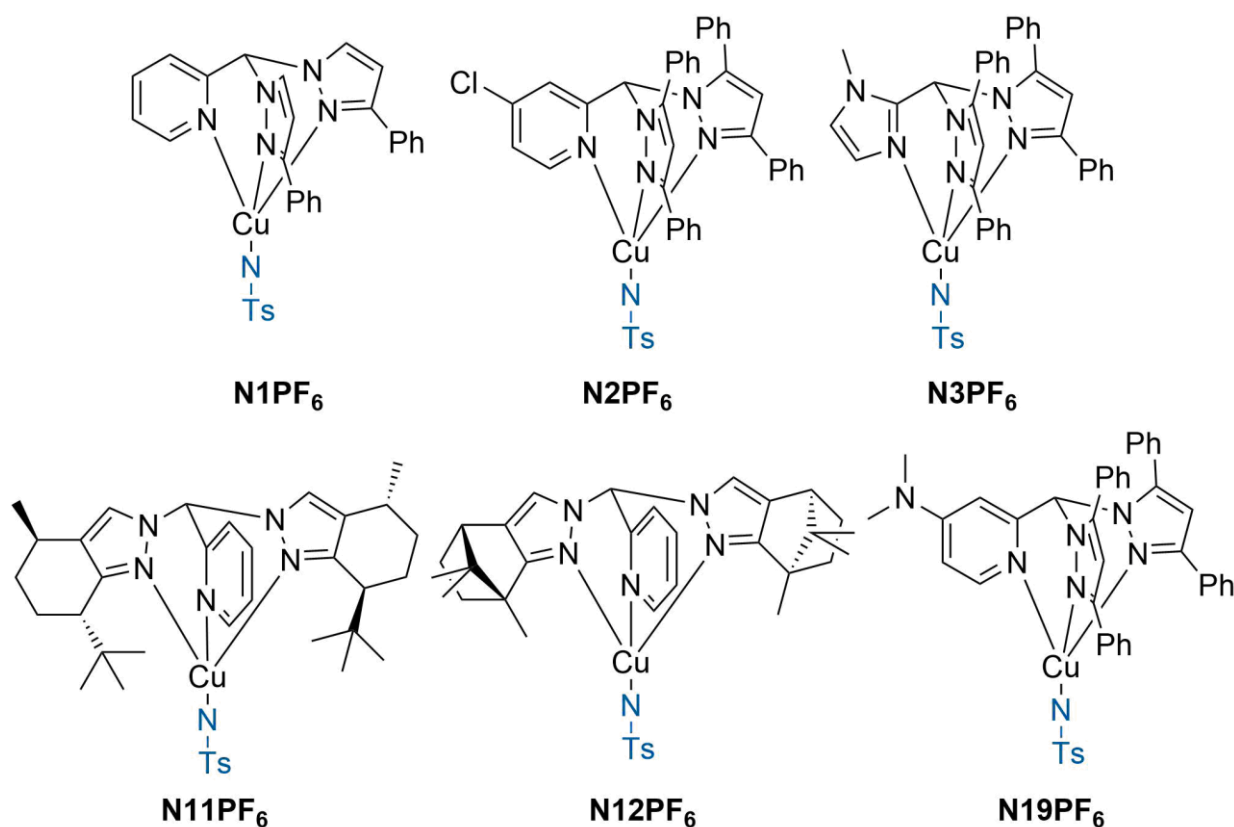


Figure 50. Novel copper nitrene complexes.

In cooperation with the Schwaneberg group in the framework of the SFB 985 (subproject A1) a tandem reaction was developed. In the first step a copper(II) catalyzed Sonogashira reaction with iodophenol yields a benzofuran derivative. This can be hydroxylated by a P450 BM3 variant to yield a bis(benzofuran) derivative. The Sonogashira reaction was optimized in different aspects. For a high reactivity a mixture of water and DMF with added phase transfer catalyst is superior to DMSO. With DMSO a conversion of 70% can be achieved after 24 h, while with the water-DMF mixture a conversion of 83% can be achieved after 12 h. The ligand design

can be optimized by the incorporation of methyl groups to the pyrazolyl unit, for the ligand HC(Pz)₂Melm (**L13**) a conversion of 70% was achieved after 24 h in DMSO. With the ligand HC(Me₃Pz)₂Melm (**L15**) a conversion of 83% was achieved after 24 h in DMSO, while for the tandem reaction itself DMSO was used as solvent and the copper complex [CuCl₂{HC(Pz)₂Melm}] (**C15**). DMSO was chosen due to the higher tolerance of the enzyme towards DMSO.^[162] And **C15** was selected due to the more efficient and scalable synthesis of both **L13** and **C15** compared to **L15**.

A second approach for a tandem reaction was the combination of the hydroxylation of xylene followed by the copper(I) catalyzed C–O coupling reaction of the xylol and an aryl bromide. While it was shown that the *in situ* formed complex [CuI{HC(Me₂Pz)₂Melm}] is an efficient catalyst, for this reaction with commercial xylol the reaction with enzymatic xylol did not yield sufficient amount of product.

In the last part of this thesis the potential of copper loaded microgel was investigated. It was shown that besides the oxidation of benzylic alcohols also the Henry reaction can be catalyzed. A major drawback was the lack of reproducibility between different microgel batches.

5.2 Outlook

On behalf of the copper nitrene complexes and their reactivity one interesting aspect which was not yet investigated is the mechanism of the aziridination and the C–H amination. This can be achieved on a theoretical level by DFT calculation of the reaction mechanism and on experimental level by a Hammett plot or a radical clock experiment.

Furthermore, the reaction between copper(I) bis(pyrazolyl)methane acetonitrile complexes and benzoyl azides should be further investigated intensively. For example, electron donating groups can be introduced to the pyrazolyl units of the ligand, as the introduction of an electron donating group on the pyridine showed an increase of the reactivity towards benzoyl azide. In addition, the reaction condition should be further optimized in terms of temperature, solvent, substrate, speed of addition of benzoyl azide and reaction time. Another aspect is the azide applied as nitrene generating agent itself. Since there is a variety of easy synthesizable benzoyl azide derivatives^[88], the influence of different functional groups on the benzoyl azide can be investigated. In addition, the reaction between iron(II) bis(pyrazolyl)methane complexes with benzoyl azide should be part of prospective studies. Additionally, the ligand design of the iron(II) complexes can be optimized to achieve a protocol for the C–H amination and aziridination with iron catalysts.

To receive a catalyst with a higher enantioselectivity the ligand design of the bis(pyrazolyl)methane allows to introduce chirality on three positions. The first possibility is the introduction of chiral substituents on the pyrazolyl, the second one is by a chiral third *N* donor unit and the last one is the apical carbon atom. However, for the third option the synthetic feasibility is doubted for a stereoselective synthesis. In contrast a feasible option would be the synthesis of a methane derivative with two different *N* donor unit followed by the introduction of a third *N* donor unit by deprotonation of the methane and the introduction of the halide of the third *N* donor unit. The obtained racemic mixture can be separated by preparative asymmetric HPLC. The first option was realized in this thesis and further chiral pyrazoles could be introduced, for example (-)-3(5)-Methyl-1-phenylethylaminomethylpyrazole. Unfortunately it was shown that the tris(pyrazolyl)borate ligand of this pyrazole only leads to low enantiomeric excess in the cyclopropanation of styrene.^[169] A chiral third *N* donor unit can be based on proline or on oxazoline. A proline based third *N* donor unit can be synthesized from prolinol. In the first step the secondary amine is arylated and in the second step the alcohol group can be transformed into an aldehyde by a Swern oxidation. The oxazoline can be introduced into a bis(pyrazolyl)methane *via* post modification by deprotonating the bis(pyrazolyl)methane apical carbon atom and subsequent adding of the oxazoline halide. However, the synthesis of the oxazoline halide is challenging.

On behalf of the development of tandem reaction the application of microgels as protective layer for both enzyme and copper catalyst should be further explored. For example, a copper loaded microgel could be immobilized on a cell with exposed enzymes. The microgel protects both the copper complex as well as the enzyme and enables a tandem reaction with an easy recoverable catalyst system. Moreover, both catalysts are in close proximity, this should also allow tandem reactions with less stable intermediates.

Other interesting products of the Sonogashira coupling reaction are indoles, which cannot be obtained from the iodoaniline. Nevertheless, by the introduction of a protective group to the amine this reaction should be feasible. Also, the reactivity of the catalyst may be increased by changing the third *N* donor unit from methyl imidazolyl to DMAP by the synthetic approach shown in this thesis to yield the ligand $\text{HC}(\text{Ph}_2\text{Pz})_2\text{DMAP}$.

6. Experimental part

6.1 General

All reactions and manipulations were carried out under nitrogen atmosphere, using standard Schlenk technique or a glovebox, unless otherwise noted. Nitrogen was dried by passage through P₂O₅. Mol sieve 3 Å were dried for 20 h at 220 °C before usage. All chemicals were purchased from commercial suppliers and used without further purification, unless otherwise noted.

6.2 Chemicals and solvents

Following chemicals were bought from commercial sources in the highest purity and used without further purification, unless otherwise noted.

Table 29. Commercial chemicals.

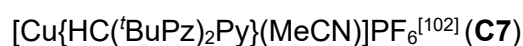
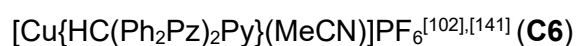
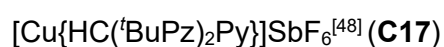
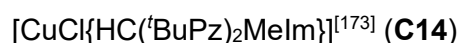
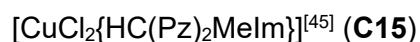
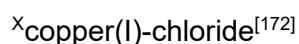
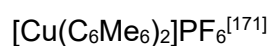
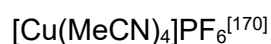
Substance	Supplier	Substance	Supplier
Acetic acid, >99%	Fisher Chemicals	α-Methylbenzylamine	Sigma-Aldrich
Acetic anhydride	VWR	Methyl propiolate	ABCR
Acetyl acetone	Sigma-Aldrich	3-Methyl-2,4-pentanone	Alfa Asear
Adamantyl azide	Sigma-Aldrich	2-Methyl-3-butyn-2-ol	TCI
Ammonium chloride	Merck	Methylimidazole	Sigma-Aldrich
Anthracene	Acros	Methylmagnesium bromide solution (3M in Et ₂ O)	Acros
Azobenzene	TCI	(1-Methylpiperidin-4-yl)methanol	ABCR
Benzene	Sigma-Aldrich	Methylphenylsulfoxide	Alfa Asear
Benzoylchloride	ABCR	2-Methylpyridine	ABCR
Benzyl alcohol	Alfa Asear	<i>n</i> Butyl lithium (2.5M in hexanes)	Acros
Benzyl bromide	Alfa Asear	<i>N,N</i> -diethylprop-2-yn-1-amine	Acros
Bibenzyl	Acros	<i>N,N</i> -dimethylprop-2-yn-1-amine	Alfa Asear
Bipyridine bromide	ABCR	<i>N,N</i> -dipropylprop-2-yn-1-amine	Alfa Asear
3,5-Bis(trifluoromethyl)aniline	Acros	Naphtalene	Fluka
Bromanisole	ABCR	Neopentyl benzene	ABCR
1-Bromo-4-(trifluoromethyl)benzene	Alfa Asear	4-Nitro-benzylaldehyde	Sigma-Aldrich
Bromobenzene	Sigma-Aldrich	Nitromethane	Sigma-Aldrich
3-Bromoprop-1-yne (80wt% in toluene)	Acros	Nitrosonium hexafluoridophosphate	Acros

Campher	Alfa Asear	Nitrosonium tetrafluoroborate	Alfa Asear
Celite	Carl Roth	4-Nitro-styrene	TCI
4-Chloropyridine-2-methanol	ABCR	O-(4-Nitrobenzoyl)hydroxyl amine	ABCR
<i>cis</i> -Stilbene	Alfa Asear	<i>para</i> -toluenesulfonamide	Alfa Asear
<i>cis</i> - β -Methyl styrene	TCI	<i>para</i> -toluenesulfonyl chloride	Acros
Cobalt(II) chloride hexahydrate	Sigma-Aldrich	Perchloric acid, 70%	Sigma-Aldrich
Copper	Sigma-Aldrich	Phenyl amine	TCI
Copper(I) bromide	Sigma-Aldrich	1-Phenyl-1-propyne	Acros
Copper(I) iodid	Alfa Asear	Phenylacetylene	ABCR
Copper(I) oxide	Riedel-de Haën	Phenylchloride	Alfa Asear
Copper(II) bromide	ABCR	Phenylflouride	TCI
Copper(II) chlorid	Acros	Pinacolone	Acros
Copper(II) oxide	Merck	Potassium carbonate	Grüssing
Cyclohexadien	Acros	Potassium hydride (30wt% in mineral oil)	Sigma-Aldrich
Cyclohexane	Acros	Potassium hydroxide	Grüssing
Cyclohexene	ABCR	Potassium phosphate	Acros
Cyclohexylmethanol	TCI	Potassium sulfate	Grüssing
(Diacetoxyiodo)benzene	Carbolution	Prop-2-yn-1-amine	TCI
Dibenzoylmethane	TCI	Pulgone	Sigma-Aldrich
Diisopropyl amine	Sigma-Aldrich	Pyrazole	Sigma-Aldrich
Dimethyl amine hydrochloride	Acros	Pyridin-2-carbaldehyde	Acros
Dimethylphenol	ABCR	Quinoline	Acros
Diphenyl amine	Acros	Quinoline aldehyde	Acros
Diphenylacetylene	Alfa Asear	Silver hexafluoridoantimonate	Acros
Di- <i>tert</i> butylperoxide	TCI	Sodium azide	TCI
DMF	Sigma-Aldrich	Sodium bistrimethylsilazane (2M in THF)	Sigma-Aldrich
Ethyl benzene	Acros	Sodium carbonate	Grüssing
Ethyl propiolate	Alfa Asear	Sodium hydride (60wt% in mineral oil)	Merck
Ethylformiate	Fisher Chemicals	Sodium hydroxide	Grüssing
2-Ethylpyridine	Sigma-Aldrich	Sodium methanolate	Acros
Europium tris[3-(heptafluoropropylhydroxymethylene)-(+)-camphorate] ([Eu(hfc) ₃])	Sigma-Aldrich	Sodium nitrite	Merck
Ferrocene	EGA-Chemie	Sodium perborate	Acros
2-Fluoropyridine	ABCR	Sodium sulfate	Grüssing
6-Formyl-2-pyridinecarboxylate	ABCR	Styrene	Merck
Heptandione	Sigma-Aldrich	Styrene β d ₂	Sigma-Aldrich
Hexaflouroacetylacetone	ABCR	TEMPO	Alfa Asear
Hexaflourophosphoric acid 55%	Sigma-Aldrich	<i>tert</i> Butanol	Alfa Asear
Hexamethyl benzene	Alfa Asear	Thionylchloride	Alfa Asear

Hydrazine monohydrate	TCI	Thiophenol	Acros
Hydrochloric acid, 37%	Fisher Chemicals	Toluene	Alfa Asear
Iodine	Grüssing	<i>trans</i> -Stilbene	Alfa Asear
Iodo aniline	ABCR	<i>trans</i> - β -Methyl styrene	Sigma-Aldrich
Iodo phenol	Sigma-Aldrich	Trichlorioscyanuric acid >95%	Sigma-Aldrich
Iron	Merck	2,4,6-Trichlorobenzoyl chloride	Carbolution
<i>i</i> sopropyl amine	ABCR	Triethylamine	ABCR
L(-)- α -Methylbenzylamine	Acros	Trifluoromethanesulfonic anhydride	Acros
Magnesium sulfate	Grüssing	Trifluoromethane acid, 99.9%	Carbolution
Manganese dioxide (activated)	Sigma-Aldrich	3-(Trifluoromethyl)pyrazole	ABCR
Mesityl amine	ABCR	4-Trifluoromethane-styrene	ABCR
3-Methoxyprop-1-yne	TCI	Triphenylmethane	Sigma-Aldrich
4-Methoxy-styrene	Alfa Asear	Triphenylphosphane	Alfa Asear
Methyl iodide	Alfa Asear		

Cobalt(II) chloride hexahydrate was absolutized with thionyl chloride and stored under inert condition in a glovebox. Ferrocene was sublimed prior to use. Sodium hydride and potassium hydride were washed with pentane and dried under reduced pressure prior to use. Styrene was distilled from calcium hydride and stored at -30 °C.

Following chemicals were resynthesized according to the literature. With ^x marked chemicals were resynthesized by coworker and provided.



[Cu{HC(^tBuPz)₂MeIm}(MeCN)]PF₆^[102] (**C8**)

[Cu{HC(CF₃Pz)₂Py}(MeCN)]PF₆^[102]

[Cu{HC((CF₃)₂Pz)₂Py}(MeCN)]PF₆^[102] (**C16**)

[Fe(MeCN)₆](BF₄)₂^[174]

[Fe{MeC(Py)₂Bpy}(MeCN)₂](OTf)₂^[159] (**C20**)

benzoylazide^[88]

mesitylazide^[175]

3,5-bis(trifluormethyl)phenylazide^[176]

Caution: Organic azides are energetic compounds and potential explosive and should always be handled carefully with proper safety measures.^[177]

O-(4-nitrobenzoyl)hydroxylamine triflate^[178]

(2-*tert*-butylsulfonyl)(*p*-toluenesulfonyl)iminoiodobenzene^[93]

(2-*tert*-butylsulfonyl)(diacetoxyiodo)iminoiodobenzene^[179]

(*p*-toluenesulfonyl)iminoiodobenzene^[180]

trimethylpyrazole^[181]

3,5-diphenylpyrazole^[182]

^x3-*tert*-butylpyrazole^[183]

(4*S*,7*R*)-7,8,8-trimethyl-4,5,6,7-tetrahydro-2*H*-4,7-methanoindazole (CamPz)^[184]

(4*R*,7*S*)-7-(*tert*-butyl)-4-methyl-4,5,6,7-tetrahydro-2*H*-indazol (PulPz)^[184]

4-chloropyridine-2-carboxaldehyde^[185]

1-methyl-imidazol-2-carboxaldehyde^[138]

^xbis(3-phenylpyrazol-1-yl)(pyrindin-2-yl)methane^[29] (**L1**)

^xbis(3,5-phenylpyrazol-1-yl)(pyrindin-2-yl)methane^[137] (**L4**)

^xbis(3-phenylpyrazol-1-yl)(quinolin-2-yl)methane^[29] (**L5**)

^xbis(3,5-ethylpyrazol-1-yl)(pyrindin-2-yl)methane^[137] (**L6**)

^xbis(3-*tert*-butylpyrazol-1-yl)(pyrindin-2-yl)methane^[29] (**L7**)

^xbis(3-*tert*-butylpyrazol-1-yl)(1-methyl-imidazol-2-yl)methane^[40] (**L8**)

^xbis(pyrazol-1-yl)(1-methyl-imidazol-2-yl)methane^[138] (**L13**)

^xbis(3,5-methylpyrazol-1-yl)(1-methyl-imidazol-2-yl)methane^[138] (**L14**)

^xbis(pyrazol-1-yl)methane^[30] (**L16**)

^xbis(3,5-methylpyrazol-1-yl)(pyrindin-2-yl)methane^[139]

^xfunctionalized pVCL microgel^[186]

3,5-Diphenylpyrazole was recrystallized from hot acetone before use.

All solvents were dried using standard procedures^[187] and degassed with three circles of freeze pump thaw, unless otherwise noted.

6.3 Analytics

6.3.1 NMR spectroscopy

The NMR spectra were measured with a *Bruker Avance II-400* or a *Bruker Avance III HD* at 25 °C. The ¹H spectra were given relative to the solvent residual signal and the ¹³C {¹H} spectra were given relative to the solvent signal (Table 30). External standards were tetramethylsilane for ¹H and ¹³C {¹H} spectra, trichlorofluoromethane for ¹⁹F {¹H} spectra and phosphoric acid for the ³¹P {¹H} spectra. The signals were assigned with the help of APT, COSY, NOESY, HSQC and HMBC measurements.

Table 30. Solvent residual signal and solvent signal of the used solvents.^[148]

Solvent	solvent residual signal [ppm]	solvent signal [ppm]
acetone- <i>d</i> ₆	2.05	29.84, 206.26
acetonitrile- <i>d</i> ₃	1.94	1.32, 118.26
benzene- <i>d</i> ₆	7.16	128.06
chloroform- <i>d</i> ₁	7.26	77.16
DCM- <i>d</i> ₂	5.32	53.84

6.3.2 Evans NMR

The effective magnetic moment (μ_{eff}) of the copper nitrene complexes (DCM-*d*₂; 6 mmol L⁻¹ in **C1-C3** and **C6**; 10 mmolL⁻¹ in **C19**) was determined by using Evans' method at low

temperatures.^{[188]–[190]} The samples were pre-cooled to -80 °C and the NMR probe head was pre-cooled to -40 °C and cooled to -80 °C immediately after the probe was inserted. The used NMR tubes were equipped with a glass capillary insert of DCM-*d*₂. The copper nitrene complexes were decayed by warming up the NMR probe head to -40 °C or to room temperature for an appropriate time. The difference in the chemical shift of the solvent in presence of the paramagnetic species to the solvent in the glass capillary insert was analyzed and the effective magnetic moment was calculated by using the following equation:

$$\mu_{\text{eff}} = 0.0618 (\Delta\delta \cdot T / (2 \cdot c))^{1/2} \text{ [188]–[190]}$$

where δ is the difference in chemical shift between the two solvent signals in ppm, T is the absolute temperature and c is the molar concentration of the precursors **C1–C3**, **C6** and **C19**. The results are summarized in Table 31.

Table 31. Values of the effective magnetic moment μ_{eff} and the spin state for **N1⁺–N3⁺**, **N6⁺** and **N19⁺**. The respective calculated spin only value for μ_{eff} is 0 μ_{B} for a singlet, 1.73 μ_{B} for a doublet and 2.83 μ_{B} for a triplet spin state.

	T [°C]	$\mu_{\text{eff}} / \mu_{\text{B}}$	Assigned spin state
N1⁺	-80	0.00	singlet
N1⁺ (decayed)	-10	1.29*	doublet
N2⁺	-80	0.00	singlet
N2⁺ (decayed)	-20	0.90*	doublet
N3⁺	-80	0.00	singlet
N3⁺ (decayed)	-30	0.88*	doublet
N6⁺	-80	0.00	singlet
N6⁺ (decayed)	r.t.	0.95	doublet
N19⁺	-80	0.00	singlet
N19⁺ (decayed)	0	1.62	doublet

* The decay products are partly insoluble in dichloromethane-*d*₂ and the formation of a green precipitate is observed. This reduces the magnetic moment of the sample.

6.3.3 UV/Vis spectroscopy

UV/Vis spectra were recorded with a *Cary 60* spectrophotometer from *Agilent Technologies* in combination with a fibre-optic quartz glass immersion probe (*Hellma*, 1 mm) customized Schlenk measurement cell.

6.3.4 ESI mass spectrometry

ESI mass spectra were recorded with a *LTQ-Orbitrap XL* from *ThermoFisher Scientific* (source voltage 4.49 kV, capillary temperature 299.54 °C, tube lens voltage 110-130 V).

6.3.5 Cryo ESI mass spectrometry

Cryospray-ionization mass spectrometry (CSI-MS) measurements were performed on an UHR-TOF *Bruker Daltonik maXis II*, an ESI-quadrupole time-of-flight (qToF) mass spectrometer capable of a resolution of at least 80.000 FWHM, which was coupled to a *Bruker Daltonik* Cryospray unit. Detection was in positive ion mode; the source voltage was 3.5 kV. The drying gas (N₂), to achieve solvent removal was held at 0 °C and the spray gas was held at –80 °C. The mass spectrometer was calibrated subsequently to every experiment *via* direct infusion of a L-proline sodium salt solution, which provided a *m/z* range of singly charged peaks up to 3000 Da in positive ion modes.

6.3.6 Single crystal x-ray diffractometry

The crystallographic data for **L2**, **L3**, **L18**, **L20**, **C1**, **C2**, **C4**, **C9**, **C10**, **C11**, **C13**, **C19** and [Cu{HC(Ph₂Pz)₂Melm}₂](PF₆)₂ are presented in Table 51-Table 57. The data for **C1**, **C10**, **C11**, **C13**, **L2** and **L3** were collected with a *Bruker D8* goniometer with *APEX CCD* using an *Incoatec* microsource with Mo-*K*_α radiation ($\lambda = 0.71073$ Å) and temperature control was achieved with an Oxford Cryostream 700. Crystals were mounted with grease on glass fibers and data were collected at 100 K in ω -scan mode. Data were collected with SMART^[191], integrated with SAINT^[191] and corrected for absorption by multi-scan methods with SADABS.^[191] The data for **C2**, **C4**, **C9**, **C19**, [Cu{HC(Ph₂Pz)₂Melm}₂](PF₆)₂, **L18** and **L20** were collected with a four-circle goniometer Stoe Stadivari with Dectris Pilatus3 R 200 K hybrid pixel detector using Geni 3D high flux Mo-K α radiation ($\lambda = 0.71073$ Å) or GeniX 3D high flux Cu radiation ($\lambda = 1.54056$ Å). The temperature was controlled by an Oxford Cryostream 800. Crystals were mounted with grease on glass fibers. Data were collected with X-Area Pilatus^[192] and integrated with X-Area Integrate^[193] and X-Area Recipe.^[194] The absorption correction was performed by Gaussian integration with Stoe X-Red32, afterwards scaling of reflections with X-Area LANA.^[195]

The structure was solved by direct and conventional Fourier methods and all non-hydrogen atoms were refined anisotropically with full-matrix least-squares based on *F*² (XPREP,^[196] ShelXS,^[197] ShelXT,^[198] ShelXL^[199] or ShelXle^[200]). Hydrogen atoms were derived from

difference Fourier maps and placed at idealised positions, riding on their parent C atoms, with isotropic displacement parameters $U_{iso}(H) = 1.2U_{eq}(C)$ and $1.5U_{eq}(C \text{ methyl})$. All methyl groups were allowed to rotate but not to tip.

Full crystallographic data for **C1**, **C2**, **C4**, **C10**, **C11**, **C13**, **L2** and **L3** have been deposited with the Cambridge Crystallographic Data Centre as supplementary no. CCDC – 1962598 for **C1**, CCDC – 1962599 for **C2**, CCDC – 1962600 for **C4**, CCDC – 1962601, CCDC – 2065190 for **C10**, CCDC – 2065189 for **C11**, CCDC – 2065191 for **C13**, for **L2** and CCDC – 1962602 for **L3**. Copies of the data can be obtained free of charge on application to CCDC, 12 Union Road, Cambridge CB2 1EZ, UK (fax: (+44)1223-336-033; e-mail: deposit@ccdc.cam.ac.uk).

6.3.7 IR spectroscopy

FT-ATR-IR were recorded on a *Shimadzu IRTrace 100* using a CsI beam splitter in combination with an ATR unit (*Quest* model from *Specac* utilizing a robust monolithic crystalline diamond) in a resolution of 2 cm^{-1} . The bands are assigned after the Wuerzburger model: vw = very weak, w = weak, m = middle, s = strong, vs = very strong.

6.3.8 Column chromatography

Column chromatography was performed with *Geduran silica gel 60* (40-63 μm) from *Merck* or with alumina B, activity Super I from *MP Biomedicals*.

6.3.9 Thin layer chromatography

Thin layer chromatography was performed with chromatography sheets from *MACHEREY-NAGEL* with a layer thickness of 0.20 mm and a precoating of a fluorescent indicator.

6.3.10 Gas chromatography

Gaschromatographic measurements were obtained with a Shimadzu GC2010plus (*FS-Supreme 5mS* capillary column, 5% phenylmethylpolysiloxane, length 30 m, diameter: 0.32 mm, film thickness: 0.25 μm , flame ionization detector).

For some samples the GC-conversion of iodophenol was determined. These have been obtained by comparison with an internal standard and the area of iodophenol. The response factor of iodophenol (0.75) was determined by Julian Moegling.^[103]

6.3.11 Cyclic voltammetry

The cyclic voltammetric measurements were performed at room temperature with a *Metrohm Autolab* PGSTAT 101 potentiostat with a three-electrode arrangement with a Pt disc working electrode (1 mm diameter), an Ag wire pseudo reference electrode and a glassy-carbon counter electrode under inert conditions. The samples were prepared with a 0.5-1.0 mM concentration of analyte and 0.1 M NnBu_4PF_6 as supporting electrolyte in dichloromethane. Ferrocene was added as internal standard after each measurement. All potentials are referenced relative to the Fc/Fc^+ couple. The cyclic voltammograms were measured with sweep rates of 20, 50, 100 and 200 mVs^{-1} .

Table 32. Oxidation potentials and half-cell potentials of the measured complexes.

	E_{ow} vs E^0 (Fc/Fc^+) [mV]	$E_{1/2}$ vs E^0 (Fc/Fc^+) [mV]
C1	780	-
C2	520	-
C3	700	-
C4	-290	-
C6	730	-
C11	660	560
C12^a	630	-
C13	1230	-
C19	1400	-

^a formed *in situ* from **C12** by the addition of 10 equiv. MeCN.

6.3.12 EPR spectroscopy

EPR spectra were recorded at 77 K on a *Miniscope MS 400* from *Magnettech* with a microwave frequency of 9.4 GHz. The concentration of the measured frozen solution was 10 mM. The B_0 field was adjusted to 325 mT with a range of 160 mT (245-405 mT) and a sweep time of 60 s. Further parameters were adjusted as follows: smooth = 0.100 s, NOPs = 4096, gain mantissa

= 5, gain exponent = 1 and $MW_{\text{attend.}} = 10$. The obtained EPR spectra were simulated using the comprehensive software packet *EasySpin* (Version 5.2.28).^[201]

6.4.13 CHN Elemental analysis

Elemental analysis were recorded on a Elementar varioEL or a Elementar varioEL cube.

6.4 Computational details

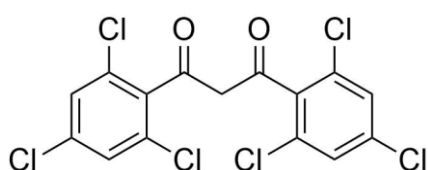
All DFT calculations were performed by Dr. Alexander Hoffmann.

Density functional theory (DFT) calculations were performed with Gaussian 16, Revision B01.^[202] The geometry optimizations were started from the geometry of the solid-state structures using the TPSSH functional^[203] and with the Ahlrichs type basis set def2-TZVP^[204] basis set as implemented in Gaussian 16, Revision B01.^[202] NBO calculations were accomplished using the program suite NBO 6.0 delivering the NBO charges and the charge-transfer energies by second order perturbation theory.^[205] As solvent model, we used the Polarizable Continuum Model (PCM) as implemented in Gaussian 16. As empirical dispersion correction, we used the D3 dispersion with Becke–Johnson damping as implemented in Gaussian16, Revision B.01.^[206] The DLPNO-CCSD(T) calculations were performed with Orca, Revision 4.2.1, starting with the optimized structures of the desired nitrenes with cc-pVDZ^[207](76) as basis set and the NormalPNO keyword.^{[152],[153],[208]} For charge decomposition analysis the program AO-Mix^[209] was used as a post-processing tool. The program APOST3D was used to determine the effective oxidation state with the Salvador's effective state analysis.^{[156],[210]}

6.5 Synthesis of starting material

6.5.1 Synthesis approach of 1,3-bis(2,4,5-trichlorophenyl)propane-1,3-dione

MeMgBr (3 M in diethyl ether, 4.3 mL, 12.8 mmol, 2 equiv.) was added to a solution of 2,4,6-trichlorobenzoyl chloride (1 mL, 6.4 mmol, 1 equiv.) in diethyl ether (5 mL) at 0 °C. The reaction mixture was stirred for 5 min at 0 °C and refluxed for 24 h. Water (20 mL) and diethyl ether (20 mL) was added. The organic phase was washed with water (3x5 mL) and dried over Na₂SO₄. The solvent was removed under reduced pressure.



The synthesis approach is based on the literature.^{[135],[136]}

The title compound couldn't be observed *via* ¹H NMR spectroscopy or mass spectroscopy.

6.6 Reagent synthesis

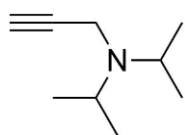
6.6.1 Synthesis approach of *N,N*-diisopropylprop-2-yn-1-amine

Approach A:

3-Bromoprop-1-yne (80w% in toluene, 0.6 mL, 5.5 mmol, 1.1 equiv.) was added to a mixture of Diisopropyl amine (0.7 mL, 5.0 mmol, 1.0 equiv.) and K₂CO₃ (138 mg, 10.0 mmol, 2.0 equiv.) in acetonitrile (20 mL). The mixture was stirred at 80 °C for 18 h and filtered over Celite. The solvent was removed under reduced pressure. The residue was solved in diethyl ether (25 mL) and washed with water (10 mL) and brine (10 mL). The organic phase is dried over Na₂SO₄ and the solvent removed under reduced pressure. The residue was filtered over a silica pad (ethyl acetate/hexane 1/10).

Approach B:

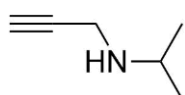
Diisopropyl amine (0.42 mL, 3.0 mmol, 1.0 equiv.) was added to suspension of Sodium hydride (128 mg, 3.2 mmol, 1.07 equiv.) in THF (7 mL) and stirred for 2 h. 3-Bromoprop-1-yne (80w% in toluene, 0.39 mL, 3.2 mmol, 1.07 equiv.) was added and the mixture was stirred for another 18 h. Water (10 mL) was added. The aqueous phase was extracted with DCM (3x15 mL). The organic phase was dried over Na₂SO₄ and the solvent was removed under reduced pressure. The residue was filtered over a silica pad (ethyl acetate/hexane 1/1).



The synthesis approach is based on the literature.^{[167],[168]} The title compound could not be isolated.

6.6.2 Synthesis approach of *N*-isopropylprop-2-yn-1-amine

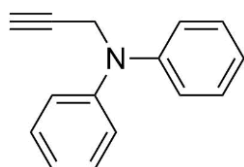
Bromoprop-1-yne (80w% in toluene, 2.2 mL, 20 mmol, 1 equiv.) was added dropwise to a solution of iso-propylamine (8.9 mL, 100 mL, 5 equiv.) in DCM (40 mL) and stirred for 24 h at room temperature. The organic phase was washed with water (3x40 mL) and dried over Na₂SO₄. The solvent was removed under reduced pressure. The residue was filtered over a silica pad (ethyl acetate/pentane 1/5).



The synthesis approach is based on the literature.^[166] The title compound could not be isolated.

6.6.3 Synthesis approach of *N,N*-diphenylprop-2-yn-1-amine

Sodium hydride (60% in mineral oil, 0.48 g, 12.0 mmol, 1.2 equiv.) was added to a solution of Diphenyl amine (1.69 g, 10.0 mmol, 1.0 equiv.) in DMF (15 mL) at 0 °C. The solution was stirred for 30 min at 0 °C. 3-Bromoprop-1-yne (80w% in toluene, 1.33 mL, 12.0 mmol, 1.2 equiv.) was added to this solution and stirred for 4 h at room temperature. NH₄Cl (saturated aqueous solution, 20 mL) was added and the aqueous phase was extracted with ethyl acetate (3x40 mL). The organic phase was washed with brine (20 mL) and dried over MgSO₄. The solvent was removed under reduced pressure. The residue was filtered over a silica pad (ethyl acetate/hexane 1/1).

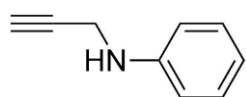


The synthesis approach is based on the literature.^[165] The title compound could not be isolated.

6.6.4 Synthesis approach of *N*-phenylprop-2-yn-1-amine

3-Bromoprop-1-yne (80w% in toluene, 0.95 mL, 8.6 mmol, 1 equiv.) was added to a mixture of aniline (1.02 mL, 11.0 mmol, 1.3 equiv.) and K₂CO₃ (1.80 g, 13.0 mmol, 1.5 equiv.) in DMF (20 mL). The mixture was stirred for 24 h at room temperature. Water (20 mL) was added and

the aqueous phase was extracted with ethyl acetate (3x40 mL). The organic phase was dried over Na₂SO₄. The solvent was removed under reduced pressure. The residue was filtered over a silica pad (ethyl acetate/hexane 1/10).



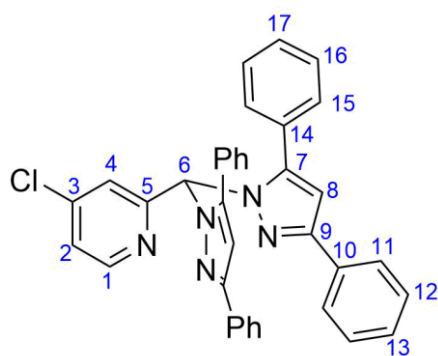
The synthesis approach is based on the literature.^[164] The title compound could not be isolated.

6.7 Ligand synthesis

6.7.1 Synthesis of HC(Ph₂Pz)₂(4-ClPy) (**L2**)

3,5-Diphenylpyrazole (4.000 g, 18.16 mmol, 2 equiv.) was added gradually to a suspension of NaH (0.436 g, 18.17 mmol, 2 equiv.) in THF (80 mL) at 0 °C and stirred for 30 min at 0 °C, the mixture was heated to 80 °C until no more gas formation was observed. The reaction mixture was cooled to 0 °C and SOCl₂ (0.66 mL, 9.08 mmol, 1 equiv.) was added dropwise. After stirring at 0 °C for 30 min and 45 min at room temperature, 4-chloropicolinaldehyde (1.285 g, 9.08 mmol, 1 equiv.) and CoCl₂ (0.118 g, 0.91 mmol, 10 mol%) were added and the reaction mixture was refluxed for 72 h. After cooling to room temperature, the reaction was stopped adding water and diethyl ether (1/1, 40 mL). The aqueous phase was extracted with diethyl ether (3x20 mL), the combined organic phases were dried over Na₂SO₄ and concentrated *in vacuo*. The residue was purified by silica gel column chromatography (*iso*-hexane/ethyl acetate, 8/2, R_f = 0.51) to give HC(Ph₂Pz)₂(4-ClPy) (3.87 g, 6.86 mmol, 75 %) as a light yellowish solid.

Crystals suitable for single crystal X-ray diffraction were obtained by vapor diffusion of pentane to a concentrated solution of HC(Ph₂Pz)₂(4-ClPy) in DCM.



Name: 2-(Bis(3,5-diphenyl-1*H*-pyrazol-1-yl)methyl)-4-chloropyridine. **Chemical formula:** C₃₆H₂₆ClN₅. **Molecular mass:** 564.09 g mol⁻¹. **¹H NMR (CD₂Cl₂, 400 MHz):** δ = 8.48 (d, ³J = 5.3 Hz, 1H, H-1), 7.82 (d, ³J = 7.0 Hz, 4H, H-11), 7.70 (s, 2H, H-4+H-6), 7.41 (t, ³J = 7.7 Hz, 4H, H-12), 7.33 (m, 5H, H-2+H-13+H-17), 7.23 (t, ³J = 7.0 Hz, 4H, H-16), 7.13 (d, ³J = 7.0 Hz, 4H, H-15), 6.84 (s, 2H, H-8) ppm. **¹³C {¹H} NMR (CD₂Cl₂, 100 MHz):** δ = 158.1 (C-5), 152.4

(C-9), 150.6 (C-1), 147.1 (C-7), 145.4 (C-3), 133.8 (C-10), 130.1 (C-14), 129.6 (C-15), 129.5 (C-16), 129.2 (C-13+C-17), 128.6 (C-12), 126.5 (C-11), 125.0 (C-4), 124.6 (C-2), 105.2 (C-8), 73.5 (C-6) ppm. **HRMS (ESI⁺, MeOH):** m/z (found) = 564.19342 (100%), 565.19678 (35%),

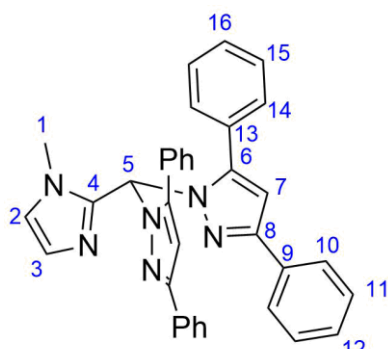
566.19080 (33%), 567.19385 (12%), 568.19720 (3%), 569.31281 (1%); m/z (calc.) = 564.19550 (100%, $^{12}\text{C}_{36}^{1}\text{H}_{27}^{14}\text{N}_5^{35}\text{Cl}^+$), 565.19885 (39%, $^{12}\text{C}_{35}^{13}\text{C}^1\text{H}_{26}^{14}\text{N}_5^{35}\text{Cl}^+$), 566.19255 (32%, $^{12}\text{C}_{36}^1\text{H}_{26}^{14}\text{N}_5^{37}\text{Cl}^+$), 567.19576 (13%, $^{12}\text{C}_{35}^{13}\text{C}^1\text{H}_{26}^{14}\text{N}_5^{37}\text{Cl}^+$), 568.19883 (3%, $^{12}\text{C}_{34}^{13}\text{C}_2^1\text{H}_{26}^{14}\text{N}_5^{37}\text{Cl}^+$), 569.20179 (1%, $^{12}\text{C}_{33}^{13}\text{C}_3^1\text{H}_{26}^{14}\text{N}_5^{37}\text{Cl}^+$). IR (ATR, neat), $\tilde{\nu}$ [cm^{-1}]: 1719 (m), 1617 (m), 1604 (m), 1573 (m), 1513 (m), 1485 (m), 1460 (m), 1409 (w), 1366 (m), 1301 (m), 1255 (m), 1229 (m), 1182 (m), 1073 (m), 1039 (w), 980 (w), 956 (w), 915 (vw), 866 (w), 816 (m), 800 (w), 767 (m), 756 (s), 719 (m), 690 (vs), 660 (w), 564 (w), 553 (m).

6.7.2 Synthesis of $\text{HC}(\text{Ph}_2\text{Pz})_2\text{Melm}$ (L3)

3,5-Diphenylpyrazole (4.000 g, 18.16 mmol, 2 equiv.) was added gradually to a suspension of NaH (0.436 g, 18.17 mmol, 2 equiv.) in toluene (80 mL) at 0 °C and stirred for 30 min at 0 °C, the mixture was heated to 80 °C until no more gas formation was observed. The reaction mixture was cooled to 0 °C and SOCl_2 (0.66 mL, 9.08 mmol, 1 equiv.) was added dropwise. After stirring at 0 °C for 30 min and 45 min at room temperature, 1-methyl-1H-imidazolylaldehyde (1.000 g, 9.08 mmol, 1 equiv.) and CoCl_2 (0.118 g, 0.91 mmol, 10 mol%) were added and the reaction mixture was refluxed for 72 h. After cooling to room temperature, the reaction was stopped adding water and diethyl ether (1/1, 40 mL). The aqueous phase was extracted with diethyl ether (3x20 mL), the combined organic phases were dried over Na_2SO_4 and concentrated *in vacuo*. The residue was purified by silica gel column chromatography (*iso*-hexane/ethyl acetate, 7/3, R_f = 0.28) to give $\text{HC}(\text{Ph}_2\text{Pz})_2\text{Melm}$ (2.37 g, 4.45 mmol, 49 %) as a colorless solid.

The reaction was also performed in THF as solvent, which leads to a lower yield.

Crystals suitable for single crystal X-ray diffraction were obtained by vapor diffusion of pentane to a concentrated solution of $\text{HC}(\text{Ph}_2\text{Pz})_2\text{Melm}$ in DCM.



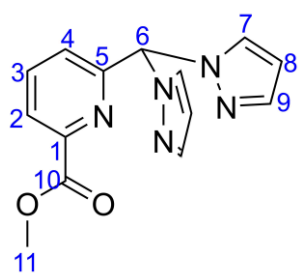
Name: 1,1'-((1-Methyl-1H-imidazol-2-yl)methylene)bis(3,5-diphenyl-1H-pyrazole). **Chemical formula:** $\text{C}_{35}\text{H}_{28}\text{N}_6$. **Molecular mass:** 532.65 g mol^{-1} . **^1H NMR (CD_2Cl_2 , 400 MHz):** δ = 7.80 (d, 3J = 7.8 Hz, 4H, H-10), 7.67 (s, 1H, H-5), 7.39 (t, 3J = 7.4 Hz, 4H, H-11), 7.32 (d, 3J = 7.3 Hz, 4H, H-12+H-16), 7.27 (t, 3J = 7.3 Hz, 4H, H-15), 7.12 (d, 3J = 7.1 Hz, 4H, H-14), 6.94 (d, 3J = 3.1 Hz, 2H, H-2+H-3), 6.65 (s, 2H, H-7), 3.70 (s, 3H, H-1) ppm. **^{13}C { ^1H } NMR (CD_2Cl_2 , 100 MHz):** δ = 151.8 (C-8),

146.4 (C-6), 142.5 (C-4), 133.7 (C-9), 129.5 (C-13), 129.4 (C-14), 129.1 (C-15), 129.1 (C-12+C-16), 128.5 (C-11), 128.0 (C-3), 126.3 (C-10), 124.3 (C-2), 106.3 (C-7), 70.0 (C-5), 34.9

(C-1) ppm. **HRMS (ESI⁺, MeOH):** *m/z* (found) = 533.24353 (100%), 534.24664 (37%), 535.25024 (7%), 536.25299 (1%); *m/z* (calc.) = 533.24537 (100%, ¹²C₃₅¹H₂₉¹⁴N₆⁺), 534.24872 (38%, ¹²C₃₄¹³C¹H₂₉¹⁴N₆⁺), 535.25207 (7%, ¹²C₃₃¹³C₂¹H₂₉¹⁴N₆⁺), 536.25543 (1%, ¹²C₃₂¹³C₃¹H₂₉¹⁴N₆⁺). **IR (ATR, neat), $\tilde{\nu}$ [cm⁻¹]:** 1605 (vw), 1551 (vw), 1485 (w), 1459 (w), 1437 (w), 1410 (vw), 1298 (vw), 1281 (vw), 1259 (w), 1202 (w), 1138 (vw), 1076 (w), 1027 (w), 1007 (w), 957 (w), 916 (w), 868 (w), 841 (w), 834 (w), 816 (m), 803 (w), 767 (m), 759 (vs), 752 (s), 704 (m), 691 (vs), 678 (m), 666 (m), 573 (m), 524 (w), 432 (vw).

6.7.3 Synthesis of HC(Pz)₂(6-CO₂MePy) (L9)

Pyrazole (0.825 g, 12.11 mmol, 2 equiv.) was added gradually to a suspension of NaH (0.298 g, 12.41 mmol, 2.05 equiv.) in THF (20 mL) at 0 °C and stirred until no more gas formation was observed, approximately 30 min, SOCl₂ (0.44 mL, 6.06 mmol, 1 equiv.) was added dropwise. After stirring at 0 °C for 30 min and 45 min at room temperature, methyl 6-formyl-2-pyridinecarboxylate (1.000 g, 6.06 mmol, 1 equiv.) and CoCl₂ (0.076 g, 0.61 mmol, 10 mol%) were added and the reaction mixture was refluxed for 24 h. After cooling to room temperature, the reaction was stopped adding water and diethyl ether (1/1, 40 mL). The aqueous phase was extracted with diethyl ether (3x20 mL), the combined organic phases were dried over Na₂SO₄ and concentrated *in vacuo*. The residue was purified by silica gel column chromatography (*iso*-hexane/ethyl acetate, 2/8, *R_f* = 0.48) to give HC(Pz)₂(6-CO₂MePy) (1.07 g, 3.78 mmol, 62 %) as a colorless solid.



Name: Methyl 6-(di(1*H*-pyrazol-1-yl)methyl)picolinate. **Chemical for-**

mula: C₁₄H₁₃N₅O₂. **Molecular mass:** 283.29 g mol⁻¹. **¹H NMR**

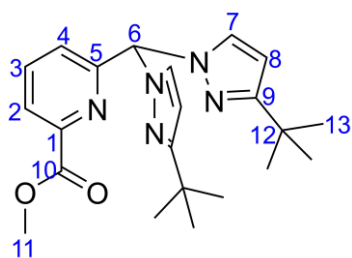
(CD₂Cl₂, 400 MHz): δ = 8.11 (d, ³J = 7.9 Hz, 1H, H-4), 7.91 (t, ³J = 7.9 Hz, 1H, H-3), 7.78 (s, 1H, H-6), 7.65 (d, ³J = 2.4 Hz, 2H, H-7), 7.60 (d, ³J = 1.5 Hz, 2H, H-9), 7.32 (d, ³J = 7.9 Hz, 1H, H-2), 6.37 (t, ³J = 2.4 Hz, 1.5 Hz, 2H, H-8), 3.95 (s, 3H, H-11) ppm. **¹³C {¹H} NMR**

(CD₂Cl₂, 100 MHz): δ = 165.6 (C-10), 155.8 (C-5), 148.6 (C-1), 141.4 (C-9), 139.0 (C-3), 130.5 (C-7), 126.3 (C-4), 125.8 (C-2), 107.3 (C-8), 78.9 (C-6), 53.3 (C-10) ppm. **HRMS (ESI⁺, MeOH):** *m/z* (found) = 306.09659 (100%), 307.09985 (16%), 308.10315 (1%); *m/z* (calc.) = 306.09669 (100%, ²³Na¹²C₁₄¹H₁₃¹⁴N₅¹⁶O₂⁺), 307.10005 (15%, ²³Na¹²C₁₃¹³C¹H₁₃¹⁴N₅¹⁶O₂⁺), 308.10340 (1%, ²³Na¹²C₁₂¹³C₂¹H₁₃¹⁴N₅¹⁶O₂⁺). **IR (ATR, neat), $\tilde{\nu}$ [cm⁻¹]:** 3096 (vw), 2953 (w), 2925 (vw), 2854 (vw), 1737 (m), 1701 (w), 1696 (w), 1587 (w), 1510 (w), 1441 (w), 1392 (m), 1289 (m), 1256 (w), 1227 (w), 1201 (m), 1179 (vw), 1167 (w), 1147 (m), 1099 (w), 1085 (m), 1051 (m), 1038 (w), 1001 (m), 993 (m), 964 (m), 920 (w), 911 (w), 900 (w), 884 (w), 841 (vw),

813 (m), 806 (m), 772 (s), 757 (m), 749 (vs), 726 (m), 691 (m), 664 (w), 656 (w), 636 (s), 617 (w), 610 (w).

6.7.4 Synthesis of HC(^tBuPz)₂(6-CO₂MePy) (**L10**)

3-*tert*-butylpyrazole (1.504 g, 12.11 mmol, 2 equiv.) was added gradually to a suspension of NaH (0.298 g, 12.41 mmol, 2.05 equiv.) in THF (20 mL) at 0 °C and stirred until no more gas formation was observed, approximately 30 min, SOCl₂ (0.44 mL, 6.06 mmol, 1 equiv.) was added dropwise. After stirring at 0 °C for 30 min and 45 min at room temperature, methyl 6-formyl-2-pyridinecarboxylate (1.000 g, 6.06 mmol, 1 equiv.) and CoCl₂ (0.076 g, 0.61 mmol, 10 mol%) were added and the reaction mixture was refluxed for 24 h. After cooling to room temperature, the reaction was stopped adding water and diethyl ether (1/1, 40 mL). The aqueous phase was extracted with diethyl ether (3x20 mL), the combined organic phases were dried over Na₂SO₄ and concentrated *in vacuo*. The residue was purified by silica gel column chromatography (*iso*-hexane/ethyl acetate, 7/3, R_f = 0.56) to give HC(^tBuPz)₂(6-CO₂MePy) (1.41 g, 3.56 mmol, 59 %) as a colorless solid.

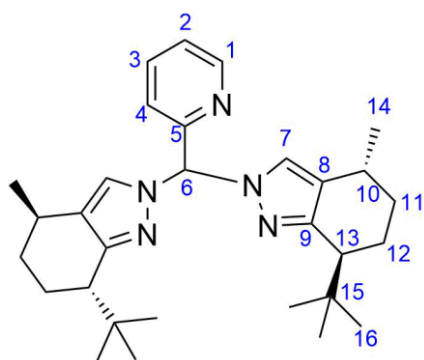


Name: Methyl 6-(bis(3-(*tert*-butyl)-1*H*-pyrazol-1-yl)methyl)picolinate. **Chemical formula:** C₂₂H₂₉N₅O₂. **Molecular mass:** 395.51 g mol⁻¹. **¹H NMR (CD₂Cl₂, 400 MHz):** δ = 8.09 (d, ³J = 7.9 Hz, 1H, H-2), 7.88 (t, ³J = 7.9 Hz, 1H, H-3), 7.56 (s, 1H, H-6), 7.38 (d, ³J = 2.4 Hz, 2H, H-7), 7.21 (d, ³J = 7.9 Hz, 1H, H-4), 6.20 (d, ³J = 2.4 Hz, 2H, H-8), 3.96 (s, 3H, H-11), 1.28 (s, 18H,

H-13) ppm. **¹³C {¹H} NMR (CD₂Cl₂, 100 MHz):** δ = 165.4 (C-10), 164.0 (C-9), 156.6 (C-5), 148.5 (C-1), 138.7 (C-3), 130.4 (C-7), 126.1 (C-4), 125.6 (C-2), 103.7 (C-8), 79.0 (C-6), 53.3 (C-11), 32.7 (C-12), 30.8 (C-13) ppm. **HRMS (ESI⁺, MeOH):** m/z(found) = 418.22119 (100%), 419.22437 (23%), 420.22760 (3%); m/z(calc.) = 418.22189 (100%, ²³Na¹²C₂₂¹H₂₉¹⁴N₅¹⁶O₂⁺), 419.22525 (24%, ²³Na¹²C₂₁¹³C₁¹H₂₉¹⁴N₅¹⁶O₂⁺), 420.22860 (3%, ²³Na¹²C₂₀¹³C₂¹H₂₉¹⁴N₅¹⁶O₂⁺). **IR (ATR), $\tilde{\nu}$ [cm⁻¹]:** 2958 (w), 2931 (vw), 2902 (w), 2867 (vw), 1751 (w), 1722 (m), 1701 (w), 1590 (w), 1577 (w), 1519 (m), 1459 (w), 1437 (w), 1397 (vw), 1362 (w), 1309 (m), 1263 (w), 1248 (m), 1225 (w), 1161 (w), 1137 (m), 1091 (w), 1056 (m), 996 (w), 982 (w), 914 (w), 820 (w), 804 (m), 781 (w), 755 (vs), 695 (w), 643 (w).

6.7.5 Synthesis of HC(PulPz)₂Py (L11)

PulPz (4.000 g, 20.8 mmol, 2 equiv.) was added gradually to a suspension of NaH (0.513 g, 21.3 mmol, 2 equiv.) in THF (50 mL) at 0 °C and stirred until no more gas formation was observed, approximated 30 min, SOCl₂ (0.76 mL, 10.4 mmol, 1 equiv.) was added dropwise. After stirring at 0 °C for 30 min and 45 min at room temperature, picolinaldehyde (0.99 mL, 10.4 mmol, 1 equiv.) and CoCl₂ (0.130 g, 1.04 mmol, 10 mol%) were added and the reaction mixture was refluxed for 72 h. After cooling to room temperature, the reaction was stopped adding water and diethyl ether (1/1, 20 mL). The aqueous phase was extracted with diethyl ether (3x10 mL), the combined organic phases were dried over Na₂SO₄ and concentrated *in vacuo*. The residue was purified by silica gel column chromatography (*iso*-hexane/ethyl acetate, 8/5, R_f = 0.70) to give HC(PulPz)₂Py (3.61 g, 7.63 mmol, 73 %) as a light yellowish oil.



Name: (4*R*,4'*R*,7*S*,7'*S*)-2,2'-(pyridin-2-ylmethylene)bis(7-(*tert*-butyl)-4-methyl-4,5,6,7-tetrahydro-2*H*-indazole).

Chemical formula: C₃₀H₄₃N₅. **Molecular mass:**

473.71 g·mol⁻¹. **¹H NMR (CD₂Cl₂, 400 MHz):** δ = 8.58 (qd, ³J = 4.8 Hz, ⁴J = 0.8 Hz, 1H, H-1), 7.70 (dt, ³J = 8.0 Hz, ⁴J = 1.6 Hz, 1H, H-3), 7.45 (s, 1H, H-6), 7.27 (m, 3H, H-2, H-7), 6.99 (d, ³J = 7.6 Hz, 1H, H-4), 2.54 (m, 4H, H-10, H-13), 2.01 (m, 2H, H-12), 1.89 (m, 2H, H-11), 1.42 (m, 2H, H-12),

1.22 (m, 2H-11), 1.12 (2xd, ³J = 6.4 Hz, 6H, H-14), 0.99 (2xs, 18H, H-16) ppm. **¹³C {¹H} NMR (CD₂Cl₂, 100 MHz):** δ = 157.0 (C-5), 152.7 (d, C-8), 149.9 (C-1), 137.3 (C-3), 126.0 (d, C-9), 125.9 (d, C-7), 124.0 (C-2), 122.6 (C-4), 79.4 (C-6), 45.5 (d, C-13), 34.6 (d, C-15), 33.9 (d, C-11), 29.0 (C-10), 28.3 (C-16), 26.8 (d, C-13), 21.7 (d, C-14) ppm. *Note: The doublets are due to the asymmetry of the pyrazolyl units, therefore no J couplings are given.* **HRMS (ESI⁺, MeOH):** m/z (found): 496.3404 (100%), 497.3441 (32%), 498.3478 (5%); m/z (calc.): 496.3444 (100%, ²³Na₁¹²C₃₀¹H₄₃¹⁴N₅⁺), 497.3441 (32%, ²³Na₁¹²C₂₉¹³C₁¹H₄₃¹⁴N₅⁺), 498.3478 (5%, ²³Na₁¹²C₂₈¹³C₂¹H₄₃¹⁴N₅⁺). **IR (ATR, neat), $\tilde{\nu}$ [cm⁻¹]:** 2952 (m), 2865 (m), 1740 (vw), 1590 (w), 1574 (w), 1564 (w), 1479 (w), 1436 (m), 1420 (m), 1392 (m), 1363 (s), 1333 (w), 1306 (m), 1239 (w), 1219 (w), 1198 (w), 1172 (m), 1148 (m), 1110 (w), 1094 (w), 1050 (w), 1030 (w), 1011 (m), 994 (w), 960 (w), 940 (vw), 885 (m), 869 (w), 848 (w), 824 (m), 798 (m), 762 (m), 748 (vs), 678 (m), 664 (w), 619 (w), 568 (vw), 516 (vw), 503 (vw), 481 (vw), 474 (vw).

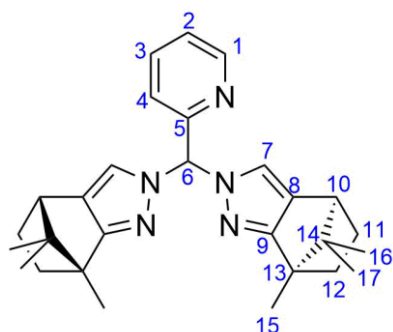
6.7.6 Synthesis of HC(CamPz)₂Py (L12)

Approach A:

CamPz (3.71 g, 21.0 mmol, 2 equiv.) was added gradually to a suspension of NaH (0.520 g, 21.7 mmol, 2.05 equiv.) in THF (30 mL) at 0 °C and stirred until no more gas formation was observed, approximately 30 min, SOCl₂ (0.76 mL, 10.5 mmol, 1 equiv.) was added dropwise. After stirring at 0 °C for 30 min and 45 min at room temperature, picolinaldehyde (1.0 mL, 10.5 mmol, 1 equiv.) and CoCl₂ (142 mg, 1.1 mmol, 10 mol%) were added and the reaction mixture was refluxed overnight. After cooling to room temperature, the reaction was stopped adding water and diethyl ether (1/1, 60 mL). The aqueous phase was extracted with diethyl ether (4x30 mL), the combined organic phases were dried over Na₂SO₄ and concentrated *in vacuo*. The residue was purified by silica gel column chromatography (*iso*-hexane/ethyl acetate/dichloromethane, 1/1/1, R_f = 0.55) and alumina column chromatography (ethyl acetate/dichloromethane, 1/5, R_f = 0.81) to give HC(CamPz)₂Py (1.20 g, 2.72 mmol, 26%) as a colorless solid.

Approach B:

CamPz (9.00 g, 51.1 mmol, 2 equiv.) was added gradually to a suspension of NaH (1.257 g, 52.4 mmol, 2.05 equiv.) in THF (50 mL) at 0 °C and stirred until no more gas formation was observed, approximately 30 min, SOCl₂ (1.85 mL, 25.5 mmol, 1 equiv.) was added dropwise. After stirring at 0 °C for 30 min and 45 min at room temperature, picolinaldehyde (2.4 mL, 25.5 mmol, 1 equiv.) and CoCl₂ (165 mg, 1.27 mmol, 5 mol%) were added and the reaction mixture was refluxed overnight. The solvent was removed under reduced pressure. To the residue dichloromethane (200 mL) was added. The organic phase was washed with water and brine (200 mL). The organic phase was dried over Na₂SO₄ and the solvent was removed under reduced pressure. The residue was purified by silica gel column chromatography (*iso*-hexane/dichloromethane, 2/1 + 5% triethylamine, R_f = 0.8) and alumina column chromatography (dichloromethane/ethyl acetate, 30/1, R_f = 0.3, followed by ethyl acetate. R_f = 1.0) to give HC(CamPz)₂Py (1.40 g, 3.17 mmol, 12%) as a light yellowish solid.



Name: (4*S*,4'*S*,7*R*,7'*R*)-2,2'-(pyridin-2-ylmethylene)bis(7,8,8-trimethyl-4,5,6,7-tetrahydro-2*H*-4,7-methanoindazole).

Chemical formula: C₂₈H₃₅N₅. **Molecular mass:**

441.29 g mol⁻¹. **¹H NMR (CD₂Cl₂, 400 MHz):** δ = 8.58 (dq, ³J = 4.8 Hz, ⁴J = 0.8 Hz, 1H, H-1), 7.70 (td, ³J = 7.8 Hz, ⁴J = 1.8 Hz, 1H, H-3), 7.44 (s, 1H, H-6), 7.27 (qd, ³J = 4.8 Hz, ⁴J = 0.9 Hz, 1H, H-2), 7.00 (s, 1H, H-7), 6.95 (s, 1H, H-7), 6.93 (dq, ³J =

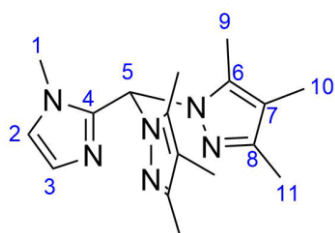
7.8 Hz, ⁴J = 0.8 Hz, 1H, H-4), 2.74 (2xd, ³J = 4.3 Hz, 2H, H-10), 2.06 (m, 2H, H-11), 1.84 (m,

2H, H-12), 1.28 (m, 2H, H-12), 1.22 (s, 3H, H-15), 1.21 (s, 3H, H-15), 1.14 (m, 2H, H-11), 0.94 (2xs, 2x3H, H-16/17), 0.66 (s, 3H, H-16/17), 0.63 (s, 3H, H-16/17) ppm. **¹³C {¹H} NMR (CD₂Cl₂, 100 MHz):** δ = 168.0 (d, C-9), 157.3 (C-5), 149.9 (C-1), 137.5 (C-3), 128.1 (d, C-8), 123.9 (C-2), 122.5 (C-4), 122.2 (d, C-7), 79.0 (C-6), 60.8 (C-14), 50.8 (C-13), 47.8 (d, C-10), 34.3 (d, C-12), 28.2 (d, C-11), 20.9 (d, C-16/17), 19.4 (C-16/17), 11.0 (d, C-15) ppm. *Note: The doublets are due to the asymmetry of the pyrazolyl units, therefore no J couplings are given.* **HRMS (ESI⁺, MeOH):** m/z (found): 464.27795 (100%), 465.28122 (29%), 466.28467 (4%); m/z (calc.) = 464.27902 (100%, ²³Na₁¹²C₂₈¹H₃₅¹⁴N₅⁺), 465.28237 (30%, ²³Na₁¹²C₂₇¹³C₁¹H₃₈¹⁴N₅⁺), 466.28573 (4%, ²³Na₁¹²C₂₆¹³C₂¹H₃₈¹⁴N₅⁺). **IR (ATR, neat), $\tilde{\nu}$ [cm⁻¹]:** 2965 (s), 2865 (w), 1590 (m), 1572 (w), 1485 (w), 1472 (m), 1457 (w), 1437 (m), 1418 (w), 1385 (m), 1376 (s), 1366 (vs), 1342 (w), 1324 (m), 1288 (s), 1277 (vs), 1268 (m), 1238 (vw), 1227 (vw), 1210 (w), 1181 (m), 1141 (m), 1120 (s), 1107 (vw), 1093 (w), 1085 (w), 1050 (vw), 998 (w), 969 (w), 963 (w), 950 (vs), 909 (w), 881 (m), 862 (w), 816 (w), 805 (m), 783 (vs), 771 (vs), 748 (m), 718 (w), 698 (m), 667 (m), 640 (w), 620 (vs), 610 (s), 570 (w).

6.7.7 Resynthesis of HC(Me₃Pz)₂Melm (**L15**)

3,4,5-methylpyrazole (4.000 g, 36.3 mmol, 2 equiv.) was added gradually to a suspension of NaH (0.8715 g, 36.3 mmol, 2 equiv.) in THF (50 mL) at 0 °C and stirred until no more gas formation was observed, approximately 30 min, SOCl₂ (1.32 mL, 18.2 mmol, 1 equiv.) was added dropwise. After stirring at 0 °C for 30 min and 45 min at room temperature, 1-methyl-2-imidazolylcarboxaldehyde (1.999 g, 18.2 mmol, 1 equiv.) and CoCl₂ (0.232 g, 1.8 mmol, 10 mol%) were added and the reaction mixture was refluxed for 72 h. After cooling to room temperature, the solvent was removed under reduced pressure. The residue was solved in DCM (100 mL) and washed with water (4x100 mL). The combined organic phases was dried over Na₂SO₄ and the solvent was removed under reduced pressure. The residue was solved in a mixture of DCM (15 mL) and diethyl ether (100 mL). The solution was layered with pentane (200 mL). After a few days colorless crystals form, which were collected by filtration and washed with cold diethyl ether to yield HC(Me₃Pz)₂Melm (1.831 g, 5.9 mmol, 33 %).

The reaction protocol from the literature^[140] was modified.

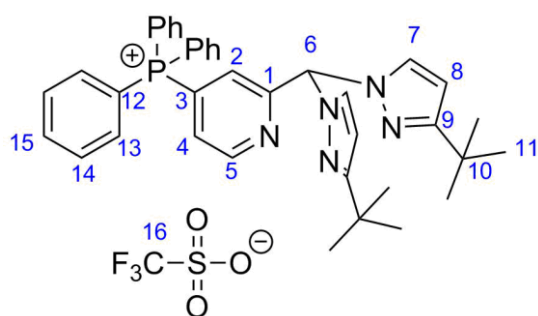


Name: 1,1'-((1-methyl-1H-imidazol-2-yl)methylene)bis(3,4,5-trimethyl-1H-pyrazole). **Chemical formula:** C₁₇H₂₄N₆. **Molecular mass:** 312.21 g mol⁻¹. **¹H NMR (CDCl₃, 400 MHz):** δ = 7.53 (s, 1H, H-5), 7.03 (s, 1H, H-3), 6.89 (s, 1H, H-2), 3.28 (s, 3H, H-1), 2.12 (s, 6H, H-9), 2.04 (s, 6H, H-10), 1.87 (s, 6H, H-11) ppm.

6.7.8 Synthesis of (HC(*t*BuPz)₂(4-PPh₃Py))OTf (**L18**)

HC(*t*BuPz)₂Py (1.687 g, 5.0 mmol, 1 equiv.) was dissolved in DCM (50 mL) at 0 °C. Tf₂O (0.84 mL, 5.0 mmol, 1 equiv.) was added dropwise over 5 minutes. The solution was stirred for 30 min at 0 °C. Triphenylphosphane (1.312 g, 5.5 mmol, 1.1 equiv.) was added, followed by three cycles of vacuum and nitrogen. The solution was stirred for 30 min at 0 °C. Triethylamine (0.69 mL, 5.0 mmol, 1 equiv.) was added and the solution was stirred for 30 min at room temperature. The reaction was stopped by adding water (50 mL) and DCM (50 mL). The organic phase was washed with water (3x50 mL) and dried over Na₂SO₄. The solution was concentrated *in vacuo* and layered with diethyl ether and stored at -30 °C. The product was isolated as colorless crystals (0.950 g, 1.3 mmol, 26%).

This reaction protocol was inspired by the literature.^{[142]–[146]}



Name: (2-(bis(3-(*tert*-butyl)-1*H*-pyrazol-1-yl)methyl)pyridin-4-yl)triphenylphosphonium triflate.

Chemical formula: C₃₉H₄₁F₃N₅O₃PS. **Molecular**

mass: 747.82 g mol⁻¹. **¹H NMR (CDCl₃, 400 MHz):** δ = 8.98 (td, ³J = 5.1 Hz, ⁴J = 0.7 Hz, 1H, H-5), 7.76 (m, 6H, H-14), 7.90 (m, 3H, H-15), 7.63 (m, 1H, H-2), 7.59 (m, 6H, H-13), 7.56 (s, 1H,

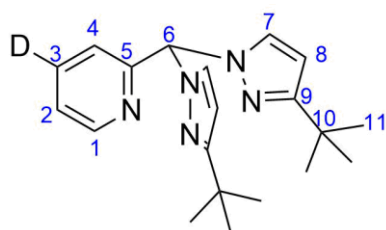
H-6), 7.36 (d, ³J = 2.5 Hz, 2H, H-7), 6.93 (d, ³J = 13.3 Hz, 1H, H-4), 6.09 (d, ³J = 2.5 Hz, 2H, H-8), 1.15 (s, 18H, H-11) ppm. **¹³C {¹H} NMR (CDCl₃, 100 MHz):** δ = 163.7 (C-9), 158.7 (d, J = 10.3 Hz, C-5), 151.7 (d, J = 10.1 Hz, C-1), 136.4 (d, J = 3.3 Hz, C-15), 134.6 (d, J = 10.1 Hz, C-13), 132.2 (d, J = 9.9 Hz, C-3), 131.2 (d, J = 13.3 Hz, C-14), 130.6 (C-7), 127.4 (d, J = 8.3 Hz, C-2), 128.6 (d, J = 12.1 Hz, C-12), 125.7 (d, J = 8.9 Hz, C-4), 121.0 (q, J = 320.6 Hz, C-16), 103.6 (C-8), 77.9 (C-6), 32.3 (C-10), 30.5 (C-11) ppm. **¹⁹F {¹H} NMR (CDCl₃, 377 MHz):** δ = -78.1 ppm. **³¹P {¹H} NMR (CDCl₃, 162 MHz):** δ = 22.6 ppm. **HRMS (ESI⁺, MeOH):** m/z (found) = 598.30969 (100%), 599.31256 (41%), 600.31580 (8%), 601.31958 (1%); m/z (calc.) = 598.30997 (100%, ¹²C₃₈¹H₄₁¹⁴N₅³¹P⁺), 599.316236 (41%, ¹²C₃₇¹³C₁¹H₄₁¹⁴N₅³¹P⁺), 600.31667 (8%, ¹²C₃₆¹³C₂¹H₄₁¹⁴N₅³¹P⁺), 601.31370 (1%, ¹²C₃₅¹³C₃¹H₄₁¹⁴N₅³¹P⁺). **IR (ATR, neat), $\tilde{\nu}$ [cm⁻¹]:** 2967 (vw), 2929 (vw), 2902 (vw), 2866 (vw), 1585 (w), 1527 (vw), 1518 (w), 1484 (vw), 1460 (vw), 1441 (w), 1388 (w), 1360 (vw), 1305 (w), 1263 (s), 1225 (s), 1207 (s), 1167 (s), 1148 (vs), 1128 (s), 1109 (vs), 1065 (m), 1056 (m), 1031 (m), 997 (m), 983 (m), 915 (w), 900 (w), 837 (w), 827 (w), 800 (w), 776 (w), 768 (m), 753 (m), 725 (m), 688 (m), 665 (w), 637 (s), 571 (m), 555 (w), 527 (s), 516 (s), 504 (s).

The reaction protocol also could be used with HC(Ph₂Pz)₂Py as starting material to yield (HC(Ph₂Pz)₂(PPh₃Pz))OTf. The product was not isolated but could be observed with ESI-

HRMS. **HRMS (ESI⁺, MeOH):** *m/z* (found) = 790.30896 (100%), 792.31525 (61%), 793.3152 (17%), 794.32300 (3%); *m/z* (calc.) = 790.30996 (100%, ¹²C₅₄¹H₄₁¹⁴N₅³¹P⁺), 791.31331 (58%, ¹²C₅₃¹³C₁¹H₄₁¹⁴N₅³¹P⁺), 792.31667 (17%, ¹²C₅₂¹³C₂¹H₄₁¹⁴N₅³¹P⁺), 793.32002 (3%, ¹²C₅₁¹³C₃¹H₄₁¹⁴N₅³¹P⁺), 794.32338 (1%, ¹²C₅₀¹³C₄¹H₄₁¹⁴N₅³¹P⁺).

6.7.9 Synthesis of HC(^tBuPz)₂(4-DPy) (**L19**)

(HC(^tBuPz)₂(PPh₃Py))OTf (50.0 mg, 0.067 mmol, 1 equiv.) and potassium carbonate (13.9 mg, 0.101 mmol, 1.5 equiv.) was solved in methanol-*d*₄ (0.20 mL) and water-*d*₂ (0.02 mL) and stirred overnight. DCM (0.22 mL) was added and the organic phase was dried over Na₂SO₄ and filtered over silica (Ethyl acetate). The solvent was removed *in vacuo*. The product was not isolated.



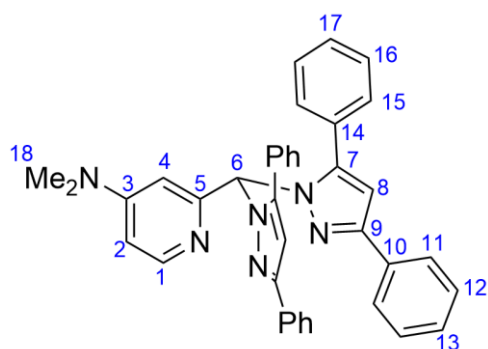
Name: 2-(bis(3-(*tert*-butyl)-1*H*-pyrazol-1-yl)methyl)pyridine-4-*d*. **Chemical formula:** C₂₀H₂₆DN₅. **Molecular mass:** 747.82 g mol⁻¹. **¹H NMR (acetone-*d*₆, 400 Hz):** δ = 8.57 (d, ³J = 4.5 Hz, 1H, H-1), 7.66 (s, 1H, H-6), 7.62 (d, ³J = 2.4 Hz, 2H, H-7), 7.37 (d, ³J = 6.6 Hz, 1H, H-2), 7.09 (d, ³J = 7.9 Hz, 1H, H-4), 6.23 (d, ³J = 2.5 Hz, 2H, H-8), 1.26 (s, 18H, H-11) ppm.

6.7.10 Synthesis of HC(Ph₂Pz)₂DMap (**L20**)

The reaction was performed under aerobic conditions in a high-pressure flask.

HC(Ph₂Pz)₂(4-ClPy) (1.500 g, 2.66 mmol, 1 equiv.) and dimethyl amine hydrochloride (1.337 g, 16.4 mmol, 6.15 equiv.) were dissolved in water (2.6 mL) and ethanol (0.52 mL). Sodium hydroxide (0.656 g, 16.4 mmol, 6.15 equiv.) was added and the flask was sealed immediately. The mixture was stirred for 4 h at 130 °C. After cooling to room temperature, dichloromethane (2 mL) was added and the solution was stirred for 5 minutes. The organic phase was separated, and the aqueous phase was extracted with dichloromethane (3x2 mL). The combined organic phase was filtered through a short aluminum oxide plug. The solvent was removed under reduced pressure. The residue was purified by silica gel column chromatography (ethyl acetate, R_f = 0.52) to give HC(Ph₂Pz)₂DMap (1.32 g, 2.31 mmol, 87%) as a light yellowish solid.

Crystals suitable for single crystal X-ray diffraction were obtained by vapor diffusion of pentane to a concentrated solution of HC(Ph₂Pz)₂DMap in DCM.



Name: 2-(bis(3,5-diphenyl-1H-pyrazol-1-yl)methyl)-N,N-dimethylpyridin-4-amine. **Chemical formula:**

$C_{38}H_{32}N_6$. **Molecular mass:** 572.72 $g\text{mol}^{-1}$. **^1H NMR**

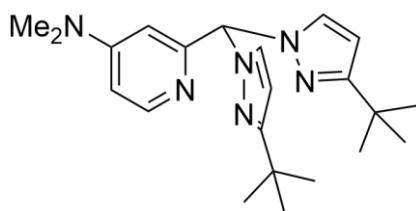
(CD_2Cl_2 , 400 MHz): δ = 8.16 (d, 3J = 8.2 Hz, 2H, H-1), 7.85 (m, 4H, H-11), 7.63 (s, 1H, H-6), 7.40 (m, 4H, H-12), 7.29 (m, 4H, H-13+17), 7.22 (m, 4H, H-16), 7.18 (m, 4H, H-15), 6.75 (d, 3J = 6.8 Hz, 1H, H-4), 6.62 (s, 2H, H-8), 6.46 (dd, 3J = 6.5 Hz, 4J = 2.6 Hz, 1H, H-2),

2.19 (s, 6H, H-18) ppm. **^{13}C { ^1H } NMR** (CD_2Cl_2 , 100 MHz): δ = 156.2 (C-5), 155.5 (C-3), 151.9 (C-9), 149.6 (C-1), 146.9 (C-7), 134.1 (C-14), 130.4 (C-10), 129.6 (C-12), 129.2 (C-13), 129.1 (C-16), 129.0 (C-15), 128.3 (C-17), 126.4 (C-11), 107.0 (C-4), 106.6 (C-2), 104.9 (C-8), 74.1 (C-6), 39.4 (C-18) ppm. **HRMS (ESI⁺, MeOH):** m/z (found) = 573.27539 (100%), 574.27820 (43%), 575.28204 (9%), 576.28552 (2%); m/z (calc.) = 573.27667 (100%, $^{12}\text{C}_{38}^{14}\text{N}_6^1\text{H}_{33}^+$), 574.28003 (41%, $^{12}\text{C}_{37}^{13}\text{C}_1^{14}\text{N}_6^1\text{H}_{33}^+$), 575.28338 (8%, $^{12}\text{C}_{36}^{13}\text{C}_2^{14}\text{N}_6^1\text{H}_{33}^+$), 576.28041 (1%, $^{12}\text{C}_{35}^{13}\text{C}_3^{14}\text{N}_6^1\text{H}_{33}^+$). **IR (ATR, neat), $\tilde{\nu}$ [cm^{-1}]:** 1604 (m), 1484 (w), 1457 (w), 1432 (w), 1407 (w), 1369 (w), 1324 (w), 1278 (w), 1223 (vw), 1204 (w), 1160 (w), 1073 (w), 1005 (w), 980 (w), 957 (w), 923 (w), 805 (w), 869 (w), 851 (w), 831 (m), 815 (m), 763 (vs), 740 (m), 698 (vs), 655 (m).

6.7.11 Synthesis approach of $\text{HC}(t\text{BuPz})_2\text{DMAP}$

The reaction was performed under aerobic conditions in a high-pressure flask.

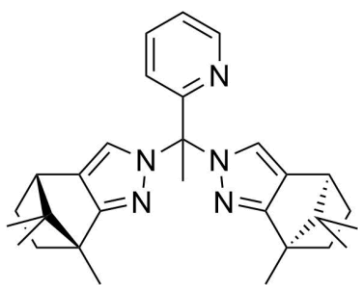
$\text{HC}(t\text{BuPz})_2(4\text{-PPh}_3\text{Py})\text{OTf}$ (0.850 g, 1.14 mmol, 1 equiv.) and dimethyl amine hydrochloride (0.557 g, 6.83 mmol, 6 equiv.) were dissolved in water (2 mL) and ethanol (0.4 mL). Sodium hydroxide (0.273 g, 6.83 mmol, 6 equiv.) was added and the flask was sealed immediately. The mixture was stirred for 18 h at 130 °C. After cooling to room temperature, the aqueous phase was diluted with water (2.5 mL) and extracted with dichloromethane (4x5 mL). The organic phase was filtered through a short aluminum oxide plug. The solvent was removed under reduced pressure.



The title compound could not be observed using ^1H NMR or HRMS-ESI.

6.7.12 Synthesis approach of MeC(CamPz)₂Py

To a solution of HC(CamPz)₂Py (44.1 mg, 0.1 mmol, 1 equiv.) in THF (1 mL) *n* butyllithium (2.5 M in hexane, 0.04 mL, 0.1 mmol, 1 equiv.) was added dropwise at room temperature. The solution was stirred for 30 min. Methyl iodide (0.02 mL, 0.3 mmol, 3 equiv.) was added and the solution was stirred at room temperature overnight. Water (2 mL) was added and the aqueous phase was extracted with diethyl ether (3x2 mL). The organic phases was dried over Na₂SO₄ and the solvent was removed under reduced pressure.



The reaction protocol was also used with potassium *tert*-butoxide (3 equiv.) and sodium bis(trimethylsilyl)amide (2 M in THF, 1. equiv.) as base.

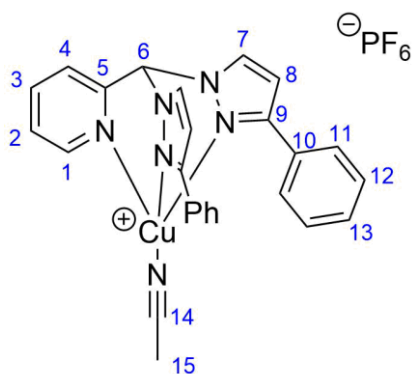
The title compound could not be observed using ¹H NMR or HRMS-ESI.

6.8 Complex synthesis

6.8.1 Synthesis of [Cu{HC(PhPz)₂Py}(MeCN)]PF₆ (**C1**)

A solution of HC(PhPz)₂Py (157 mg, 0.42 mmol, 1 equiv.) in THF (5 mL) was added dropwise to a solution of [Cu(MeCN)₄]PF₆ (155 mg, 0.42 mmol, 1 equiv.) in THF (5 mL). The solution was stirred at room temperature overnight. The complex was crystallized by vapor diffusion of diethyl ether to this solution for a few days. The substance was filtrated, washed with THF/Et₂O (1/2, 3x1 mL) and dried *in vacuo* to yield the complex [Cu{HC(PhPz)₂Py}(MeCN)]PF₆ (202 mg, 0.32 mmol, 76 %).

Crystals suitable for single crystal X-ray diffraction were obtained from a concentrated solution of [Cu{HC(PhPz)₂Py}(MeCN)]PF₆ in THF, which was layered with diethyl ether.



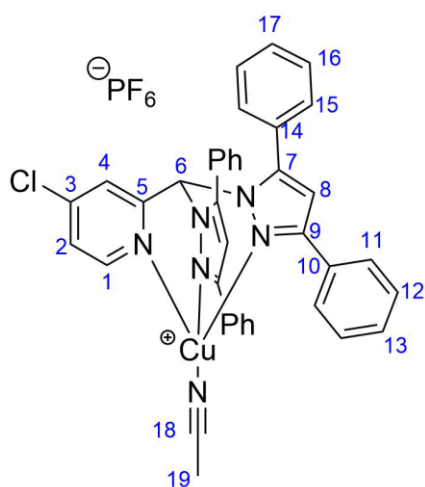
Chemical formula: C₂₆H₂₂CuF₆N₆P. **Molecular mass:** 627.01 gmol⁻¹. **¹H NMR (CD₂Cl₂, 400 MHz):** δ = 8.65 (dq, ³J = 5.0 Hz, ⁴J = 0.9 Hz, 1H, H-1), 8.19 (d, ³J = 2.6 Hz, 2H, H-7), 8.03 (dt, ³J = 7.6 Hz, ⁴J = 0.9 Hz, 1H, H-4), 7.97 (td, ³J = 7.6 Hz, ⁴J = 1.7 Hz, 1H, H-3), 7.94 (s, 1H, H-6), 7.86 (m, 4H, H-11), 7.50 (m, 1H, H-2), 7.44 (m, 6H, H12+13), 6.60 (d, ³J = 2.6 Hz, 2H, H-8), 2.20 (s, 3H, H-15) ppm. **¹H NMR (CDCl₃, 400 MHz):** δ = 8.66 (d, ³J = 5.0 Hz, 1H, H-1), 8.21 (d, ³J =

2.6 Hz, 2H, H-7), 8.03 (d, ³J = 7.8 Hz, 1H, H-4), 8.00 (s, 1H, H-6), 7.81 (m, 5H, H-3+H-11), 7.40 (m, 7H, H-2+H-12+H-13), 6.49 (d, ³J = 2.6 Hz, 2H, H-8), 2.24 (s, 3H, H-15) ppm. **¹³C {¹H} NMR (CDCl₃, 100 MHz):** δ = 153.6 (C-9), 151.4 (C-5), 149.7 (C-1), 139.6 (C-3), 133.6 (C-7), 131.5 (C-10+C-14), 129.3 (C-13), 128.6 (C-12), 127.2 (C-11), 125.7 (C-2), 125.4 (C-4), 105.0 (C-8), 71.9 (C-6), 2.7 (C-15) ppm. **¹⁹F {¹H} NMR (CD₃Cl, 377 MHz):** δ = -71.4 (d, J = 711.6 Hz) ppm. **³¹P {¹H} NMR (CD₃Cl, 162 MHz):** δ = -143.9 (sept, J = 712.0 Hz) ppm. **HRMS (ESI⁺, MeOH):** m/z (found) = 440.09317 (97%), 441.09634 (24%), 442.09128 (42%), 443.09433 (11%), 444.09744 (2%); m/z (calc.) = 440.09364 (100%, ¹²C₂₄¹H₁₉¹⁴N₅⁶³Cu⁺), 441.09700 (26%, ¹²C₂₃¹³C¹H₁₉¹⁴N₅⁶³Cu⁺), 442.09184 (45%, ¹²C₂₄¹H₁₉¹⁴N₅⁶⁵Cu⁺), 443.09519 (12%, ¹²C₂₃¹³C¹H₁₉¹⁴N₅⁶⁵Cu⁺), 444.09854 (1%, ¹²C₂₂¹³C₂¹H₁₉¹⁴N₅⁶³Cu⁺). **IR (ATR, neat), $\tilde{\nu}$ [cm⁻¹]:** 3142 (vw), 3129 (vw), 3065 (vw), 3026 (vw), 2968 (vw), 1599 (w), 1531 (w), 1501 (w), 1478 (vw), 1462 (w), 1445 (w), 1431 (w), 1415 (vw), 1367 (vw), 1353 (vw), 1343 (vw), 1308 (vw), 1285 (vw), 1266 (vw), 1233 (w), 1215 (w), 1182 (vw), 1158 (vw), 1106 (w), 1077 (w), 1055 (w), 1028 (w), 1015 (w), 955 (vw), 904 (vw), 877 (w), 844 (s), 831 (vs), 788 (m), 762 (m), 754 (s), 738 (m), 699 (m), 691 (m), 685 (w), 673 (m), 639 (w), 556 (s), 527 (vw), 513 (w), 411 (w).

6.8.2 Synthesis of [Cu{HC(Ph₂Pz)₂(4-ClPy)}(MeCN)]PF₆ (**C2**)

A solution of HC(Ph₂Pz)₂(4-ClPy) (756.7 mg, 1.34 mmol, 1 equiv.) in DCM (3 mL) was added dropwise to a solution of [Cu(MeCN)₄]PF₆ (500.0 mg, 1.34 mmol, 1 equiv.) in DCM (5 mL). The solution was stirred at room temperature overnight. The complex was crystallized by vapor diffusion of pentane to this solution for a few days. The substance was filtrated, washed with DCM/pentane (1/2, 3x1 mL) and dried *in vacuo* to yield the complex [Cu{HC(Ph₂Pz)₂(4-ClPy)}(MeCN)]PF₆ (1008.0 mg, 1.24 mmol, 92%).

Crystals suitable for single crystal X-ray diffraction were obtained from a concentrated solution of [Cu{HC(Ph₂Pz)₂(4-ClPy)}(MeCN)]PF₆ in DCM, which was layered with *n*-pentane.



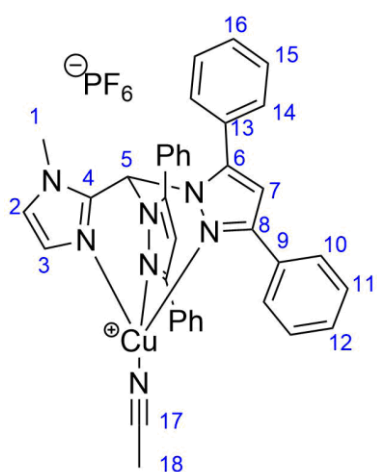
Chemical formula: C₃₈H₂₉ClCuF₆N₆P. **Molecular mass:**

813.65 g mol⁻¹. **¹H NMR (CD₂Cl₂, 400 MHz):** δ = 8.81 (d, ³J = 5.5 Hz, 1H, H-1), 7.90 (m, 4H, H-15), 7.70 (dd, ³J = 5.4 Hz, ⁴J = 1.8 Hz, 1H, H-2), 7.49 (m, 8H, H-12+H-16), 7.43 (s, 1H, H-6), 7.37 (t, ³J = 7.4 Hz, 4H, H-13+H-17; d, 1H, H-4), 7.15 (d, ³J = 7.3 Hz, 4H, H-11), 6.65 (s, 2H, H-8), 2.28 (s, 3H, H-19) ppm. **¹³C {¹H} NMR (CD₂Cl₂, 100 MHz):** δ = 153.8 (C-7), 152.5 (C-5), 152.2 (C-1), 148.1 (C-9), 147.2 (C-3), 131.4 (C-14), 130.3 (C-12), 130.2 (C-13+C-17), 129.3 (C-16), 129.2 (C-11), 127.9 (C-10), 127.8 (C-

15), 127.1 (C-2), 124.4 (C-4), 117.0 (C-18), 106.6 (C-8), 67.1 (C-6), 3.2 (C-19) ppm. **¹⁹F {¹H} NMR (CD₂Cl₂, 377 MHz):** δ = -73.4 (d, J = 710.3 Hz) ppm. **³¹P {¹H} NMR (CD₂Cl₂, 162 MHz):** δ = -144.3 (sept, J = 710.6 Hz) ppm. **HRMS (ESI⁺, MeOH):** m/z (found) = 626.11487 (100%), 627.11823 (37%), 628.11304 (76%), 629.11609 (28%), 630.11060 (12%), 631.11389 (6%), 632.11743 (1%); m/z (calc.) = 626.11727 (100%, ¹²C₃₆¹H₂₆³⁵Cl¹⁴N₆⁶³Cu⁺), 627.12063 (39%, ¹²C₃₅¹³C¹H₂₆³⁵Cl¹⁴N₆⁶³Cu⁺), 628.11581 (85%, ¹²C₃₆¹H₂₆³⁵Cl¹⁴N₆⁶⁵Cu⁺), ¹²C₃₆¹H₂₆³⁷Cl¹⁴N₆⁶³Cu⁺), 629.11836 (33%, ¹²C₃₅¹³C¹H₂₆³⁵Cl¹⁴N₆⁶⁵Cu⁺), ¹²C₃₅¹³C¹H₂₆³⁷Cl¹⁴N₆⁶³Cu⁺), 630.11251 (14%, ¹²C₃₆¹H₂₆³⁷Cl¹⁴N₆⁶⁵Cu⁺), 631.11587 (6%, ¹²C₃₅¹³C¹H₂₆³⁷Cl¹⁴N₆⁶⁵Cu⁺), 632.11922 (1%, ¹²C₃₄¹³C₂¹H₂₆³⁷Cl¹⁴N₆⁶⁵Cu⁺). **IR (ATR, neat), $\tilde{\nu}$ [cm⁻¹]:** 2962 (vw), 1581 (w), 1559 (w), 1483 (w), 1460 (m), 1438 (w), 1408 (w), 1375 (w), 1261 (m), 1218 (w), 1206 (w), 1085 (m), 1029 (m), 964 (w), 925 (vw), 878 (w), 837 (vs), 819 (s), 771 (m), 762 (s), 740 (w), 697 (s), 665 (w), 575 (w), 556 (w), 527 (w), 493 (w).

6.8.3 Synthesis of [Cu{HC(Ph₂Pz)₂Melm}(MeCN)]PF₆ (**C3**)

A solution of HC(Ph₂Pz)₂Melm (714.5 mg, 1.34 mmol, 1 equiv.) in DCM (3 mL) was added dropwise to a solution of [Cu(MeCN)₄]PF₆ (500.0 mg, 1.34 mmol, 1 equiv.) in DCM (5 mL). The solution was stirred at room temperature overnight. The complex was crystallized by vapor diffusion of pentane to this solution for a few days. The substance was filtrated, washed with DCM/pentane (1/2, 3x1 mL) and dried *in vacuo* to yield the complex [Cu{HC(Ph₂Pz)₂Melm}(MeCN)]PF₆ (908.0 mg, 1.16 mmol, 87%).



Chemical formula: C₃₇H₃₁CuF₆N₇P. **Molecular mass:**

782.21 g mol⁻¹. **¹H NMR (CD₂Cl₂, 400 MHz):** δ = 7.88 (dd, ³J = 7.5 Hz, ⁴J = 2.1 Hz, 4H, H-10), 7.57 (s, 1H, H-5), 7.50 (m, 8H, H-11+H-15), 7.38 (t, ³J = 7.3 Hz, 4H, H-12+H-16), 7.24 (d, ³J = 1.2 Hz, 1H, H-3), 7.14 (dd, ³J = 7.3 Hz, ⁴J = 1.2 Hz, 4H, H-14), 7.09 (d, ³J = 1.2 Hz, 1H, H-2), 6.65 (s, 2H, H-7), 3.42 (s, 3H, H-1), 2.15 (s, 3H, H-18) ppm. **¹³C {¹H} NMR (CD₂Cl₂, 100 MHz):** δ = 154.1 (C-8), 146.8 (C-6), 140.7 (C-4), 131.6 (C-13), 131.2 (C-9), 130.3 (C-12+C-16), 129.3 (C-11+C-15), 129.2 (C-3), 129.1 (C-14), 128.0 (C-17), 127.9 (C-10), 123.3 (C-2), 106.8

(C-7), 60.4 (C-5), 34.0 (C-1), 2.8 (C-18) ppm. **¹⁹F {¹H} NMR (CD₂Cl₂, 377 MHz):** δ = -73.3 (d, J = 710.3 Hz) ppm. **³¹P {¹H} NMR (CD₂Cl₂, 162 MHz):** δ = -144.5 (sept, J = 709.7 Hz) ppm.

HRMS (ESI⁺, MeOH): m/z (found) = 595.16638 (97%), 596.16913 (39%), 597.16522 (51%), 598.16736 (18%), 599.17114 (4%), 600.17401 (1%); m/z (calc.) = 595.16714 (100%, ¹²C₃₅¹H₂₈¹⁴N₆⁶³Cu⁺), 596.17050 (38%, ¹²C₃₄¹³C¹H₂₈¹⁴N₆⁶³Cu⁺), 597.16533 (45%, ¹²C₃₅¹H₂₈¹⁴N₆⁶⁵Cu⁺), 598.16869 (17%, ¹²C₃₄¹³C¹H₂₈¹⁴N₆⁶⁵Cu⁺), 599.17204 (3%, ¹²C₃₃¹³C₂¹H₂₈¹⁴N₆⁶⁵Cu⁺), 600.17540 (1%, ¹²C₃₂¹³C₃¹H₂₈¹⁴N₆⁶⁵Cu⁺). **IR (ATR, neat), $\tilde{\nu}$ [cm⁻¹]:** 2953 (vw), 1719 (w), 1611 (m), 1595 (m), 1504 (vw), 1484 (w), 1458 (w), 1437 (w), 1374 (w), 1298 (m), 1274 (m), 1203 (w), 1141 (vw), 1088 (m), 1031 (w), 1007 (vw), 980 (vw), 963 (vw), 878 (m), 836 (vs), 760 (m), 698 (m), 679 (m), 666 (m), 576 (w), 556 (m), 495 (vw).

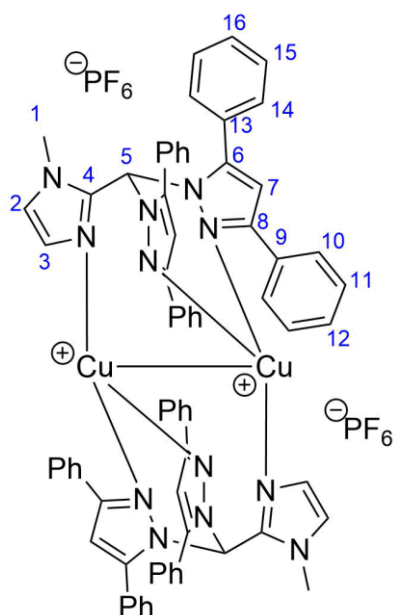
6.8.4 Synthesis of [Cu₂{HC(Ph₂Pz)₂Melm}₂](PF₆)₂ (**C4**)

Approach A:

A solution of [Cu{HC(Ph₂Pz)₂Melm}(MeCN)]PF₆ (72.0 mg, 0.09 mmol) in THF (4 mL) was layered with diethyl ether (2 mL). Overnight, colorless crystals formed, which were suitable for single crystal X-ray diffraction.

Approach B:

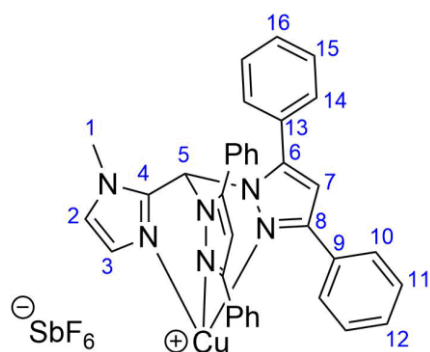
A solution of $[\text{Cu}\{\text{HC}(\text{Ph}_2\text{Pz})_2\text{Melm}\}(\text{MeCN})]\text{PF}_6$ (78.9 mg, 0.10 mmol) in chloroform (5 mL) was layered with hexane (2 mL). Overnight, colorless crystals formed, which were suitable for single crystal X-ray diffraction.



Chemical formula: $\text{C}_{70}\text{H}_{56}\text{Cu}_2\text{F}_{12}\text{N}_{12}\text{P}_2$. **Molecular mass:** $1482.32 \text{ g mol}^{-1}$. **^1H NMR (CD_2Cl_2 , 400 MHz):** $\delta = 7.65$ (d, $^3J = 7.3 \text{ Hz}$, 4H, H-10), 7.56 (t, $^3J = 7.5 \text{ Hz}$, 2H, H-15), 7.46 (t, $^3J = 7.7 \text{ Hz}$, 4H, H-16), 7.39 (s, 1H, H-5), 7.24 (t, $^3J = 7.3 \text{ Hz}$, 2H, H-12), 7.06 (t, $^3J = 7.5 \text{ Hz}$, 4H, H-11), 6.97 (d, $^3J = 7.3 \text{ Hz}$, 4H, H-14), 6.74 (m, 3H, H-7+H-2), 6.28 (s, 1H, H-3), 2.71 (s, 3H, H-1) ppm. **^{13}C $\{^1\text{H}\}$ NMR (CD_2Cl_2 , 100 MHz):** $\delta = 156.3$ (C-8), 148.7 (C-6), 139.8 (C-4), 132.1 (C-15), 131.0 (C-12), 130.5 (C-16), 130.0 (C-9), 129.4 (C-14), 129.0 (C-11), 128.7 (C-3), 127.8 (C-10), 126.8 (C-13), 124.7 (C-2), 107.7 (C-7), 62.7 (C-5), 34.0 (C-1) ppm. **^{19}F $\{^1\text{H}\}$ NMR (CD_2Cl_2 , 377 MHz):** $\delta = -73.0$ (d, $J = 710.8 \text{ Hz}$) ppm. **^{31}P $\{^1\text{H}\}$ NMR (CD_2Cl_2 , 162 MHz):** $\delta = -144.4$ (sept, $J = 711.2 \text{ Hz}$) ppm. **IR (ATR, neat), $\tilde{\nu}$ [cm^{-1}]:** 1559 (w), 1482 (w), 1459 (w), 1442 (w), 1416 (vw), 1375 (vw), 1364 (w), 1299 (m), 1232 (vs), 1201 (s), 1152 (s), 1125 (s), 1075 (m), 1031 (w), 1009 (w), 982 (m), 930 (vw), 876 (w), 862 (m), 831 (vs), 823 (vs), 779 (w), 766 (m), 758 (m), 753 (m), 718 (w), 710 (m), 702 (m), 692 (m), 666 (m), 641 (w), 575 (w), 556 (s), 520 (m), 510 (m).

6.8.5 *In situ* synthesis of $[\text{Cu}\{\text{HC}(\text{Ph}_2\text{Pz})_2\text{Melm}\}]\text{SbF}_6$ (**C5**)

A solution of $\text{HC}(\text{Ph}_2\text{Pz})_2\text{Melm}$ (6.4 mg, $1.2 \times 10^{-5} \text{ mol}$, 1 equiv.) in $\text{DCM-}d_2$ (0.5 mL) was added to a solution of CuCl (1.2 mg, $1.2 \times 10^{-5} \text{ mol}$, 1 equiv.) in $\text{DCM-}d_2$ (1 mL). The solution was stirred for two hours. Then, a solution of AgSbF_6 (4.1 mg, $1.2 \times 10^{-5} \text{ mol}$, 1 equiv) in $\text{DCM-}d_2$ (0.5 mL) was added and the formation of AgCl was observed. The supernatant was analyzed *via* NMR.



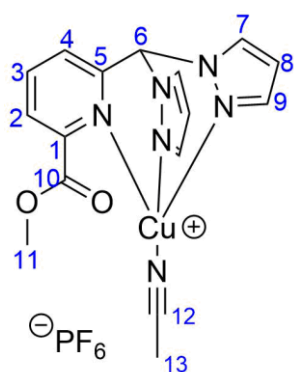
Chemical formula: $\text{C}_{35}\text{H}_{28}\text{CuF}_6\text{N}_6\text{Sb}$. **Molecular mass:** $831.95 \text{ g mol}^{-1}$. **^1H NMR (CD_2Cl_2 , 400 MHz):** $\delta = 7.62$ (d, $^3J = 7.0 \text{ Hz}$, 4H, H-10), 7.57 (t, $^3J = 7.5 \text{ Hz}$, 2H, H-15), 7.46 (t, $^3J = 7.4 \text{ Hz}$, 4H, H-16), 7.39 (s, 1H, H-5), 7.24 (t, $^3J = 7.4 \text{ Hz}$, 2H, H-12), 7.06 (t, $^3J = 7.8 \text{ Hz}$, 4H, H-11), 6.96 (d, $^3J = 7.4 \text{ Hz}$, 4H, H-14), 6.74 (s, 2H, H-7), 6.68 (d, $^3J = 1.3 \text{ Hz}$, 1H, H-2), 6.30 (d, $^3J = 1.3 \text{ Hz}$, 1H, H-3), 2.69 (s,

3H, H-1) ppm. ^{13}C { ^1H } NMR (CD_2Cl_2 , 100 MHz): δ = 156.4 (C-8), 148.8 (C-6), 139.9 (C-4), 132.2 (C-15), 131.0 (C-12), 130.6 (C-16), 130.0 (C-9), 129.4 (C-14), 129.1 (C-10), 128.9 (C-3), 127.9 (C-11), 126.9 (C-13), 124.5 (C-2), 107.8 (C-7), 62.8 (C-5), 34.0 (C-1) ppm.

6.8.6 Synthesis of $[\text{Cu}\{\text{HC}(\text{Pz})_2(6\text{-CO}_2\text{MePy})\}(\text{MeCN})]\text{PF}_6$ (**C9**)

A solution of $\text{HC}(\text{Pz})_2(6\text{-CO}_2\text{MePy})$ (114.0 mg, 0.40 mmol, 1 equiv.) in acetone (5 mL) was added dropwise to a solution of $[\text{Cu}(\text{MeCN})_4]\text{PF}_6$ (150.0 mg, 0.40 mmol, 1 equiv.) in acetone (10 mL). The solution was stirred at room temperature overnight. The complex was crystallized by layering the solution with pentane to this solution for a few days. The substance was filtered, washed with acetone/pentane (1/2, 3x1 mL) and dried *in vacuo* to yield the complex $[\text{Cu}\{\text{HC}(\text{Pz})_2(6\text{-CO}_2\text{MePy})\}(\text{MeCN})]\text{PF}_6$ (172 mg, 0.32 mmol, 80%).

Crystals suitable for single crystal X-ray diffraction were obtained from a concentrated solution of $[\text{Cu}\{\text{HC}(\text{Pz})_2(6\text{-CO}_2\text{MePy})\}(\text{MeCN})]\text{PF}_6$ in DCM, which was layered with *n*-hexane.



Chemical formula: $\text{C}_{16}\text{H}_{16}\text{CuF}_6\text{N}_6\text{O}_2\text{P}$. **Molecular mass:**

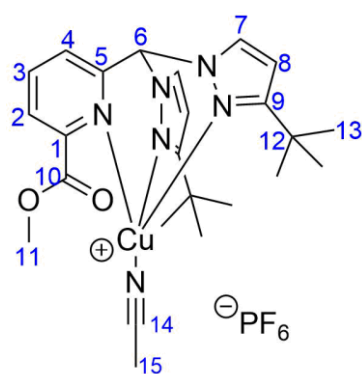
$532.85 \text{ g mol}^{-1}$. ^1H NMR (CD_2Cl_2 , 400 MHz): δ = 8.27 (m, 3H, H-4, H-9), 8.15 (t, 3J = 7.9 Hz, 1H, H-3), 3.08 (s, 1H, H-6), 7.77 (m, 2H, H-7), 7.62 (d, 3J = 7.6 Hz, 1H, H-2), 6.49 (s, 2H, H-8), 4.07 (s, 3H, H-11), 2.25 (s, 3H, H-13) ppm. ^{13}C { ^1H } NMR (CD_2Cl_2 , 100 MHz): δ = 165.9 (C-10), 153.4 (C-5), 147.2 (C-3), 143.4 (C-7), 141.6 (C-1), 134.4 (C-9), 129.0 (C-2), 127.4 (C-4), 117.4 (C-12), 108.0 (C-8), 73.2 (C-6), 54.2 (C-11), 3.0 (C-13) ppm. ^{19}F { ^1H } NMR (CD_2Cl_2 , 377 MHz): δ

= - 72.3 (d, J = 711.7 Hz) ppm. ^{31}P { ^1H } NMR (CD_2Cl_2 , 162 MHz): δ = -144.3 (sept, J = 709.1 Hz) ppm. **HRMS (ESI⁺, MeOH):** m/z (found): 346.03598 (100%), 347.03931 (15%), 348.03406 (43%), 349.03729 (7%); m/z (calc.): 346.03652 (100%, $^{12}\text{C}_{14}^{1}\text{H}_{13}^{63}\text{Cu}^{14}\text{N}_5^{16}\text{O}_2^+$), 347.03988 (15%, $^{12}\text{C}_{13}^{13}\text{C}_1^{1}\text{H}_{13}^{63}\text{Cu}^{14}\text{N}_5^{16}\text{O}_2^+$), 348.03471 (45%, $^{12}\text{C}_{14}^{1}\text{H}_{13}^{65}\text{Cu}^{14}\text{N}_5^{16}\text{O}_2^+$), 349.03807 (7%, $^{12}\text{C}_{13}^{13}\text{C}_1^{1}\text{H}_{13}^{65}\text{Cu}^{14}\text{N}_5^{16}\text{O}_2^+$). **IR (ATR, neat), $\tilde{\nu}$ [cm^{-1}]:** 3140 (vw), 2959 (vw), 2924 (vw), 1710 (w), 1597 (vw), 1518 (vw), 1444 (w), 1403 (w), 1319 (w), 1289 (w), 1256 (vw), 1221 (vw), 1174 (vw), 1144 (vw), 1096 (w), 1057 (vw), 993 (w), 907 (vw), 827 (vs), 759 (s), 740 (w), 723 (w), 705 (w), 642 (w), 632 (w), 608 (vw), 556 (s).

6.8.7 Synthesis of [Cu{HC(^tBuPz)₂(6-CO₂MePy)}(MeCN)]PF₆ (**C10**)

A solution of HC(^tBuPz)₂(6-CO₂MePy) (159.2 mg, 0.40 mmol, 1 equiv.) in acetone (5 mL) was added dropwise to a solution of [Cu(MeCN)₄]PF₆ (150.0 mg, 0.40 mmol, 1 equiv.) in acetone (10 mL). The solution was stirred at room temperature overnight. The complex was crystallized by layering the solution with pentane to this solution for a few days. The substance was filtered, washed with acetone/pentane (1/2, 3x1 mL) and dried *in vacuo* to yield the complex [Cu{HC(^tBuPz)₂(6-CO₂MePy)}(MeCN)]PF₆ (215 mg, 0.33 mmol, 82%).

Crystals suitable for single crystal X-ray diffraction were obtained from a concentrated solution of [Cu{HC(^tBuPz)₂(6-CO₂MePy)}(MeCN)]PF₆ in DCM, which was layered with *n*-hexane.



Chemical formula: C₂₄H₃₂CuF₆N₆O₂P. **Molecular mass:**

645.07 g mol⁻¹. **¹H NMR (CD₂Cl₂, 400 MHz):** δ = 8.16 (m, 2H, H-3, H-4), 8.01 (d, ³J = 2.6 Hz, 2H, H-7), 7.91 (d, ³J = 7.3 Hz, 1H, H-2), 7.85 (s, 1H, H-6), 6.27 (d, ³J = 2.6 Hz, 2H, H-8), 4.03 (s, 3H, H-11), 2.31 (s, 3H, H-15), 1.39 (s, 18H, H-13) ppm. **¹³C {¹H} NMR (CD₂Cl₂, 100 MHz):** δ = 165.5 (C-10), 165.2 (C-9), 153.4 (C-5), 147.9 (C-3), 141.4 (C-1), 133.5 (C-7), 128.8 (C-2), 127.0 (C-4), 117.1 (C-14), 104.6 (C-8), 73.2 (C-6), 54.2 (C-11), 32.7

(C-12), 30.5 (C-13), 3.1 (C-15) ppm. **¹⁹F {¹H} NMR (CD₂Cl₂, 377 MHz):** δ = -71.9 (d, J = 711.0 Hz) ppm. **³¹P {¹H} NMR (CD₂Cl₂, 162 MHz):** δ = -144.2 (sept, J = 711.2 Hz) ppm. **HRMS (ESI⁺, MeOH):** m/z (found): 458.16077 (100%), 459.16364 (24%), 460.15900 (48%), 461.16190 (10%), 462.16489 (1%); m/z (calc.): 458.16172 (100%, ¹²C₂₂¹H₂₉⁶³Cu¹⁴N₅¹⁶O₂⁺), 459.16508 (24%, ¹²C₂₁¹³C₁¹H₂₉⁶³Cu¹⁴N₅¹⁶O₂⁺), 460.15991 (45%, ¹²C₂₂¹H₂₉⁶⁵Cu¹⁴N₅¹⁶O₂⁺), 461.16327 (11%, ¹²C₂₁¹³C₁¹H₂₉⁶⁵Cu¹⁴N₅¹⁶O₂⁺), 462.16662 (1%, ¹²C₂₀¹³C₂¹H₂₉⁶⁵Cu¹⁴N₅¹⁶O₂⁺). **IR (ATR, neat), $\tilde{\nu}$ [cm⁻¹]:** 2958 (w), 2931 (vw), 2902 (w), 2867 (vw), 1751 (w), 1722 (m), 1701 (w), 1590 (w), 1577 (w), 1519 (m), 1459 (w), 1437 (w), 1397 (vw), 1362 (w), 1309 (m), 1263 (w), 1248 (m), 1225 (w), 1161 (w), 1137 (m), 1091 (w), 1056 (m), 996 (w), 982 (w), 914 (w), 820 (w), 804 (m), 781 (w), 755 (vs), 695 (w), 643 (w).

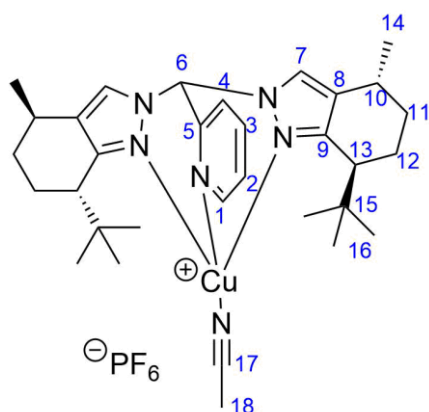
6.8.8 Synthesis of [Cu{HC(PuIPz)₂Py}(MeCN)]PF₆ (**C11**)

A solution of HC(PuIPz)₂Pz (380 mg, 0.80 mmol, 1 equiv.) in acetone (20 mL) was added dropwise over 25 min to a solution of [Cu(MeCN)₄]PF₆ (300 mg, 0.80 mmol, 1 equiv.) in acetone (20 mL). The solution was stirred for 72 h at room temperature. The solution was concentrated under reduced pressure, to approximately the half volume and layered with hexane (50 mL).

Overnight greenish crystalline precipitate forms, which was collected by filtration and washed with hexane to yield $[\text{Cu}\{\text{HC}(\text{PulPz})_2\text{Py}\}(\text{MeCN})]\text{PF}_6$ (497 mg, 0.69 mmol, 86%).

The crystals obtained from this synthesis were suitable for X-ray diffraction.

A low concentration and a slow addition of the ligand solution is necessary to avoid the formation of a $[\text{Cu}_2\text{L}_2](\text{PF}_6)_2$ coordination motif.



Chemical formula: $\text{C}_{32}\text{H}_{46}\text{CuF}_6\text{N}_6\text{P}$. **Molecular mass:**

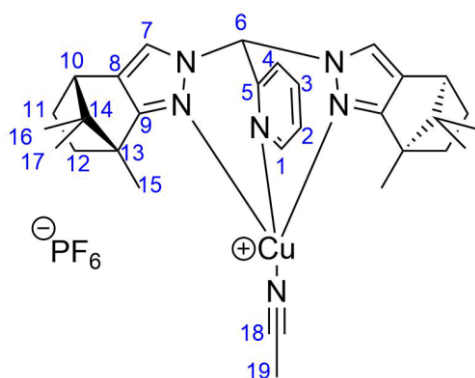
723.27 g mol^{-1} . **$^1\text{H-NMR}$ (CD_2Cl_2 , 400 MHz):** δ = 8.56 (d, 3J = 4.8 Hz, 1H, H-1), 7.94 (m, 2H, H-3, H-4), 7.61 (d, 3J = 6.8 Hz, 2H, H-7), 7.49 (m, 2H, H-2, H-6), 2.66 (t, 3J = 8.0 Hz, 2H, H-13), 2.50 (m, 2H, H-10), 2.34 (s, 3H, H-18), 1.90 (m, 2H, H-12), 1.84 (m, 2H, H-11), 1.67 (m, 2H, H-12), 1.08 (2xs, 6H, H-14), 0.96 (m, 2H, H-11), 0.82 (2xs, 18H, H-16) ppm. **$^{13}\text{C}\{^1\text{H}\}\text{-NMR}$ (CD_2Cl_2 , 100 MHz):** δ = 154.6 (C-5), 153.5 (C-8), 152.6 (C-17), 149.3 (C-1), 139.9 (C-3),

128.5 (d, C-7), 126.9 (d, C-9), 125.8 (C-2), 125.4 (C-4), 73.0 (d, C-6), 43.1 (d, C-13), 36.3 (d, C-15), 32.9 (d, C-11), 28.6 (d, C-16), 27.9 (d, C-10), 25.0 (d, C-12), 21.3 (d, C-14), 3.4 (C-18) ppm. *Note: The doublets are due to the asymmetry of the pyrazolyl units, therefore no J couplings are given.* **$^{19}\text{F}\{^1\text{H}\}\text{NMR}$ (CD_2Cl_2 , 377 MHz):** δ = -73.1 (d, J = 711 Hz) ppm. **$^{31}\text{P}\{^1\text{H}\}\text{NMR}$ (CD_2Cl_2 , 162 MHz):** δ = 144.1 (sept, J = 715 Hz) ppm. **HRMS (ESI⁺, MeOH):** m/z (found): 536.2807 (100%), 537.2838 (35%), 538.2830 (44%), 539.2821 (14%); m/z (calc.): 536.2814 (100%, $^{12}\text{C}_{30}^{1}\text{H}_{43}^{63}\text{Cu}_1^{14}\text{N}_5^+$), 537.2848 (32%, $^{12}\text{C}_{29}^{13}\text{C}_1^1\text{H}_{43}^{63}\text{Cu}_1^{14}\text{N}_5^+$), 538.2796 (44%, $^{12}\text{C}_{30}^1\text{H}_{43}^{65}\text{Cu}_1^{14}\text{N}_5^+$), 539.2830 (14%, $^{12}\text{C}_{29}^{13}\text{C}_1^1\text{H}_{43}^{65}\text{Cu}_1^{14}\text{N}_5^+$). **IR (ATR, neat), $\tilde{\nu}$ [cm^{-1}]:** 2969 (w), 2873 (vw), 1704 (vw), 1600 (w), 1479 (w), 1450 (w), 1429 (w), 1396 (w), 1366 (w), 1310 (w), 1300 (vw), 1282 (vw), 1217 (w), 1165 (w), 1150 (w), 1089 (vw), 1036 (vw), 1016 (w), 997 (w), 907 (vw), 879 (w), 867 (w), 834 (vs), 780 (w), 767 (m), 761 (w), 738 (w), 729 (vw), 721 (w), 682 (w), 664 (w), 637 (w), 556 (s).

6.8.9 Synthesis of $[\text{Cu}\{\text{HC}(\text{CamPz})_2\text{Py}\}(\text{MeCN})]\text{PF}_6$ (**C12**)

A solution of $\text{HC}(\text{CamPz})_2\text{Py}$ (22.1 mg, 0.05 mmol, 1 equiv.) in THF (2 mL) was added slowly dropwise to a solution of $[\text{Cu}(\text{MeCN})_4]\text{PF}_6$ (18.6 mg, 0.05 mmol, 1 equiv.) in THF (2 mL). The solution was stirred for 10 min. Diethyl ether (15 mL) was added and a precipitate forms, which was collected by filtration and washed with diethyl ether to yield $[\text{Cu}\{\text{HC}(\text{CamPz})_2\text{Py}\}(\text{MeCN})]\text{PF}_6$ (29.7 mg, 0.04 mmol, 80%).

A low concentration and a very slow addition of the ligand solution is necessary to avoid the formation of a $[\text{Cu}_2\text{L}_2](\text{PF}_6)_2$ coordination motif. The formation of the title compound is implicated by a pale yellowish color of the solution and precipitate, while the formation of a $[\text{Cu}_2\text{L}_2](\text{PF}_6)_2$ coordination motif is implicated by an intense yellow color of the solution and the precipitate. Trials to scale up the reaction were not successful. When the title compound is solved the formation of a $[\text{Cu}_2\text{L}_2](\text{PF}_6)_2$ coordination motif can be observed, which can be reversed by the dropwise addition of about 10-20 equiv. of acetonitrile to the solution. The addition of too much acetonitrile leads to the formation of $[\text{Cu}(\text{MeCN})_4]\text{PF}_6$, this is implicated by a complete loss in color of the solution.



Chemical formula: $\text{C}_{30}\text{H}_{38}\text{CuF}_6\text{N}_6\text{P}$. **Molecular**

mass: $691.19 \text{ g mol}^{-1}$. **$^1\text{H-NMR}$ (CD_2Cl_2 , 400 MHz):** δ = 8.61 (d, 3J = 4.8 Hz, 1H, H-1), 7.89 (td, 3J = 7.8 Hz, 4J = 1.6 Hz, 1H, H-3), 7.82 (d, 3J = 7.8 Hz, 1H, H-4), 7.44 (m, 3H, H2+H-7), 7.36 (s, 1H, H-6), 2.75 (t, 3J = 4.3 Hz, 2H, H-10), 2.01 (m, 5H, H-11+H-19), 1.82 (m, 2H, H-12), 1.30 (2xs, 6H, H-15), 1.21-1.00 (m, 4H, H-11+H-12), 0.91 (2xs, 6H, H-16/17), 0.48 (2xs, 6H, H-

16/17) ppm. **$^{13}\text{C}\{^1\text{H}\}\text{-NMR}$ (CD_2Cl_2 , 100 MHz):** δ = 167.2 (d, C-9), 152.1 (C-5), 148.2 (C-1), 138.3 (C-3), 126.6 (d, C-8), 124.0 (C-2), 123.6 (C-4), 122.9 (d, C-7), 115.6 (C-18), 71.2 (C-6), 59.9 (C-13), 50.0 (C-14), 46.3 (C-10), 32.3 (d, C-12), 26.3 (d, C-11), 19.1 (d, C-16/17), 17.7 (d, C-16/17), 9.3 (d, C-15), 0.9 (C-19) ppm. *Note: The doublets are due to the asymmetry of the pyrazolyl units, therefore no J couplings are given.* **$^{19}\text{F}\{^1\text{H}\}\text{ NMR}$ (CD_2Cl_2 , 377 MHz):** δ = 72.1 (d, J = 711 Hz) ppm. **$^{31}\text{P}\{^1\text{H}\}\text{ NMR}$ (CD_2Cl_2 , 162 MHz):** δ = -144.1 (sept, J = 711 Hz) ppm. *Note: As above mentioned the NMR spectras have to be recorded in the present of acetonitrile.*

HRMS (ESI⁺, MeOH): m/z (found): 545.24506 (100%), 546.24791 (37%), 547.24364 (52%), 548.24629 (17%), 549.24915 (3%); m/z (calc.): 545.24539 (100%, $^{12}\text{C}_{30}^{1}\text{H}_{38}^{63}\text{Cu}_1^{14}\text{N}_6^+$), 546.24875 (32%, $^{13}\text{C}_1^{12}\text{C}_{29}^1\text{H}_{38}^{63}\text{Cu}_1^{14}\text{N}_6^+$), 547.24358 (45%, $^{12}\text{C}_{30}^1\text{H}_{38}^{65}\text{Cu}_1^{14}\text{N}_6^+$), 548.24694 (14%, $^{13}\text{C}_1^{12}\text{C}_{29}^1\text{H}_{38}^{65}\text{Cu}_1^{14}\text{N}_6^+$), 549.25029 (2%, $^{13}\text{C}_2^{12}\text{C}_{28}^1\text{H}_{38}^{65}\text{Cu}_1^{14}\text{N}_6^+$). **IR (ATR, neat), $\tilde{\nu}$ [cm^{-1}]:** 3127 (vw), 2965 (w), 2872 (vw), 1599 (w), 1392 (w), 1343 (vw), 1278 (w), 1241 (vw), 1179 (vw), 1141 (w), 1088 (vw), 1008 (w), 981 (vw), 878 (w), 838 (vs), 786 (w), 770 (w), 740 (w), 691 (w), 674 (w), 630 (vw), 613 (vw), 603 (vw), 557 (s).

6.8.10 Synthesis of $[\text{Cu}_2\{\text{HC}(\text{CamPz})_2\text{Py}\}_2(\text{PF}_6)_2$ (**C13**)

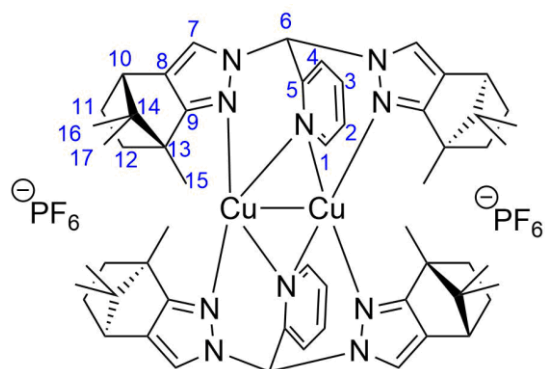
A solution of $\text{HC}(\text{CamPz})_2\text{Py}$ (22.1 mg, 0.05 mmol, 1 equiv.) in acetone (0.5 mL) was added to a solution of $[\text{Cu}(\text{MeCN})_4]\text{PF}_6$ (18.6 mg, 0.05 mmol, 1 equiv.) in acetone (0.5 mL). The

solution was stirred overnight. Hexane (4 mL) was added and a precipitate forms, which was collected by filtration and washed with hexane to yield $[\text{Cu}_2\{\text{HC}(\text{CamPz})_2\text{Py}\}_2](\text{PF}_6)_2$ (26.3 mg, 0.02 mmol, 80%).

The reaction can also be performed with DCM and THF as solvent.

Crystals suitable for single crystal X-ray diffraction were obtained from a concentrated solution of $[\text{Cu}_2\{\text{HC}(\text{CamPz})_2\text{Py}\}_2](\text{PF}_6)_2$ in DCM, which was layered with *n*-hexane.

A high concentration is beneficial to avoid the formation of a $[\text{CuL}(\text{MeCN})]\text{PF}_6$ coordination motif, which may occur as a side product.



Chemical formula: $\text{C}_{56}\text{H}_{70}\text{Cu}_2\text{F}_{12}\text{N}_{10}\text{P}_2$. **Molecular**

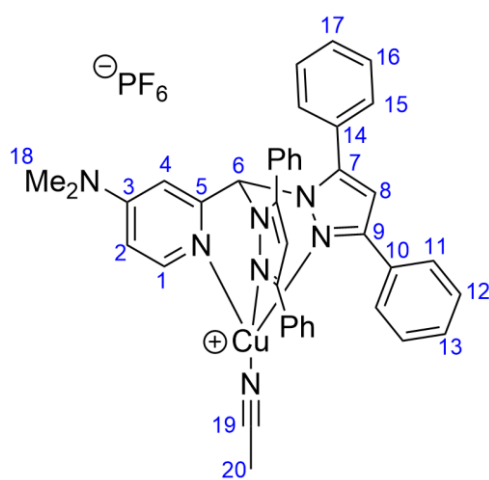
mass: $1300.27 \text{ g mol}^{-1}$. **$^1\text{H-NMR}$ (CD_2Cl_2 , 400 MHz):** $\delta = 8.22$ (d, $^3J = 7.6 \text{ Hz}$, 2H, H-1), 8.14 (td, $^3J = 8.1 \text{ Hz}$, $^4J = 1.5 \text{ Hz}$, 2H, H-2), 8.07 (s, 2H, H-6), 8.01 (s, 2H, H-7), 7.95 (s, 2H, H-7), 7.65 (dd, $^3J = 5.1 \text{ Hz}$, $^4J = 1.5 \text{ Hz}$, 2H, H-4), 7.42 (t, $^3J = 6.2 \text{ Hz}$, 2H, H-3), 2.92 (m, 4H, H-10), 2.09 (m, 4H, H-11), 1.73 (m, 4H, H-12), 1.20 (m, 4H, H-11),

1.03 (m, 4H, H-12), 0.87 (s, 6H, H-16/17), 0.85 (s, 6H, H-16/17), 0.62 (s, 6H, H-16/17), 0.55 (s, 6H, H-15), 0.53 (s, 6H, H-15), 0.50 (s, 6H, H-16/17) ppm. **$^{13}\text{C}\{^1\text{H}\}\text{-NMR}$ (CD_2Cl_2 , 100 MHz):** $\delta = 171.3$ (C-9), 170.2 (C-9), 151.4 (C-5), 150.6 (C-4), 142.0 (C-2), 129.8 (d, C-8), 129.1 (C-1), 128.1 (d, C-7), 126.9 (C-3), 73.0 (C-6), 62.7 (C-14), 61.4 (C-14), 51.9 (d, C-13), 47.6 (d, C-10), 34.0 (d, C-12), 27.3 (d, C-11), 20.9 (d, C-16/17), 18.9 (d, C-16/17), 10.9 (d, C-15) ppm. *Note: The doublets are due to the asymmetry of the pyrazolyl units, therefore no J couplings are given.* **$^{19}\text{F}\{^1\text{H}\}\text{NMR}$ (CD_2Cl_2 , 377 MHz):** $\delta = -71.3$ (d, $J = 711 \text{ Hz}$) ppm. **$^{31}\text{P}\{^1\text{H}\}\text{NMR}$ (CD_2Cl_2 , 162 MHz):** $\delta = -143.9$ (sept, $J = 711 \text{ Hz}$) ppm. **HRMS (ESI⁺, MeOH):** m/z (found): 1153.40076 (98%), 1154.40427 (60%), 1155.40034 (100%), 1156.40307 (55%), 1157.40151 (30%), 1158.40221 (13%), 1159.40505 (4%); m/z (calc.): 1153.40187 (100%, $^{12}\text{C}_{56}^{1}\text{H}_{70}^{63}\text{Cu}_2^{14}\text{N}_{10}^{31}\text{P}_1^{19}\text{F}_6^+$), 1154.40522 (61%, $^{13}\text{C}_1^{12}\text{C}_{55}^1\text{H}_{70}^{63}\text{Cu}_2^{14}\text{N}_{10}^{31}\text{P}_1^{19}\text{F}_6^+$), 1155.40006 (89%, $^{12}\text{C}_{56}^1\text{H}_{70}^{65}\text{Cu}_1^{63}\text{Cu}_1^{14}\text{N}_{10}^{31}\text{P}_1^{19}\text{F}_6^+$), 1156.40341 (54%, $^{13}\text{C}_1^{12}\text{C}_{55}^1\text{H}_{70}^{65}\text{Cu}_1^{63}\text{Cu}_1^{14}\text{N}_{10}^{31}\text{P}_1^{19}\text{F}_6^+$), 1157.40110 (27%, $^{12}\text{C}_{56}^1\text{H}_{70}^{65}\text{Cu}_2^{14}\text{N}_{10}^{31}\text{P}_1^{19}\text{F}_6^+$, $^{13}\text{C}_2^{12}\text{C}_{54}^1\text{H}_{70}^{65}\text{Cu}_1^{63}\text{Cu}_1^{14}\text{N}_{10}^{31}\text{P}_1^{19}\text{F}_6^+$), 1158.40161 (12%, $^{13}\text{C}_1^{12}\text{C}_{55}^1\text{H}_{70}^{65}\text{Cu}_2^{14}\text{N}_{10}^{31}\text{P}_1^{19}\text{F}_6^+$), 1159.40496 (4%, $^{13}\text{C}_2^{12}\text{C}_{54}^1\text{H}_{70}^{65}\text{Cu}_2^{14}\text{N}_{10}^{31}\text{P}_1^{19}\text{F}_6^+$), 1160.40831 (1%, $^{13}\text{C}_3^{12}\text{C}_{53}^1\text{H}_{70}^{65}\text{Cu}_2^{14}\text{N}_{10}^{31}\text{P}_1^{19}\text{F}_6^+$). **IR (ATR, neat), $\tilde{\nu}$ [cm^{-1}]:** 3127 (vw), 2962 (w), 2918 (vw), 2872 (vw), 1598 (w), 1392 (w), 1343 (w), 1276 (w), 1267 (w), 1242 (vw), 1210 (w), 1176 (w), 1140 (w), 1007 (w), 984 (vw), 835 (vs), 786 (w), 772 (m), 739 (w), 691 (w), 674 (w), 631 (w), 615 (vw), 604 (vw), 556 (s).

6.8.11 Synthesis of [Cu{HC(Ph₂Pz)₂DMAP}(MeCN)]PF₆ (**C19**)

A solution of HC(Ph₂Pz)₂DMAP (57.2 mg, 0.10 mmol, 1 equiv.) in DCM (1 mL) was added dropwise to a solution of [Cu(MeCN)₄]PF₆ (37.2 mg, 0.10 mmol, 1 equiv.) in DCM (1 mL). The solution was stirred at room temperature overnight. The complex was crystallized by layering the solution with hexane. The substance was filtrated, washed with DCM/hexane (1/2, 3x1 mL) and dried *in vacuo* to yield the complex [Cu{HC(Ph₂Pz)₂DMAP}(MeCN)]PF₆ (71.9 mg, 0.874 mmol, 87%).

Crystals suitable for single crystal X-ray diffraction were obtained from a concentrated solution of [Cu{HC(Ph₂Pz)₂DMAP}(MeCN)]PF₆ in DCM, which was layered with *n*-hexane.



Chemical formula: C₄₀H₃₅CuF₆N₇P. **Molecular mass:** 822.28 g mol⁻¹. **¹H NMR (CD₂Cl₂, 400 MHz):** δ

= 8.27 (d, ³J = 6.2 Hz, 1H, H-1), 7.93 (m, 4H, H-11), 7.48 (m, 8H, H-12+H-16), 7.34 (t, ³J = 7.5 Hz, 4H, H-13+H-17), 7.24 (s, 1H, H-6), 7.18 (dd, ³J = 8.4 Hz, ⁴J = 1.1 Hz, 4H, H-15), 6.63 (m, 3H, H-2+H-8), 6.30 (d, ³J = 2.4 Hz, 1H, H-4), 3.06 (s, 6H, H-18), 2.22 (s, 3H, H-20) ppm. **¹³C {¹H} NMR (CD₂Cl₂, 100 MHz):** δ = 156.0 (C-3), 153.1 (C-9), 151.5 (C-1), 150.3 (C-5), 146.8 (C-7), 131.8 (C-10), 130.8 (C-14), 130.0 (C-17), 129.8 (C-

16), 129.4 (C-15), 129.1 (C-12), 128.4 (C-13), 127.7 (C-11), 116.4 (C-19), 107.4 (C-2), 106.1 (C-8), 105.8 (C-4), 68.4 (C-6), 39.8 (C-18), 2.9 (C-20) ppm. *Note: The signal of C-19 is only observable using HMBC.* **¹⁹F {¹H} NMR (CD₂Cl₂, 377 MHz):** δ = -73.4 (d, J = 710 Hz) ppm. **³¹P {¹H} NMR (CD₂Cl₂, 162 MHz):** δ = -144.8 (sept, J = 710 Hz) ppm. **HRMS (ESI⁺, MeOH):** m/z (found): 635.19623 (100%), 636.19910 (41%), 637.19513 (47%), 638.19739 (19%), 639.20105 (4%); m/z (calc.): 635.19844 (100%, ¹²C₃₈¹H₃₂¹⁴N₆⁶³Cu⁺), 636.20180 (41%, ¹²C₃₇¹³C₁¹H₃₂¹⁴N₆⁶⁵Cu⁺), 637.19663 (45%, ¹²C₃₈¹H₃₂¹⁴N₆⁶³Cu⁺), 638.19999 (18%, ¹²C₃₇¹³C₁¹H₃₂¹⁴N₆⁶⁵Cu⁺), 639.20334 (4%, ¹²C₃₆¹³C₂¹H₃₂¹⁴N₆⁶⁵Cu⁺). **IR (ATR, neat), $\tilde{\nu}$ [cm⁻¹]:** 3062 (vw), 2923 (vw), 1612 (m), 1554 (w), 1541 (w), 1527 (w), 1483 (w), 1460 (m), 1442 (w), 1415 (w), 1390 (w), 1340 (vw), 1323 (vw), 1299 (vw), 1278 (w), 1265 (w), 1230 (vw), 1197 (w), 1168 (vw), 1127 (vw), 1087 (vw), 1075 (vw), 1020 (w), 1012 (w), 980 (vw), 965 (vw), 922 (vw), 899 (w), 875 (w), 851 (m), 834 (vs), 808 (s), 779 (m), 758 (s), 738 (m), 708 (m), 697 (m), 671 (m), 627 (vw), 616 (vw), 572 (w), 556 (s), 507 (w), 487 (w), 430 (w), 421 (w).

6.8.12 Synthesis approach of $[\text{Cu}\{\text{C}(\text{tBuPz})_2\text{Py}\}]$

Approach A:

A solution of $\text{HC}(\text{tBuPz})_2\text{Py}$ (67.4 mg, 0.2 mmol, 1 equiv.) in THF (1 mL) was added dropwise to a solution of $[\text{Cu}(\text{MeCN})_4]\text{OTf}$ (75.4 mg, 0.2 mmol, 1 equiv.) in THF (1 mL) and stirred at room temperature for 1 h. The solution was cooled to $-20\text{ }^\circ\text{C}$ and NaNTMS_2 (2 M in THF, 0.1 mL, 0.2 mmol, 1 equiv.) was added dropwise and the solution was stirred for 1 h at this temperature and then warmed slowly to room temperature. All volatiles were removed under reduced pressure.

The title compound could not be observed in the ^1H NMR spectra, the formation of $[\text{Cu}\{\text{HC}(\text{tBuPz})_2\text{Py}\}(\text{NTMS}_2)]$ is indicated.

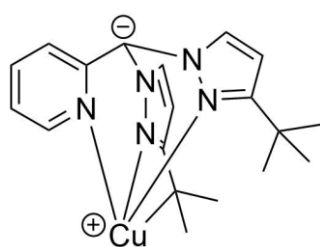
Approach B:

NaNTMS_2 (2 M in THF, 0.13 mL, 0.26 mmol 1.3 equiv.) is added dropwise to a solution of $\text{HC}(\text{tBuPz})_2\text{Py}$ (67.4 mg, 0.2 mmol, 1 equiv.) in THF (1 mL) at room temperature and stirred for 30 min. This solution is added dropwise to a suspension of CuCl (19.8 mg, 0.2 mmol, 1 equiv.) in THF (1 mL). The solution is stirred for 30 min. All volatiles were removed under reduced pressure.

The title compound could not be observed in the ^1H NMR spectra, the formation of $[\text{Cu}\{\text{HC}(\text{tBuPz})_2\text{Py}\}(\text{NTMS}_2)]$ is indicated.

Approach C:

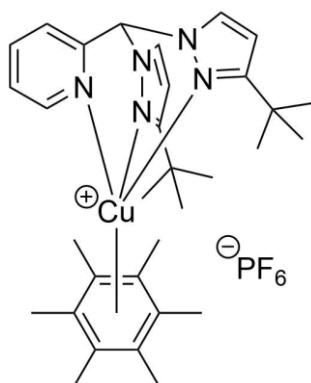
n-Butyllithium (2.5 M in hexane, 0.1 mL, 0.25 mmol 1 equiv.) is added dropwise to a solution of $\text{HC}(\text{tBuPz})_2\text{Py}$ (84.4 mg, 0.25 mmol, 1 equiv.) in THF (2.5 mL) at room temperature and stirred for 30 min. All volatiles were removed under reduced pressure. The residue is washed with hexane and solved in toluene. This solution is added to CuCl (24.8 mg, 0.25 mmol, 1 equiv.). The solution is stirred overnight. All volatiles were removed under reduced pressure.



The reaction was also performed using THF for the complexation of copper(I) chloride. The title compound could not be observed in the ^1H NMR spectra, a disproportionation is indicated.

6.8.13 Synthesis approach of $[\text{Cu}\{\text{HC}(\text{tBuPz})_2\text{Py}\}(\text{C}_6\text{Me}_6)]\text{PF}_6$

A solution of $\text{HC}(\text{tBuPz})_2\text{Py}$ (16.9 mg, 0.05 mmol, 1 equiv.) in DCM (0.5 mL) was added dropwise to a solution of $[\text{Cu}(\text{Me}_6\text{C}_6)_2]\text{PF}_6$ (26.7 mg, 0.05 mmol, 1 equiv.) in DCM (0.5 mL). The solution was stirred at room temperature overnight. Hexane (4 mL) was added. And the precipitate was filtered and washed with hexane. All volatiles were removed under reduced pressure.



The protocol was also used with $\text{HC}(\text{tBuPz})_2\text{Melm}$ as starting material and THF as solvent. The title compound could not be observed using ^1H NMR, a $[\text{Cu}_2\text{L}_2](\text{PF}_6)_2$ coordination motif is indicated.

6.9 Nitrene analytic

6.9.1 Nitrene formation test

The nitrene precursor complex (2.63×10^{-5} mol, 1 equiv.) was dissolved in DCM (7.0 mL) at -80 °C. A solution of nitrene generating agent (2.63×10^{-5} mol, 1 equiv.) in DCM (0.75 mL) was added. The reaction was monitored using UV/Vis spectroscopy. When no reaction occurred at low temperatures, the temperature was increased stepwise to room temperature.

For some reaction with organic azides the concentration was doubled.

In some cases, the precursor complex is formed *in situ*. Therefore, the ligand and $[\text{Cu}(\text{MeCN})_4]\text{PF}_6$ were stirred in DCM for 24 h to yield a $[\text{CuL}(\text{MeCN})]\text{PF}_6$ complex. To yield $[\text{CuL}]\text{SbF}_6$ complexes the ligand (1.5 equiv.) and copper(I) chloride (1.5 equiv.) were stirred in DCM overnight and AgSbF_6 (1.5 equiv.) is added and a precipitate is formed. The supernatant was then diluted and applied to the standard procedure.

Table 33. Overview of nitrene formation tests.

	$^s\text{PhINTs}$	MesN_3	$\text{Ph}(\text{CF}_3)_2\text{N}_3$	AdN_3	PhCON_3	$\text{H}_2\text{NTs} + ^t\text{Bu}_2\text{O}_2$	PhNNPh	Carbamate
$[\text{Cu}\{\text{HC}(\text{Ph}_2\text{Pz})_2\text{Py}\}(\text{MeCN})]\text{PF}_6$	+		-			-	~	~
$[\text{Cu}\{\text{HC}(\text{Et}_2\text{Pz})_2\text{Py}\}(\text{MeCN})]\text{PF}_6^a$	(+)							
$[\text{Cu}\{\text{HC}(\text{PhPz})_2\text{Py}\}(\text{MeCN})]\text{PF}_6$	+							
$[\text{Cu}\{\text{HC}(\text{PhPz})_2\text{Qu}\}(\text{MeCN})]\text{PF}_6^a$	~							
$[\text{Cu}\{\text{HC}(\text{Ph}_2\text{Pz})_2\text{Melm}\}(\text{MeCN})]\text{PF}_6$	+							
$[\text{Cu}_2\{\text{HC}(\text{Ph}_2\text{Pz})_2\text{Melm}\}_2](\text{PF}_6)_2$	-							
$[\text{Cu}\{\text{HC}(\text{Ph}_2\text{Pz})_2\text{Melm}\}]\text{SbF}_6^a$			~					
$[\text{Cu}\{\text{HC}(\text{Ph}_2\text{Pz})_2(4\text{-ClPy})\}(\text{MeCN})]\text{PF}_6$	+							
$[\text{Cu}\{\text{HC}(^t\text{BuPz})_2\text{Py}\}(\text{MeCN})]\text{PF}_6$	$^{+b}$	-	-		-			
$[\text{Cu}\{\text{HC}(^t\text{BuPz})_2\text{Py}\}]\text{SbF}_6^a$			~					
$[\text{Cu}\{\text{HC}(^t\text{BuPz})_2\text{Melm}\}(\text{MeCN})]\text{PF}_6$	$^{+b}$	-	-		(+)			
$[\text{Cu}\{\text{HC}(^t\text{BuPz})_2\text{Melm}\}]\text{SbF}_6^a$		\sim^d	\sim^d	\sim^d	(+)			
$[\text{Cu}\{\text{HC}(^t\text{BuPz})_2(\text{CO}_2\text{MePy})\}(\text{MeCN})]\text{PF}_6$	~							
$[\text{Cu}\{\text{HC}(\text{PuIPz})_2\text{Py}\}(\text{MeCN})]\text{PF}_6$	+							

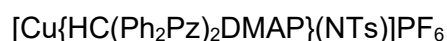
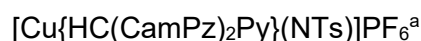
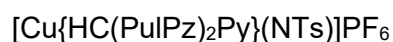
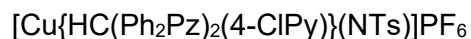
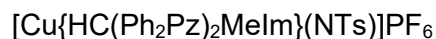
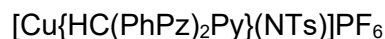
$[\text{Cu}\{\text{HC}(\text{CamPz})_2\text{Py}\}(\text{MeCN})]\text{PF}_6^{\text{c}}$	+		
$[\text{Cu}_2\{\text{HC}(\text{CamPz})_2\text{Py}\}_2](\text{PF}_6)_2$	-		
$[\text{Cu}\{\text{HC}(\text{Ph}_2\text{Pz})_2\text{DMAP}\}(\text{MeCN})]\text{PF}_6$	+	(+)	
$[\text{Fe}\{\text{MeCPy}_2\text{Bpy}\}(\text{MeCN})_2]\text{OTf}_2$	~	~	~

^a complex is formed *in situ*. ^b according to literature^[102]. ^c complex is formed *in situ* from $[\text{Cu}_2\{\text{HC}(\text{CamPz})_2\text{Py}\}_2](\text{PF}_6)_2$ by the addition of 10 equiv. of MeCN; ^d reaction was also performed with the doubled concentration. + : stable nitrene formation observed; (+) : instable nitrene formation observed; - : no reaction observed; ~ : reaction observed.

6.9.2 Titration against ^sPhINTs

The nitrene precursor complex (2.63×10^{-5} mol, 1 equiv.) was dissolved in DCM (7.0 mL) at -80 °C and titrated with ^sPhINTs (0.2 equiv. steps in 0.15 mL DCM up to 1.3 equiv.). After each addition of ^sPhINTs, the maximal UV/Vis absorption is awaited.

Analyzed nitrene complexes:



^a titration performed at -60 °C, pre cursor complex **C12** formed *in situ* from **C13** by the addition of 10 equiv. of MeCN

6.9.3 Nitrene yield determination

The nitrene precursor complex (2.63×10^{-5} mol, 1 equiv.) was dissolved in DCM (7.0 mL) at -80 °C. A solution of ^sPhINTs (13.0 mg, 2.63×10^{-5} mol, 1 equiv.) in DCM (0.75 mL) was added. The maximal UV/Vis absorption was awaited. Ferrocene (146.5 mg, 7.89×10^{-4} mol, 30 equiv.) dissolved in DCM (1.0 mL) was added. The maximal UV/Vis absorption for the ferrocenium band at 624 nm was awaited. The extinction coefficient of ferrocenium ($\epsilon_{624} =$

507 L^{*}mol⁻¹*cm⁻¹) allowed the calculation of the concentration of ferrocenium from Lambert-Beer's law. This corresponds to the concentration of formed nitrene.

Table 34. Measured nitrene yields.

Analyzed nitrene complex	Nitrene yield [%]
[Cu{HC(PhPz) ₂ Py}(NTs)]PF ₆	89
[Cu{HC(Ph ₂ Pz) ₂ Melm}(NTs)]PF ₆	90
[Cu{HC(Ph ₂ Pz) ₂ (4-ClPy)}(NTs)]PF ₆	89
[Cu{HC(PuIPz) ₂ Py}(NTs)]PF ₆	50
[Cu{HC(CamPz) ₂ Py}(NTs)]PF ₆	50 ^a
[Cu{HC(Ph ₂ Pz) ₂ DMAP}(NTs)]PF ₆	58

^a reaction performed at -60 °C

[Cu{HC(Ph₂Pz)₂DMAP}(MeCN)]PF₆ (10.8 mg, 1.32*10⁻⁵ mol, 1 equiv.) was dissolved in DCM (3.5 mL) at -80 °C. A solution of ⁹PhINTs (6.5 mg, 1.32*10⁻⁵ mol, 1 equiv.) in DCM (0.38 mL) was added. The solution was stirred for 5 min. Triphenylphosphane (68.7 mg, 2.63*10⁻⁴ mol, 0 equiv.) dissolved in DCM (0.5 mL) at -42 °C was added. The solution was stirred at -42 °C for one hour. The solvent volume was reduced to approximal 1.0 mL *in vacuo*. The yield was determined by ³¹P {¹H} NMR spectroscopy to 16%.

6.9.4 Thermal stability

The nitrene precursor complex (2.63*10⁻⁵ mol, 1 equiv.) was dissolved in DCM (7.0 mL) at -80 °C. A solution of ⁹PhINTs (13.0 mg, 2.63*10⁻⁵ mol, 1 equiv.) in DCM (0.75 mL) was added. The maximal UV/Vis absorption was awaited. The thermal decay was monitored at -42 °C.

For ESI mass spectrometry sample of the nitrene decay products the solvent of the decayed nitrene solution was removed *in vacuo* and the residue was analyzed *via* ESI mass spectrometry.

Table 35. Measured half-life time at -42 °C.

Analyzed nitrene complex	t _{1/2} [min]
[Cu{HC(PhPz) ₂ Py}(NTs)]PF ₆	50
[Cu{HC(Ph ₂ Pz) ₂ Melm}(NTs)]PF ₆	42

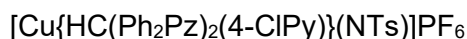
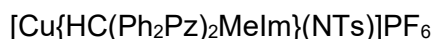
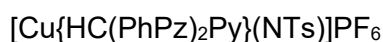
[Cu{HC(Ph ₂ Pz) ₂ (4-ClPy)}(NTs)]PF ₆	5
[Cu{HC(Ph ₂ Pz) ₂ (4-ClPy)}(NTs)]PF ₆ (DCM- <i>d</i> ₂)	6
[Cu{HC(Ph ₂ Pz) ₂ (4-ClPy)}(NTs)]PF ₆ (CHCl ₃)	2
[Cu{HC(Ph ₂ Pz) ₂ (4-ClPy)}(NTs)]PF ₆ (c = 1.7 mmolL ⁻¹)	3
[Cu{HC(Ph ₂ Pz) ₂ (4-ClPy)}(NTs)]PF ₆ (c = 6.8 mmolL ⁻¹)	30
[Cu{HC(Ph ₂ Pz) ₂ Py}(NTs)]PF ₆	14
[Cu{HC(PuIPz) ₂ Py}(NTs)]PF ₆	2
[Cu{HC(CamPz) ₂ Py}(NTs)]PF ₆ ^a	20
[Cu{HC(Ph ₂ Pz) ₂ DMAP}(NTs)]PF ₆	6

^a nitrene formation performed at -60 °C precursor complex **C12** formed *in situ* from **C13** by the addition of 10 equiv. of MeCN

6.9.5 Preparation of Cryo ESI MS sample

A solution of ^sPhINTs (3.0 mg, 6*10⁻⁶ mol, 1 equiv.) in DCM (0.5 mL) was added to a solution of nitrene precursor complex (6*10⁻⁶ mol, 1 equiv.) in DCM (0.5 mL) at -80 °C. The solution was stirred for 5 min. 0.1 mL of the nitrene solution was diluted with DCM (0.5 mL) at -80 °C. The diluted solution was measured with cryo ESI mass spectroscopy at -80 °C.

The following nitrenes were characterized with this method

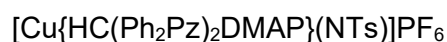
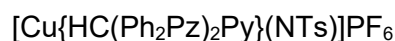
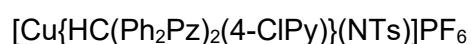
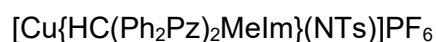
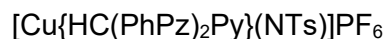


A solution of benzoyl azide in DCM (0.1 mM, 0.06 mL, 6.0*10⁻⁶ mol, 1 equiv.) was added to a solution of [Cu{HC(Ph₂Pz)₂DMAP}(MeCN)]PF₆ (4.9 mg, 6.0*10⁻⁶ mmol, 1 equiv.) in DCM (0.94 mL) at room temperature. The solution was stirred for approximated 10 seconds and then cooled to -80 °C. 0.1 mL of the nitrene solution was diluted with DCM (0.5 mL) at -80 °C. The diluted solution was measured with cryo ESI mass spectroscopy at -80 °C.

6.9.6 Preparation of low temperature Evans' NMR

A solution of $^9\text{PhINTs}$ (6.0 mg, 1.2×10^{-5} mol, 1 equiv.) in $\text{DCM-}d_2$ (0.4 mL) was added to a solution of nitrene precursor complex (1.2×10^{-5} mmol, 1 equiv.) in $\text{DCM-}d_2$ (1.6 mL) at -80°C . The solution was stirred for 5 min. Approximated 0.5 mL of the nitrene solution was transferred to a cooled NMR tube and measured at -80°C using ^1H NMR spectroscopy.

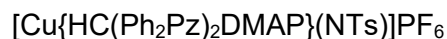
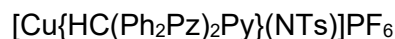
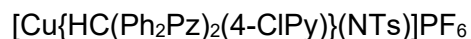
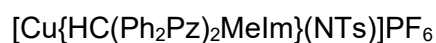
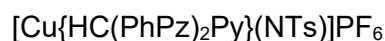
Analyzed nitrene complexes:



6.9.7 Preparation of low temperature NMR

A solution of $^9\text{PhINTs}$ (10.0 mg, 2.0×10^{-5} mol, 1 equiv.) in $\text{DCM-}d_2$ (0.4 mL) was added to a solution of nitrene precursor complex (2.0×10^{-5} mmol, 1 equiv.) in $\text{DCM-}d_2$ (1.6 mL) at -80°C . The solution was stirred for 5 min. Approximated 0.5 mL of the nitrene solution was transferred to a cooled NMR tube and measured at -80°C using ^1H NMR spectroscopy and HSQC.

Analyzed nitrene complexes:



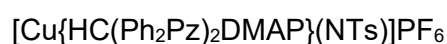
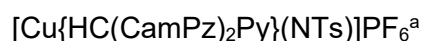
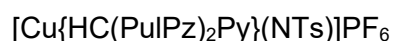
6.9.8 Preparation of EPR samples

A solution of benzoyl azide in DCM (0.1 mM, 0.2 mL, 2.0×10^{-5} mol, 1 equiv.) was added to a solution of $[\text{Cu}\{\text{HC}(\text{Ph}_2\text{Pz})_2\text{DMAP}\}(\text{MeCN})]\text{PF}_6$ (16.4 mg, 2.0×10^{-5} mmol, 1 equiv.) in DCM (1.8 mL) at room temperature. The solution was stirred for approximated 10 seconds and then

cooled to -80 °C. Approximated 0.2 mL of the nitrene solution was transferred to a cooled EPR tube. The EPR sample was measured at -196 °C. After the measurement the nitrene was allowed to decay at -33 °C and measured again at -196 °C.

A solution of $^5\text{PhINTs}$ (10.0 mg, 2.0×10^{-5} mol, 1 equiv.) in DCM (0.4 mL) was added to a solution of nitrene precursor complex (2.0×10^{-5} mmol, 1 equiv.) in DCM (1.6 mL) at -80 °C. The solution was stirred for 5 min. Approximated 0.5 mL of the nitrene solution was transferred to a cooled EPR tube. The EPR sample was measured at -196 °C. After the measurement the nitrene was allowed to decay at -33 °C and measured again at -196 °C.

Analyzed nitrene complexes:

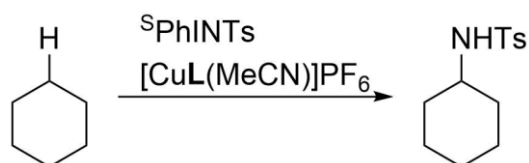


^a formation performed at -63 °C, complex formed *in situ* from **C13** by the addition of 10 equiv. MeCN.

6.10 Catalytic reactions

6.10.1 C–H amination

C–H amination of aliphatic substrates



Cyclohexane (0.3 mL, 2.8×10^{-3} mol, 28 equiv.) and chlorobenzene (0.3 mL) were added to the catalyst (1.00×10^{-5} mol, 0.1 equiv.), $^5\text{PhINTs}$ (49.4 mg, 1.00×10^{-4} mol, 1 equiv.) and molecular sieve (3 Å). The reaction mixture was stirred for 48 h at room temperature. The solvent and remaining substrate were removed *in vacuo*. The residue was dissolved in $\text{CDCl}_3/\text{MeNO}_2$ (1 mL, 10 mL/20 μL) and filtrated. The yield was determined by ^1H NMR spectroscopy.

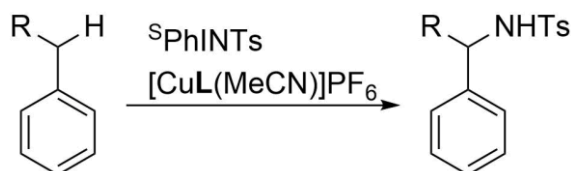
Table 36. C–H amination of cyclohexane.

#	Catalyst	Solvent (V[mL])	Equiv.	Yield [%]
1	[Cu(MeCN) ₄]PF ₆	PhCl	188	0
2	C1	PhCl	56	30
3	C2	PhCl	56	18
4	C3	PhCl	56	18
5	C6	DCM	56	traces
6	C6	PhCl	56	7
7	C6	PhCl (0.15)	10	19
8	C6	MeCN	56	11
9	C11	PhCl	56	38
10	C12^a	PhCl	56	0
11	C12^a	DCM	56	7

^a *In situ* formed from **C13** by the addition of 10 equiv. of MeCN.

C–H amination of benzylic substrates

C–H amination of toluene with ^sPhINTs



Toluene (1 ml, 9.40*10⁻³ mol, 188 equiv.) and chlorobenzene (1 mL) were added to the catalyst (5.00*10⁻⁶ mol, 0.1 equiv.), ^sPhINTs (24.7 mg, 5.00*10⁻⁵ mol, 1 equiv.) and molecular sieve (3 Å). The reaction mixture was stirred for 24 h at room temperature. The solvent and remaining substrate were removed *in vacuo*. The residue was dissolved in CDCl₃/MeNO₂ (1 mL, 10 mL/20 µL) and filtrated. The yield was determined by ¹H NMR spectroscopy.

Table 37. C–H amination of toluene.

#	Catalyst	Toluene [equiv.]	Solvent (V [mL])	Yield [%]
1	[Cu(MeCN) ₄]PF ₆	188	PhCl	22
2	C1	188	PhCl	69

3	C2	188	PhCl	21
4	C3	188	PhCl	22
5	C6	188	PhCl	76
6	C6	188	-	41
7	C6	1	PhCl (0.15)	57
8	C6	10	C ₆ D ₅ Cl	32 ^a
9	C6	10	PhCl	43
10	C11	188	PhCl	56
11	C12^b	188	PhCl	3
12	C12^b	188	DCM	8
13	C17	188	DCM (0.5)	0
14	C18	188	DCM	0
15	C19	188	PhCl	76

^a reaction time 30 min. ^b *In situ* formed from **C13** by the addition of 10 equiv. of MeCN.

C–H amination of toluene with organic azides

Toluene, solvent and Benzoylazide in DCM (0.1 M, 0.5 mL, 5.0*10⁻⁵ mol, 1 equiv.) were added to catalyst (0.5*10⁻⁵ mol, 0.1 equiv.) and molecular sieve (3 Å). The reaction mixture was stirred for 24 h at room temperature. The solvent and remaining substrate were removed *in vacuo*. The residue was dissolved in CDCl₃/MeNO₂ (1 mL, 10 mL/20 µL) and filtrated. The yield was determined by ¹H NMR spectroscopy.

Table 38. C–H amination of toluene with benzoylazide.

#	catalyst	Toluene [equiv.]	Solvent (V [mL])	Yield [%]
1	C19	188	DCM (0.5)	1
2	C19^a	188	DCM (0.5)	4
3	C19^b	188	DCM (0.5)	2
4	C19	188	PhF (0.5)	traces
5	C19^a	188	PhF (0.5)	traces
6	C19^b	188	PhF (0.5)	traces

^a stepwise addition in 5 portions of the benzoylazide over 10 min, reaction time after complete addition 30 min. ^b reaction time 40 min.

AgSbF₆ (5.1 mg, 2.0*10⁻⁵ mol, 1 equiv.) in DCM (1.0 mL) was added to a solution of [CuCl{HC(^tBuPz)₂Py}] or [CuCl{HC(^tBuPz)₂Melm}] (2.0*10⁻⁵ mol, 1 equiv.) in DCM (1.5 mL). An aliquot of 0.25 mL of the supernatant was added to a solution of bis(trifluoromethyl)phenylazid (3.2 mg, 2.0*10⁻⁵ mol, 1 equiv.) in DCM (0.75 mL) and toluene (0.75 mL) over molecular sieve (3 Å). The reaction mixture was stirred for 24 h at room temperature. The solvent and remaining substrate were removed *in vacuo*. The residue was dissolved in CDCl₃/MeNO₂ (1 mL, 10 mL/20 µL) and filtrated. The yield was determined by ¹H NMR spectroscopy. No product was observed.

C–H amination of toluene with an amine and a peroxid

A mixture of [Cu{HC(Ph₂Pz)₂Py}(MeCN)]PF₆ (1.5 mg, 2.0*10⁻⁵ mol, 0.1 equiv.), H₂NTs (34.2 mg, 2.0*10⁻⁴ mol, 1 equiv.), Di-*tert*-butylperoxid (0.44 mL, 2.4*10⁻⁴ mol, 1.2 equiv.) and molecular sieve (3 Å) in DCM (1.0 mL) and toluene (1.0 mL) was stirred for 24 h at room temperature. The solvent and remaining substrate were removed *in vacuo*. The residue was dissolved in CDCl₃/MeNO₂ (1 mL, 10 mL/20 µL) and filtrated. The yield was determined by ¹H NMR spectroscopy. No product was observed.

C–H amination of ethylbenzene with ^SPhINTs

Ethylbenzene (1 ml, 8.19*10⁻³ mol, 164 equiv.) and chlorobenzene (1 mL) were added to the catalyst (5.00*10⁻⁶ mol, 0.1 equiv.), ^SPhINTs (24.7 mg, 5.00*10⁻⁵ mol, 1 equiv.) and molecular sieve (3 Å). The reaction mixture was stirred for 24 h at room temperature. The solvent and remaining substrate were removed *in vacuo*. The residue was dissolved in CDCl₃/MeNO₂ (1 mL, 10 mL/20 µL) and filtrated. The yield was determined by ¹H NMR spectroscopy. The enantiomeric ratio was determined by ¹H NMR spectroscopy in C₆D₆ and with [Eu(hfc)₃] and an external reference with a known enantiomeric ratio.

Table 39. C–H amination ethylbenzene.

#	Catalyst	substrate [equiv.]	Solvent (V [mL])	Yield [%] (e.r. R:S)
1	[Cu(MeCN) ₄]PF ₆	164	PhCl	17
2	C1	164	PhCl	49
3	C2	164	PhCl	57
4	C3	164	PhCl	10
5	C6	164	PhCl	32

6	C7	164	PhCl	40
7	C8	164	DCM	40
8	C10	164	PhCl	9
9	C11	164	PhCl	43 (50:50)
10	C12	164	PhCl	0
11	C12	164	DCM	25 (55:45)
12	C12^b	164	DCM	7 (52:48)
13	C12^b	164	DCM	traces (55:45) ^c
14	C13	164	DCM	0
15	C19	164	PhCl	56
16	C7	164	PhCl	19 ^a
17	C7	164	DCM	12
18	C7	164	MeCN	30
19	C7	164	THF	3
20	C7	81	PhCl (0.5)	12
21	C7	49	PhCl (0.3)	14
22	C7	81	PhCl (1.0)	16
23	C7	49	PhCl (1.0)	12
24	C7	5	PhCl (1.0)	10
25	C7	5	PhCl (0.5)	11

^a PhINTs as nitrene generating agent. ^b *In situ* formed from **C13** by the addition of 10 equiv. of MeCN. ^c Reaction temperature 0 °C, reaction time: 6 h

C–H amination of ethylbenzene with organic azide

Ethylbenzene, solvent and Benzoylazide in DCM (0.1 M, 0.5 mL, 5.0*10⁻⁵ mol, 1 equiv.) were added to catalyst (0.5*10⁻⁵ mol, 0.1 equiv.) and molecular sieve (3 Å). The reaction mixture was stirred for 24 h at room temperature. The solvent and remaining substrate were removed *in vacuo*. The residue was dissolved in CDCl₃/MeNO₂ (1 mL, 10 mL/20 µL) and filtrated. The yield was determined by ¹H NMR spectroscopy.

Table 40. C–H amination of ethylbenzene with benzoylazide.

#	catalyst	Ethylbenzene [equiv.]	Solvent (V [mL])	Yield [%]
1	C7	164	DCM (0.5)	0

2	C18	164	DCM (0.5)	4
3	C8	164	DCM (0.5)	12
4	C8	82	-	10
5	C19	82	-	16
6	C19	164	DCM (0.5)	11
7 ^a	C19	164	DCM (0.5)	6
8 ^b	C19	164	DCM (0.5)	6
9	C19	164	PhF (0.5)	traces
10 ^a	C19	164	PhF (0.5)	traces
11 ^b	C19	164	PhF (0.5)	traces
12 ^c	C19	164	PhF (0.5)	3
13 ^{a,c}	C19	164	PhF (0.5)	3
14 ^{b,c}	C19	164	PhF (0.5)	3
15 ^d	C19	164	DCM (0.9)	traces
16 ^d	C19	164	DCM (0.9)	traces
17 ^d	C19	164	DCM (0.9)	traces
18 ^{d,c}	C19	164	PhF (0.9)	traces
19 ^{d,c}	C19	164	PhF (0.9)	traces
20 ^{d,c}	C19	164	PhF (0.9)	traces

^a stepwise addition in 5 portions of the benzoylazide over 10 min, reaction time after complete addition 30 min. ^b reaction time 40 min. ^c Benzoylazide solution in PhF. ^d the concentration of the benzoylazide solution was 0.5 M. Therefore, 0.1 mL Benzoylazide solution was added.

C–H amination of bibenzyl, neopentyl benzene and benzyl bromide with ^sPhINTs

Substrate (2.5*10⁻⁴ mol, 5 equiv.) and solvent (1 mL) were added to the catalyst (5.00*10⁻⁶ mol, 0.1 equiv.), ^sPhINTs (24.7 mg, 5.00*10⁻⁵ mol, 1 equiv.) and molecular sieve (3 Å). The reaction mixture was stirred for 24 h at room temperature. The solvent and remaining substrate were removed *in vacuo*. The residue was dissolved in CDCl₃/MeNO₂ (1 mL, 10 mL/20 µL) and filtered. The yield was determined by ¹H NMR spectroscopy.

Table 41. C–H amination of bibenzyl, neopentyl benzene and benzyl bromide with ^sPhINTs.

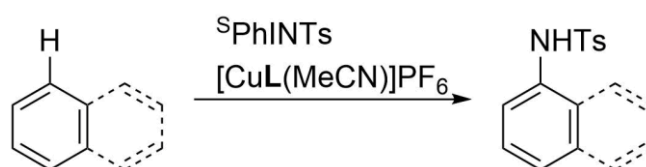
#	Catalyst	Substrate	Solvent	Yield [%]
1	C12^a	Bibenzyl	DCM	traces
2	C13	Bibenzyl	DCM	traces
3	C7	Bibenzyl	PhCl	16

4	C7	Bibenzyl	THF	0
5	C7	Bibenzyl	DCM	23
6	C7	Bibenzyl	MeCN	7
7	C12^a	Neopentyl benzene	DCM	traces
8	C7	Neopentyl benzene	PhCl	traces
9	C7	Neopentyl benzene	THF	0
10	C7	Neopentyl benzene	DCM	traces
11	C7	Neopentyl benzene	MeCN	traces
12	C7	Benzyl bromide	PhCl	traces
13	C7	Benzyl bromide	THF	traces
14	C7	Benzyl bromide	DCM	3
15	C7	Benzyl bromide	MeCN	0

^a *In situ* formed from **C13** by the addition of 10 equiv. of MeCN.

C–H amination of aromatic substrates

C–H amination of benzene with ^sPhINTs



Benzene and solvent were added to the catalyst (5.00×10^{-6} mol, 0.1 equiv.), ^sPhINTs (24.7 mg, 5.00×10^{-5} mol, 1 equiv.) and molecular sieve (3 Å). The reaction mixture was stirred for 48 h at room temperature. The solvent and remaining substrate were removed *in vacuo*. The residue was dissolved in CDCl₃/MeNO₂ (1 mL, 10 mL/20 μL) and filtrated. The yield was determined by ¹H NMR spectroscopy.

Table 42. C–H amination of benzene.

#	Catalyst	Solvent ([mL])	Benzene [equiv.]	Yield [%]
1	[Cu(MeCN) ₄]PF ₆	PhCl (1.0)	188	0
2	C6	PhCl (1.0)	188	16
3	C6	PhCl (0.5)	94	16
4	C6	PhCl (0.3)	56	17
5	C6	PhCl (0.5)	5	9
6	C6	-	188	17

7	C6	-	94	25
8	C6	DCM (0.5)	94	30
9 ^a	C6	DCM (0.5)	94	7
10	C6	MeCN (0.5)	94	35
11	C6	MeCN (0.5)	94	10
12	C6	MeCN (1.0)	188	26
13	C6	MeCN (0.5)	94	31
14	C6	MeCN (0.3)	56	37
15	C6	MeCN (0.5)	5	45
16	C6	MeCN (0.3)	5	30
17	C1	MeCN (0.5)	5	35
18	C2	MeCN (0.5)	5	24
19	C3	MeCN (0.5)	5	22
20	C7	MeCN (0.5)	5	29
21	C16	MeCN (0.5)	5	28

^a PhINTs was used as nitrene generating agent.

C–H amination of naphthalene and further aromatic substrates with ^sPhINTs

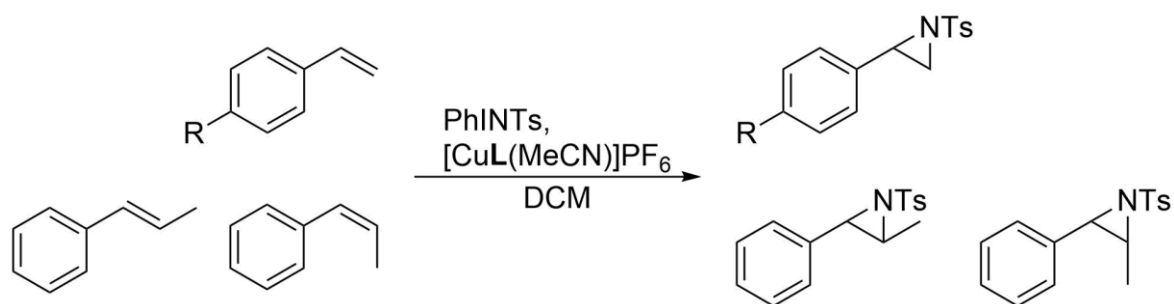
Naphthalene (32.0 mg, 2.5*10⁻⁴ mol, 5 equiv.) and solvent were added to the catalyst (5.00*10⁻⁶ mol, 0.1 equiv.), ^sPhINTs (24.7 mg, 5.00*10⁻⁵ mol, 1 equiv.) and molecular sieve (3 Å). The reaction mixture was stirred for 48 h at room temperature. The solvent was removed *in vacuo*. The residue was dissolved in CDCl₃/MeNO₂ (1 mL, 10 mL/20 µL) and filtrated. The yield was determined by ¹H NMR spectroscopy.

Table 43. C–H amination of naphthalene, anthracene, quinoline chlorobenzene and bromobenzene.

#	Catalyst	Solvent (V [mL])	Substrate ([equiv.])	Yield [%]
1	[Cu(MeCN) ₄]PF ₆	DCM (0.5)	Naphthalene (5)	0
2	C6	PhCl (1.0)	Naphthalene (5)	3
3	C6	DCM (1.0)	Naphthalene (5)	16
4	C6	MeCN (1.0)	Naphthalene (5)	15
5	C6	DCM (0.5)	Naphthalene (5)	25
6	C6	MeCN (0.5)	Naphthalene (5)	27
7	C6	DCM (0.3)	Naphthalene (5)	18

8	C6	MeCN (0.3)	Naphthalene (5)	25
9	C6	MeCN (0.5)	Naphthalene (10)	18
10	C1	DCM (0.5)	Naphthalene (5)	7
11	C2	MeCN (0.5)	Naphthalene (5)	25
12	C3	MeCN (0.5)	Naphthalene (5)	23
13	C6	MeCN (0.5)	Bromobenzene (5)	0
14	C6	MeCN (0.5)	Chlorobenzene (5)	0
15	C6	MeCN (0.5)	Anthracene (5)	0
16	C6	MeCN (0.5)	Quinoline (5)	0

6.10.2 Aziridination



Aziridination of styrene derivatives with PhINTs

Styrene (8.73×10^{-5} mol, 1 equiv.) and DCM (0.5 mL) were added to the catalyst (5×10^{-6} mol, 0.04 equiv.), PhINTs (38.6 mg, 1.0×10^{-4} mol, 1.15 equiv.) and molecular sieve (3 Å). The reaction mixture was stirred for 24 h at room temperature. The solvent and remaining substrate were removed *in vacuo*. The residue was dissolved in $\text{CDCl}_3/\text{MeNO}_2$ (1 mL, 10 mL/20 μL) and filtrated. The yield was determined by ^1H NMR spectroscopy. The enantiomeric excess was determined by ^1H NMR spectroscopy in C_6D_6 and with $[\text{Eu}(\text{hfc})_3]$.

Table 44. Overview of styrene aziridination.

#	Substrate	Equiv. (Styrene)	Equiv. (PhINTs)	Catalyst	Y [%] (cis/trans) {ee}
1	<i>cis</i> -methyl styrene	1.0	1.15	$[\text{Cu}(\text{MeCN})_4]\text{PF}_6$	21 (25/75)
2	<i>trans</i> -methyl styrene	1.0	1.15	$[\text{Cu}(\text{MeCN})_4]\text{PF}_6$	30 (0/100)
3	4- CF_3 -styrene	1.0	1.15	C6	44 ^f
4	4- NO_2 -styrene	1.0	1.15	C6	24
5	<i>cis</i> -methyl styrene	1.0	1.15	C6	42 (88/12)

6	<i>trans</i> -methyl rene	sty-	1.0	1.15	C6	48 (0/100)
7	styrene		1.0	1.15	C1	69
8	styrene ^a		1.0	1.0	C1	70
9	styrene ^b		2.0	1.0	C1	46
10	styrene ^c		3.0	1.0	C1	60
11	styrene ^d		4.0	1.0	C1	58
12	styrene ^e		5.0	1.0	C1	59
13	4-CF ₃ -styrene		1.0	1.15	C1	29
14	4-NO ₂ -styrene		1.0	1.15	C1	41
15	4-OMe-styrene		1.0	1.15	C1	14
16	<i>cis</i> -methyl styrene		1.0	1.15	C1	57 (86/14)
17	<i>trans</i> -methyl rene	sty-	1.0	1.15	C1	45 (0/100)
18	styrene		1.0	1.15	C2	50
19	4-CF ₃ -styrene		1.0	1.15	C2	32
20	4-NO ₂ -styrene		1.0	1.15	C2	13
21	4-OMe-styrene		1.0	1.15	C2	4
22	<i>cis</i> -methyl styrene		1.0	1.15	C2	39 (90/10)
23	<i>trans</i> -methyl rene	sty-	1.0	1.15	C2	41 (0/100)
24	styrene		1.0	1.15	C3	39
25	4-CF ₃ -styrene		1.0	1.15	C3	56
26	4-NO ₂ -styrene		1.0	1.15	C3	40
27	4-OMe-styrene		1.0	1.15	C3	7
28	<i>cis</i> -methyl styrene		1.0	1.15	C3	32 (63/37)
29	<i>trans</i> -methyl rene	sty-	1.0	1.15	C3	47 (0/100)
30	Styrene		1.0	1.15	C11	16 {0}
31	4-CF ₃ -styrene		1.0	1.15	C11	46 {0}
32	4-NO ₂ -styrene		1.0	1.15	C11	42 {0}
33	<i>cis</i> -methyl styrene		1.0	1.15	C11	39 (33/67)
34	<i>trans</i> -methyl rene	sty-	1.0	1.15	C11	38 (0/100) {0}
35	Styrene		1.0	1.15	C12^g	55 {4}
36	Styrene		1.0	1.15	C12^g	30 {12} ^h
37	4-CF ₃ -styrene		1.0	1.15	C12^g	52 {10}

38	4-NO ₂ -styrene	1.0	1.15	C12^g	58 {8}
39	4-OMe-styrene	1.0	1.15	C12^g	32
40	<i>cis</i> -methyl styrene	1.0	1.15	C12^g	49 (57/43)
41	<i>trans</i> -methyl styrene	1.0	1.15	C12^g	55 (0/100) {8}
42	<i>cis</i> -stilbene	1.0	1.15	C12^g	24 (49/51)
43	<i>trans</i> -stilbene	1.0	1.15	C12^g	13 (0/100) {30}
44	<i>cis</i> -stilbene	1.0	1.15	C7	38 (81/19)
45	<i>trans</i> -stilbene	1.0	1.15	C7	41 (0/100)
46	styrene	1.0	1.15	C19	58

^a styrene (1.0*10⁻⁴ mol, 1 equiv.), PhINTs (1.0*10⁻⁴ mol, 1 equiv.); ^b styrene (2.0*10⁻⁴ mol, 2 equiv.), PhINTs (1.0*10⁻⁴ mol, 1 equiv.); ^c styrene (3.0*10⁻⁴ mol, 3 equiv.), PhINTs (1.0*10⁻⁴ mol, 1 equiv.); ^d styrene (4.0*10⁻⁴ mol, 4 equiv.), PhINTs (1.0*10⁻⁴ mol, 1 equiv.); ^e styrene (5.0*10⁻⁴ mol, 5 equiv.), PhINTs (1.0*10⁻⁴ mol, 1 equiv.). ^f t = 30 min, solvent = DCM-*d*₂, this experiment was performed in a young NMR tube. ^g *In situ* formed from **C13** by the addition of 10 equiv. of MeCN. ^h Reaction temperature 0 °C, reaction time: 6 h.

Aziridination of styrene with benzoylazide

Benzoylazide in DCM (0.1 M, 1 mL, 1.0*10⁻⁴ mol, 1.15 equiv.) were added to styrene (8.73*10⁻⁵ mol, 1 equiv.), catalyst (0.4*10⁻⁶ mol, 0.1 equiv.) and molecular sieve (3 Å). The reaction mixture was stirred for 24 h at room temperature. The solvent and remaining substrate were removed *in vacuo*. The residue was dissolved in CDCl₃/MeNO₂ (1 mL, 10 mL/20 µL) and filtrated. The yield was determined by ¹H NMR spectroscopy.

Table 45. Overview of aziridination using benzoylazide.

#	Substrate	Catalyst	Solvent (V [mL])	Y [%]
1	styrene	C19	-	5
2 ^a	styrene	C19	DCM (0.3)	traces

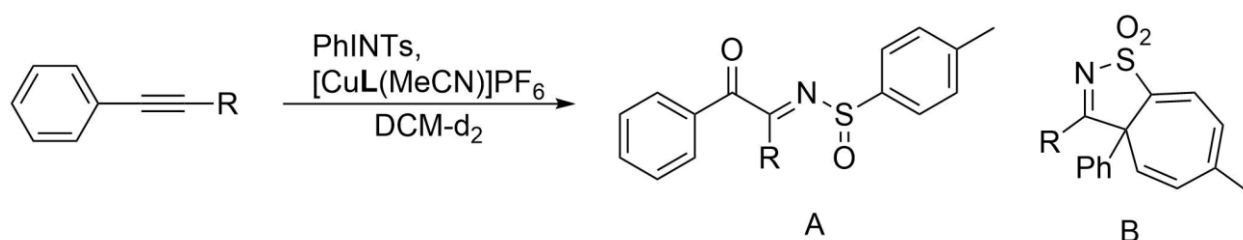
^a The concentration of the benzoylazide solution was 0.5 M. Therefore, 0.2 mL Benzoylazide solution was added.

β-*d*₂ styrene

A mixture of styrene-β-*d*₀ and styrene-β-*d*₂ (1:1; 58 µL, 0.5 mmol, 2 equiv.) and DCM (1.2 mL) were added to the [Cu{HC(PhPz)₂Py}(MeCN)]PF₆ (7.8 mg, 0.0125 mmol, 0.05 equiv.), PhINTs (93.3 mg, 0.25 mmol, 1 equiv.) and molecular sieve (3 Å). The reaction mixture was stirred for

24 h at room temperature. The solvent and remaining substrate were removed *in vacuo*. The residue was purified by silica gel column chromatography, first with hexane to remove the styrene ($R_f = 0.66$), and then with hexane/ethyl acetate (10/1) to yield the aziridine (27.3 mg, 0.10 mmol, 40%, $R_f = 0.26$) as a colorless solid. The ratio of d_0/d_2 aziridines (CD_3CN , 120 s relaxation delay) and styrene ($CDCl_3$, 120 s relaxation delay) is evaluated by 1H NMR spectroscopy.

6.10.3 Alkyne rearrangement

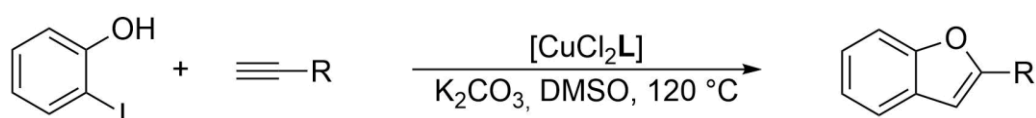


Alkyne (1.0 mmol, 10 equiv.) and $DCM-d_2$ (1.5 mL) were added to mixture of PhINTs (37.2 mg, 0.1 mmol, 1 equiv.) and catalyst (0.005 mmol, 0.1 equiv.). The mixture was stirred for 4 h at room temperature. 0.5 mL of the reaction mixture were analyzed *via* 1H NMR spectroscopy.

Table 46. Overview of alkyne rearrangement.

#	Catalyst	R =	Yield [%] (A:B)
1	C6	H	91 (100:0)
2	C6	Me	22 (60:40)
3	C6	Ph	10 (n.d.)
4	C16	H	30 (100:0)
5	C16	Me	21 (36:64)
6	C16	Ph	0

6.10.4 Sonogashira coupling reaction



All Sonogashira coupling reactions were performed under aerobic conditions.

Standard protocol A:

K₂CO₃ (276 mg, 2 mmol, 2 equiv.), catalyst (0.1 mmol, 0.1 equiv.) and iodophenol (220 mg, 1 mmol, 1 equiv.) were dissolved in DMSO (2 mL) and heated to 80 °C. Alkyne (1 mmol, 1 equiv.) was added and the mixture was stirred at 120 °C for 24 h. The conversion of iodophenol was analyzed with gas chromatography.

Standard protocol B:

Ligand (0.1 mmol, 0.1 equiv.) and CuCl₂ (0.1 mmol, 0.1 equiv.) were dissolved in DMSO (2 mL) and stirred for 10 min. Subsequently K₂CO₃ (276 mg, 2 mmol, 2 equiv.) and iodophenol (220 mg, 1 mmol, 1 equiv.) were added and the reaction mixture was heated to 80 °C and alkyne (1 mmol, 1 equiv.) was added and the mixture was stirred at 120 °C for 24 h. The conversion of iodophenol was analyzed with gas chromatography, 50 µL of 3,5-dimethoxybenzene was added as internal standard.

Table 47. Optimization of benzofuran synthesis.

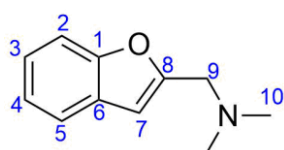
#	Catalyst	solvent	R =	T [°C]	t [h]	X [%]
1	[CuCl ₂ {HC(Pz) ₂ MeIm}]	DMSO	CH ₂ NMe ₂	80	24	70
2	[CuCl ₂ {HC(Me ₂ Pz) ₂ MeIm}]	DMSO	CH ₂ NMe ₂	80	24	80
3	[CuCl ₂ {HC(Me ₃ Pz) ₂ MeIm}]	DMSO	CH ₂ NMe ₂	80	24	83
4	[CuCl ₂ {HC(Pz) ₂ MeIm}]	DMSO	CH ₂ NMe ₂	120	24	100
5	[CuCl ₂ {HC(Pz) ₂ MeIm}]	DMSO	CH ₂ NEt ₂	120	24	100
6	[CuCl ₂ {HC(Pz) ₂ MeIm}]	DMSO	CH ₂ N ⁿ Pr ₂	120	24	100
7	[CuCl ₂ {HC(Pz) ₂ MeIm}]	DMF/H ₂ O	CH ₂ NMe ₂	80	12	70
8	[CuCl ₂ {HC(Pz) ₂ MeIm}]	DMF/H ₂ O ^a	CH ₂ NMe ₂	80	12	83

^a *n*Bu₄NBr (48.4 mg, 0.15 mmol, 0.15 equiv.) as phase transfer catalyst was added.

Synthesis of *N,N*-dimethyl-2-benzofuranmethanamine

K₂CO₃ (552 mg, 4 mmol, 2 equiv.), [CuCl₂{HC(Pz)₂(MeIm)}] (72 mg, 0.2 mmol, 0.1 equiv.) and 2-iodophenol (440 mg, 2 mmol, 1 equiv.) were dissolved in DMSO (4 mL) and heated to 80 °C. 3-Dimethyl-amino-1-propyne (220 µL, 2 mmol, 1 equiv.) was added and the mixture was stirred at 120 °C for 24 h. The reaction mixture was cooled to room temperature and water was added (20 mL). The mixture was extracted with ethyl acetate (3 × 20 mL). The combined organic phase was dried with anhydrous Na₂SO₄ and the solvent was removed under reduced

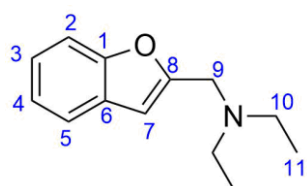
pressure. Column chromatography (EtOAc/MeOH; 95:5; R_f = 0.57) yielded the target compound to 77% (270.8 mg, 1.54 mmol) as a dark yellow oil.



^1H NMR (CDCl_3 , 400 MHz): δ = 7.54 (m, 1H, H-2), 7.45 (m, 1H, H-5), 7.24 (m, 2H, H-3+4), 6.60 (m, 1H, H-7), 3.59 (s, 2H, H-9), 2.29 (s, 6H, H-10) ppm. **^{13}C { ^1H } NMR (CDCl_3 , 100 MHz):** δ = 156.5 (C-8), 155.6 (C-6), 129.0 (C-1), 124.3 (C-3), 123.1 (C-4), 121.2 (C-2), 111.5 (C-5), 105.5 (C-7), 56.8 (C-9), 45.5 (C-10) ppm. **HRMS (ESI⁺, MeOH):** m/z (found): 176.10660 (100%), 177.10986 (12%); m/z (calc.): 176.10753 (100%, $^{12}\text{C}_{11}^{1}\text{H}_{14}^{14}\text{N}_1^{16}\text{O}_1^+$), 177.11095 (12%, $^{13}\text{C}_1^{12}\text{C}_{10}^{1}\text{H}_{14}^{14}\text{N}_1^{16}\text{O}_1^+$). **EA:** calc.: C = 75.40, H = 7.48, N = 7.99, found: C = 74.83 H = 7.37 N = 8.48.

Synthesis of *N,N*-diethyl-2-benzofuranmethanamine

The synthesis is performed analogous to the synthesis of *N,N*-dimethyl-2-benzofuranmethanamine.

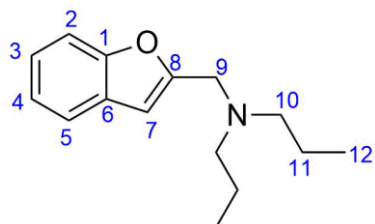


R_f = 0.55; Yield: 381.1 mg, 1.87 mmol, 94%.

^1H NMR (CD_2Cl_2 , 400 MHz): δ = 7.53 (m, 1H, H-2), 7.45 (m, 1H, H-5), 7.21 (m, 2H, H-3, H-4), 6.57 (s, 1H, H-7), 3.75 (s, 2H, H-9), 2.58 (q, 3J = 7.1 Hz, H-4, H-10), 1.07 (t, 3J = 7.1 Hz, 6H, H-11) ppm. **^{13}C { ^1H } NMR (CD_2Cl_2 , 100 MHz):** δ = 157.2 (C-8), 155.5 (C-6), 129.2 (C-1), 124.1 (C-3), 123.1 (C-4), 121.1 (C-2), 111.5 (C-5), 105.3 (C-7), 50.5 (C-9), 47.7 (C-10), 12.5 (C-11) ppm. **HRMS (ESI⁺, MeOH):** m/z (found): 204.13812 (100%), 205.14136 (13%), 206.15354 (1%); m/z (calc.): 204.13884 (100%, $^{12}\text{C}_{13}^{1}\text{H}_{18}^{14}\text{N}_1^{16}\text{O}_1^+$), 205.141940 (14%, $^{13}\text{C}_1^{12}\text{C}_{12}^{1}\text{H}_{18}^{14}\text{N}_1^{16}\text{O}_1^+$), 206.14555 (1%, $^{13}\text{C}_2^{12}\text{C}_{11}^{1}\text{H}_{18}^{14}\text{N}_1^{16}\text{O}_1^+$). **EA:** calc.: C = 76.81, H = 8.43, N = 6.89, found: C = 76.33, H = 8.26, N = 7.80.

Synthesis of *N,N*-dipropyl-2-benzofuranmethanamine

The synthesis is performed analogous to the synthesis of *N,N*-dimethyl-2-benzofuranmethanamine.



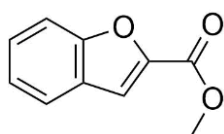
R_f = 0.56; Scale: 1 mmol. Yield: 188.0 mg, 0.81 mmol, 88%

^1H NMR (CD_2Cl_2 , 400 MHz): δ = 7.51 (d, 3J = 7.1 Hz, 1H, H-2), 7.43 (d, 3J = 7.8 Hz, 1H, H-5), 7.21 (m, 2H, H-3, H-4), 6.57 (s, 1H, H-7), 3.76 (s, 2H, H-9), 2.45 (m, 4H, H-10), 1.50 (m, 4H, H-11), 0.91 (t, 3J = 7.3 Hz, 6H, H-12) ppm. **^{13}C { ^1H } NMR (CDCl_3 , 100 MHz):** δ = 157.6 (C-8),

155.5 (C-6), 129.2 (C-1), 124.1 (C-3), 123.0 (C-4), 121.1 (C-2), 111.5 (C-5), 105.1 (C-7), 56.7 (C-10), 51.5 (C-9), 42.5 (C-10), 21.1 (C-11), 12.2 (C-12) ppm. **HRMS (ESI⁺, MeOH):** m/z (found): 232.16910 (100%), 233.17241 (15%), 234.14879 (1%); m/z (calc.): 232.17013 (100%, ¹²C₁₅¹H₂₂¹⁴N₁¹⁶O₁⁺), 233.17349 (16%, ¹³C₁¹²C₁₄¹H₂₂¹⁴N₁¹⁶O₁⁺), 234.17685 (1%, ¹³C₂¹²C₁₃¹H₂₂¹⁴N₁¹⁶O₁⁺).

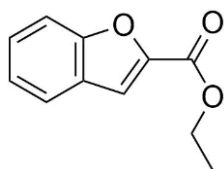
Synthesis of methyl benzofuran-2-carboxylate

The synthesis is performed analogous to standard protocol A. Only traces of the product are observed in the GC spectra.



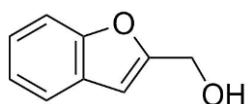
Synthesis of ethyl benzofuran-2-carboxylate

The synthesis is performed analogous to standard protocol A. Only traces of the product are observed in the GC spectra.



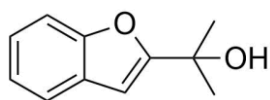
Synthesis of benzofuran-2-ylmethanol

The synthesis is performed analogous to standard protocol A. Only traces of the product are observed in the GC spectra.



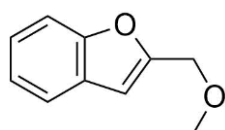
Synthesis of 2-(benzofuran-2-yl)propan-2-ol

The synthesis is performed analogous to standard protocol A. The product was not isolated, the yield is 62%. The yield was calculated from the GC-conversion of iodophenol, no side products are observable.



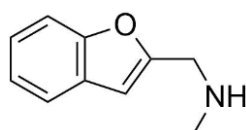
Synthesis of 2-(methoxymethyl)benzofuran

The synthesis is performed analogous to standard protocol A. The product was not isolated, the yield is 30%. The yield was calculated from the GC-conversion of iodophenol, no side products are observable.



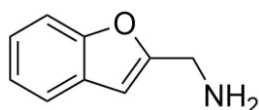
Synthesis of *N*-methyl-2-benzofuranmethanamine

The synthesis is performed analogous to standard protocol A. Only traces of the product are observed in the GC spectra.



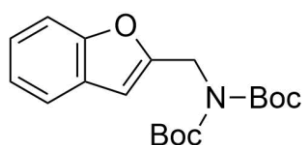
Synthesis of 2-benzofuranmethanamine

The synthesis is performed analogous to standard protocol A. Only traces of the product are observed in the GC spectra.



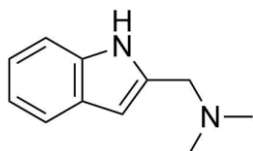
Synthesis of *N,N*-di-*tert*-butoxycarbonyl-2-benzofuranmethanamine

The synthesis is performed analogous to standard protocol A. Only traces of the product are observed in the GC spectra.

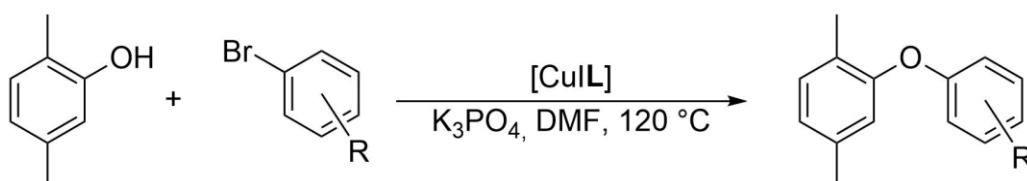


Synthesis of 1-(1*H*-indol-2-yl)-*N,N*-dimethylmethanamine

The synthesis is performed analogous to standard protocol A. Only traces of the product are observed in the GC spectra.



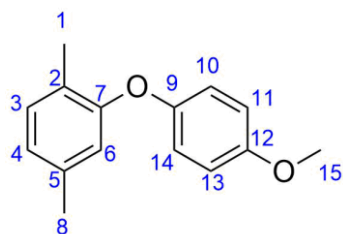
6.10.5 C–O coupling reaction



Standard protocol

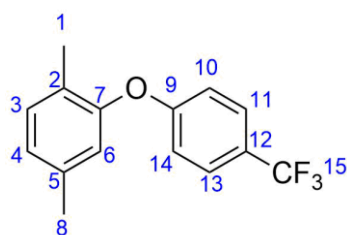
Copper(I) iodide (19.0 mg, 0.1 mmol, 0.1 equiv.), $\text{HC}(\text{Me}_2\text{Pz})_2\text{Py}$ (28.1 mg, 0.1 mmol, 0.1 equiv.) and K_3PO_4 (424.0 mg, 2.0 mmol, 2.0 equiv.) were solved in DMF (2 mL) and stirred for 10 min. 2,5-Dimethyl phenol (146.6 mg, 1.0 mmol, 1.0 equiv.) and bromarene (1.0 mmol, 1.0 equiv.) were added. The reaction mixture was stirred for 36 h at 100 °C. The solvent was removed under reduced pressure and the product isolated by silica gel column chromatography (ethyl acetate).

Synthesis of 2-(4-methoxyphenoxy)-1,4-dimethylbenzene



$R_f = 0.81$; Purity = 50%, $Y = 217.3$ mg, 0.47 mmol, 47%. **$^1\text{H NMR}$ (CDCl_3 , 100 MHz):** $\delta = 7.02$ (m, 2H, H-10, H-14), 6.91 (m, 1H, H-3), 6.60 (m, 1H, H-4), 6.54 (m, 3H, H-6, H-11, H-13), 3.72 (s, 3H, H-15), 2.20 (s, 3H, H-1), 2.14 (s, 3H, H-8) ppm.

Synthesis of 1,4-dimethyl-2-(4-(trifluoromethyl)phenoxy)benzene



$R_f = 0.84$; $Y = 234.5$ mg, 0.88 mmol, 88%. $^1\text{H NMR}$ (CDCl_3 , 100 MHz): $\delta = 7.52$ (m, 2H, H-10, H-14), 7.15 (m, 1H, H-3), 6.93 (m, 3H, H-4, H-11, H-13), 6.79 (s, 1H, H-6), 2.31 (s, 3H, H-1), 2.14 (s, 3H, H-8) ppm. ^{19}F $\{^1\text{H}\}$ NMR (CDCl_3 , 377 MHz): $\delta = -61.4$ ppm.

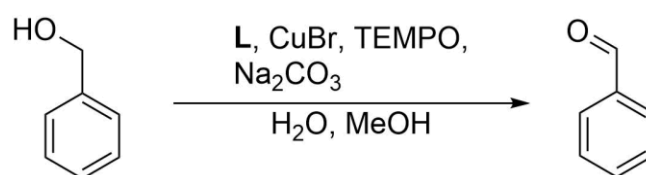
Reaction with 2,5-Dimethyl phenol provided by the Schwaneberg group

The raw mixture of enzymatically produced 2,5-dimethyl phenol (1 L, 50 mg, 0.41 mmol, 1.0 equiv.) was extracted with diethyl ether (5x100 mL). The solvent was removed under reduced pressure and solved in DMF (0.2 mL). Copper(I) iodide (6.5 mg, 0.04 mmol, 0.1 equiv.), $\text{HC}(\text{Me}_2\text{Pz})_2\text{Py}$ (9.6 mg, 0.04 mmol, 0.1 equiv.) and K_3PO_4 (144.6 mg, 0.82 mmol, 2.0 equiv.) were solved in DMF (0.5 mL) and stirred for 10 min. To this solution the 2,5-dimethyl phenol solution and 1-bromo-4-(trifluoromethyl)benzene (47.1 μL , 0.41 mmol, 1.0 equiv.) was added and the reaction mixture was stirred for 36 h at 100 $^\circ\text{C}$. An aliquot was analyzed via NMR spectroscopy. Trace amount of the product could be observed.

6.10.6 Preliminary work on copper loaded microgel

All reactions were performed under aerobic conditions.

Oxidation of benzylic alcohols



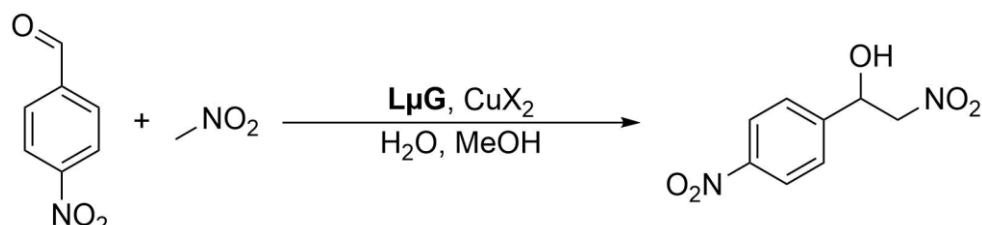
Copper(I) bromide (7.2 mg, 0.05 mmol, 0.05 equiv.), ligand (0.05 mmol, 0.05 equiv.), TEMPO (7.8 mg, 0.05 mmol, 0.05 equiv.), Na_2CO_3 (106.0 mg, 1.0 mmol, 1.0 equiv.) and benzyl alcohol (103.9 μL , 1.0 mmol, 1.0 equiv.) were solved in methanol (4 mL) and stirred for 5 h at room temperature. 0.1 mL of the reaction solution was diluted in 0.6 mL of CDCl_3 and analyzed with $^1\text{H NMR}$ spectroscopy.

Table 48. Oxidation of benzylic alcohols.

#	Ligand	Variation	Product observable
1	L16	-	Yes

2	L16	Without TEMPO	No
3	L7	-	Yes
4	L7	Without TEMPO	No

Henry reaction

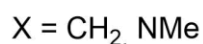
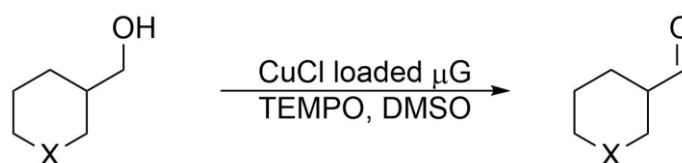


A suspension of functionalized microgel (0.5 mL, 10 $\mu\text{mol/mL}$ ligand, 0.1 equiv.) in water was added to copper(II)bromide (1.1 mg, 5.0 μmol , 0.1 equiv.) and stirred for 15 min. Methanol (0.5 mL), 4-nitrobenzylaldehyde (75.6 mg, 0.05 mmol, 1 equiv.) and nitromethane (107 μL , 0.2 mmol, 4 equiv.) were added. The reaction mixture was stirred for 48 h at room temperature. Ammonium chloride (saturated aqueous solution, 1 mL). The aqueous phase was extracted with ethyl acetate (3x1 mL). The organic phase was dried over Na_2SO_4 and the solvent was removed under reduced pressure. The residue was analyzed with ^1H NMR spectroscopy, 1,3 dimethoxybenzene was added as an internal standard (3.9 $\mu\text{L}/1\text{ mL}$ CDCl_3).

Table 49. Henry reaction.

#	Copper salt	Y [%]
1	CuBr_2	16
2	CuCl_2	4
3	$[\text{Cu}(\text{MeCN})_4]\text{OTf}_2$	15

Oxidation of aliphatic alcohols



Microgel (pVCL, functionalized with 10w% Ligand, 21.3 mg, 0.015 mmol ligand, 0.05 equiv.) and copper(I) chloride (1.5 mg, 0.015 mmol, 0.05 equiv.) was suspended in DMSO (4 mL). Substrate (0.3 mmol, 1 equiv.) and TEMPO (2.3 mg, 0.015 mmol, 0.05 equiv.) was added and the mixture was stirred for 24 h at room temperature at 900 rpm. Ammonium chloride (saturated aqueous solution, 1 mL). The aqueous phase was extracted with ethyl acetate (3x1 mL).

The organic phase was dried over Na₂SO₄ and the solvent was removed under reduced pressure. The residue was analyzed with ¹H NMR spectroscopy.

Table 50. Oxidation of aliphatic alcohol.

#	Substrate	Y [%]
1	Cyclohexylmethanol	traces
2	(1-methylpiperidin-4-yl)methanol	traces

7. Literature

- [1] a) P. Mal, B. Breiner, K. Rissanen, J. R. Nitschke, *Science* **2009**, 324, 1697; b) J.-U. Rohde, J.-H. In, M. H. Lim, W. W. Brennessel, M. R. Bukowski, A. Stubna, E. Münck, W. Nam, L. Que, *Science* **2003**, 299, 1037; c) J. Wencel-Delord, F. Glorius, *Nat. Chem.* **2013**, 5, 369; d) T. Rösener, A. Hoffmann, S. Herres-Pawlis, *Eur. J. Inorg. Chem.* **2018**, 2018, 3164; e) R. D. Rittinghaus, P. M. Schäfer, P. Albrecht, C. Conrads, A. Hoffmann, A. N. Ksiazkiewicz, O. Bienemann, A. Pich, S. Herres-Pawlis, *ChemSusChem* **2019**, 12, 2161; f) S. Kundu, W. Y. Kim, J. A. Bertke, T. H. Warren, *J. Am. Chem. Soc.* **2017**, 139, 1045; g) Y. Xiao, Z. Sun, H. Guo, O. Kwon, *Beilstein J. Org. Chem.* **2014**, 10, 2089.
- [2] S. Kriek, A. Koch, K. Hinze, C. Müller, J. Lange, H. Görls, M. Westerhausen, *Eur. J. Inorg. Chem.* **2016**, 2016, 2332.
- [3] S. Trofimenko, *Scorpionates: The Coordination Chemistry of Polypyrazolyborate Ligands*, Imperial College Press, London, **1999**.
- [4] S. Trofimenko, *Chem. Rev.* **1993**, 93, 943.
- [5] S. Trofimenko, *J. Am. Chem. Soc.* **1967**, 89, 3170.
- [6] B. R. Manzano, F. A. Jalón, M. C. Carrión, G. Durá, *Eur. J. Inorg. Chem.* **2016**, 2016, 2272.
- [7] C. Santini, M. Pellei, G. G. Lobbia, G. Papini, *Mini-Reviews in Organic Chemistry* **2010**, 7, 84.
- [8] S. Fischer, J. Hoyano, L. K. Peterson, *Can. J. Chem.* **1976**, 54, 2710.
- [9] E. E. Pullen, D. Rabinovich, C. D. Incarvito, T. E. Concolino, A. L. Rheingold, *Inorg. Chem.* **2000**, 39, 1561.
- [10] R. Panzer, C. Guhrenz, D. Haubold, R. Hübner, N. Gaponik, A. Eychmüller, J. J. Weigand, *Angew. Chem. Int. Ed.* **2017**, 56, 14737; *Angew. Chem.* **2017**, 129, 14932.
- [11] A. Maleckis, J. W. Kampf, M. S. Sanford, *J. Am. Chem. Soc.* **2013**, 135, 6618.
- [12] W. Hückel, H. Bretschneider, *Ber. Dtsch. Chem. Ges.* **1937**, 70, 2024.
- [13] S. Trofimenko, *J. Am. Chem. Soc.* **1966**, 88, 1842.
- [14] a) S. Trofimenko, *J. Am. Chem. Soc.* **1967**, 89, 3904; b) S. Trofimenko, *J. Am. Chem. Soc.* **1967**, 89, 6288.
- [15] S. Trofimenko, J. C. Calabrese, J. S. Thompson, *Inorg. Chem.* **1987**, 26, 1507.
- [16] D. L. Reger, *Comments Inorganic Chem.* **1999**, 21, 1.
- [17] a) L. M. Martins, *Coord. Chem. Rev.* **2019**, 396, 89; b) M. M. Díaz-Requejo, P. J. Pérez, *Eur. J. Inorg. Chem.* **2020**, 2020, 879.
- [18] D. L. Reger, J. R. Gardinier, S. Bakbak, R. F. Semeniuc, U. H. F. Bunz, M. D. Smith, *New J. Chem.* **2005**, 29, 1035.
- [19] L. M. D. R. S. Martins, A. J. L. Pombeiro, *Eur. J. Inorg. Chem.* **2016**, 2016, 2236.
- [20] W. Kläui, M. Berghahn, G. Rheinwald, H. Lang, *Angew. Chem. Int. Ed.* **2000**, 39, 2464; *Angew. Chem.* **2000**, 112, 2590.
- [21] A. Sánchez-Méndez, G. F. Silvestri, E. de Jesús, F. J. de la Mata, J. C. Flores, R. Gómez, P. Gómez-Sal, *Eur. J. Inorg. Chem.* **2004**, 2004, 3287.
- [22] H. E. Wagner, S. Hohnstein, M. G. Schußmann, L. A. Steppe, F. Breher, *Dalton Trans.* **2019**, 15397.
- [23] I. Kuzu, I. Krummenacher, I. J. Hewitt, Y. Lan, V. Mereacre, A. K. Powell, P. Höfer, J. Harmer, F. Breher, *Chem. Eur. J.* **2009**, 15, 4350.
- [24] M. G. Cushman, J. Meyer, A. Heath, A. D. Schwarz, I. Fernández, F. Breher, P. Mountford, *Organometallics* **2010**, 29, 1174.
- [25] a) T. Ruman, Z. Ciunik, S. Wołowicz, *Polyhedron* **2004**, 23, 219; b) T. Ruman, Z. Ciunik, A. Goclan, M. Łukasiewicz, S. Wołowicz, *Polyhedron* **2001**, 20, 2965.

- [26] A. Otero, J. Fernández-Baeza, A. Lara-Sánchez, L. F. Sánchez-Barba, *Coord. Chem. Rev.* **2013**, 257, 1806.
- [27] a) K. I. The, L. K. Peterson, E. Kiehlmann, *Can. J. Chem.* **1973**, 51, 2448; b) K. I. Thé, L. K. Peterson, *Can. J. Chem.* **1973**, 51, 422.
- [28] A. D. Schofield, M. L. Barros, M. G. Cushion, A. D. Schwarz, P. Mountford, *Dalton Trans.* **2009**, 85.
- [29] A. Hoffmann, U. Flörke, M. Schürmann, S. Herres-Pawlis, *Eur. J. Org. Chem.* **2010**, 2010, 4136.
- [30] L. D. Field, B. A. Messerle, M. Rehr, L. P. Soler, T. W. Hambley, *Organometallics* **2003**, 22, 2387.
- [31] a) J. T. Hoffman, B. L. Tran, C. J. Carrano, *Dalton Trans.* **2006**, 3822; b) A. Otero, J. Fernández-Baeza, A. Lara-Sánchez, J. Tejada, L. F. Sánchez-Barba, *Eur. J. Inorg. Chem.* **2008**, 2008, 5309.
- [32] Y.-R. Luo, *Comprehensive handbook of chemical bond energies*, Taylor & Francis, Boca Raton, **2007**.
- [33] A. Otero, J. Fernández-Baeza, A. Antiñolo, J. Tejada, A. Lara-Sánchez, L. Sánchez-Barba, M. Sánchez-Molina, S. Franco, I. López-Solera, A. M. Rodríguez, *Eur. J. Inorg. Chem.* **2006**, 2006, 707.
- [34] A. Otero, J. Fernández-Baeza, A. Antiñolo, J. Tejada, A. Lara-Sánchez, L. Sánchez-Barba, M. Sánchez-Molina, S. Franco, I. López-Solera, A. M. Rodríguez, *Dalton Trans.* **2006**, 4359.
- [35] A. Otero, F. Carrillo-Hermosilla, P. Terreros, T. Expósito, S. Rojas, J. Fernández-Baeza, A. Antiñolo, I. López-Solera, *Eur. J. Inorg. Chem.* **2003**, 2003, 3233.
- [36] A. Otero, J. Fernández-Baeza, A. Antiñolo, J. Tejada, A. Lara-Sánchez, L. Sánchez-Barba, A. M. Rodríguez, M. A. Maestro, *J. Am. Chem. Soc.* **2004**, 126, 1330.
- [37] a) R. Trammell, K. Rajabimoghadam, I. Garcia-Bosch, *Chem. Rev.* **2019**, 119, 2954; b) Q.-S. Gu, Z.-L. Li, X.-Y. Liu, *Acc. Chem. Res.* **2020**, 53, 170.
- [38] A. Hossain, A. Bhattacharyya, O. Reiser, *Science* **2019**, 364, eaav9713–9724.
- [39] M. Pellei, V. Gandin, L. Marchiò, C. Marzano, L. Bagnarelli, C. Santini, *Molecules* **2019**, 24, 1761.
- [40] C. Wilfer, P. Liebhäuser, A. Hoffmann, H. Erdmann, O. Grossmann, L. Runtsch, E. Paffenholz, R. Schepper, R. Dick, M. Bauer, M. Dürr, I. Ivanović-Burmazović, S. Herres-Pawlis, *Chem. Eur. J.* **2015**, 21, 17639.
- [41] J. Moegling, A. Hoffmann, S. Herres-Pawlis, *Synthesis* **2016**, 49, 225.
- [42] a) J. Elflein, F. Platzmann, N. Burzlaff, *Eur. J. Inorg. Chem.* **2007**, 2007, 5173; b) T. Godau, F. Platzmann, F. W. Heinemann, N. Burzlaff, *Dalton Trans.* **2009**, 254.
- [43] T. Godau, S. M. Bleifuss, A. L. Müller, T. Roth, S. Hoffmann, F. W. Heinemann, N. Burzlaff, *Dalton Trans.* **2011**, 6547.
- [44] K. Sonogashira, Y. Tohda, N. Hagihara, *Tetrahedron Lett.* **1975**, 16, 4467.
- [45] J. Moegling, A. D. Benischke, J. M. Hammann, N. A. Vepřek, F. Zoller, B. Rendenbach, A. Hoffmann, H. Sievers, M. Schuster, P. Knochel, S. Herres-Pawlis, *Eur. J. Org. Chem.* **2015**, 2015, 7475.
- [46] a) A. N. Campbell, S. S. Stahl, *Acc. Chem. Res.* **2012**, 45, 851; b) S. D. McCann, S. S. Stahl, *Acc. Chem. Res.* **2015**, 48, 1756.
- [47] S. Itoh, S. Fukuzumi, *Acc. Chem. Res.* **2007**, 40, 592.
- [48] A. Hoffmann, C. Citek, S. Binder, A. Goos, M. Rübhausen, O. Troeppner, I. Ivanović-Burmazović, E. C. Wasinger, T. D. P. Stack, S. Herres-Pawlis, *Angew. Chem. Int. Ed.* **2013**, 52, 5398; *Angew. Chem.* **2013**, 125, 5508.
- [49] P. Liebhäuser, K. Keisers, A. Hoffmann, T. Schnappinger, I. Sommer, A. Thoma, C. Wilfer, R. Schoch, K. Stührenberg, M. Bauer, M. Dürr, I. Ivanović-Burmazović, S. Herres-Pawlis, *Chem. Eur. J.* **2017**, 23, 12171.

- [50] T. A. G. Duarte, A. P. Carvalho, L. M. D. R. S. Martins, *Catal. Sci. Technol.* **2018**, *8*, 2285.
- [51] B. G. M. Rocha, T. C. O. Mac Leod, M. F. C. Guedes da Silva, K. V. Luzyanin, L. M. D. R. S. Martins, A. J. L. Pombeiro, *Dalton Trans.* **2014**, 15192.
- [52] M. J. Moure, R. SanMartin, E. Domínguez, *Adv. Synth. Catal.* **2014**, 356, 2070.
- [53] A. M. Thomas, A. Sujatha, G. Anilkumar, *RSC Adv.* **2014**, *4*, 21688.
- [54] F. Liu, D. Ma, *J. Org. Chem.* **2007**, *72*, 4844.
- [55] a) F. Ullmann, *Ber. Dtsch. Chem. Ges.* **1904**, *37*, 853; b) F. Ullmann, P. Sponagel, *Ber. Dtsch. Chem. Ges.* **1905**, *38*, 2211.
- [56] F. Monnier, M. Taillefer, *Angew. Chem. Int. Ed.* **2009**, *48*, 6954; *Angew. Chem.* **2009**, *121*, 7088.
- [57] Q. Cai, B. Zou, D. Ma, *Angew. Chem. Int. Ed.* **2006**, *45*, 1276; *Angew. Chem.* **2006**, *118*, 1298.
- [58] N. Xia, M. Taillefer, *Chem. Eur. J.* **2008**, *14*, 6037.
- [59] H. Rao, Y. Jin, H. Fu, Y. Jiang, Y. Zhao, *Chem. Eur. J.* **2006**, *12*, 3636.
- [60] F. Collet, R. H. Dodd, P. Dauban, *Chem. Commun.* **2009**, 5061.
- [61] R. Hili, A. K. Yudin, *Nat. Chem. Biol.* **2006**, *2*, 284.
- [62] S. D. Roughley, A. M. Jordan, *J. Med. Chem.* **2011**, *54*, 3451.
- [63] B. Niu, K. Yang, B. Lawrence, H. Ge, *ChemSusChem* **2019**, *12*, 2955.
- [64] O. Baudoin, *Angew. Chem. Int. Ed.* **2020**, *59*, 17798; *Angew. Chem.* **2020**, *132*, 17950.
- [65] V. Bagchi, P. Paraskevopoulou, P. Das, L. Chi, Q. Wang, A. Choudhury, J. S. Mathieson, L. Cronin, D. B. Pardue, T. R. Cundari, G. Mitrikas, Y. Sanakis, P. Stavropoulos, *J. Am. Chem. Soc.* **2014**, *136*, 11362.
- [66] a) D. N. Barman, K. M. Nicholas, *Tetrahedron Lett.* **2010**, *51*, 1815; b) R. Bhuyan, K. M. Nicholas, *Org. Lett.* **2007**, *9*, 3957; c) I. Cano, M. C. Nicasio, P. J. Pérez, *Dalton Trans.* **2009**, 730; d) R. T. Gephart, T. H. Warren, *Organometallics* **2012**, *31*, 7728; e) T. T. Ponduru, Z. Sun, T. R. Cundari, H. V. Rasika Dias, *ChemCatChem* **2019**, *11*, 4966.
- [67] M. M. Díaz-Requejo, T. R. Belderráin, M. C. Nicasio, S. Trofimenko, P. J. Pérez, *J. Am. Chem. Soc.* **2003**, *125*, 12078.
- [68] M. R. Fructos, S. Trofimenko, M. M. Díaz-Requejo, P. J. Pérez, *J. Am. Chem. Soc.* **2006**, *128*, 11784.
- [69] A. N. Vedernikov, K. G. Caulton, *Chem. Commun.* **2004**, 162.
- [70] a) L. D. Amisial, X. Dai, R. A. Kinney, A. Krishnaswamy, T. H. Warren, *Inorg. Chem.* **2004**, *43*, 6537; b) T. Ando, S. Minakata, I. Ryu, M. Komatsu, *Tetrahedron Lett.* **1998**, *39*, 309; c) I. Arenas, M. Á. Fuentes, E. Alvarez, Y. Díaz, A. Caballero, S. Castellón, P. J. Pérez, *Inorg. Chem.* **2014**, *53*, 3991; d) B. M. Chanda, R. Vyas, A. V. Bedekar, *J. Org. Chem.* **2001**, *66*, 30; e) P. Comba, M. Merz, H. Pritzkow, *Eur. J. Inorg. Chem.* **2003**, 2003, 1711; f) D. A. Evans, M. T. Bilodeau, M. M. Faul, *J. Am. Chem. Soc.* **1994**, *116*, 2742; g) K. M. Gillespie, E. J. Crust, R. J. Deeth, P. Scott, *Chem. Commun.* **2001**, 785; h) E. Haldón, M. Delgado-Rebollo, A. Prieto, E. Alvarez, C. Maya, M. C. Nicasio, P. J. Pérez, *Inorg. Chem.* **2014**, *53*, 4192; i) N. Nebra, C. Lescot, P. Dauban, S. Mallet-Ladeira, B. Martin-Vaca, D. Bourissou, *Eur. J. Org. Chem.* **2013**, 2013, 984; j) A. N. Vedernikov, K. G. Caulton, *Org. Lett.* **2003**, *5*, 2591; k) H. Wu, L.-W. Xu, C.-G. Xia, J. Ge, W. Zhou, L. Yang, *Catal. Commun.* **2005**, *6*, 221.
- [71] P. Comba, C. Haaf, A. Lienke, A. Muruganantham, H. Wadepohl, *Chem. Eur. J.* **2009**, *15*, 10880.
- [72] P. Comba, C. Lang, C. Lopez de Laorden, A. Muruganantham, G. Rajaraman, H. Wadepohl, M. Zajackowski, *Chem. Eur. J.* **2008**, *14*, 5313.
- [73] M. J. B. Aguila, Y. M. Badiei, T. H. Warren, *J. Am. Chem. Soc.* **2013**, *135*, 9399.
- [74] Z. Li, R. W. Quan, E. N. Jacobsen, *J. Am. Chem. Soc.* **1995**, *117*, 5889.
- [75] D. N. Barman, P. Liu, K. N. Houk, K. M. Nicholas, *Organometallics* **2010**, *29*, 3404.

- [76] P. Brandt, M. J. Södergren, P. G. Andersson, P.-O. Norrby, *J. Am. Chem. Soc.* **2000**, *122*, 8013.
- [77] I. Cano, E. Álvarez, M. C. Nicasio, P. J. Pérez, *J. Am. Chem. Soc.* **2011**, *133*, 191.
- [78] L. Maestre, W. M. C. Sameera, M. M. Díaz-Requejo, F. Maseras, P. J. Pérez, *J. Am. Chem. Soc.* **2013**, *135*, 1338.
- [79] S. M. Tekarli, T. G. Williams, T. R. Cundari, *J. Chem. Theory. Comput.* **2009**, *5*, 2959.
- [80] a) R. J. Scamp, B. Scheffer, J. M. Schomaker, *Chem. Commun.* **2019**, *55*, 7362; b) R. Rey-Rodriguez, G. Grelier, L. Habert, P. Retailleau, B. Darses, I. Gillaizeau, P. Dauban, *J. Org. Chem.* **2017**, *82*, 11897.
- [81] G. Dequirez, V. Pons, P. Dauban, *Angew. Chem. Int. Ed.* **2012**, *51*, 7384; *Angew. Chem.* **2012**, *124*, 7498.
- [82] a) M. Goswami, V. Lyaskovskyy, S. R. Domingos, W. J. Buma, S. Woutersen, O. Troeppner, I. Ivanović-Burmazović, H. Lu, X. Cui, X. P. Zhang, E. J. Reijerse, S. De-Beer, M. M. van Schooneveld, F. F. Pfaff, K. Ray, B. de Bruin, *J. Am. Chem. Soc.* **2015**, *137*, 5468; b) N. D. Paul, S. Mandal, M. Otte, X. Cui, X. P. Zhang, B. de Bruin, *J. Am. Chem. Soc.* **2014**, *136*, 1090; c) P. F. Kuijpers, M. J. Tiekink, W. B. Breukelaar, D. L. J. Broere, N. P. van Leest, J. I. van der Vlugt, J. N. H. Reek, B. de Bruin, *Chem. Eur. J.* **2017**, *23*, 7945.
- [83] P. F. Kuijpers, J. I. van der Vlugt, S. Schneider, B. de Bruin, *Chem. Eur. J.* **2017**, *23*, 13819.
- [84] N. Jung, S. Bräse, *Angew. Chem. Int. Ed.* **2012**, *51*, 5538; *Angew. Chem.* **2012**, *124*, 5632.
- [85] a) K. M. Carsch, J. T. Lukens, I. M. DiMucci, D. A. Iovan, S.-L. Zheng, K. M. Lancaster, T. A. Betley, *J. Am. Chem. Soc.* **2020**, *142*, 2264; b) C. Wentrup, *Angew. Chem. Int. Ed.* **2018**, *57*, 11508; *Angew. Chem.* **2018**, *130*, 11680.
- [86] K. M. Carsch, I. M. DiMucci, D. A. Iovan, A. Li, S.-L. Zheng, C. J. Titus, S. J. Lee, K. D. Irwin, D. Nordlund, K. M. Lancaster, T. A. Betley, *Science* **2019**, *365*, 1138.
- [87] Y. M. Badiei, A. Krishnaswamy, M. M. Melzer, T. H. Warren, *J. Am. Chem. Soc.* **2006**, *128*, 15056.
- [88] A. G. Bakhoda, Q. Jiang, Y. M. Badiei, J. A. Bertke, T. R. Cundari, T. H. Warren, *Angew. Chem. Int. Ed.* **2019**, *58*, 3421; *Angew. Chem.* **2019**, *131*, 3459.
- [89] S. Wiese, Y. M. Badiei, R. T. Gephart, S. Mossin, M. S. Varonka, M. M. Melzer, K. Meyer, T. R. Cundari, T. H. Warren, *Angew. Chem. Int. Ed.* **2010**, *49*, 8850; *Angew. Chem.* **2010**, *122*, 9034.
- [90] Y. M. Badiei, A. Dinescu, X. Dai, R. M. Palomino, F. W. Heinemann, T. R. Cundari, T. H. Warren, *Angew. Chem. Int. Ed.* **2008**, *47*, 9961; *Angew. Chem.* **2008**, *120*, 10109.
- [91] K. W. Fiori, J. Du Bois, *J. Am. Chem. Soc.* **2007**, *129*, 562.
- [92] T. Corona, L. Ribas, M. Rovira, E. R. Farquhar, X. Ribas, K. Ray, A. Company, *Angew. Chem.* **2016**, *128*, 14211; *Angew. Chem. Int. Ed.* **2016**, *55*, 14005.
- [93] S. Kundu, E. Miceli, E. Farquhar, F. F. Pfaff, U. Kuhlmann, P. Hildebrandt, B. Braun, C. Greco, K. Ray, *J. Am. Chem. Soc.* **2012**, *134*, 14710.
- [94] S.-L. Abram, I. Monte-Pérez, F. F. Pfaff, E. R. Farquhar, K. Ray, *Chem. Commun.* **2014**, *50*, 9852.
- [95] I. Monte-Pérez, S. Kundu, K. Ray, *Z. Anorg. Allg. Chem.* **2015**, *641*, 78.
- [96] J. A. La Molina de Torre, I. Pérez-Ortega, Á. Beltrán, M. R. Rodríguez, M. M. Díaz-Requejo, P. J. Pérez, A. C. Albéniz, *Chem. Eur. J.* **2019**, *25*, 556.
- [97] E. Haldón, M. Besora, I. Cano, X. C. Cambeiro, M. A. Pericàs, F. Maseras, M. C. Nicasio, P. J. Pérez, *Chem. Eur. J.* **2014**, *20*, 3463.
- [98] M. R. Rodríguez, Á. Beltrán, Á. L. Mudarra, E. Álvarez, F. Maseras, M. M. Díaz-Requejo, P. J. Pérez, *Angew. Chem. Int. Ed.* **2017**, *56*, 12842; *Angew. Chem.* **2017**, *129*, 13022.

- [99] A. M. Rodríguez, M. R. Rodríguez, M. M. Díaz-Requejo, P. J. Pérez, *Isr. J. Chem.* **2020**, *60*, 485.
- [100] F. Dielmann, O. Back, M. Henry-Ellinger, P. Jerabek, G. Frenking, G. Bertrand, *Science* **2012**, *337*, 1526.
- [101] F. Dielmann, D. M. Andrada, G. Frenking, G. Bertrand, *J. Am. Chem. Soc.* **2014**, *136*, 3800.
- [102] J. Moegling, A. Hoffmann, F. Thomas, N. Orth, P. Liebhäuser, U. Herber, R. Rampmaier, J. Stanek, G. Fink, I. Ivanović-Burmazović, S. Herres-Pawlis, *Angew. Chem. Int. Ed.* **2018**, *57*, 9154; *Angew. Chem.* **2018**, *130*, 9294.
- [103] Julian Moegling, *Dissertation*, RWTH Aachen University, Aachen, **2018**.
- [104] W. M. Haynes (Hrsg.) *CRC handbook of chemistry and physics. A ready-reference book of chemical and physical data*, CRC Press, Boca Raton, **2017**.
- [105] D. S. McGuinness, E. L. Marshall, V. C. Gibson, J. W. Steed, *J. Polym. Sci. A Polym. Chem.* **2003**, *41*, 3798.
- [106] B. Plietker, A. Röske, *Catal. Sci. Technol.* **2019**, *9*, 4188.
- [107] H. Yu, Z. Li, C. Bolm, *Angew. Chem. Int. Ed.* **2018**, *57*, 324; *Angew. Chem.* **2018**, *130*, 330.
- [108] N. W. Goldberg, A. M. Knight, R. K. Zhang, F. H. Arnold, *J. Am. Chem. Soc.* **2019**, *141*, 19585.
- [109] Y.-D. Du, C.-Y. Zhou, W.-P. To, H.-X. Wang, C.-M. Che, *Chem. Sci.* **2020**, *11*, 4680.
- [110] M. J. T. Wilding, D. A. Iovan, T. A. Betley, *J. Am. Chem. Soc.* **2017**, *139*, 12043.
- [111] D. A. Iovan, T. A. Betley, *J. Am. Chem. Soc.* **2016**, *138*, 1983.
- [112] S. Hong, K. D. Sutherlin, A. K. Vardhaman, J. J. Yan, S. Park, Y.-M. Lee, S. Jang, X. Lu, T. Ohta, T. Ogura, E. I. Solomon, W. Nam, *J. Am. Chem. Soc.* **2017**, *139*, 8800.
- [113] S. Hong, X. Lu, Y.-M. Lee, M. S. Seo, T. Ohta, T. Ogura, M. Clémancey, P. Maldivi, J.-M. Latour, R. Sarangi, W. Nam, *J. Am. Chem. Soc.* **2017**, *139*, 14372.
- [114] F. Rudroff, M. D. Mihovilovic, H. Gröger, R. Snajdrova, H. Iding, U. T. Bornscheuer, *Nat. Catal.* **2018**, *1*, 12.
- [115] a) Z. C. Litman, Y. Wang, H. Zhao, J. F. Hartwig, *Nature* **2018**, *560*, 355; b) M. Saifuddin, C. Guo, L. Biewenga, T. Saravanan, S. J. Charnock, G. J. Poelarends, *ACS catalysis* **2020**, *10*, 2522; c) S. Schmidt, K. Castiglione, R. Kourist, *Chem. Eur. J.* **2018**, *24*, 1755.
- [116] S. Dutta, N. Kumari, S. Dubbu, S. W. Jang, A. Kumar, H. Ohtsu, J. Kim, S. H. Cho, M. Kawano, I. S. Lee, *Angew. Chem. Int. Ed.* **2020**, *59*, 3416; *Angew. Chem.* **2020**, *132*, 3444.
- [117] G. Rulli, N. Duangdee, K. Baer, W. Hummel, A. Berkessel, H. Gröger, *Angew. Chem. Int. Ed.* **2011**, *50*, 7944; *Angew. Chem.* **2011**, *123*, 8092.
- [118] H. Sato, W. Hummel, H. Gröger, *Angew. Chem. Int. Ed.* **2015**, *54*, 4488; *Angew. Chem.* **2015**, *127*, 4570.
- [119] F. A. Plamper, W. Richtering, *Acc. Chem. Res.* **2017**, *50*, 131.
- [120] S. Schneider, F. Jung, O. Mergel, J. Lammertz, A. C. Nickel, T. Caumanns, A. Mhamdi, J. Mayer, A. Mitsos, F. A. Plamper, *Polym. Chem.* **2020**, *11*, 315.
- [121] W. Xu, A. Rudov, A. Oppermann, S. Wypysek, M. Kather, R. Schroeder, W. Richtering, I. I. Potemkin, D. Wöll, A. Pich, *Angew. Chem. Int. Ed.* **2020**, *59*, 1248; *Angew. Chem.* **2020**, *132*, 1264.
- [122] A. J. D. Krüger, J. Köhler, S. Cichosz, J. C. Rose, D. B. Gehlen, T. Haraszti, M. Möller, L. de Laporte, *Chem. Commun.* **2018**, *54*, 6943.
- [123] A. C. Nickel, A. Scotti, J. E. Houston, T. Ito, J. Crassous, J. S. Pedersen, W. Richtering, *Nano Lett.* **2019**, *19*, 8161.
- [124] A. Scotti, S. Bochenek, M. Brugnoni, M. A. Fernandez-Rodriguez, M. F. Schulte, J. E. Houston, A. P. H. Gelissen, I. I. Potemkin, L. Isa, W. Richtering, *Nat. Commun.* **2019**, *10*, 1418.

- [125] I. Berndt, J. S. Pedersen, W. Richtering, *Angew. Chem. Int. Ed.* **2006**, *45*, 1737; *Angew. Chem.* **2006**, *118*, 1769.
- [126] A. A. Polotsky, F. A. Plamper, O. V. Borisov, *Macromolecules* **2013**, *46*, 8702.
- [127] A. V. Dolgoplov, K. N. Graftskaia, P. V. Bovsunovskaya, E. R. Melnikova, D. A. Ivanov, A. Pich, X. Zhu, M. Möller, *Photochem. Photobiol. Sci.* **2019**, *18*, 1709.
- [128] L. Hu, Y. Wan, Q. Zhang, M. J. Serpe, *Adv. Funct. Mater.* **2020**, *30*, 1903471.
- [129] W. Xu, A. A. Rudov, R. Schroeder, I. V. Portnov, W. Richtering, I. I. Potemkin, A. Pich, *Biomacromolecules* **2019**, *20*, 1578.
- [130] R. A. Meurer, S. Kemper, S. Knopp, T. Eichert, F. Jakob, H. E. Goldbach, U. Schwaneberg, A. Pich, *Angew. Chem. Int. Ed.* **2017**, *56*, 7380; *Angew. Chem.* **2017**, *129*, 7486.
- [131] D. Kleinschmidt, M. S. Fernandes, M. Mork, A. A. Meyer, J. Krischel, M. V. Anakhov, R. A. Gumerov, I. I. Potemkin, M. Rueping, A. Pich, *J. Colloid Interface Sci.* **2020**, *559*, 76.
- [132] Z. Zou, E. Gau, I. El-Awaad, F. Jakob, A. Pich, U. Schwaneberg, *Bioconj. Chem.* **2019**, *30*, 2859.
- [133] M. Faulde, E. Siemes, D. Wöll, A. Jupke, *Polymers* **2018**, *10*.
- [134] H. Khanam, Shamsuzzaman, *Eur. J. Med. Chem.* **2015**, *97*, 483.
- [135] R. C. Fuson, J. H. van Campen, D. E. Wolf, *J. Am. Chem. Soc.* **1938**, *60*, 2269.
- [136] W. E. Ross, R. C. Fuson, *J. Am. Chem. Soc.* **1937**, *59*, 1508.
- [137] U. Herber, J. Moegling, R. Siris, A. Hoffmann, P. Mayer, C. Göbel, C. Lochenie, B. Weber, S. Herres-Pawlis, *Z. Anorg. Allg. Chem.* **2018**, *644*, 1576.
- [138] S. E. Howson, L. E. N. Allan, N. P. Chmel, G. J. Clarkson, R. J. Deeth, A. D. Faulkner, D. H. Simpson, P. Scott, *Dalton Trans.* **2011**, 10416.
- [139] J. Zhang, A. Li, T. S. A. Hor, *Dalton Trans.* **2009**, 9327.
- [140] Maria-Fatima Tepedino, *Dissertation*, Friedrich-Alexander-Universität, Erlangen-Nürnberg, **2012**.
- [141] Fabian Thomas, *Masterarbeit*, RWTH Aachen University, Aachen, **2017**.
- [142] R. G. Anderson, B. M. Jett, A. McNally, *Angew. Chem. Int. Ed.* **2018**, *57*, 12514; *Angew. Chem.* **2018**, *130*, 12694.
- [143] R. Dolewski, M. Hilton, A. McNally, *Synlett* **2018**, *29*, 8.
- [144] M. C. Hilton, R. D. Dolewski, A. McNally, *J. Am. Chem. Soc.* **2016**, *138*, 13806.
- [145] J. L. Koniarczyk, D. Hesk, A. Overgard, I. W. Davies, A. McNally, *J. Am. Chem. Soc.* **2018**, *140*, 1990.
- [146] C. Patel, M. Mohnike, M. C. Hilton, A. McNally, *Org. Lett.* **2018**, *20*, 2607.
- [147] L. Yang, D. R. Powell, R. P. Houser, *Dalton Trans.* **2007**, 955.
- [148] G. R. Fulmer, A. J. M. Miller, N. H. Sherden, H. E. Gottlieb, A. Nudelman, B. M. Stoltz, J. E. Bercaw, K. I. Goldberg, *Organometallics* **2010**, *29*, 2176.
- [149] M. Wagner, C. Limberg, T. Tietz, *Chem. Eur. J.* **2009**, *15*, 5567.
- [150] A. Hoffmann, S. Herres-Pawlis, *Phys. Chem. Chem. Phys.* **2016**, *18*, 6430.
- [151] P. Comba, D. Faltermeier, S. Krieg, B. Martin, G. Rajaraman, *Dalton Trans.* **2020**, 2888.
- [152] C. Riplinger, F. Neese, *J. Chem. Phys.* **2013**, *138*, 34106.
- [153] C. Riplinger, B. Sandhoefer, A. Hansen, F. Neese, *J. Chem. Phys.* **2013**, *139*, 134101.
- [154] a) A. Hoffmann, M. Rohrmüller, A. Jesser, I. dos Santos Vieira, W. G. Schmidt, S. Herres-Pawlis, *J. Comput. Chem.* **2014**, *35*, 2146; b) A. Jesser, M. Rohrmüller, W. G. Schmidt, S. Herres-Pawlis, *J. Comput. Chem.* **2014**, *35*, 1.
- [155] a) S. Dapprich, G. Frenking, *J. Phys. Chem.* **1995**, *99*, 9352; b) K. Kitaura, K. Morokuma, *Int. J. Quantum Chem.* **1976**, *10*, 325; c) T. Ziegler, A. Rauk, *Theoret. Chim. Acta* **1977**, *46*, 1.
- [156] E. Ramos-Cordoba, V. Postils, P. Salvador, *J. Chem. Theory. Comput.* **2015**, *11*, 1501.
- [157] D. A. Evans, M. M. Faul, M. T. Bilodeau, *J. Org. Chem.* **1991**, *56*, 6744.
- [158] F. Thomas, M. Oster, F. Schön, K. Göbgen, B. Amarouch, D. Steden, A. Hoffmann, S. Herres-Pawlis, *Dalton Trans.* **2021**, *50*, 6444-6462.

- [159] L. Chen, X.-J. Su, J. W. Jurss, *Organometallics* **2018**, 37, 4535.
- [160] K. Keisers, H. M. Hüppe, L. Iffland-Mühlhaus, A. Hoffmann, C. Göbel, U.-P. Apfel, B. Weber, S. Herres-Pawlis, *Inorg. Chem.* **2020**, 20, 15343.
- [161] a) R. S. Foster, H. Jakobi, J. P. A. Harrity, *Org. Lett.* **2012**, 14, 4858; b) D. S. Laitar, C. J. N. Mathison, W. M. Davis, J. P. Sadighi, *Inorg. Chem.* **2003**, 42, 7354; c) X. Zhou, Z. Jiang, L. Xue, P. Lu, Y. Wang, *Eur. J. Org. Chem.* **2015**, 2015, 5789.
- [162] T. S. Wong, F. H. Arnold, U. Schwaneberg, *Biotechnol. Bioeng.* **2004**, 85, 351.
- [163] M. A. S. Mertens, F. Thomas, M. Nöth, J. Moegling, I. El-Awaad, D. F. Sauer, G. V. Dhoke, W. Xu, A. Pich, S. Herres-Pawlis, U. Schwaneberg, *Eur. J. Org. Chem.* **2019**, 2019, 6341.
- [164] D. Zhu, Z. Wu, B. Luo, Y. Du, P. Liu, Y. Chen, Y. Hu, P. Huang, S. Wen, *Org. Lett.* **2018**, 20, 4815.
- [165] G. Li, H. Nakamura, *Angew. Chem. Int. Ed.* **2016**, 55, 6758; *Angew. Chem.* **2016**, 128, 6870.
- [166] P. Brunel, J. Monot, C. E. Kefalidis, L. Maron, B. Martin-Vaca, D. Bourissou, *ACS Catal.* **2017**, 7, 2652.
- [167] A. R. Hamann, C. de Kock, P. J. Smith, W. A. L. van Otterlo, M. A. L. Blackie, *Bioorg. Med. Chem. Lett.* **2014**, 24, 5466.
- [168] T. Sugiishi, A. Kimura, H. Nakamura, *J. Am. Chem. Soc.* **2010**, 132, 5332.
- [169] U. P. Singh, P. Babbar, B. Hassler, H. Nishiyama, H. Brunner, *J. Mol. Catal. A: Chem.* **2002**, 185, 33.
- [170] G. J. Kubas, B. Monzyk, A. L. Crumbliss, *Inorganic Synthesis* **1990**, 90.
- [171] A. M. Wright, B. J. Irving, G. Wu, A. J. H. M. Meijer, T. W. Hayton, *Angew. Chem. Int. Ed.* **2015**, 54, 3088; *Angew. Chem.* **2015**, 127, 3131.
- [172] H.-D. Hardt, *Z. Anorg. Allg. Chem.* **1959**, 301, 87.
- [173] P. Liebhäuser, *Dissertation*, RWTH Aachen University, Aachen, **2018**.
- [174] B. J. Hathaway, D. G. Holah, A. E. Underhill, *J. Chem. Soc.* **1962**, 2444.
- [175] S. W. Kwok, J. R. Fotsing, R. J. Fraser, V. O. Rodionov, V. V. Folkin, *Org. Lett.* **2010**, 19, 4217.
- [176] D. S. Laitar, C. J. N. Mathison, W. M. Davis, J. P. Sadighi, *Inorg. Chem.* **2003**, 42, 7354.
- [177] S. Bräse, C. Gil, K. Knepper, V. Zimmermann, *Angew. Chem. Int. Ed.* **2005**, 44, 5188; *Angew. Chem.* **2005**, 117, 5320.
- [178] J. Liu, K. Wu, T. Shen, Y. Liang, M. Zou, Y. Zhu, X. Li, X. Li, N. Jiao, *Chem. Eur. J.* **2017**, 23, 563.
- [179] D. Macikenas, E. Skrzypczak-Jankun, J. D. Protasiewicz, *J. Am. Chem. Soc.* **1999**, 121, 7164.
- [180] Y. Yamada, T. Yamamoto, M. Okawara, *Chem. Lett.* **1975**, 4, 361.
- [181] T. J. Morin, S. Wanniarachchi, C. Gwengo, V. Makura, H. M. Tatlock, S. V. Lindeman, B. Bennett, G. J. Long, F. Grandjean, J. R. Gardinier, *Dalton Trans.* **2011**, 8024.
- [182] P. Govindaswamy, Y. A. Mozharivskyj, M. R. Kollipara, *J. Organomet. Chem.* **2004**, 689, 3265.
- [183] S. Trofimenko, J. C. Calabrese, J. S. Thompson, *Inorg. Chem.* **1987**, 26, 1507.
- [184] D. D. LeCloux, C. J. Tokar, M. Osawa, R. P. Houser, M. C. Keyes, W. B. Tolman, *Organometallics* **1994**, 13, 2855.
- [185] H. Fuchida, S. Tabata, N. Shindo, I. Takashima, Q. Leng, Y. Hatsuyama, I. Hamachi, A. Ojida, *Bull. Chem. Soc. Jpn.* **2015**, 88, 784.
- [186] D. Schäfer, F. Fink, D. Kleinschmidt, K. Keisers, F. Thomas, A. Hoffmann, A. Pich, S. Herres-Pawlis, *Chem. Commun.* **2020**, 56, 5601.
- [187] J. Leonard, B. Lygo, G. Procter, *Praxis der organischen Chemie; Ein Handbuch*, VCH, Weinheim, **1996**.
- [188] D. F. Evans, *J. Chem. Soc.* **1959**, 2003.

- [189] D. F. Evans, D. A. Jakubovic, *J. Chem. Soc., Dalton Trans.* **1988**, 2927.
- [190] R. S. J. Löllinger, *J. Chem. Edu.* **1972**, 49, 646.
- [191] Bruker AXS Inc., SMART (Version 5.631), SAINT (Version 8.37A) and SADABS (Version 2008/1), Madison, Wisconsin, USA, 2008.
- [192] *X-Area Pilatus3_SV 1.31.131.0*, STOE, **2017**.
- [193] *X-Area Integrate 1.71.0.0*, STOE, **2016**.
- [194] *X-Area Precipe 1.33.0.0*, STOE, **2015**.
- [195] *X-Area LANA 1.74.4.0*, STOE, **2017**.
- [196] Bruker, *Xprep V5.1*, Bruker AXS Inc., Madison, Wisconsin, USA, **1997**.
- [197] G. M. Sheldrick, *Acta Crystallogr. Sect. A* **2008**, 64, 112.
- [198] G. M. Sheldrick, *Acta Crystallogr. Sect. A* **2015**, 71, 3.
- [199] G. M. Sheldrick, *Acta Crystallogr. Sect. C* **2015**, 71, 3.
- [200] C. B. Hübschle, G. M. Sheldrick, B. Dittrich, *J. Appl. Crystallogr.* **2011**, 44, 1281.
- [201] S. Stoll, A. Schweiger, *J. Magn. Reson.* **2006**, 178, 42.
- [202] Gaussian 16, Revision B.01, M. J. Frisch, G. W. Trucks, H. B. Schlegel, G. E. Scuseria, M. A. Robb, J. R. Cheeseman, G. Scalmani, V. Barone, G. A. Petersson, H. Nakatsuji, X. Li, M. Caricato, A. V. Marenich, J. Bloino, B. G. Janesko, R. Gomperts, B. Mennucci, H. P. Hratchian, J. V. Ortiz, A. F. Izmaylov, J. L. Sonnenberg, D. Williams-Young, F. Ding, F. Lipparini, F. Egidi, J. Goings, B. Peng, A. Petrone, T. Henderson, D. Ranasinghe, V. G. Zakrzewski, J. Gao, N. Rega, G. Zheng, W. Liang, M. Hada, M. Ehara, K. Toyota, R. Fukuda, J. Hasegawa, M. Ishida, T. Nakajima, Y. Honda, O. Kitao, H. Nakai, T. Vreven, K. Throssell, J. A. Montgomery, Jr., J. E. Peralta, F. Ogliaro, M. J. Bearpark, J. J. Heyd, E. N. Brothers, K. N. Kudin, V. N. Staroverov, T. A. Keith, R. Kobayashi, J. Normand, K. Raghavachari, A. P. Rendell, J. C. Burant, S. S. Iyengar, J. Tomasi, M. Cossi, J. M. Millam, M. Klene, C. Adamo, R. Cammi, J. W. Ochterski, R. L. Martin, K. Morokuma, O. Farkas, J. B. Foresman, and D. J. Fox, Gaussian, Inc., Wallingford CT, 2016.
- [203] a) J. Tao, J. P. Perdew, V. N. Staroverov, G. E. Scuseria, *Phys. Rev. Lett.* **2003**, 91, 146401; b) V. N. Staroverov, G. E. Scuseria, J. Tao, J. P. Perdew, *J. Chem. Phys.* **2003**, 119, 12129; *J. Chem. Phys.*, **2004**, 121, 11507.
- [204] a) F. Weigend, R. Ahlrichs, *Phys. Chem. Chem. Phys.* **2005**, 7, 3297; b) A. Schäfer, C. Huber, R. Ahlrichs, *J. Chem. Phys.* **1994**, 100, 5829; c) K. Eichkorn, F. Weigend, O. Treutler, R. Ahlrichs, *Theor. Chem. Acc.* **1997**, 97, 119.
- [205] a) E. D. Glendening, C. R. Landis, F. Weinhold, *J. Comput. Chem.* **2013**, 34, 1429; b) F. Weinhold and C. Landis, *Valency and Bonding – A Natural Bond Orbital Donor–Acceptor Perspective*, Cambridge University Press, New York **2005**; c) E. D. Glendening, J. K. Badenhoop, A. E. Reed, J. E. Carpenter, J. A. Bohmann, C. M. Morales, C. R. Landis, F. Weinhold, NBO 6.0, Theoretical Chemistry Institute, University of Wisconsin: Madison **2013**, available at: www.chem.wisc.edu/nbo6, accessed Feb. 1, 2013.
- [206] a) S. Grimme, S. Ehrlich, L. Goerigk, *J. Comput. Chem.* **2011**, 32, 1456; b) L. Goerigk, S. Grimme, *Phys. Chem. Chem. Phys.* **2011**, 13, 6670; c) For TPSSh, the values of the original paper have been substituted by the corrected values kindly provided by S. Grimme as private communication and published in: A. Hoffmann, R. Grunzke, S. Herres-Pawlis, *J. Comput. Chem.* **2014**, 35, 1943.
- [207] a) N. B. Balabanov, K. A. Peterson, *J. Chem. Phys.* **2005**, 123, 64107; b) N. B. Balabanov, K. A. Peterson, *J. Chem. Phys.* **2006**, 125, 74110; c) T. H. Dunning, *J. Chem. Phys.* **1989**, 90, 1007; d) D. E. Woon, T. H. Dunning, *J. Chem. Phys.* **1993**, 98, 1358.
- [208] a) Y. Guo, C. Riplinger, U. Becker, D. G. Liakos, Y. Minenkov, L. Cavallo, F. Neese, *J. Chem. Phys.* **2018**, 148, 11101; b) F. Neese, *WIREs Comput Mol Sci.* **2012**, 2, 73; c) F. Neese, *WIREs Comput Mol Sci.* **2018**, 8, 33.

- [209] a) I. S. Gorelsky, AOMix: Program for Molecular Orbital Analysis, version 6.80, University of Ottawa, 2013, <http://www.sg-chem.net/>; b) I. S. Gorelsky, A. B. P. Lever, *J. Organomet. Chem.* **2001**, 525, 187.
- [210] P. Salvador, E. Ramos-Cordoba, Program APOST-3D, Version 2.00, Girona, 2014.
- [211] A. L. Spek, PLATON, A Multipurpose Crystallographic Tool, Utrecht University, Utrecht (The Netherlands) 2008.
- [212] A. L. Spek, *Acta crystallographica. Section D, Biological crystallography* **2009**, 65, 148.

8. Appendix

8.1 Crystallographic data

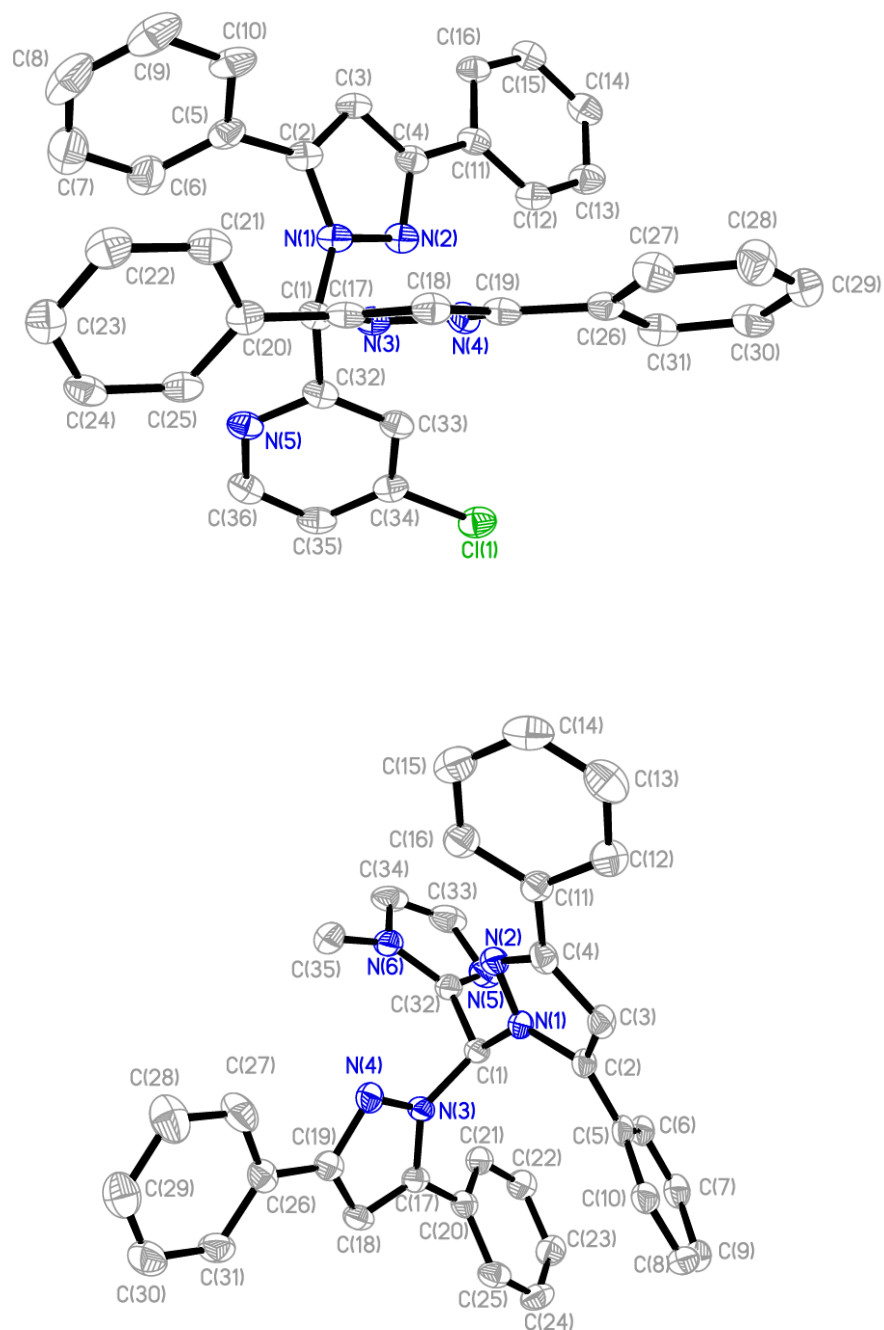


Figure 51. Molecular structures of **L2** (top) and **L3** (bottom). All hydrogen atoms are omitted for clarity. Displacement ellipsoids represent the 50% of probability level.

Table 51. Crystallographic data of **L2** and **L3**.

	L2	L3
Empirical formula	C ₃₆ H ₂₆ ClN ₅	C ₃₅ H ₂₈ N ₆
Formula weight [g mol ⁻¹]	564.07	532.63
Crystal size [mm]	0.33 x 0.26 x 0.17	0.32 x 0.29 x 0.28
<i>T</i> [K]	100	100
Crystal system	triclinic	monoclinic
Space group	P $\bar{1}$	P2 ₁ /c
<i>a</i> [Å]	11.375(2)	11.707(4)
<i>b</i> [Å]	11.866(2)	21.831(7)
<i>c</i> [Å]	12.420(3)	11.757(4)
α [°]	107.92(3)	90
β [°]	106.74(3)	113.371(7)
γ [°]	101.25(3)	90
<i>V</i> [Å ³]	1451.3(6)	2758.3(15)
<i>Z</i>	2	4
$\rho_{\text{caclcd.}}$ [g cm ⁻³]	1.291	1.283
μ [mm ⁻¹]	0.166	0.078
λ [Å]	0.71073	0.71073
F(000)	588	1120
<i>hkl</i> range	±13, ±14, ±14	±14, ±26, ±14
Reflections collected	16224	25280
Independent reflections	5328	4760
<i>R</i> _{int}	0.0940	0.1257
Number of parameters	379	371
<i>R</i> ₁ [<i>I</i> ≥ 2σ(<i>I</i>)]	0.0600	0.0506
<i>wR</i> ₂ (all data)	0.1606	0.1157
Goodness-of-fit	1.008	0.792
Largest diff. peak, hole [eÅ ⁻³]	0.385, -0.368	0.221, -0.255

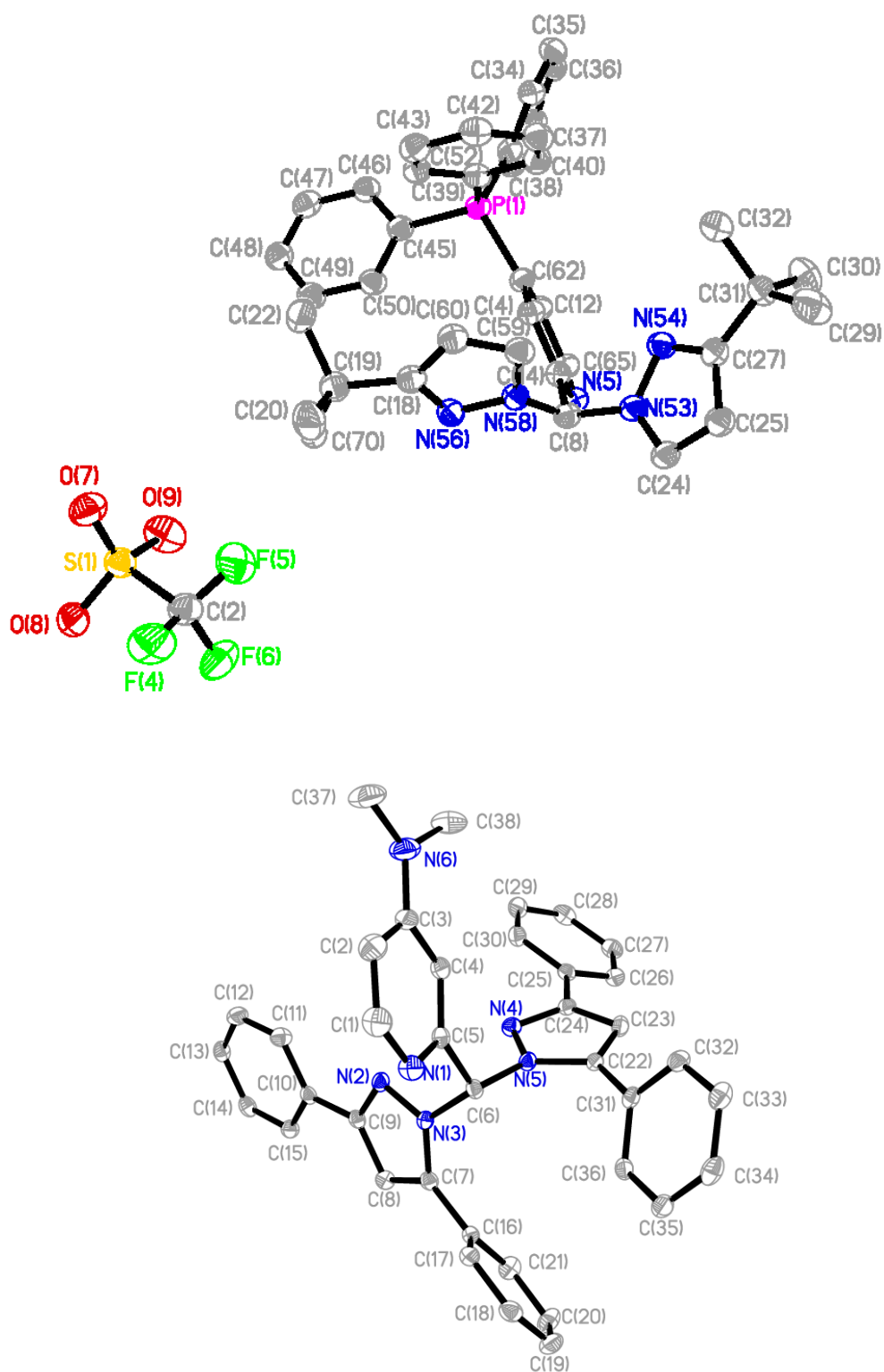


Figure 52. Molecular structures of **L18** (top) and **L20** (bottom). All hydrogen atoms are omitted for clarity. Displacement ellipsoids represent the 50% of probability level.

Table 52. Crystallographic data of **L18** and **L20**.

	L18	L20
Empirical formula	C ₃₉ H ₄₁ F ₃ N ₅ O ₃ PS	C ₃₈ H ₃₂ N ₆
Formula weight [g mol ⁻¹]	747.80	572.69
Crystal size [mm]	0.17 x 0.16 x 0.15	0.19 x 0.18 x 0.25
<i>T</i> [K]	100	100
Crystal system	triclinic	Monoclinic
Space group	P $\bar{1}$	P2 ₁ /n
<i>a</i> [Å]	10.172(2)	12.934(2)
<i>b</i> [Å]	13.112(3)	18.103(4)
<i>c</i> [Å]	14.465(3)	13.275(3)
α [°]	86.31(3)	90
β [°]	72.94(3)	102.30(3)
γ [°]	85.16(3)	90
<i>V</i> [Å ³]	1836.2(7)	3036.8(11)
<i>Z</i>	2	4
$\rho_{\text{caclcd.}}$ [g cm ⁻³]	1.353	1.253
μ [mm ⁻¹]	0.192	0.076
λ [Å]	0.71073	0.71073
F(000)	784	1208
<i>hkl</i> range	±15, -14 to 20, -19 to 22	-16 to 11, -23 to 22, ±16
Reflections collected	29343	25906
Independent reflections	13455	6595
<i>R</i> _{int.}	0.0334	0.0353
Number of parameters	476	399
<i>R</i> ₁ [<i>I</i> ≥ 2σ(<i>I</i>)]	0.0677	0.0407
<i>wR</i> ₂ (all data)	0.2012	0.0996
Goodness-of-fit	0.998	1.001
Extinction coefficient	0.040(3)	-
Largest diff. peak, hole [eÅ ⁻³]	1.007, -0.669	0.363, -0.261

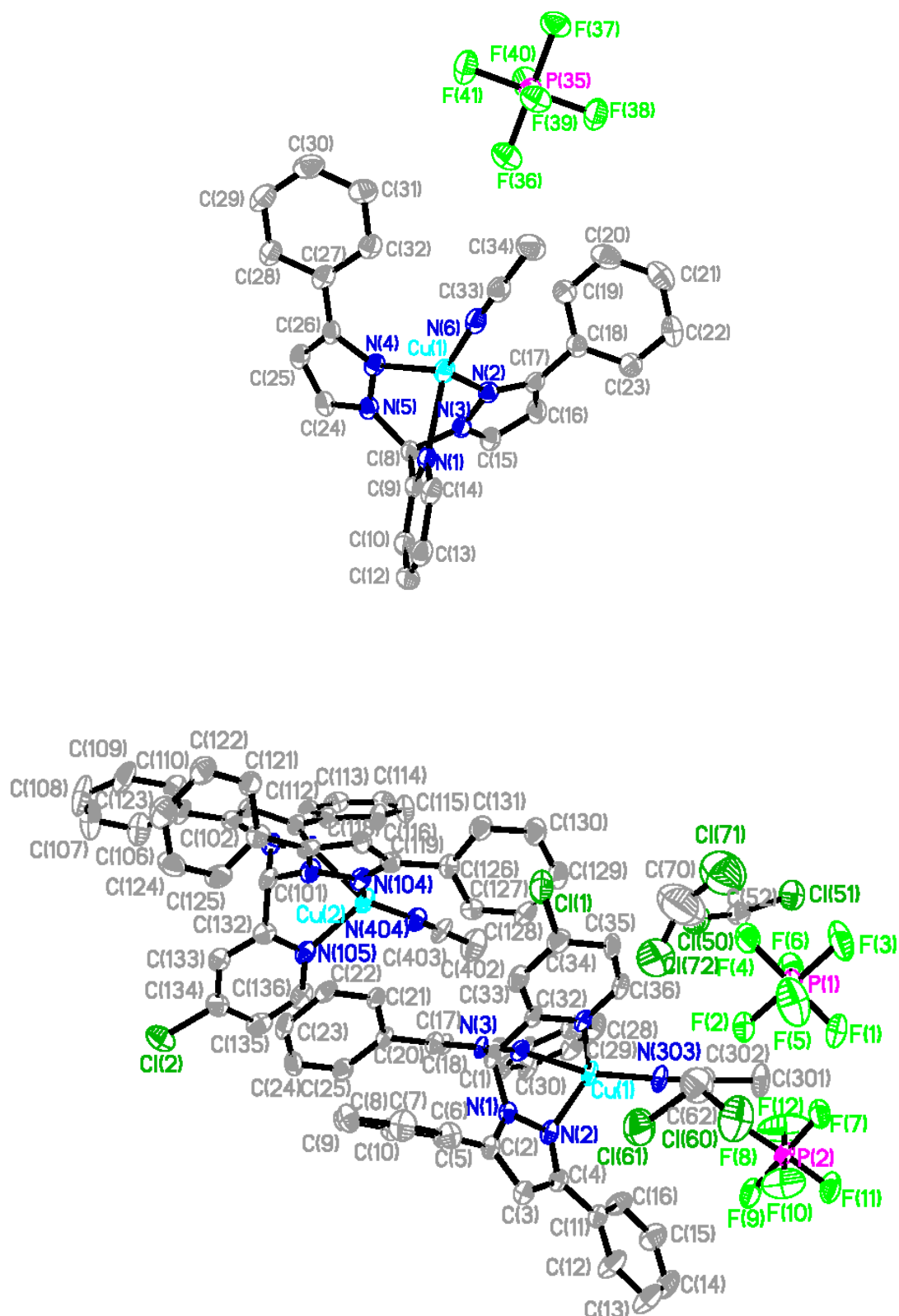


Figure 53. Molecular structures of **C1** (top) and **C2 · 1 DCM** (bottom). All hydrogen atoms are omitted for clarity. Displacement ellipsoids represent the 50% of probability level.

Table 53. Crystallographic data of **C1** and **C2**.

	C1	C2 · 1 DCM
Empirical formula	C ₂₆ H ₂₂ CuF ₆ N ₆ P	C ₇₉ H ₆₄ Cl ₈ Cu ₂ F ₁₂ N ₁₂ P ₂
Formula weight [g mol ⁻¹]	627.00	1882.04
Crystal size [mm]	0.44 x 0.33 x 0.22	0.21 x 0.13 x 0.08
<i>T</i> [K]	100	100
Crystal system	monoclinic	triclinic
Space group	P2 ₁ /n	P $\bar{1}$
<i>a</i> [Å]	12.778(3)	11.931(2)
<i>b</i> [Å]	13.899(3)	15.931(3)
<i>c</i> [Å]	16.116(3)	21.581(4)
α [°]	90	89.59(3)
β [°]	112.11(3)	76.64(3)
γ [°]	90	87.33(3)
<i>V</i> [Å ³]	2651.8(11)	3986.6(15)
<i>Z</i>	4	2
$\rho_{\text{caclcd.}}$ [g cm ⁻³]	1.570	1.568
μ [mm ⁻¹]	0.955	4.205
λ [Å]	0.71073	1.54186
F(000)	1272	1908
<i>hkl</i> range	±15, ±16, ±19	-12 ≤ <i>h</i> ≤ 14, -11 ≤ <i>k</i> ≤ 19, -26 ≤ <i>l</i> ≤ 25
Reflections collected	28696	23297
Independent reflections	4884	12881
<i>R</i> _{int}	0.0867	0.1012
Number of parameters	362	1038
<i>R</i> ₁ [<i>I</i> ≥ 2σ(<i>I</i>)]	0.0448	0.0823
<i>wR</i> ₂ (all data)	0.1195	0.2393
Goodness-of-fit	1.034	0.978
Largest diff. peak, hole [eÅ ⁻³]	0.660, -0.507	0.881, -1.168

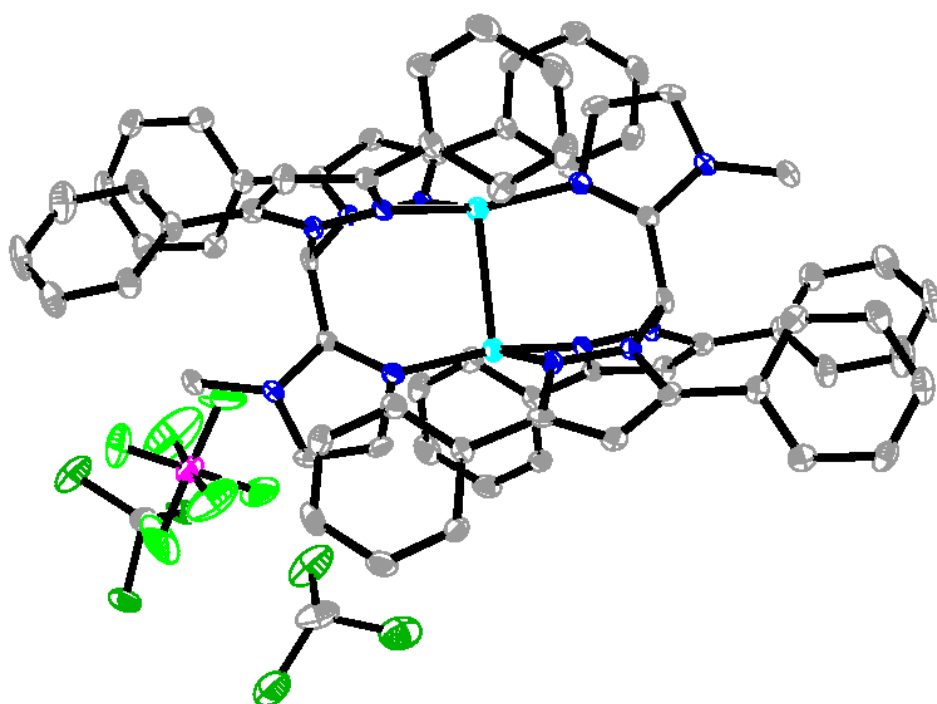
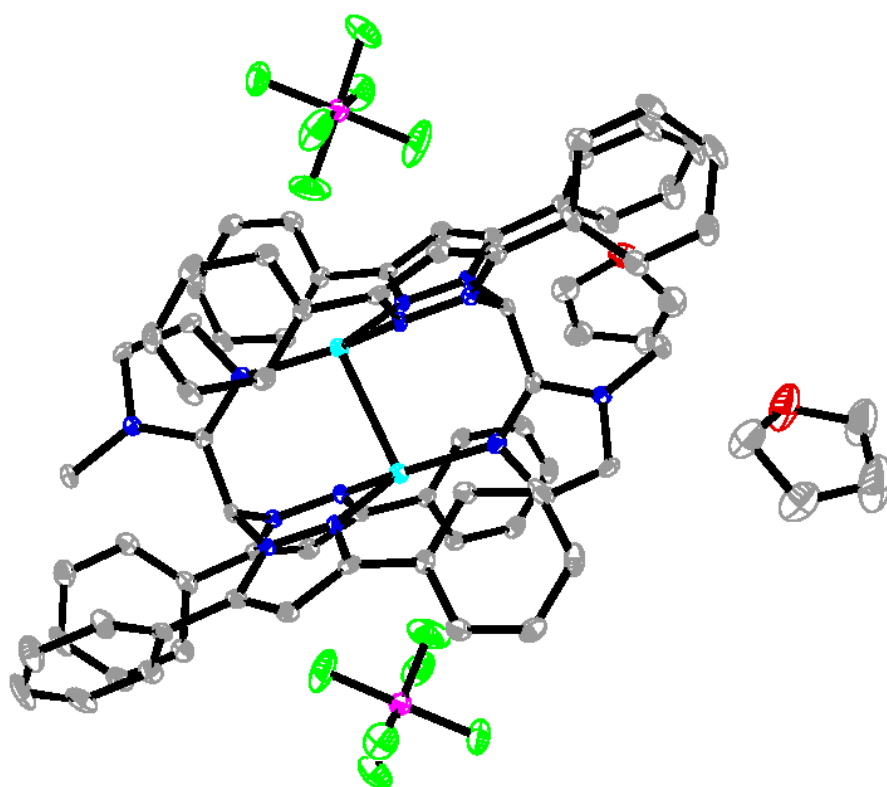


Figure 54. Molecular structures of **C4 · 4 THF** (top) and **C4 · 4 CHCl₃** (bottom). All hydrogen atoms are omitted for clarity. Displacement ellipsoids represent the 50% of probability level. Numberation is given in Figure 55 on the asymmetric unit for clarity.

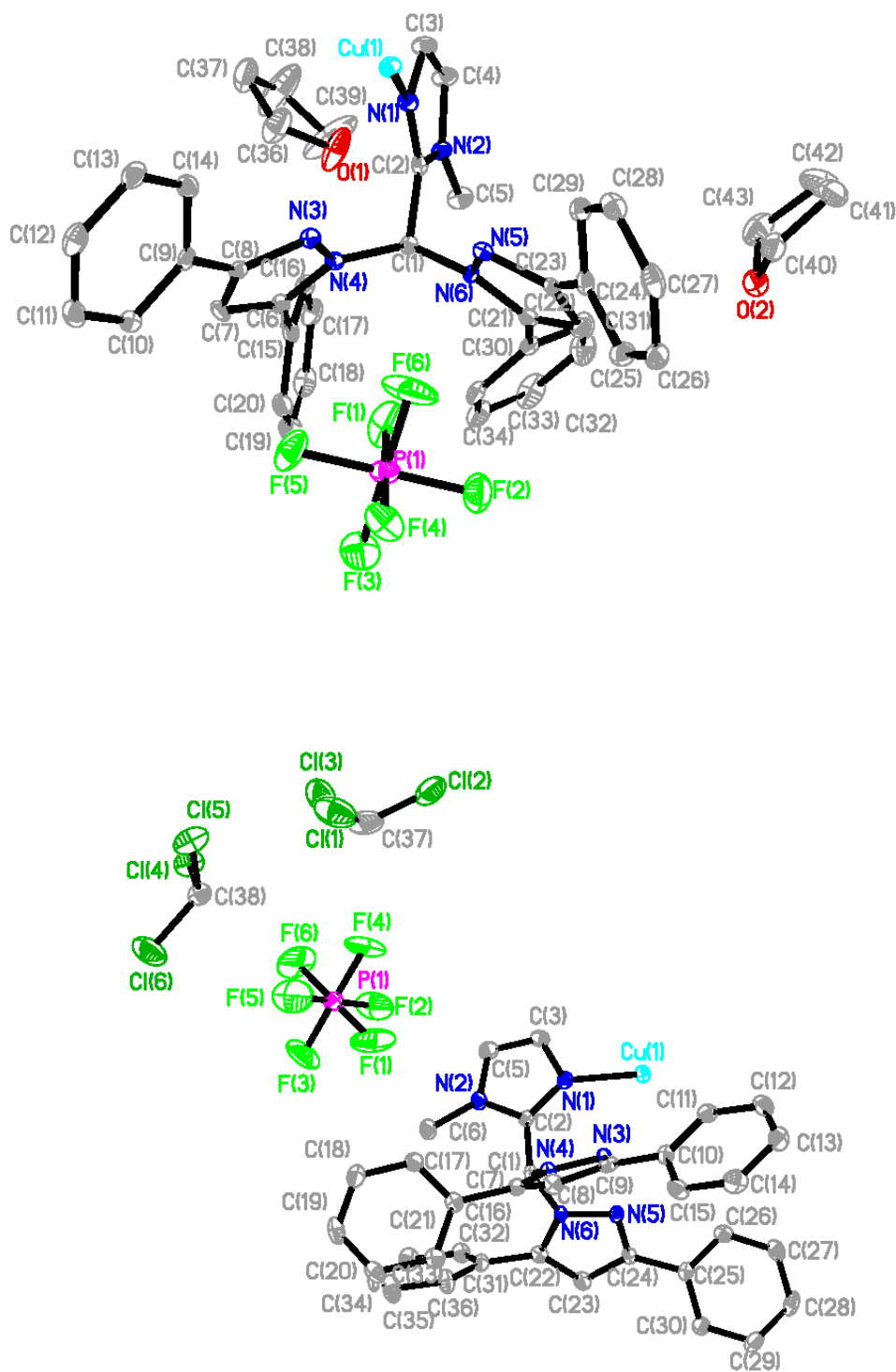


Figure 55. Molecular structures of the asymmetric unit **C4 · 4 THF** (top) and **C4 · 4 CHCl₃** (bottom). All hydrogen atoms are omitted for clarity. Displacement ellipsoids represent the 50% of probability level.

Table 54. Crystallographic data of **C4 · 4 CHCl₃** and **C4 · 4 THF**.

	C4 · 4 CHCl₃	C4 · 4 THF
Empirical formula	C ₇₄ H ₆₀ Cl ₁₂ Cu ₂ F ₁₂ N ₁₂ P ₂	C ₈₆ H ₈₈ Cu ₂ F ₁₂ N ₁₂ O ₄ P ₂
Formula weight [g mol ⁻¹]	1959.76	1770.70
Crystal size [mm]	0.14 x 0.12 x 0.10	0.13 x 0.11 x 0.09
<i>T</i> [K]	100	100
Crystal system	monoclinic	triclinic
Space group	P2 ₁ /c	P $\bar{1}$
<i>a</i> [Å]	11.877(2)	11.105(2)
<i>b</i> [Å]	18.917(4)	13.053(3)
<i>c</i> [Å]	18.418(4)	15.834(3)
α [°]	90	108.78(3)
β [°]	96.14(3)	101.14(3)
γ [°]	90	105.51(3)
<i>V</i> [Å ³]	4114.2(15)	1993.4(8)
<i>Z</i>	2	1
$\rho_{\text{caclcd.}}$ [g cm ⁻³]	1.582	1.475
μ [mm ⁻¹]	1.024	0.663
λ [Å]	0.71073	0.71073
F(000)	1976	916
<i>hkl</i> range	-16 ≤ <i>h</i> ≤ 17, -20 ≤ <i>k</i> ≤ 27, ±27	-16 to 17, -20 to 13, -21 to 24
Reflections collected	50395	28039
Independent reflections	13673	14071
<i>R</i> _{int.}	0.0881	0.0713
Number of parameters	515	533
<i>R</i> ₁ [<i>I</i> ≥ 2σ(<i>I</i>)]	0.0503	0.0475
<i>wR</i> ₂ (all data)	0.1073	0.0917
Goodness-of-fit	0.811	0.803
Largest diff. peak, hole [eÅ ⁻³]	1.723, -1.130	0.748, -0.717

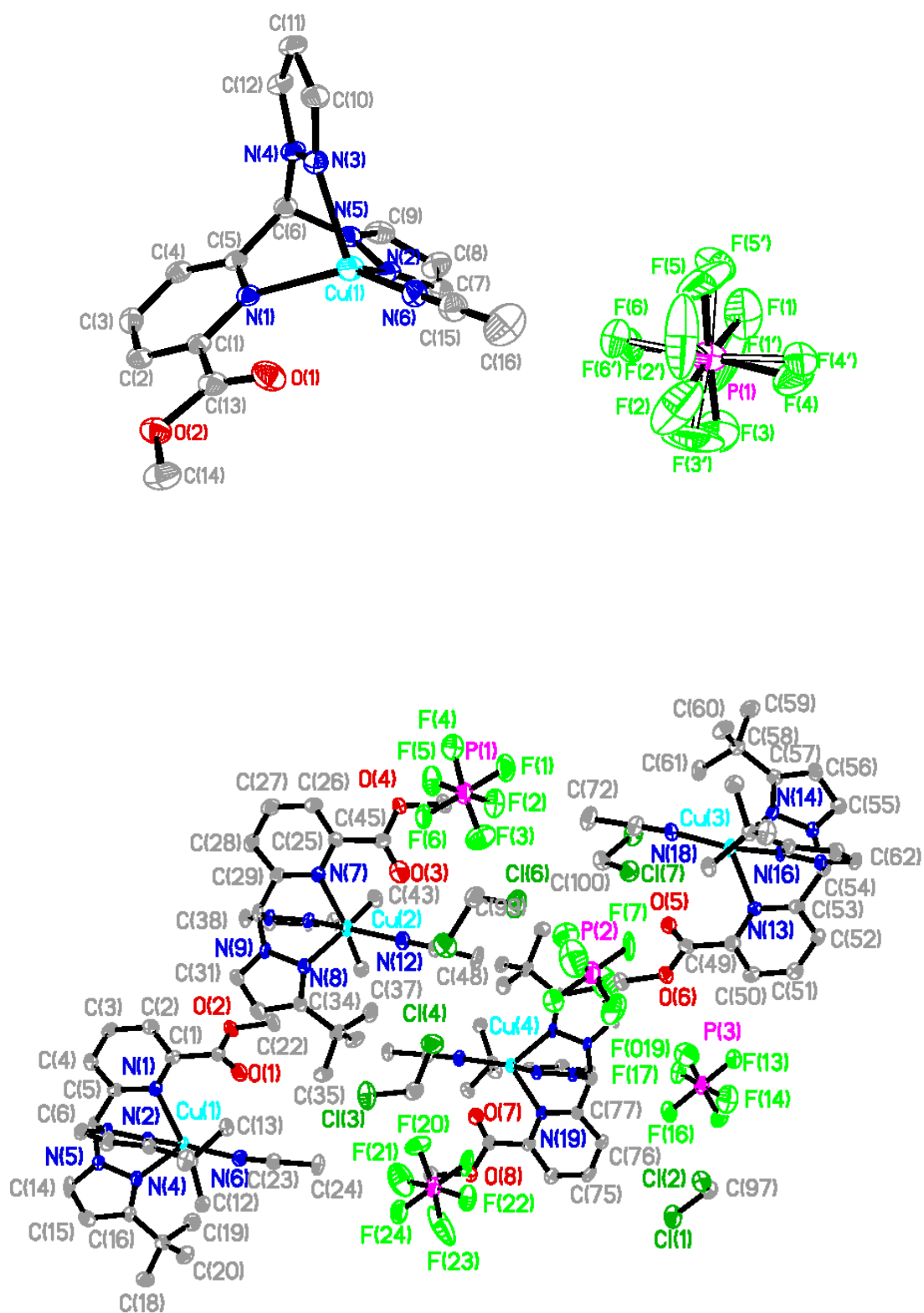


Figure 56. Molecular structures of **C9** (top) and **C10 · DCM** (bottom). All hydrogen atoms are omitted for clarity. Displacement ellipsoids represent the 50% of probability level.

Table 55. Crystallographic data of **C9** and **C10 · DCM**. In **C9** it was not possible to model the disordered solvent molecule CH₂Cl₂ in an adequate manner, and the data set was treated with the SQUEEZE routine as implemented in PLATON^{[211],[212]}.

	C9	C10 · DCM
Empirical formula	C ₁₆ H ₁₆ Cu ₁ F ₆ N ₆ PO ₂	C ₂₅ H ₃₄ Cl ₂ CuF ₆ N ₆ PO ₂
Formula weight [g mol ⁻¹]	532.86	729.99
Crystal size [mm]	0.21 x 0.16 x 0.09	0.31 x 0.12 x 0.10
<i>T</i> [K]	100	100
Crystal system	monoclinic	monoclinic
Space group	P2 ₁ /c	Pn
<i>a</i> [Å]	12.538(3)	15.545(1)
<i>b</i> [Å]	13.105(3)	26.281(3)
<i>c</i> [Å]	13.897(3)	16.685(2)
α [°]	90	90
β [°]	107.85(3)	111.65(1)
γ [°]	90	90
<i>V</i> [Å ³]	2173.6(8)	6335.6(10)
<i>Z</i>	4	8
$\rho_{\text{caclcd.}}$ [g cm ⁻³]	1.628	1.531
μ [mm ⁻¹]	1.155	0.978
λ [Å]	0.71073	0.71073
<i>F</i> (000)	1072	2992
<i>hkl</i> range	15 to 14, ± 15 , -16 to 15	± 21 , ± 36 , ± 22
Reflections collected	12977	93490
Independent reflections	4017	34423
<i>R</i> _{int.}	0.0299	0.0660
Number of parameters	346	1582
<i>R</i> ₁ [$ I \geq 2\sigma(I)$]	0.0563	0.0661
<i>wR</i> ₂ (all data)	0.1173	0.1885
Goodness-of-fit	1.172	1.054
Largest diff. peak, hole [eÅ ⁻³]	0.633, -0.460	1.721, -1.051

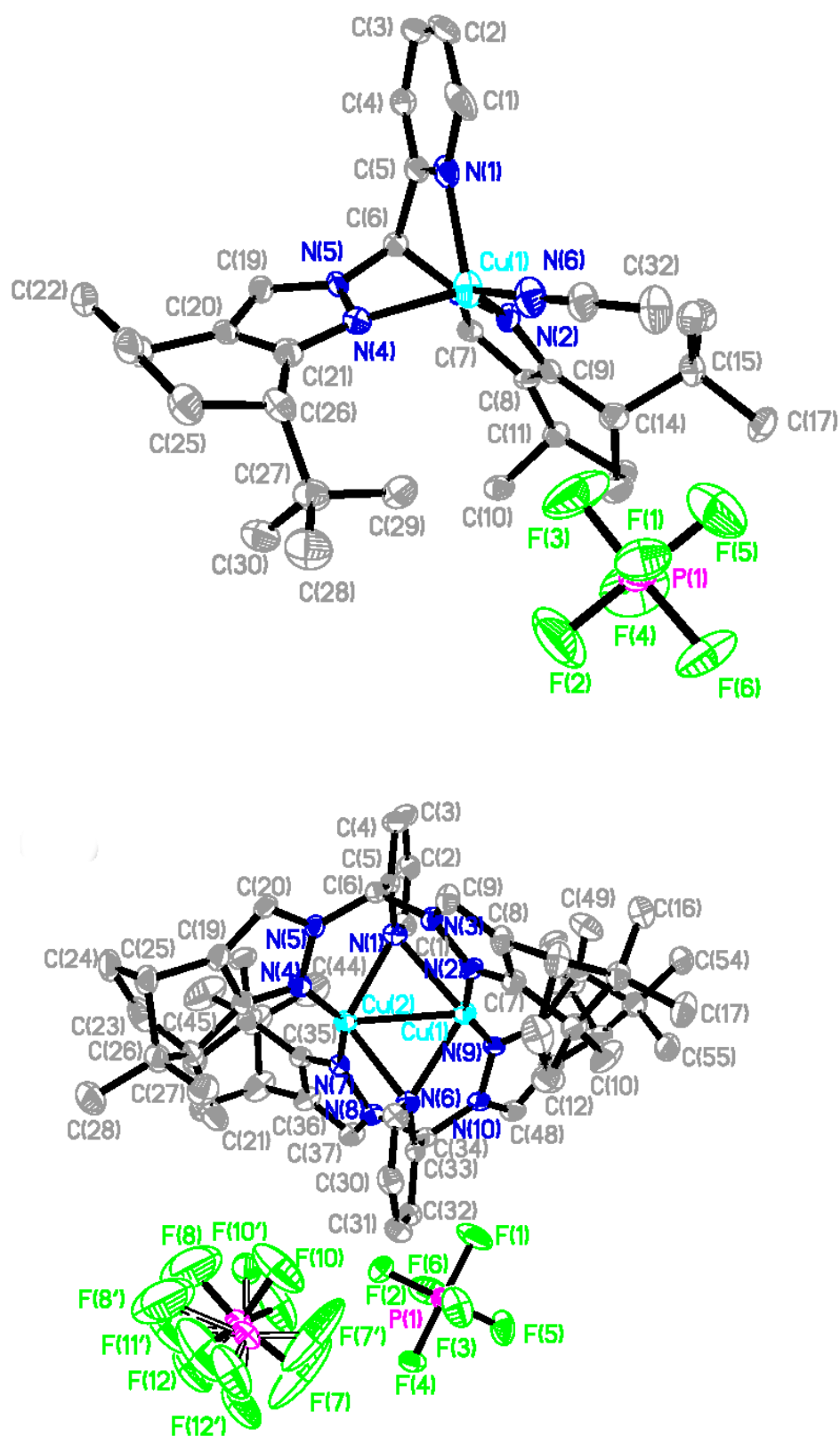


Figure 57. Molecular structures of **C11** (top) and **C13** (bottom). All hydrogen atoms are omitted for clarity. Displacement ellipsoids represent the 50% of probability level.

Table 56. Crystallographic data of **C11** and **C13**. In **C13** it was not possible to model the two disordered solvent molecule pentane in an adequate manner, and the data set was treated with the SQUEEZE routine as implemented in PLATON^{[211],[212]}.

	C11	C13
Empirical formula	C ₃₂ H ₄₆ CuF ₆ N ₆ P	C ₅₆ H ₇₀ Cu ₂ F ₁₂ N ₁₀ P ₂
Formula weight [g mol ⁻¹]	723.26	1300.24
Crystal size [mm]	0.15 x 0.07 x 0.04	0.36 x 0.26 x 0.18
<i>T</i> [K]	100	100
Crystal system	Monoclinic	Monoclinic
Space group	P2(1)	P2(1)
<i>a</i> [Å]	12.233(2)	11.2192(5)
<i>b</i> [Å]	8.024(16)	23.2860(11)
<i>c</i> [Å]	17.133(3)	13.0331(6)
α [°]	90	90
β [°]	98.89(3)	93.42(1)
γ [°]	90	90
<i>V</i> [Å ³]	1698.5(6)	3398.9(3)
<i>Z</i>	2	2
$\rho_{\text{caclcd.}}$ [g cm ⁻³]	1.414	1.270
μ [mm ⁻¹]	0.755	0.746
λ [Å]	0.71073	0.71073
F(000)	756	1344
<i>hkl</i> range	±16, ±11, ±24	±17, ±35, ±20
Reflections collected	26149	114764
Independent reflections	9866	26016
<i>R</i> _{int.}	0.0894	0.0579
Number of parameters	424	779
<i>R</i> ₁ [<i>I</i> ≥ 2σ(<i>I</i>)]	0.0638	0.0444
<i>wR</i> ₂ (all data)	0.1329	0.1202
Goodness-of-fit	1.038	1.065
Largest diff. peak, hole [eÅ ⁻³]	0.480, -0.549	0.744, -0.434

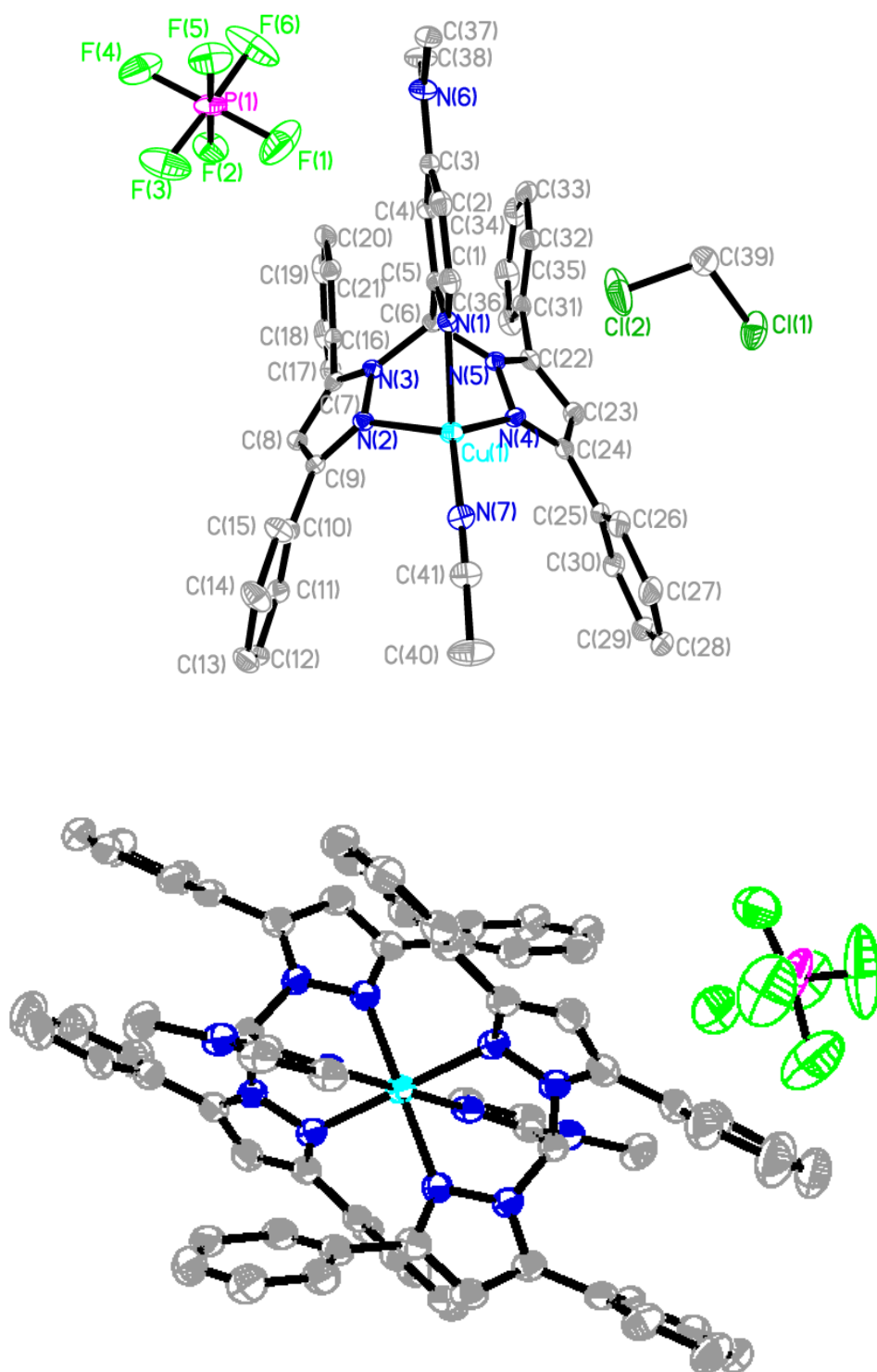


Figure 58. Molecular structures of **C19 · DCM** (top) and $[\text{Cu}\{\text{HC}(\text{Ph}_2\text{Ph})_2\text{Melm}\}_2](\text{PF}_6)$ (bottom). All hydrogen atoms are omitted for clarity. Displacement ellipsoids represent the 50% of probability level. Numeration is given in Figure 59 on the asymmetric unit for clarity.

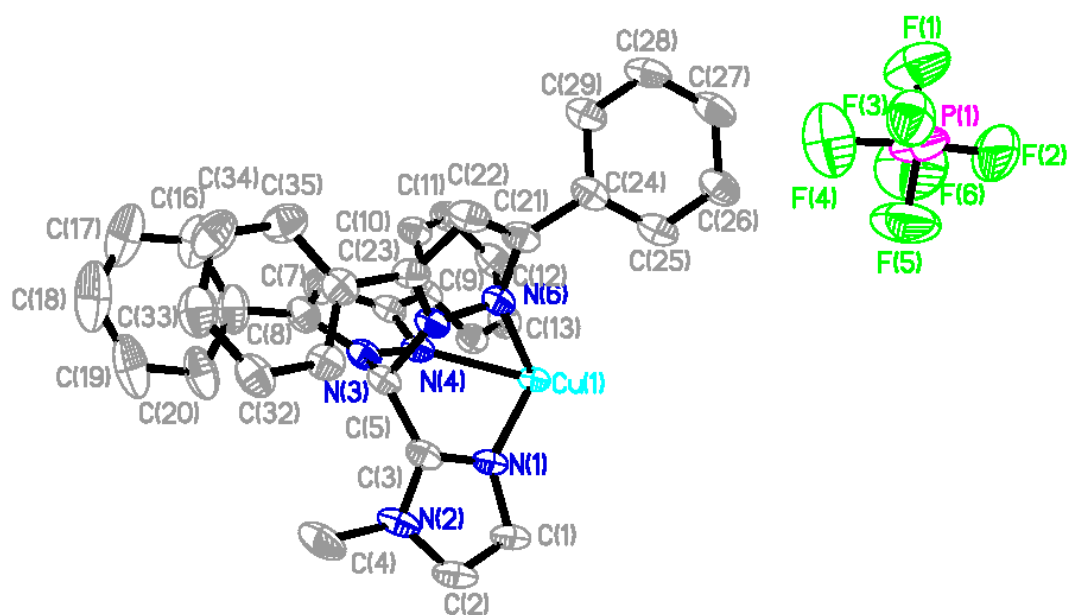


Figure 59. Molecular structure of the asymmetric unit of $[\text{Cu}\{\text{HC}(\text{Ph}_2\text{Pz})_2\text{MeIm}\}_2(\text{PF}_6)_2]$. All hydrogen atoms are omitted for clarity. Displacement ellipsoids represent the 50% of probability level.

Table 57. Crystallographic data of **C19 · DCM** and $[\text{Cu}\{\text{HC}(\text{Ph}_2\text{Pz})_2\text{Melm}\}_2](\text{PF}_6)_2$. In $[\text{Cu}\{\text{HC}(\text{Ph}_2\text{Pz})_2\text{Melm}\}_2](\text{PF}_6)_2$ it was not possible to model the three disordered solvent molecule CD_2Cl_2 in an adequate manner, and the data set was treated with the SQUEEZE routine as implemented in PLATON^{[211],[212]}.

	C19 · DCM	$[\text{Cu}\{\text{HC}(\text{Ph}_2\text{Pz})_2\text{Melm}\}_2](\text{PF}_6)_2$
Empirical formula	$\text{C}_{41}\text{H}_{37}\text{Cl}_2\text{CuF}_6\text{N}_7\text{P}$	$\text{C}_{70}\text{H}_{56}\text{CuF}_{12}\text{N}_{12}\text{P}_2$
Formula weight [g mol^{-1}]	907.18	1418.74
Crystal size [mm]	0.21 x 0.18 x 0.13	0.24 x 0.16 x 0.10
<i>T</i> [K]	100	100
Crystal system	orthorhombic	Monoclinic
Space group	Pbca	C2/c
<i>a</i> [Å]	16.264(3)	16.2952(3)
<i>b</i> [Å]	18.198(4)	19.2367(3)
<i>c</i> [Å]	27.118(5)	24.0649(4)
α [°]	90	90
β [°]	90	97.542(2)
γ [°]	90	90
<i>V</i> [Å ³]	8026(3)	7478.3(2)
<i>Z</i>	8	4
$\rho_{\text{caclcd.}}$ [g cm^{-3}]	1.501	1.260
μ [mm^{-1}]	0.786	1.477
λ [Å]	0.71073	0.71073
<i>F</i> (000)	3712	2908
<i>hkl</i> range	±20, -23 to 18, -31 to 34	-19 to 14, -23 to 16, -29 to 28
Reflections collected	71041	60598
Independent reflections	8715	7093
<i>R</i> _{int.}	0.0447	0.0475
Number of parameters	526	440
<i>R</i> ₁ [$ I \geq 2\sigma(I)$]	0.0383	0.1027
<i>wR</i> ₂ (all data)	0.1044	0.2795
Goodness-of-fit	1.053	1.064
Largest diff. peak, hole [eÅ^{-3}]	1.585, -0.784	1.569, -1.594

8.2 Cryo-ESI-MS

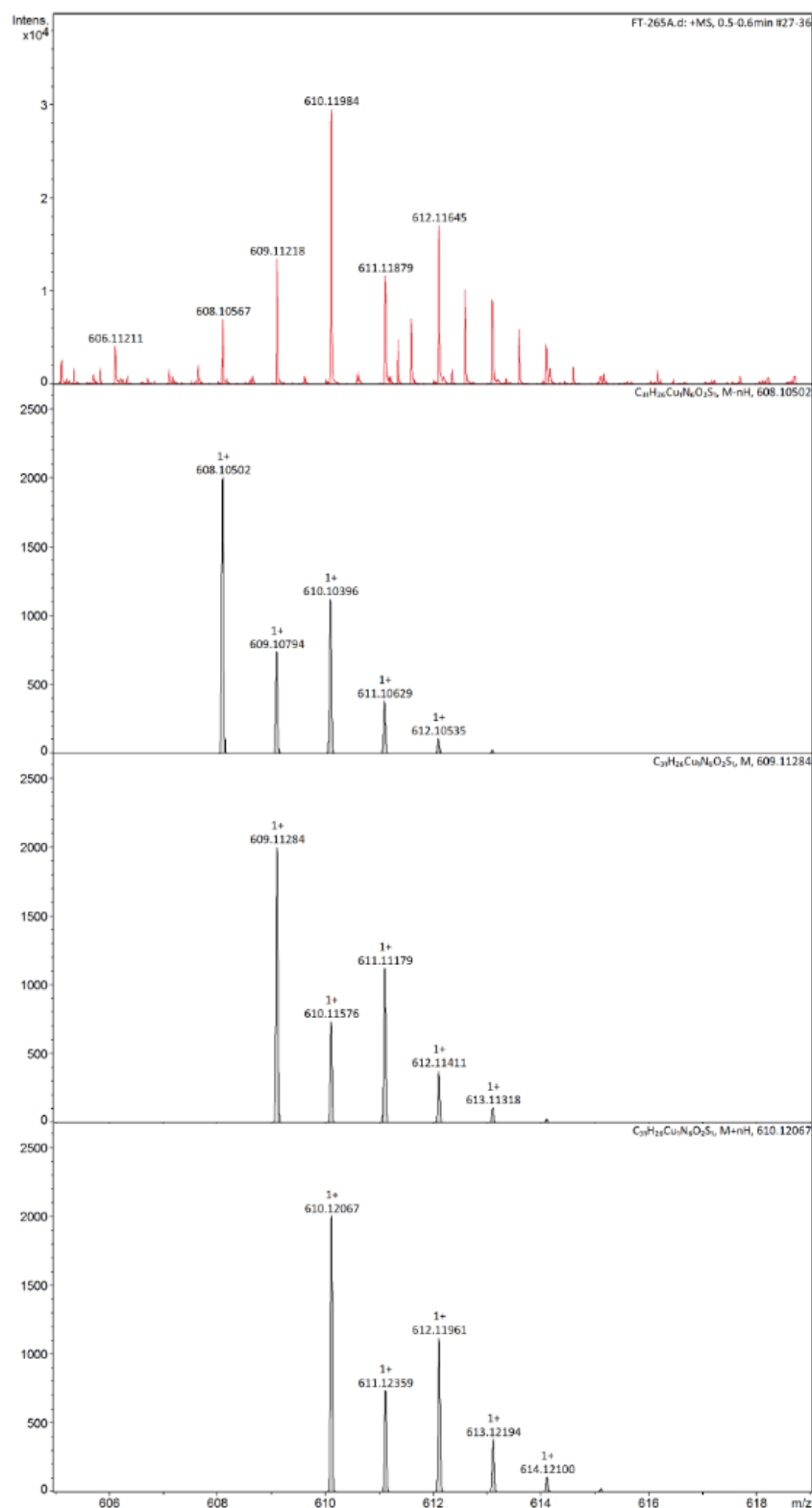


Figure 60. Cryo-UHR-ESI mass spectrum (red) of $[\text{Cu}\{\text{HC}(\text{PhPz})_2\text{Py}\}(\text{NTs})]^+$ (**N1**⁺) at 183.15 K and simulation (black) of $[\text{Cu}\{\text{HC}(\text{PhPz})_2\text{Py}\}(\text{NTs})-\text{H}]^+$ (top), $[\text{Cu}\{\text{HC}(\text{PhPz})_2\text{Py}\}(\text{NTs})]^+$ (middle) and $[\text{Cu}\{\text{HC}(\text{PhPz})_2\text{Py}\}(\text{NTs})+\text{H}]^+$ (bottom).

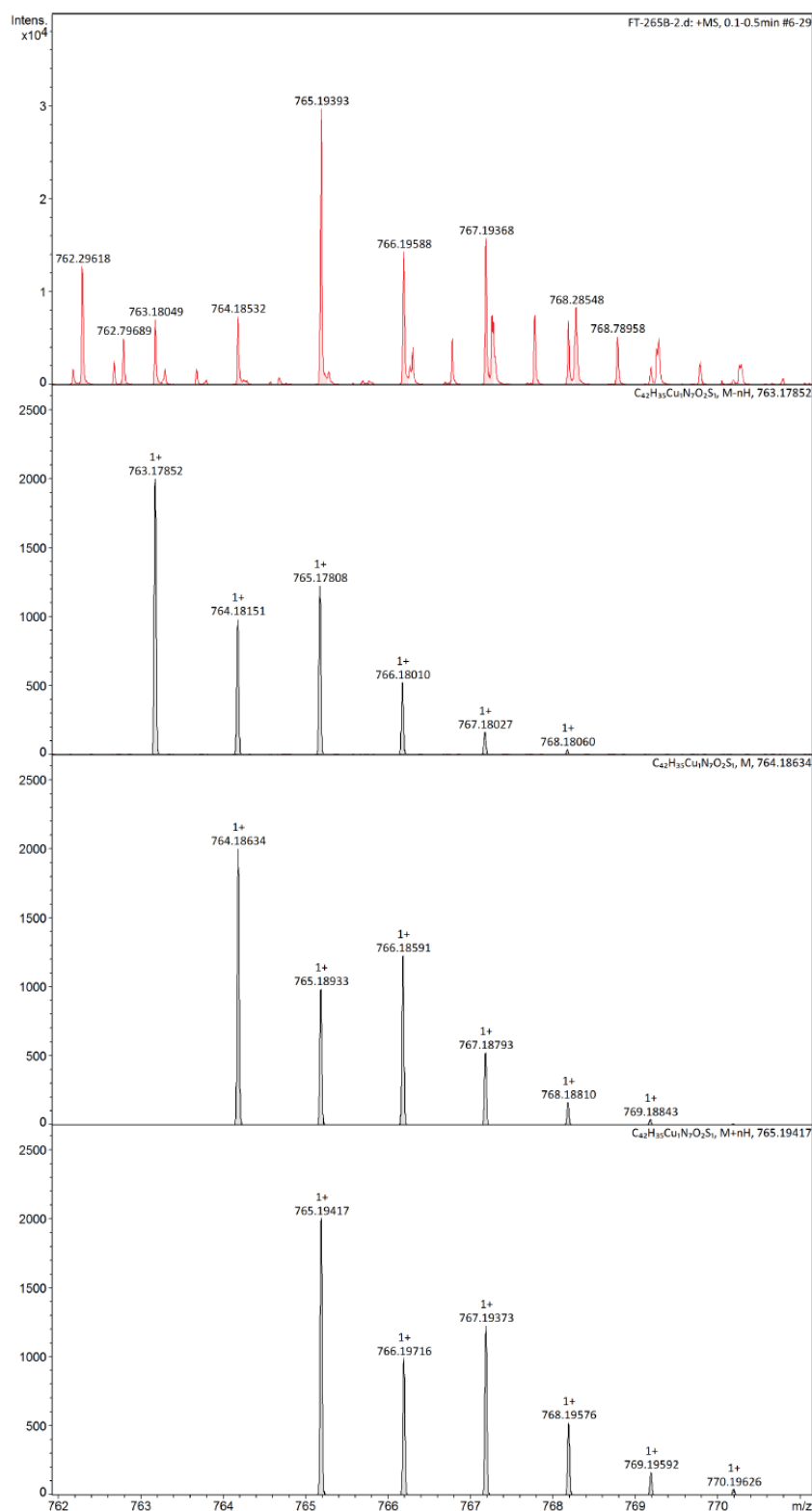


Figure 61. Cryo-UHR-ESI mass spectrum (red) of $[Cu\{HC(Ph_2Pz)_2Melm\}(NTs)]^+$ ($N3^+$) at 183.15 K and simulation (black) of $[Cu\{HC(Ph_2Pz)_2Melm\}(NTs)-H]^+$ (top), $[Cu\{HC(Ph_2Pz)_2Melm\}(NTs)]^+$ (middle) and $[Cu\{HC(Ph_2Pz)_2Melm\}(NTs)+H]^+$ (bottom).

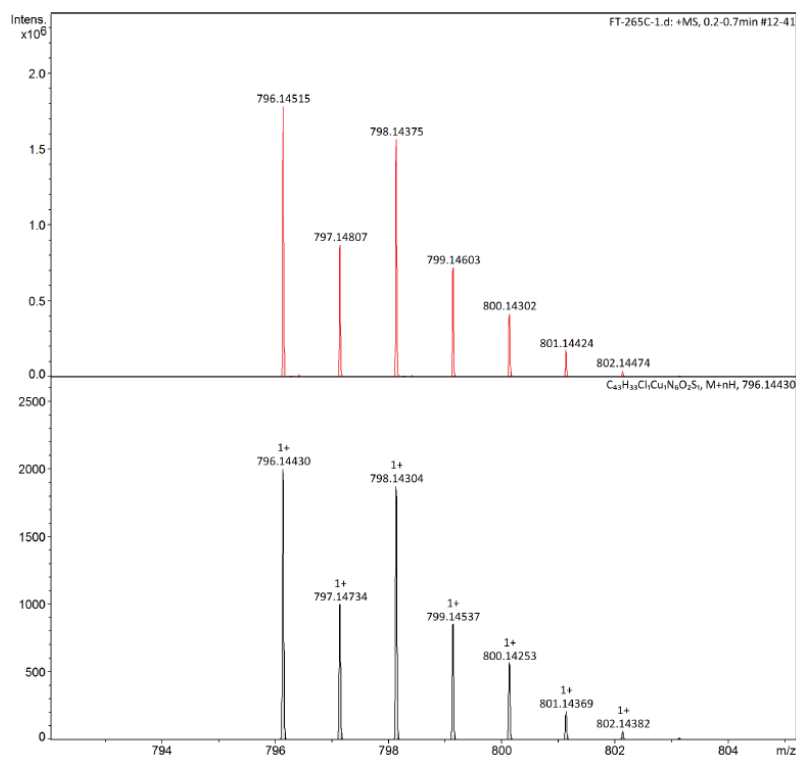


Figure 62. Cryo-UHR-ESI mass spectrum (red) of $[\text{Cu}\{\text{HC}(\text{Ph}_2\text{Pz})_2(4\text{-ClPy})\}(\text{NTs})]^+$ (N_2^+) at 183.15 K and simulation (black) of $[\text{Cu}\{\text{HC}(\text{Ph}_2\text{Pz})_2(4\text{-ClPy})\}(\text{NTs})+\text{H}]^+$.

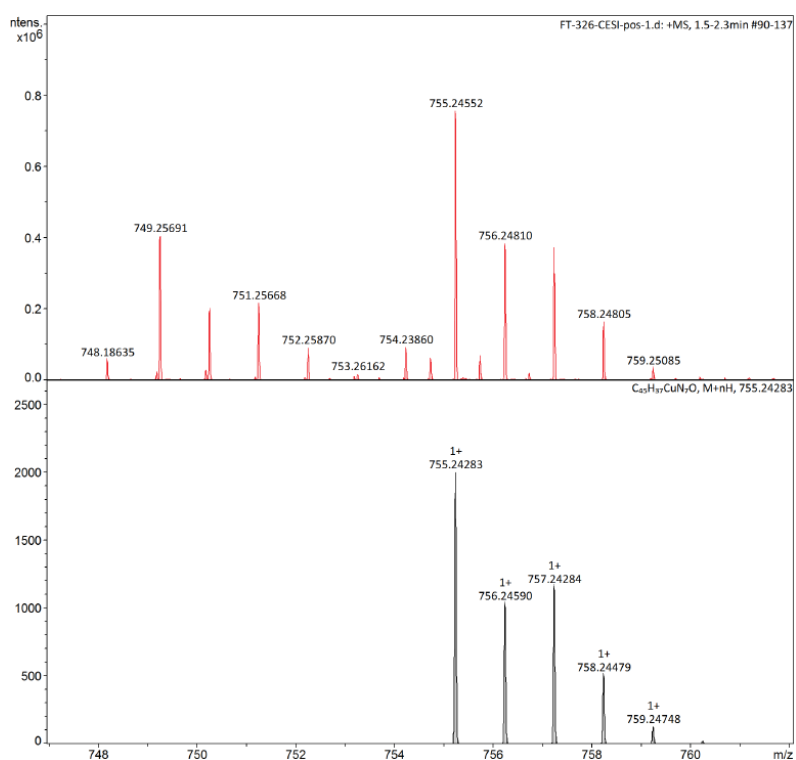
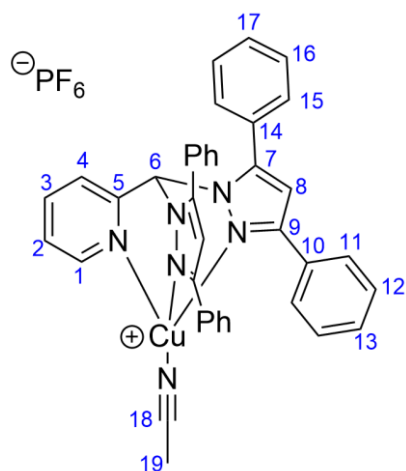


Figure 63. Cryo-UHR-ESI mass spectrum (red) of $[\text{Cu}\{\text{HC}(\text{Ph}_2\text{Pz})_2\text{DMAP}\}(\text{NCOPh})]^+$ at 183.15 K and simulation (black) of $[\text{Cu}\{\text{HC}(\text{Ph}_2\text{Pz})_2\text{DMAP}\}(\text{NCOPh})+\text{H}]^+$.

8.3 Additional analytic of [Cu{HC(Ph₂Pz)₂Py}(MeCN)]PF₆

The compound was resynthesized according to the literature^[102] to yield additional analytic.



¹H NMR (CD₂Cl₂, 400 MHz): δ = 8.84 (d, ³J = 4.5 Hz, 1H, H-1), 8.07 (dt, ³J = 7.8 Hz, ⁴J = 1.7 Hz, 1H, H-3), 7.91 (m, 4H, H-15), 7.66 (m, 1H, H-2), 7.51 (s, 1H, H-6), 7.47 (m, 9H, H-4+12+16), 7.36 (t, ³J = 7.6 Hz, 4H, H-13+17), 7.15 (m, 4H, H-11), 6.63 (s, 2H, H-8), 2.27 (s, 3H, H-19) ppm.

8.4 UV/Vis Spectra

8.4.1 Titration

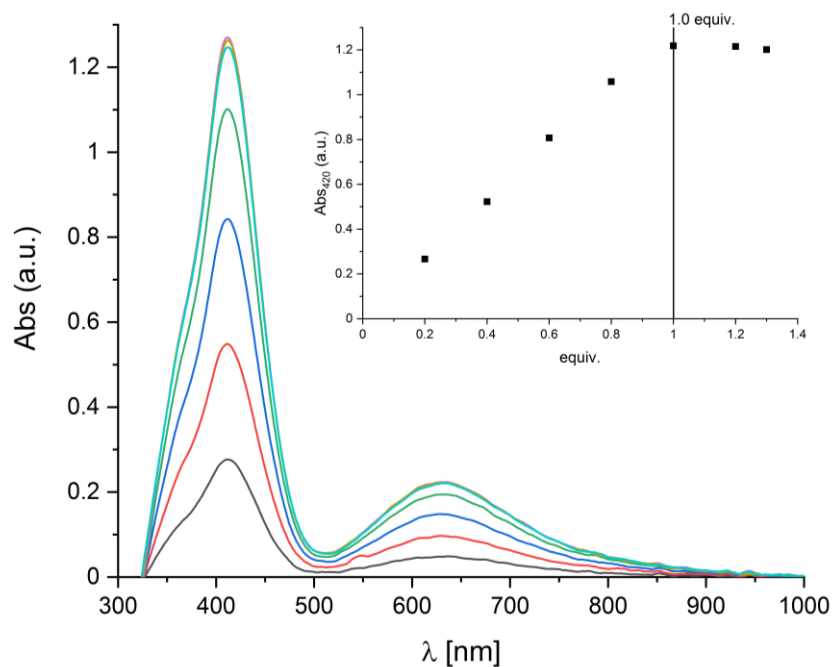


Figure 64. Titration experiment of **C1** against $SPhINTs$ in DCM at -80 °C. Inset: UV/Vis absorbance of **N1PF₆** at 420 nm with equivalents of added $SPhINTs$.

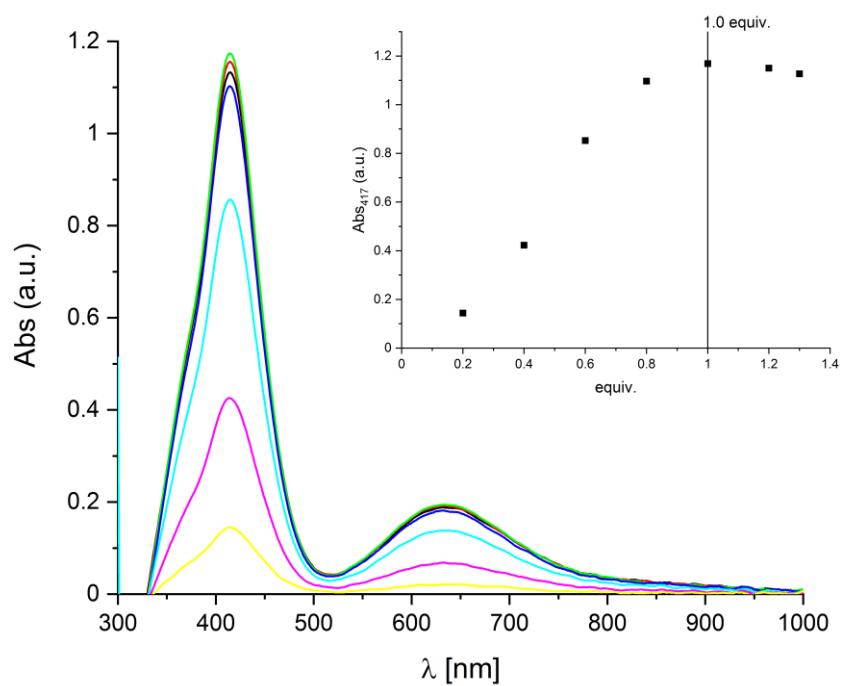


Figure 65. Titration experiment of **C2** against $SPhINTs$ in DCM at -80 °C. Inset: UV/Vis absorbance of **N2PF₆** at 417 nm with equivalents of added $SPhINTs$.

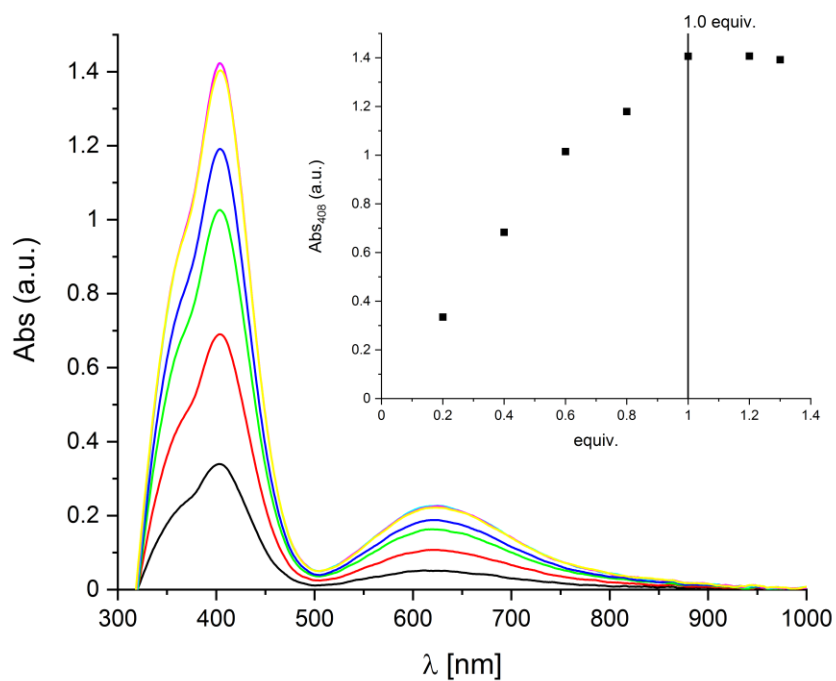


Figure 66. Titration experiment of **C3** against $^3\text{PhINTs}$ in DCM at $-80\text{ }^{\circ}\text{C}$. Inset: UV/Vis absorbance of **N3PF₆** at 408 nm with equivalents of added $^3\text{PhINTs}$.

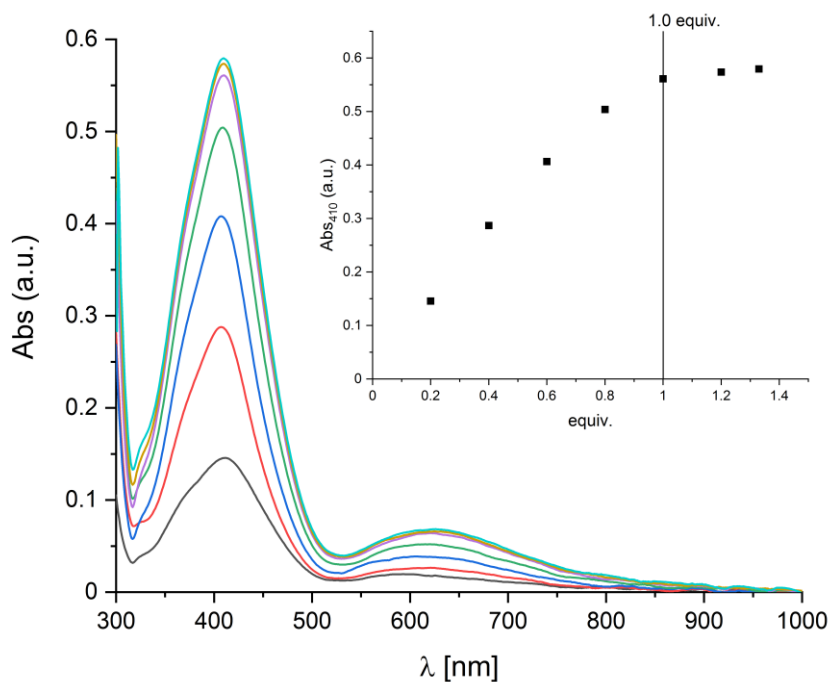


Figure 67. Titration experiment of **C11** against $^3\text{PhINTs}$ in DCM at $-80\text{ }^{\circ}\text{C}$. Inset: UV/Vis absorbance of **N11PF₆** at 410 nm with equivalents of added $^3\text{PhINTs}$.

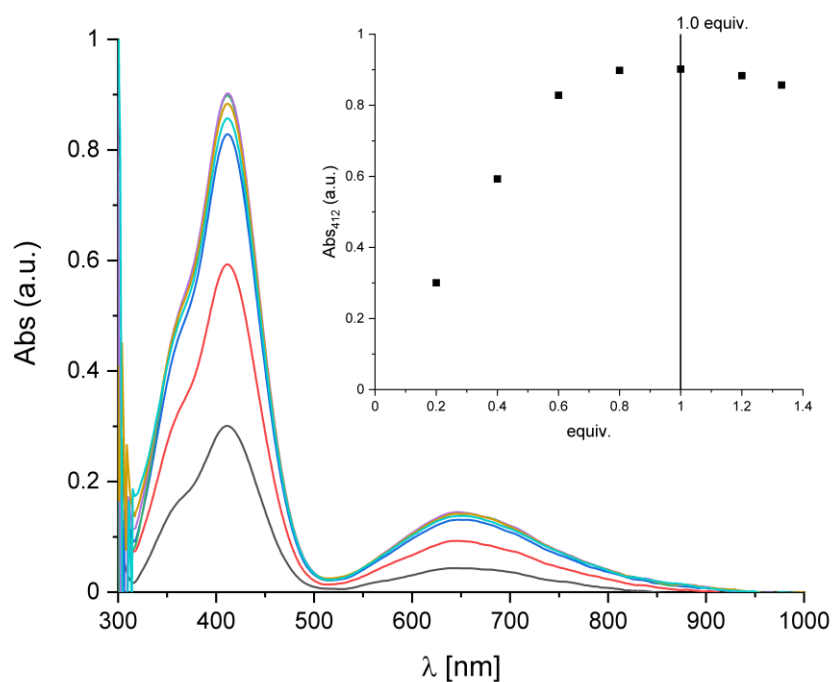


Figure 68. Titration experiment of **C12** against $^3\text{PhINTs}$ in DCM at $-63\text{ }^\circ\text{C}$. **C12** was formed *in situ* by the addition of 10 equiv. of MeCN to **C13**. Inset: UV/Vis absorbance of **N12PF₆** at 412 nm with equivalents of added $^3\text{PhINTs}$.

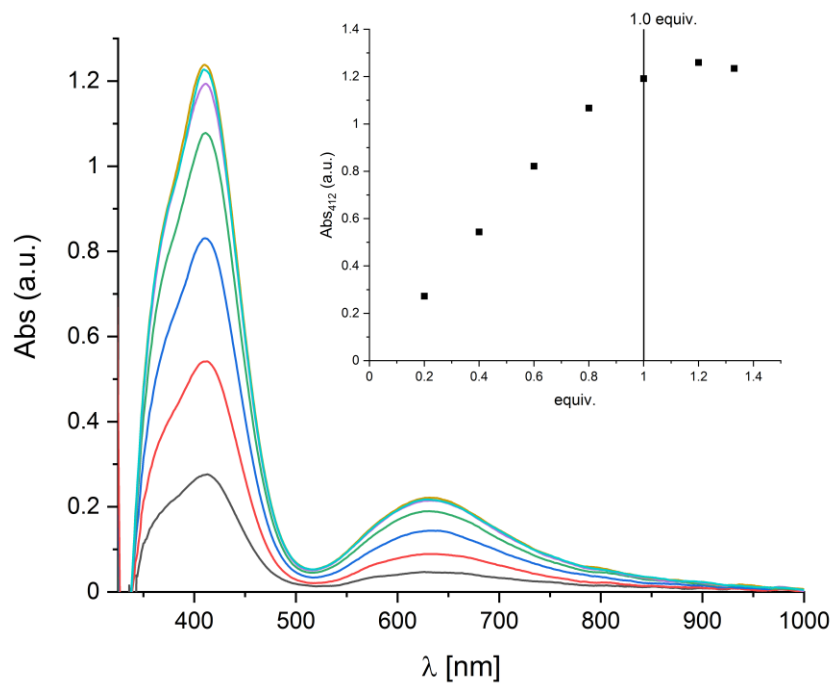


Figure 69. Titration experiment of **C19** against $^3\text{PhINTs}$ in DCM at $-80\text{ }^\circ\text{C}$. Inset: UV/Vis absorbance of **N19PF₆** at 412 nm with equivalents of added $^3\text{PhINTs}$.

8.4.2. Decay

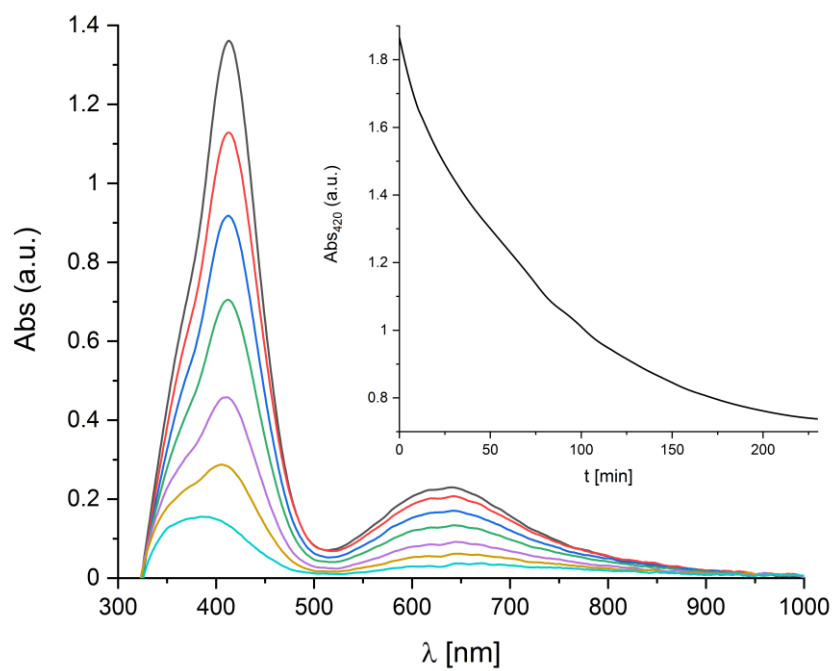


Figure 70. Thermal decay of **N1PF₆** at -42 °C in DCM. Inset: absorption trace at 420 nm.

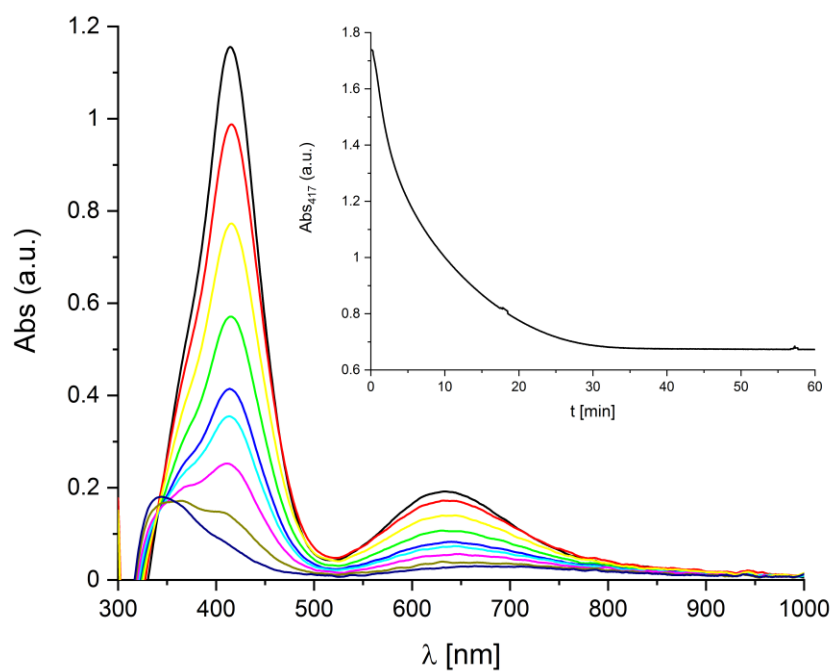


Figure 71. Thermal decay of **N2PF₆** at -42 °C in DCM. Inset: absorption trace at 417 nm.

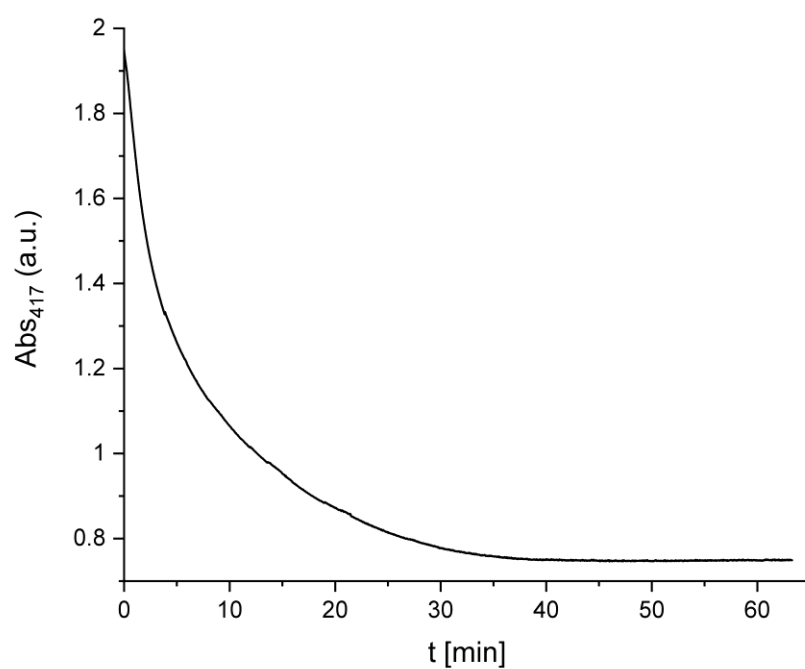


Figure 72. Absorption trace at 417 nm of the thermal decay of **N2PF₆** at -42 °C in DCM-*d*₂.

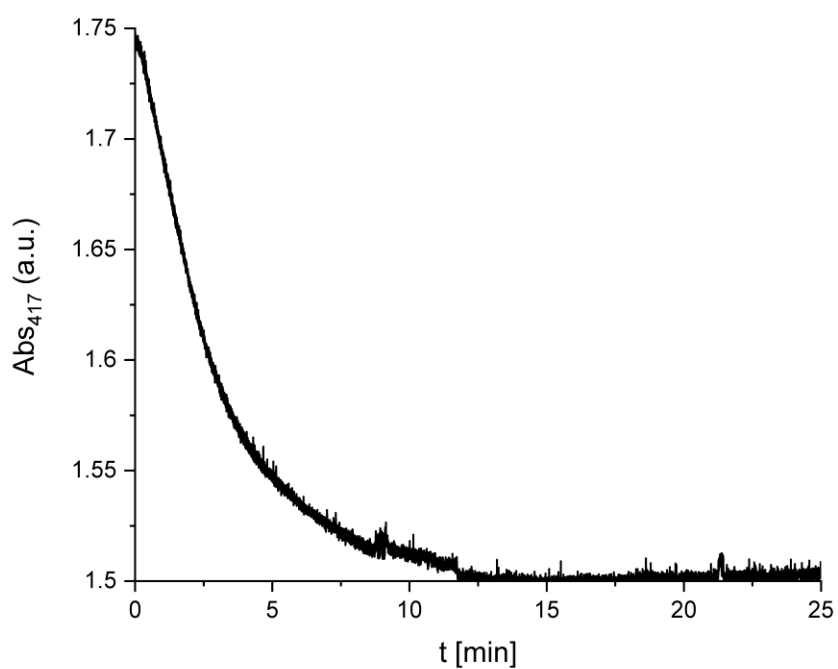


Figure 73. Absorption trace at 417 nm of the thermal decay of **N2PF₆** at -42 °C in DCM. Concentration: 1.7 mM.

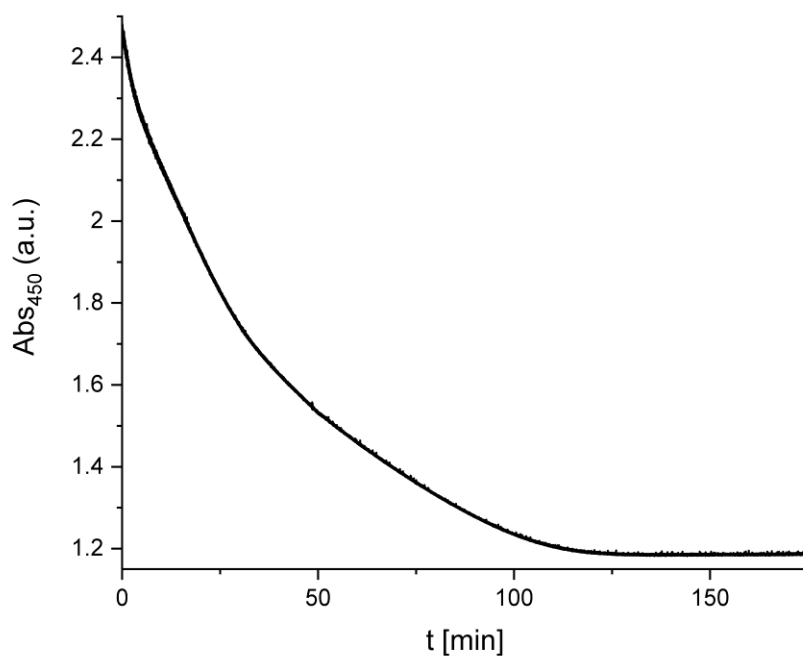


Figure 74. Absorption trace at 450 nm of the thermal decay of **N2PF₆** at -42 °C in DCM. Concentration: 6.8 mM.

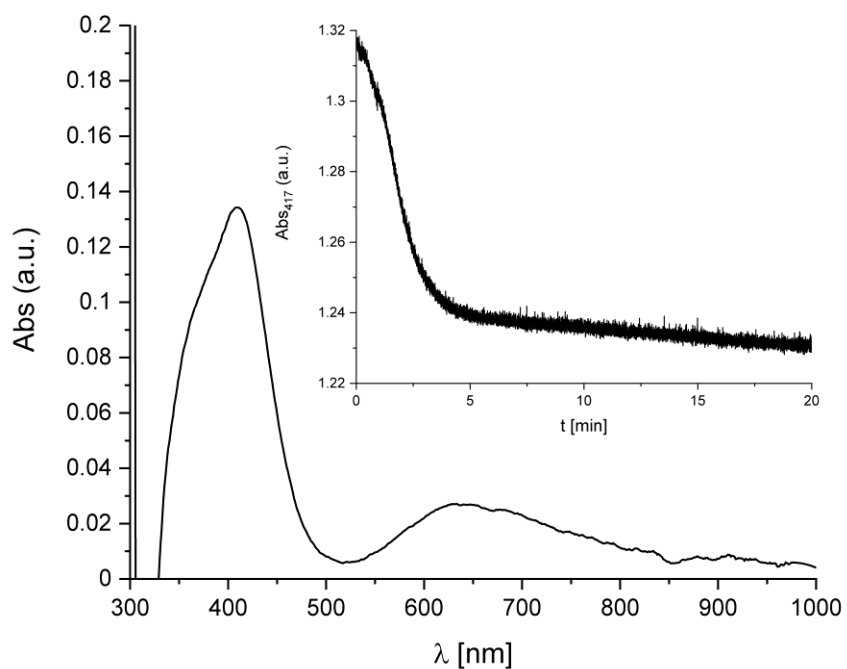


Figure 75. Formation of **N2PF₆** at -60 °C in chloroform. Inset: Absorption trace at 417 nm of the thermal decay of **N2PF₆** at -42 °C

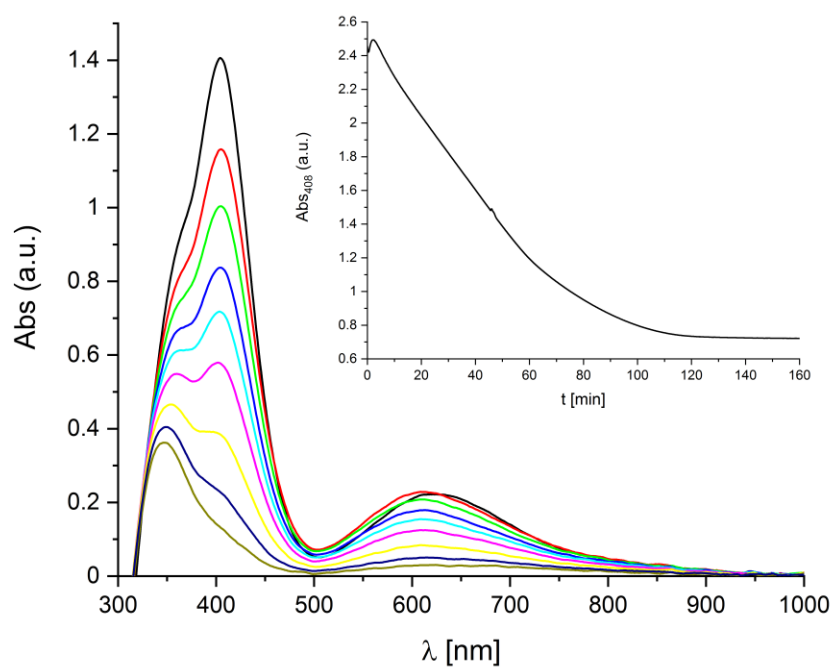


Figure 76. Thermal decay of **N3PF₆** at -42 °C in DCM. Inset: absorption trace at 417 nm.

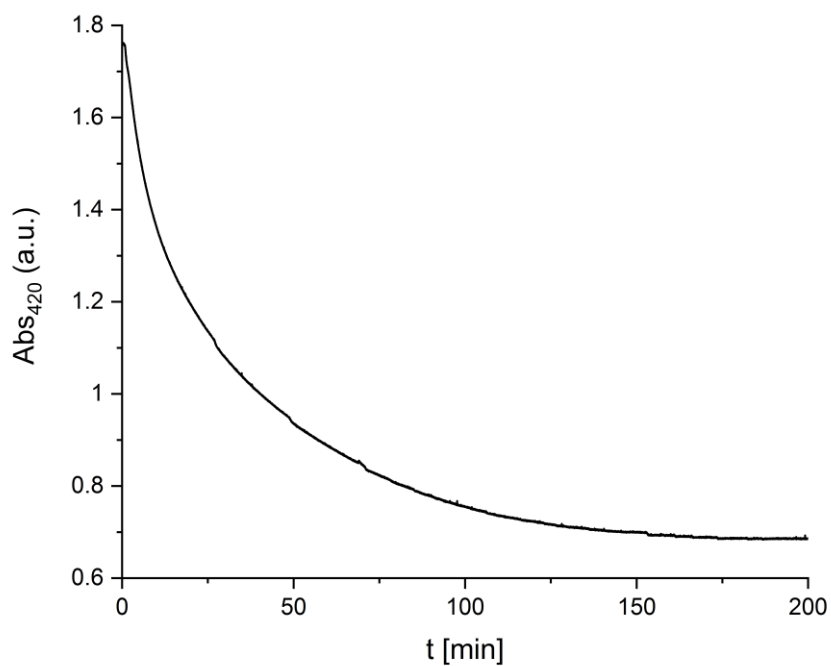


Figure 77. Reproduction of the thermal decay of **N3PF₆** at -42 °C in DCM, absorption trace at 420 nm.

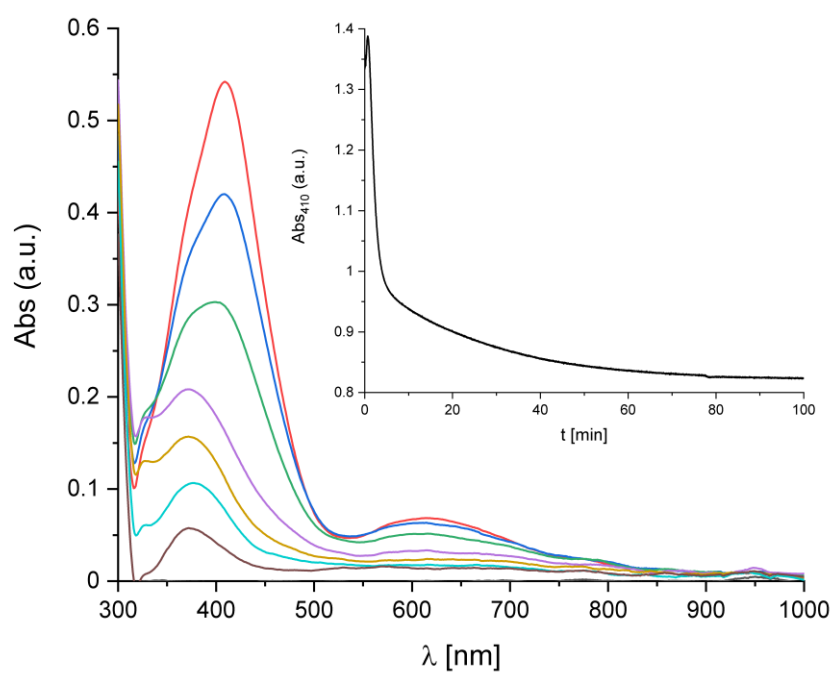


Figure 78. Thermal decay of **N11PF₆** at -42 °C in DCM. Inset: absorption trace at 410 nm.

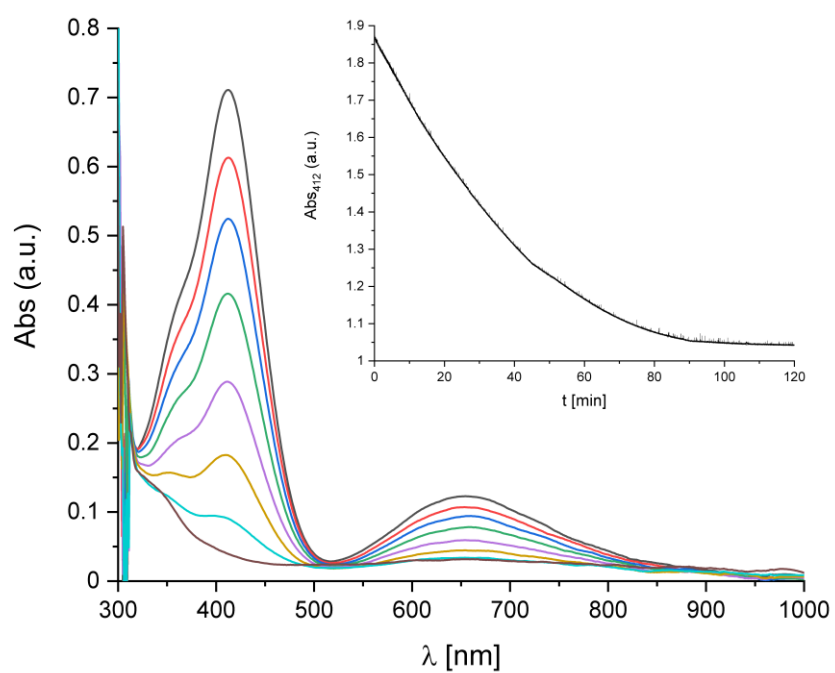


Figure 79. Thermal decay of **N12PF₆** at -42 °C in DCM. Inset: absorption trace at 410 nm. **C12** was formed *in situ* by the addition of 10 equiv. of MeCN.

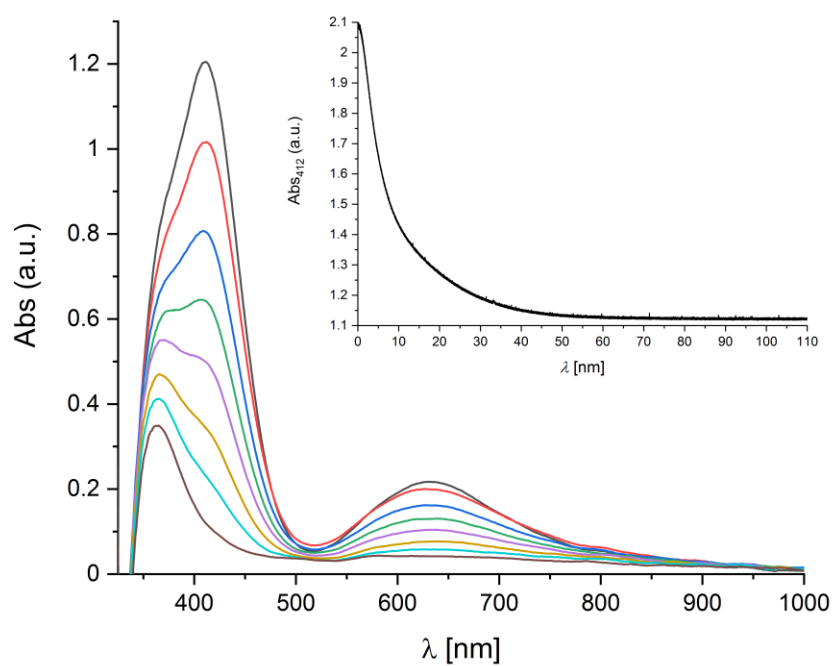


Figure 80. Thermal decay of **N19PF₆** at -42 °C in DCM. Inset: absorption trace at 412 nm.

8.4.3 Nitrene reduction with ferrocene

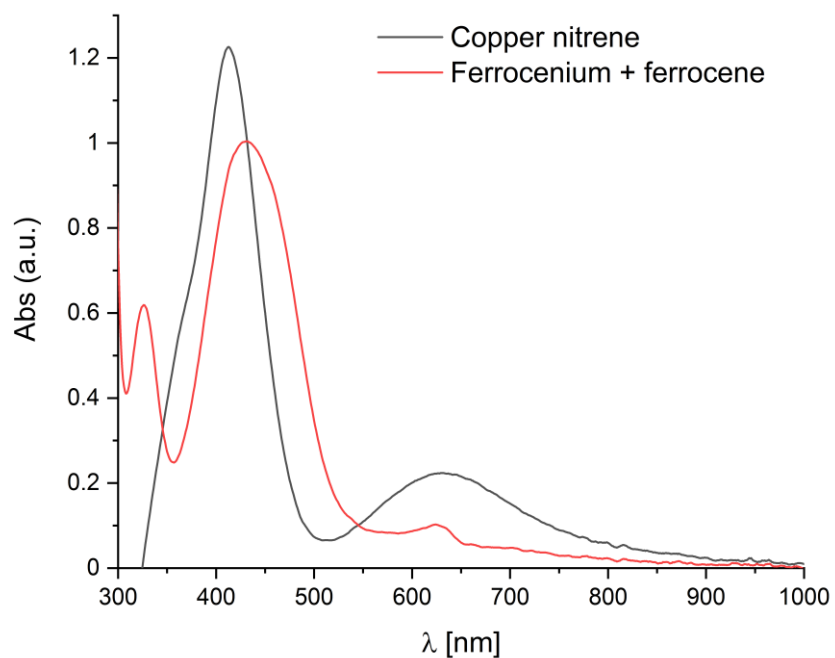


Figure 81. Nitrene reduction in DCM at -80 °C with **N19PF₆**.

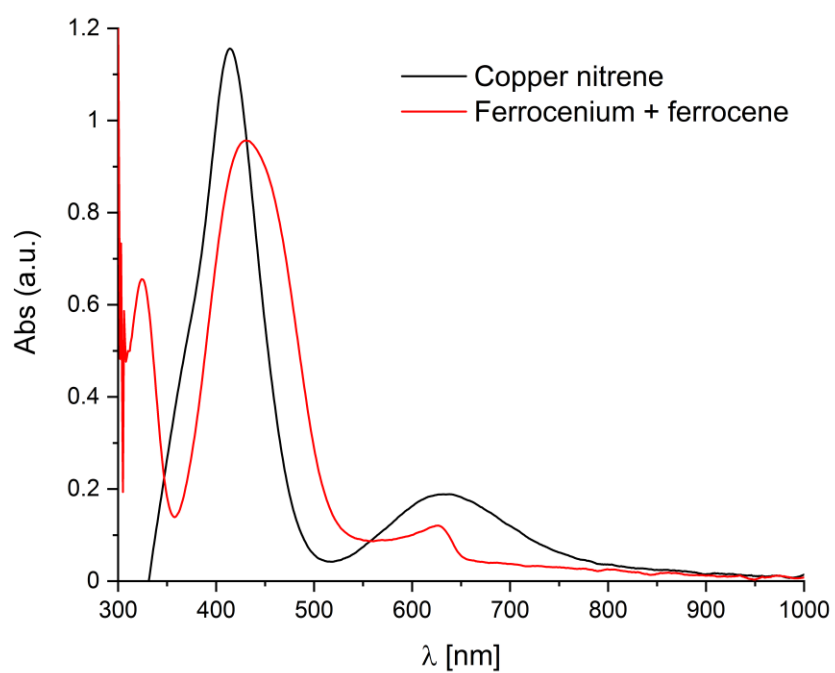


Figure 82. Nitrene reduction in DCM at -80 °C with N_2PF_6 .

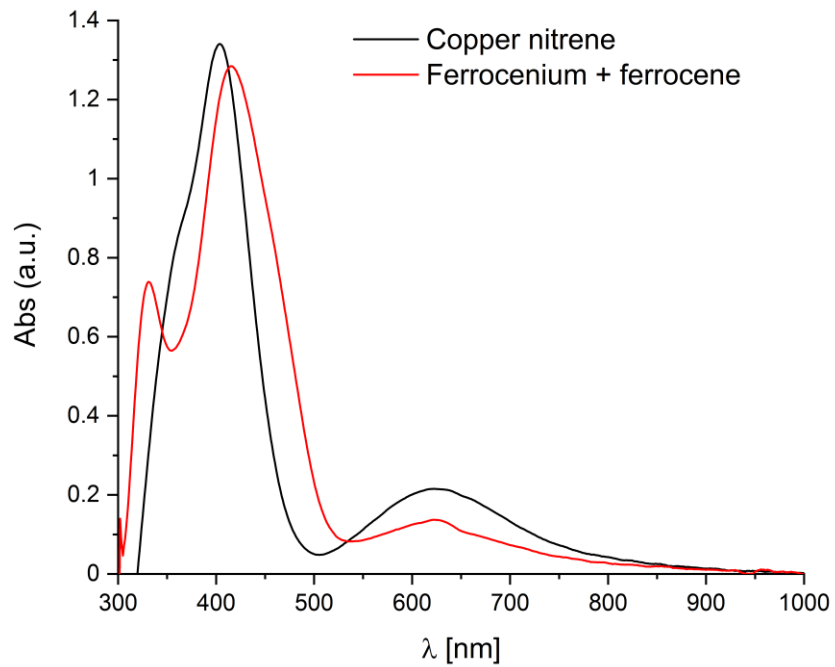


Figure 83. Nitrene reduction in DCM at -80 °C with N_3PF_6 .

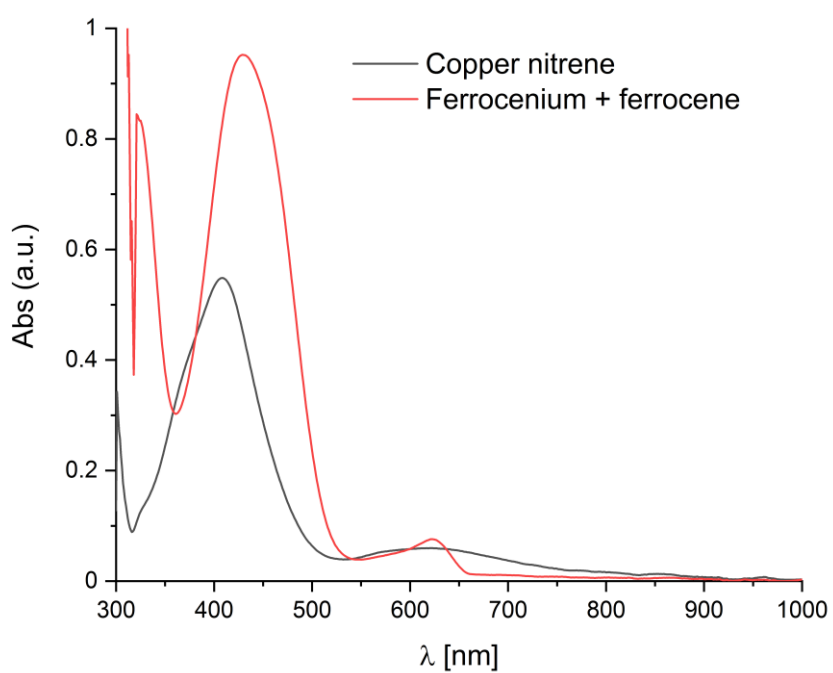


Figure 84. Nitrene reduction in DCM at -80 °C with **N11PF₆**.

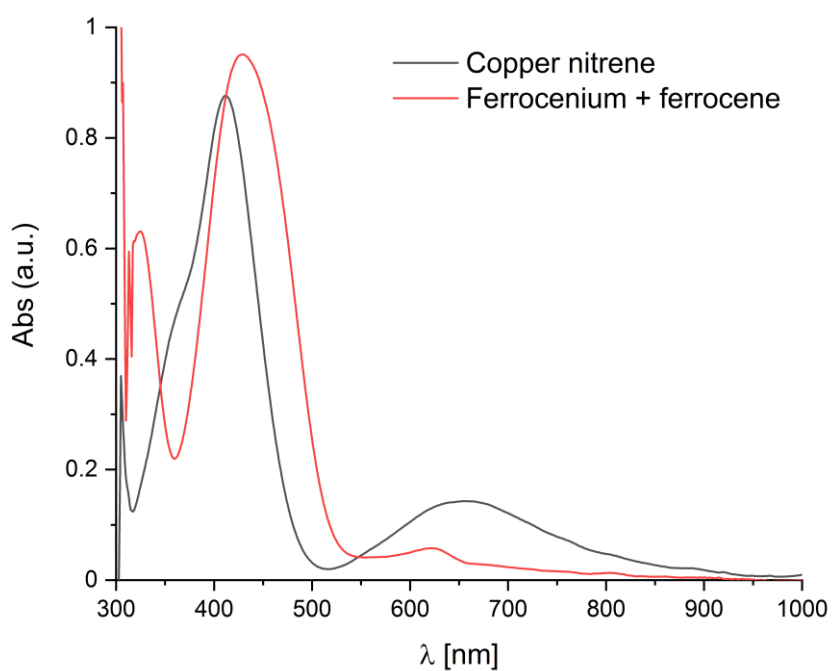


Figure 85. Nitrene reduction in DCM at -63 °C with **N12PF₆**. **C12** was formed *in situ* by the addition of 10 equiv. of MeCN to **C13**.

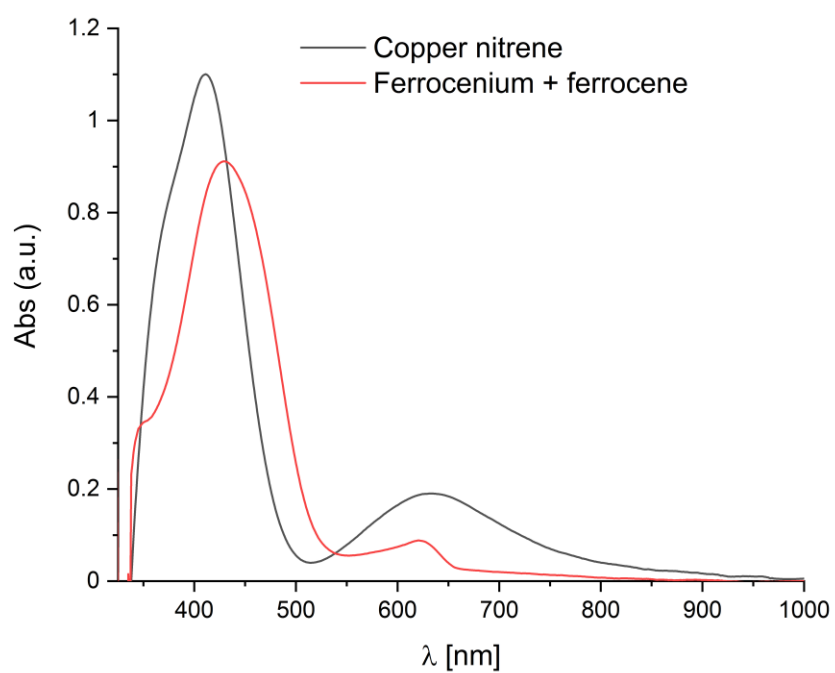


Figure 86. Nitrene reduction in DCM at -80 °C with **N19PF₆**.

8.4.4 Nitrene formation test

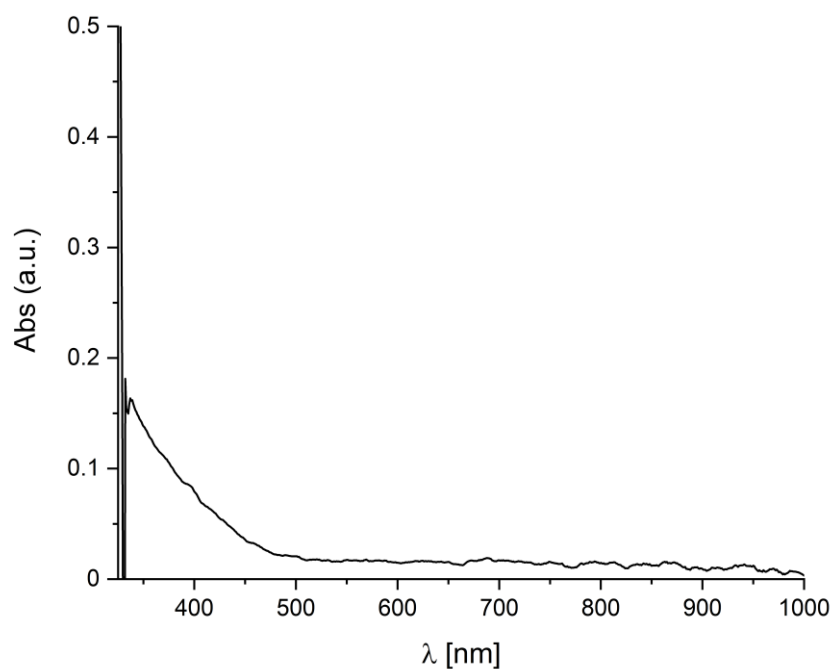


Figure 87. Nitrene formation test with *in situ* formed $[\text{Cu}\{\text{HC}(\text{QuPz})_2\text{Py}\}(\text{MeCN})]\text{PF}_6$ ($[\text{CuL5}(\text{MeCN})]\text{PF}_6$) and $^s\text{PhINTs}$ in DCM at -80 °C.

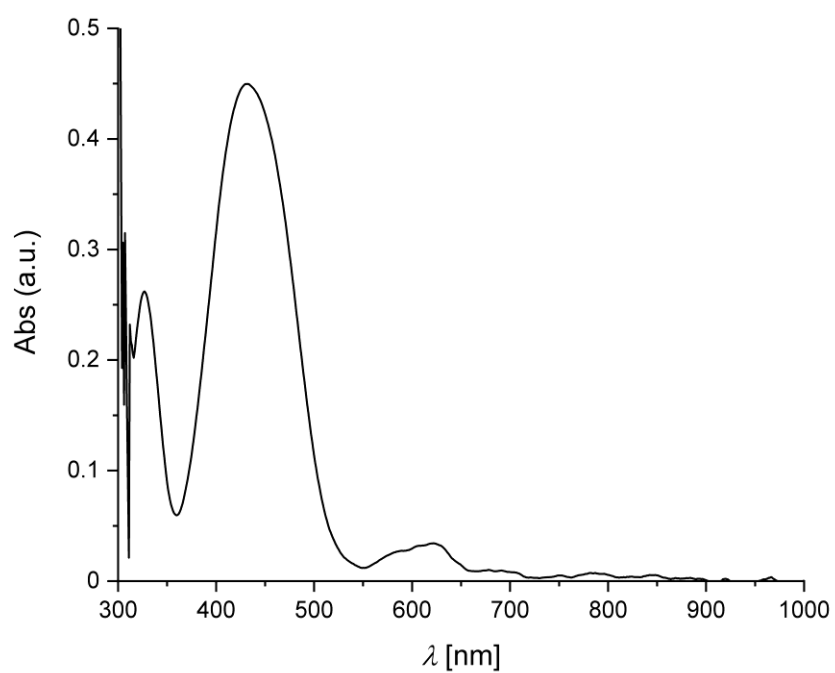


Figure 88. Nitrene formation test with *in situ* formed $[\text{Cu}\{\text{HC}(\text{Et}_2\text{Pz})_2\text{Py}\}(\text{MeCN})]\text{PF}_6$ (**[CuL6(MeCN)]PF₆**) and $^s\text{PhINTs}$ in DCM at -80°C .

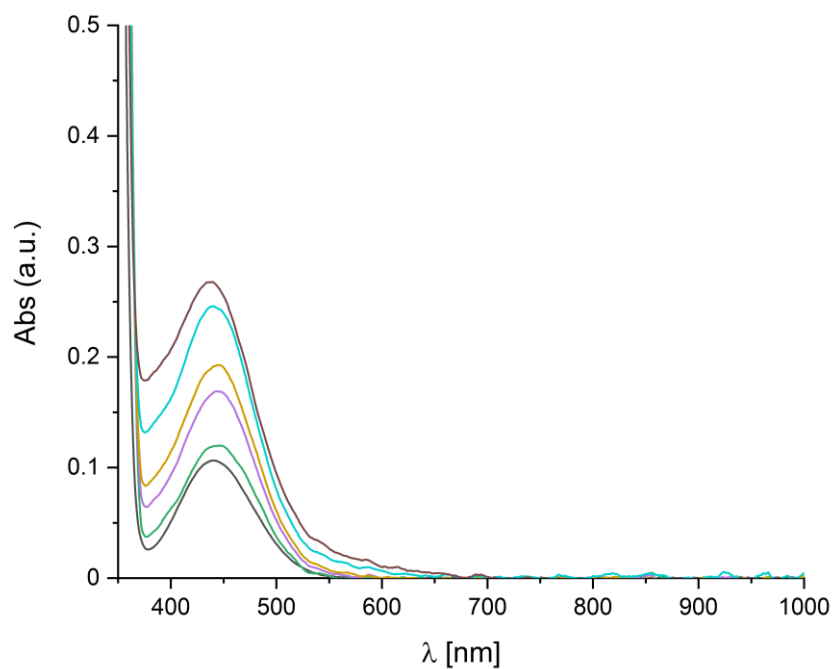


Figure 89. Nitrene formation test with $[\text{Cu}\{\text{HC}(\text{Ph}_2\text{Pz})_2(\text{Py})\}(\text{MeCN})]\text{PF}_6$ (**C4**) and azobenzene in DCM at -80°C .

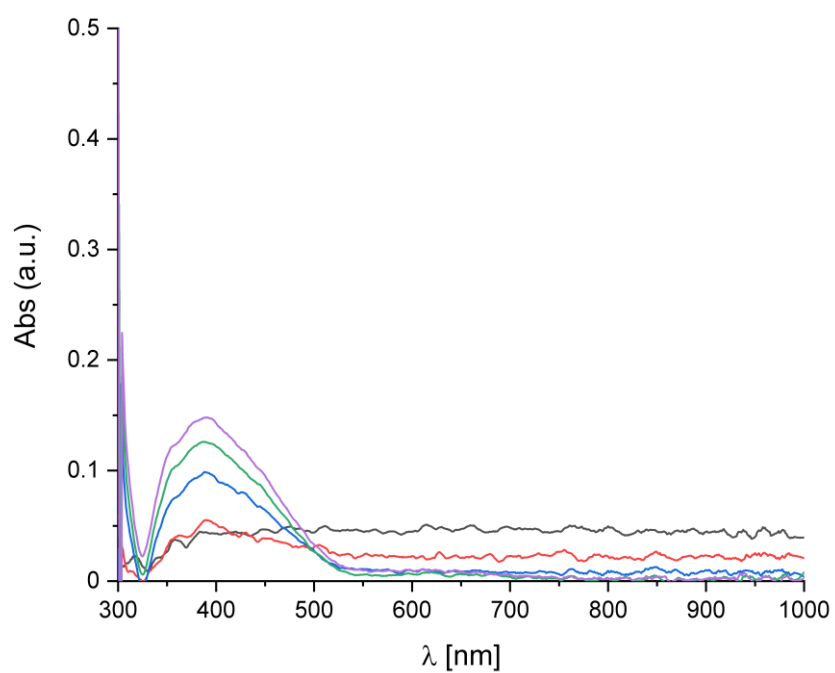


Figure 90. Nitrene formation test with $[\text{Cu}\{\text{HC}(\text{Ph}_2\text{Pz})_2(\text{Py})\}(\text{MeCN})]\text{PF}_6$ (**C4**) and *O*-(4-nitrobenzoyl)hydroxylamine triflate in DCM at -80°C .

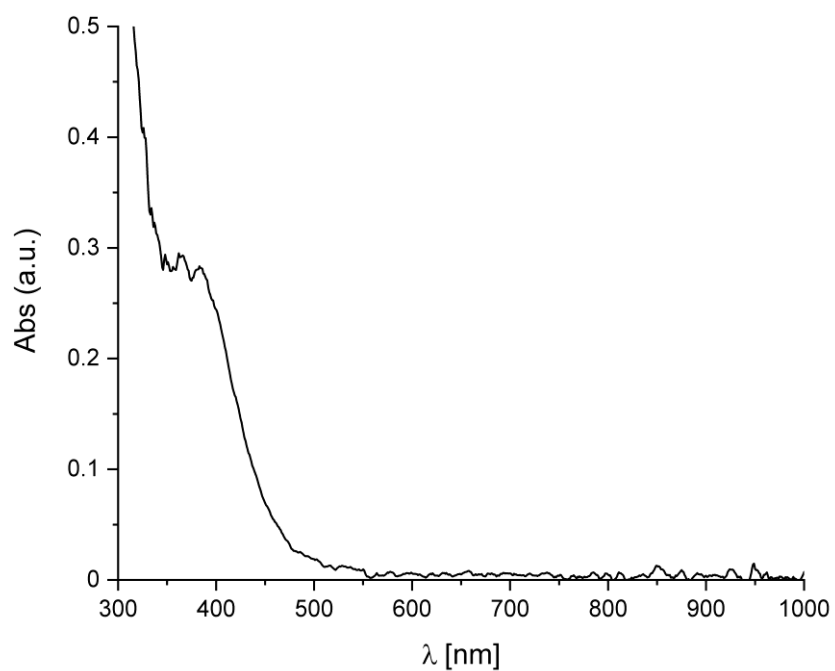


Figure 91. Nitrene formation test with $[\text{Cu}\{\text{HC}(\text{tBuPz})_2(6\text{-CO}_2\text{MePy})\}(\text{MeCN})]\text{PF}_6$ (**C10**) and $^s\text{PhINTs}$ in DCM at -80°C .

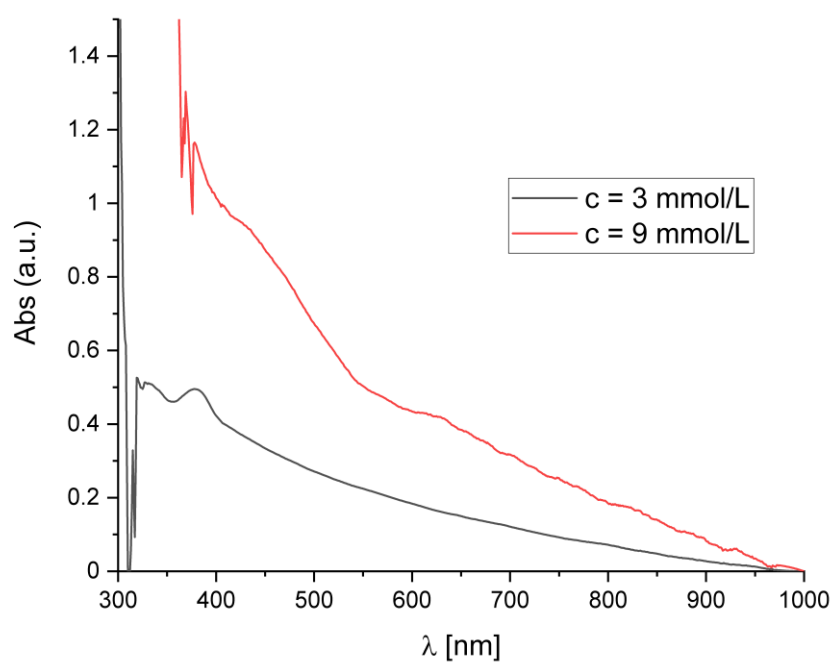


Figure 92. Nitrene formation test with $[\text{Cu}\{\text{HC}(\text{'BuPz})_2\text{Py}\}]\text{SbF}_6$ (**C18**) and bis(trifluormethyl)phenyl azide in DCM at room temperature. Due to the formation of a precipitate a baseline shift occurs, which was corrected. Reaction time: 20 h

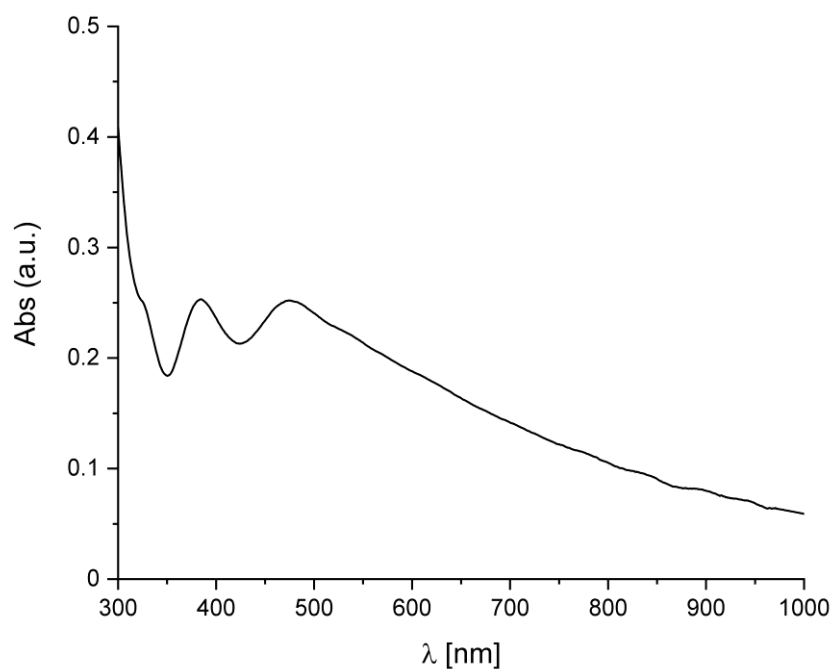


Figure 93. Nitrene formation test with $[\text{Cu}\{\text{HC}(\text{'BuPz})_2\text{Py}\}]\text{SbF}_6$ (**C17**) and bis(trifluormethyl)phenyl azide in DCM starting from $-42\text{ }^{\circ}\text{C}$ ending at room temperature. Concentration: 3.4 mmol/L

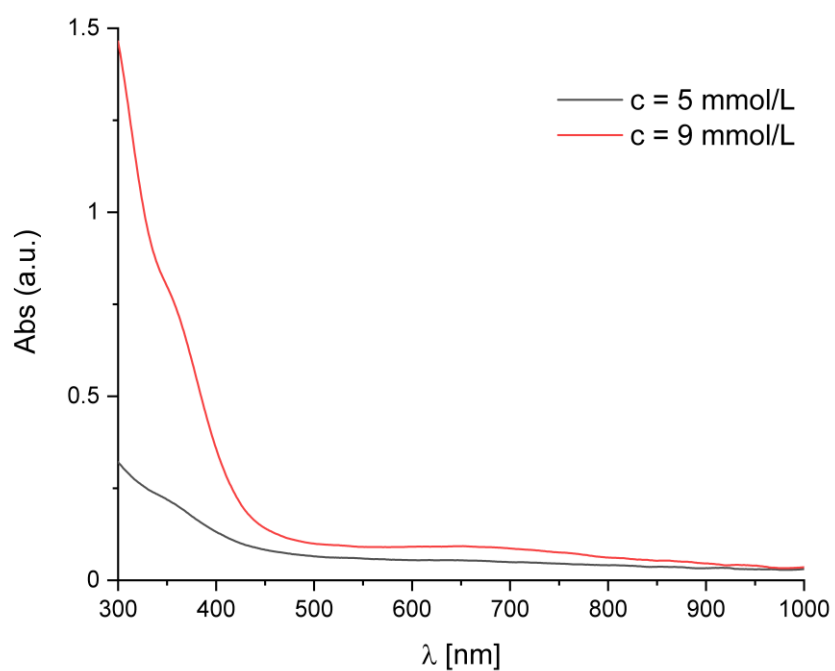


Figure 94. Nitrene formation test with $[\text{Cu}\{\text{HC}(\text{tBuPz})_2\text{Melm}\}]\text{SbF}_6$ (**C18**) and adamantyl azide in DCM at room temperature. Reaction time: 72 h

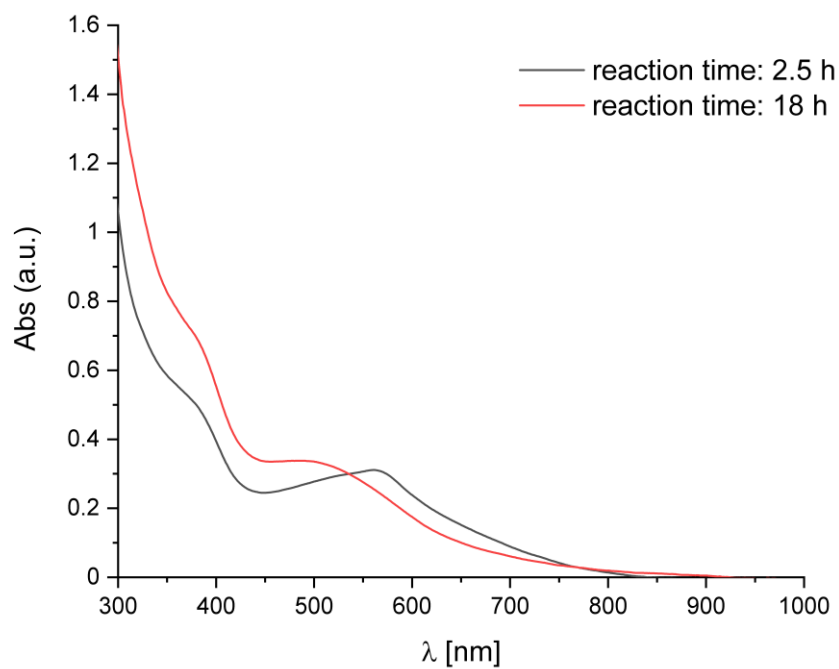


Figure 95. Nitrene formation test with $[\text{Cu}\{\text{HC}(\text{tBuPz})_2\text{Melm}\}]\text{SbF}_6$ (**C18**) and mesityl azide in DCM at room temperature. Concentration: 5 mmol/L

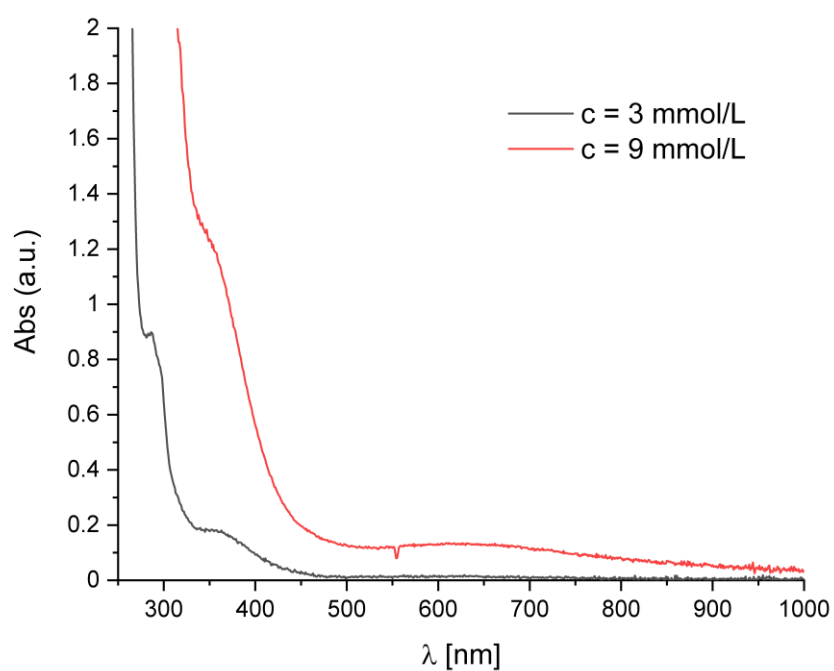


Figure 96. Nitrene formation test with $[\text{Cu}\{\text{HC}(\text{tBuPz})_2\text{Py}\}]\text{SbF}_6$ (**C18**) and bis(trifluoromethyl)phenyl azide in DCM at room temperature. Reaction time: 20 h

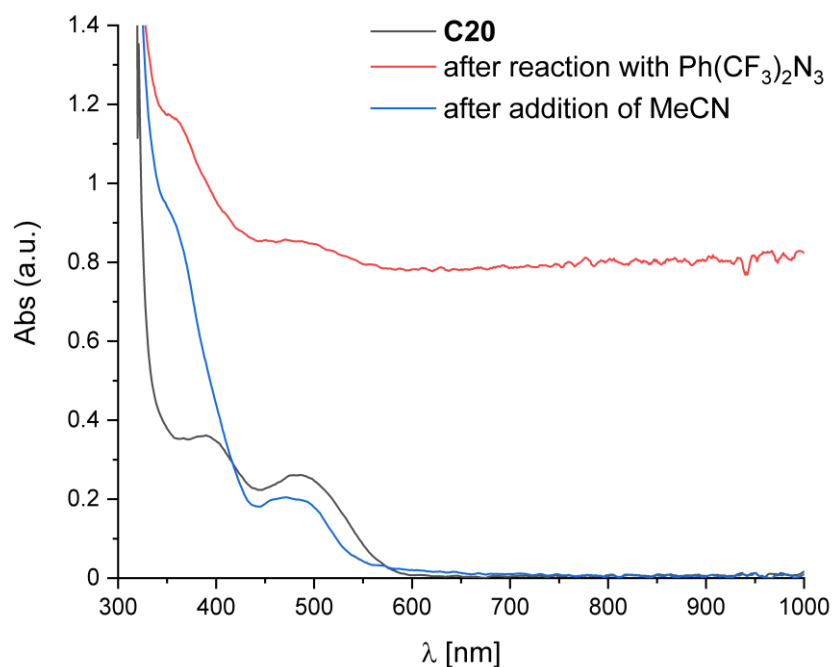


Figure 97. Nitrene formation test with $[\text{Fe}\{\text{MeC}(\text{Py})_2\text{Bpy}\}(\text{MeCN})_2]\text{OTf}_2$ (**C20**) and bis(trifluoromethyl)phenyl azide in DCM at room temperature. After the reaction with bis(trifluoromethyl)phenyl azide a precipitate form, which can be solved by addition of 2 mL of MeCN. Reaction time: 20 h

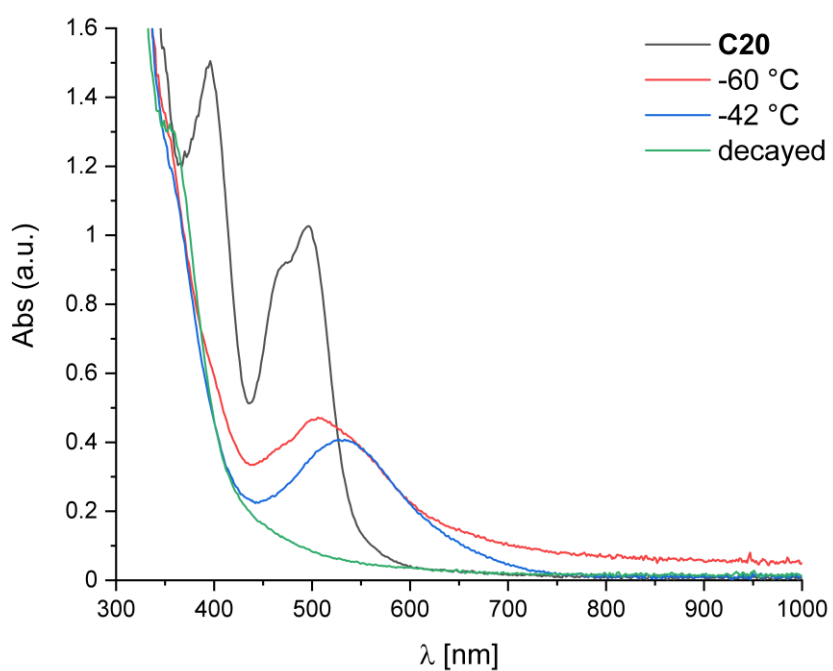


Figure 98. Nitrene formation test with $[\text{Fe}\{\text{MeC}(\text{Py})_2\text{Bpy}\}(\text{MeCN})_2]\text{OTf}_2$ (**C20**) and $^s\text{PhINTs}$ in DCM.

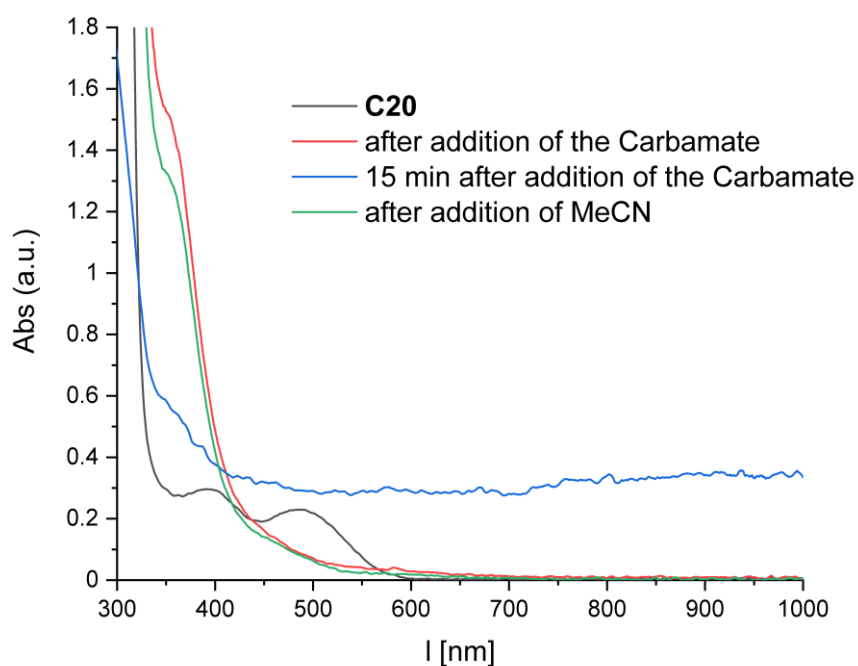


Figure 99. Nitrene formation test with $[\text{Fe}\{\text{MeC}(\text{Py})_2\text{Bpy}\}(\text{MeCN})_2](\text{OTf})_2$ (**C20**) and *O*-(4-Nitrobenzoyl)hydroxylamine triflate in DCM at room temperature. Due to the low solubility of *O*-(4-Nitrobenzoyl)hydroxylamine triflate in DCM, it was added in THF.

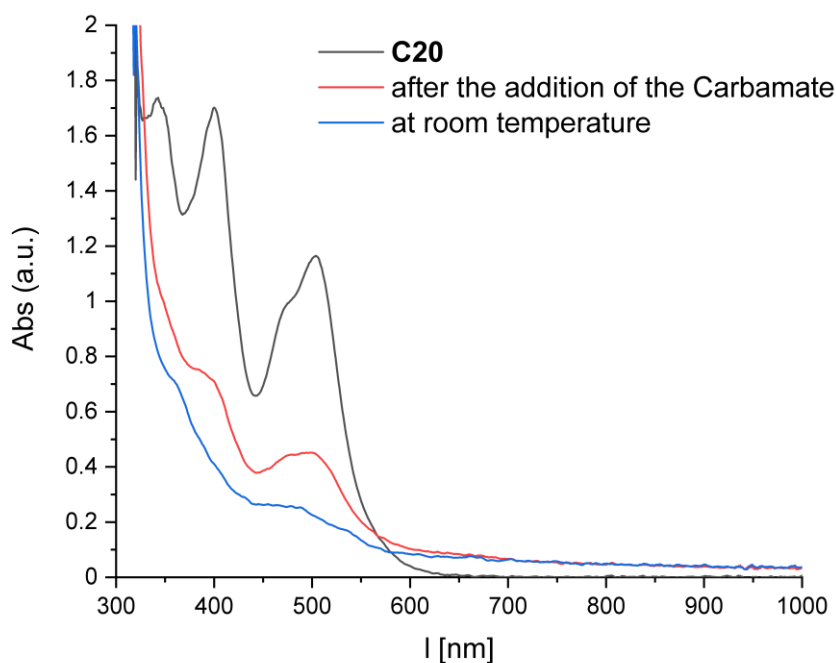


Figure 100. Nitrene formation test with $[\text{Fe}\{\text{MeC}(\text{Py})_2\text{Bpy}\}(\text{MeCN})_2](\text{OTf})_2$ (**C20**) and *O*-(4-Nitrobenzoyl)hydroxylamine triflate in THF at $-80\text{ }^\circ\text{C}$. Due to the low solubility of **C20** in THF, **C20** was added in DCM.

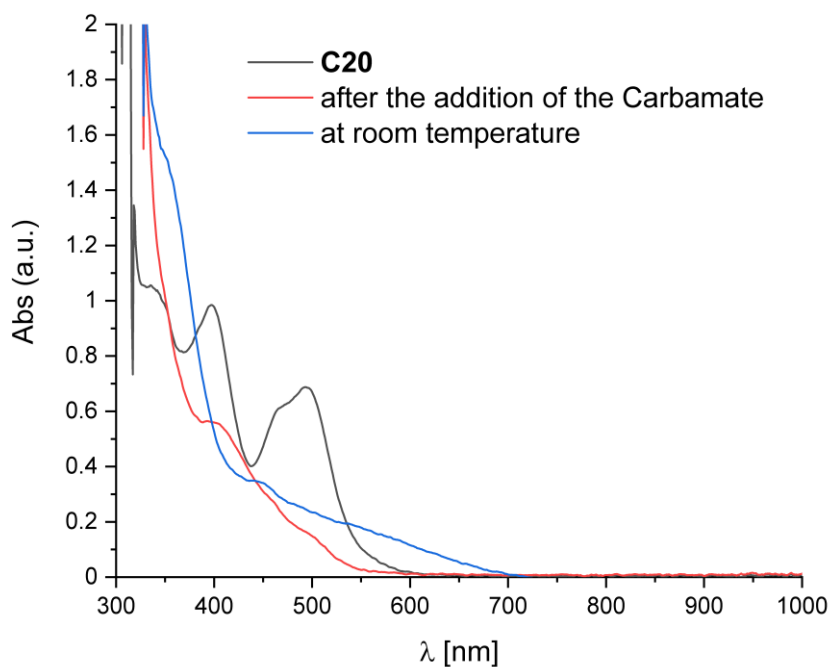


Figure 101. Nitrene formation test with $[\text{Fe}\{\text{MeC}(\text{Py})_2\text{Bpy}\}(\text{MeCN})_2]\text{OTf}_2$ (**C20**) and *O*-(4-Nitrobenzoyl)hydroxylamine triflate in acetone at $-80\text{ }^\circ\text{C}$.

8.5 EPR spectroscopy

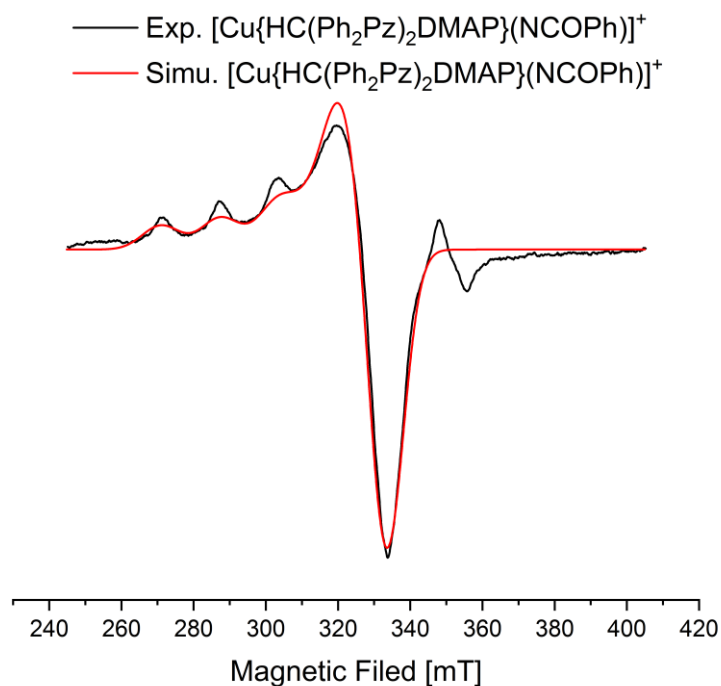


Figure 102. X-Band EPR spectrum of a sample of the reaction between **C19** and **113**. (simulation parameters: $g_{\parallel} = 2.10$, $g_{\perp} = 2.33$, $A_{\parallel}(\text{Cu}) = 32$ MHz, $A_{\perp}(\text{Cu}) = 522$ MHz, $A_{\parallel}(\text{N}) = 41$ MHz, $A_{\perp}(\text{N}) = 41$ MHz, $A_{\parallel}(\text{H}) = 9$ MHz, $A_{\perp}(\text{H}) = 10$ MHz, Gaussian line shape linewidth: 9.3 mT).

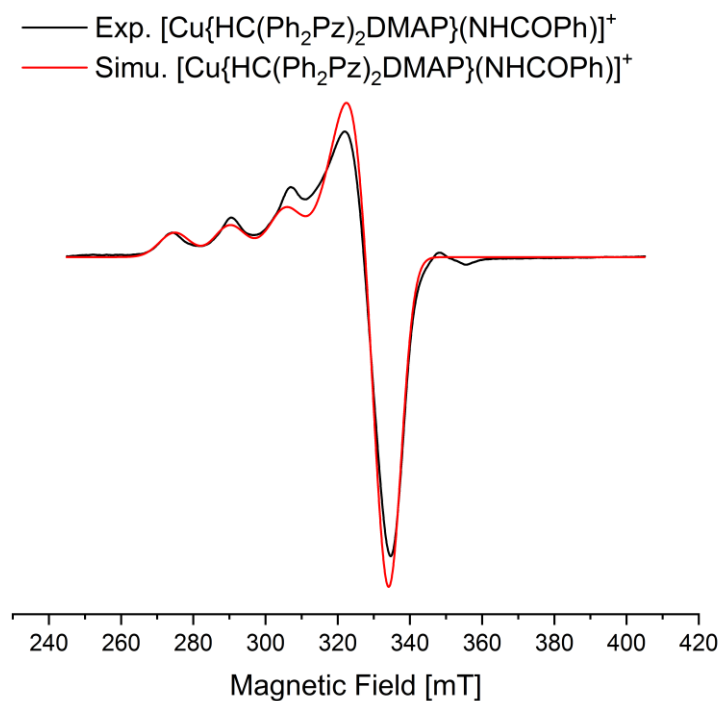


Figure 103. X-Band EPR spectrum of a decayed sample of the reaction between **C19** and **113**. (simulation parameters: $g_{\parallel} = 2.09$, $g_{\perp} = 2.31$, $A_{\parallel}(\text{Cu}) = 41$ MHz, $A_{\perp}(\text{Cu}) = 490$ MHz, $A_{\parallel}(\text{N}) = 44$ MHz, $A_{\perp}(\text{N}) = 49$ MHz, $A_{\parallel}(\text{H}) = 23$ MHz, $A_{\perp}(\text{H}) = 25$ MHz, Gaussian line shape linewidth: 6.0 mT).

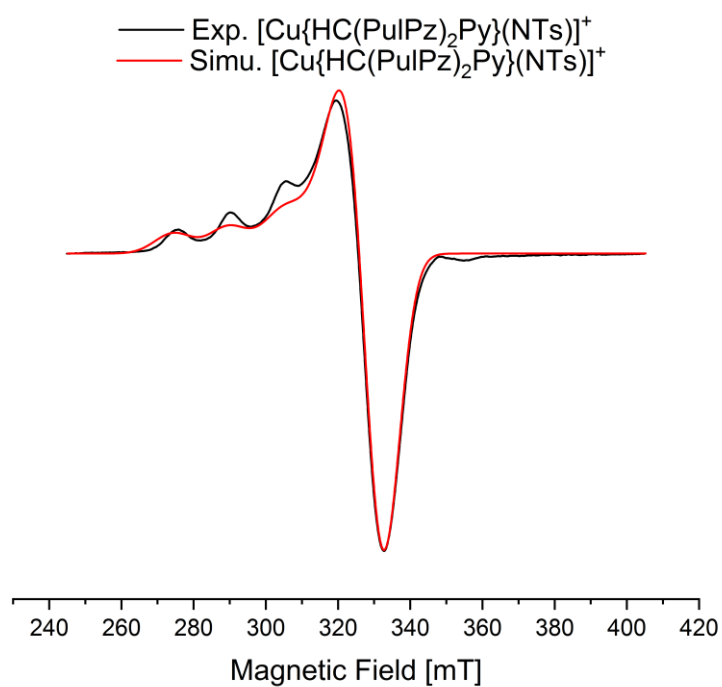


Figure 104. X-Band EPR spectrum of a sample of **N11PF₆**. (simulation parameters: $g_{\parallel} = 2.11$, $g_{\perp} = 2.32$, $A_{\parallel}(\text{Cu}) = 36$ MHz, $A_{\perp}(\text{Cu}) = 479$ MHz, $A_{\parallel}(\text{N}) = 31$ MHz, $A_{\perp}(\text{N}) = 97$ MHz, Gaussian line shape linewidth: 9.0 mT).

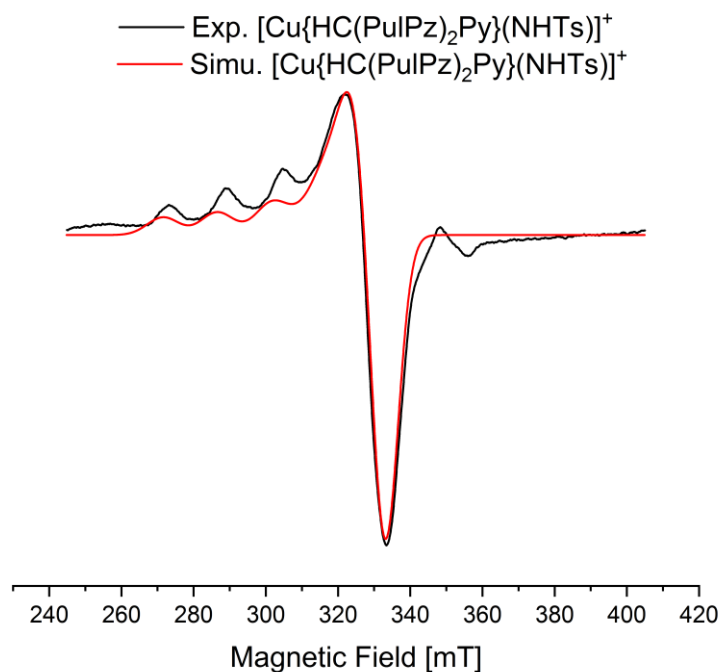


Figure 105. X-Band EPR spectrum of a decayed sample of **N11PF₆**. (simulation parameters: $g_{\parallel} = 2.10$, $g_{\perp} = 2.34$, $A_{\parallel}(\text{Cu}) = 29$ MHz, $A_{\perp}(\text{Cu}) = 428$ MHz, $A_{\parallel}(\text{N}) = 31$ MHz, $A_{\perp}(\text{N}) = 54$ MHz, $A_{\parallel}(\text{H}) = 11$ MHz, $A_{\perp}(\text{H}) = 73$ MHz, Gaussian line shape linewidth: 7.0 mT).

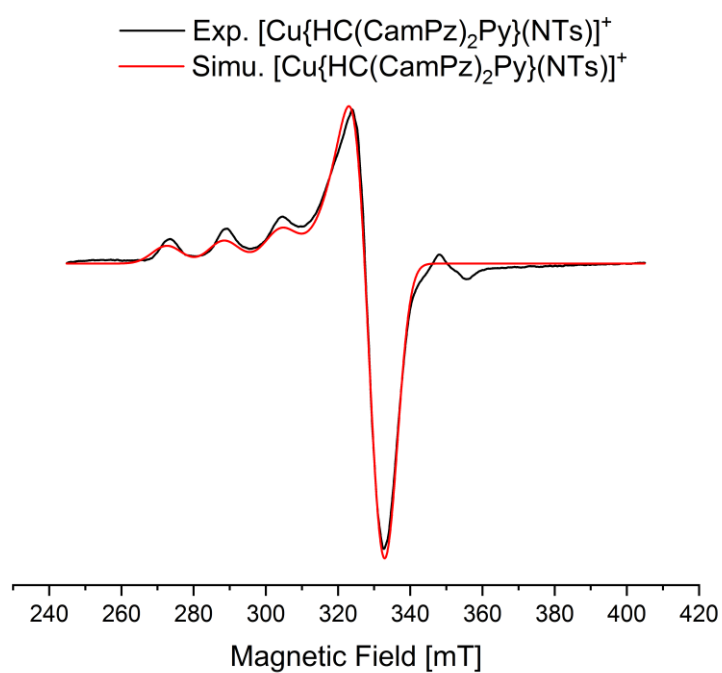


Figure 106. X-Band EPR spectrum of a sample of **N12PF₆**. (simulation parameters: $g_{\parallel} = 2.09$, $g_{\perp} = 2.32$, $A_{\parallel}(\text{Cu}) = 21$ MHz, $A_{\perp}(\text{Cu}) = 501$ MHz, $A_{\parallel}(\text{N}) = 4$ MHz, $A_{\perp}(\text{N}) = 52$ MHz, Gaussian line shape linewidth: 5.9 mT).

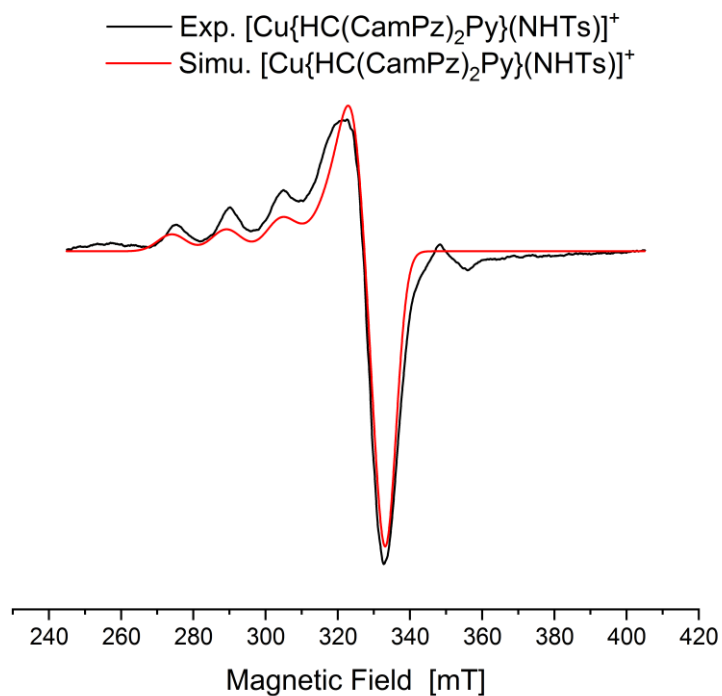


Figure 107. X-Band EPR spectrum of a decayed sample of **N12PF₆**. (simulation parameters: $g_{\parallel} = 2.10$, $g_{\perp} = 2.32$, $A_{\parallel}(\text{Cu}) = 54$ MHz, $A_{\perp}(\text{Cu}) = 515$ MHz, $A_{\parallel}(\text{N}) = 31$ MHz, $A_{\perp}(\text{N}) = 39$ MHz, $A_{\parallel}(\text{H}) = 37$ MHz, $A_{\perp}(\text{H}) = 22$ MHz, Gaussian line shape linewidth: 5.5 mT).

8.6 Key parameters determined by DFT calculation

Table 58. Key geometric parameters of the complexes **C1** – **C4** and **C6** (Gaussian16; TPSSh/def2-TZVP and PCM solvent model for dichloromethane and the empirical dispersion correction with Becke-Johnson damping).

	C1	C2	C3	C4	C6
<i>Bond lengths [Å]</i>					
Cu – N(Pz, Pz')	2.070/2.070	2.057/2.068	2.092/2.128	1.978/2.024	2.061/2.099
Cu – N(Py, Im)	2.099	2.105	2.057	1.930	2.085
Cu – N(MeCN)	1.871	1.870	1.866	-	1.869
Cu – Cu	-	-	-	2.530	

Table 59. NBO charges (in e⁻ units) and charge transfer energies (in kcal/mol) for selected atoms (*italic*) for **C1** – **C4** (NBO6.0. TPSSh/def2-TZVP and PCM solvent model for dichloromethane and the empirical dispersion correction with Becke-Johnson damping).

	C1	C2	C3	C4
<i>NBO charges</i>				
Cu	0.94	0.94	0.93	0.88
N(Pz, Pz')	-0.37/-0.37	-0.37/-0.37	-0.36/-0.36	-0.41/-0.40
N(Py, Im)	-0.52	-0.52	-0.55	-0.58
N(MeCN)	-0.52	-0.53	-0.52	
<i>Charge transfer energies</i>				
N(Pz, Pz') → Cu	25.7/25.2	24.3/26.0	22.5/20.2	21.7/26.3
N(Py, Im) → Cu	19.8	19.5	26.3	32.2
N(MeCN) → Cu	46.3	46.2	45.8	

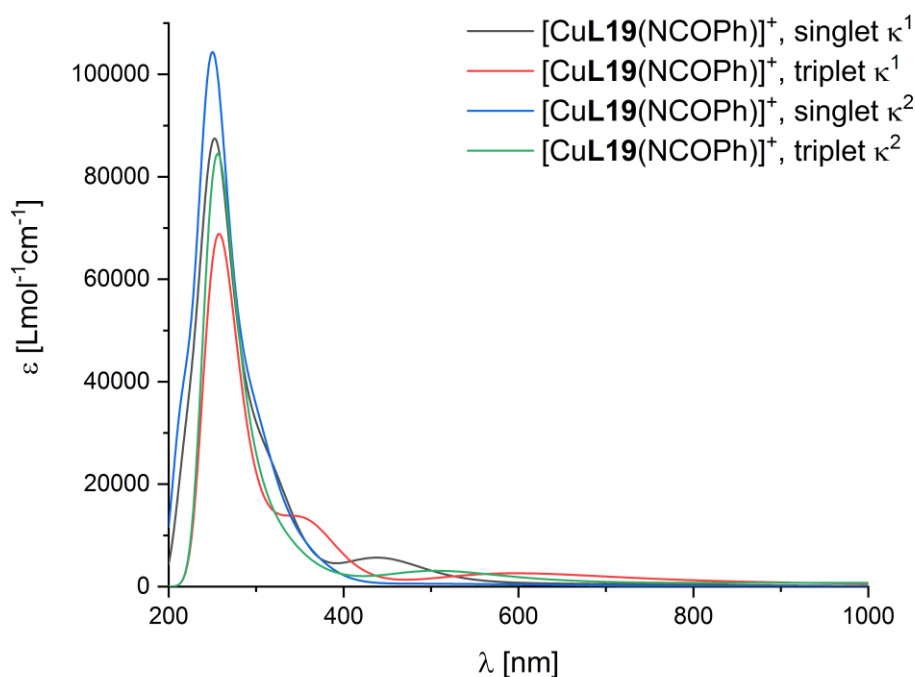


Figure 108. Calculated UV/Vis spectra of [CuL19(NCOPh)]⁺ in dichloromethane.

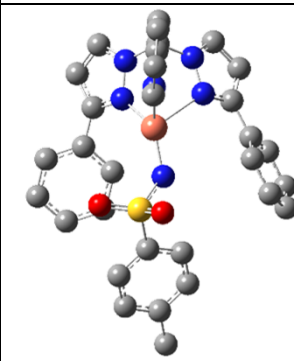
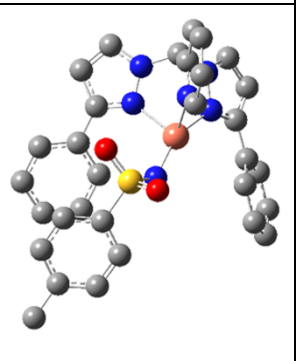
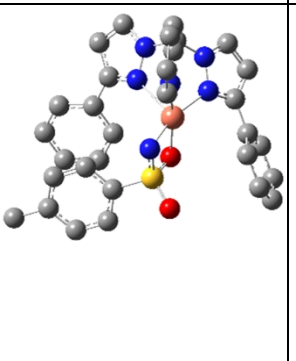
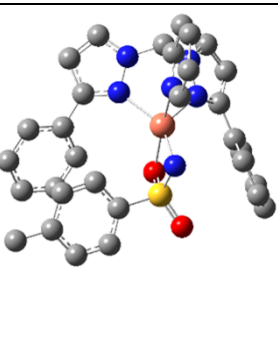
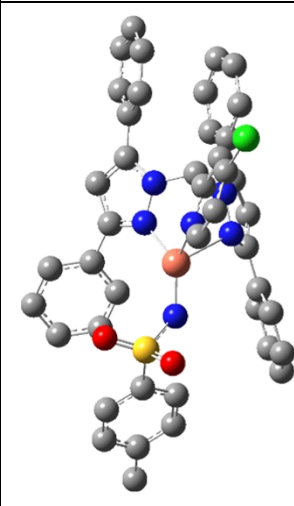
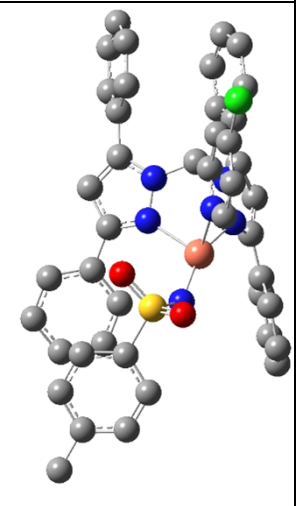
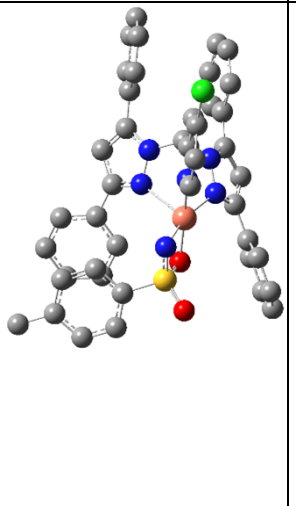
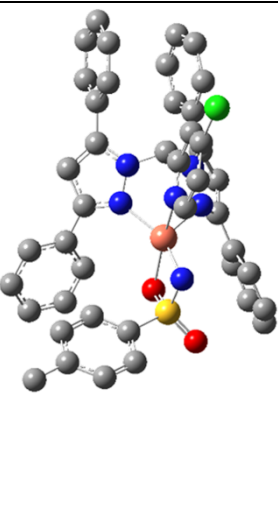
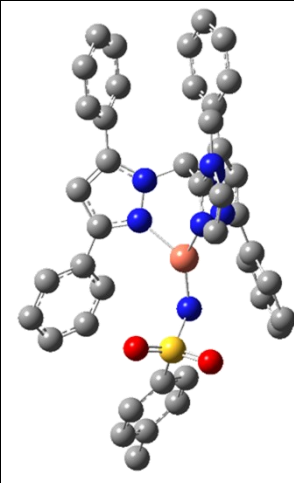
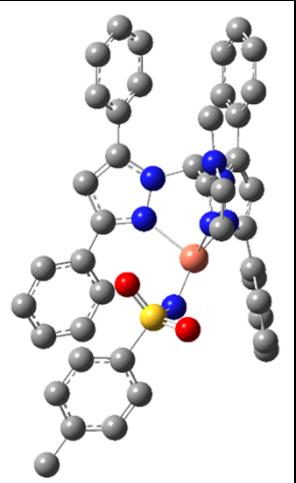
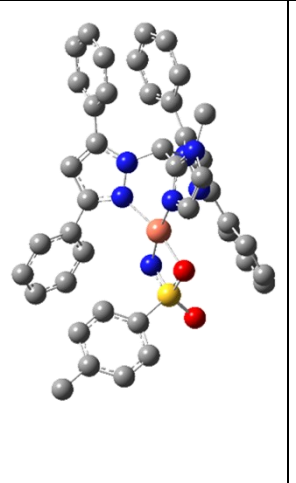
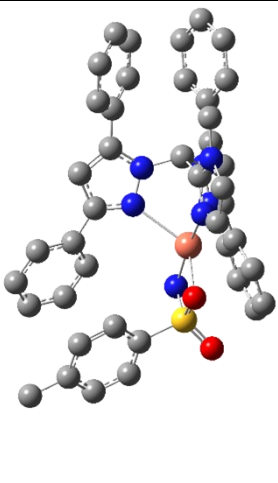
singlet- κ^1 -mode of $N1^+$	triplet- κ^1 -mode of $N1^+$	singlet- κ^2 -mode of $N1^+$	triplet- κ^2 -mode of $N1^+$
			
singlet- κ^1 -mode of $N2^+$	triplet- κ^1 -mode of $N2^+$	singlet- κ^2 -mode of $N2^+$	triplet- κ^2 -mode of $N2^+$
			
singlet- κ^1 -mode of $N3^+$	triplet- κ^1 -mode of $N3^+$	singlet- κ^2 -mode of $N3^+$	triplet- κ^2 -mode of $N3^+$
			

Figure 109. κ^1 - and κ^2 -coordination motifs of the nitrene moieties in the copper nitrenes.